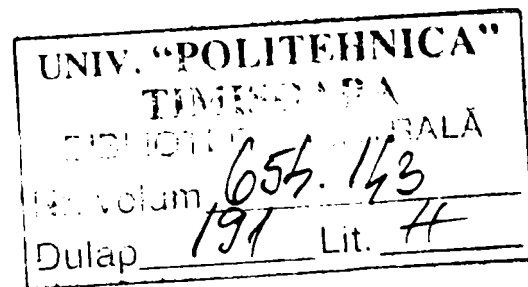


Miklos IVANYI Jr.

PhD. THESIS

**ULTIMATE LIMIT STATE ANALYSIS AND DESIGN
OF A NEW TYPE OF ORTHOTROPIC STEEL PLATE
FOR COMPOSITE BRIDGES
ACCORDING TO EUROCODES**



PhD. Thesis analysis and sustain board

Chairman:

Prof. Ioan BORZA, PhD. Eng.,
Faculty of Civil Engineering,
"Politehnica" University of Timisoara

Members:

Prof. Radu BANCILA, PhD. Eng., Supervisor
"Politehnica" University of Timisoara
Prof. Josef FINK, PhD. Eng., Reviewer
Technical University of Vienna, Austria
Prof. Aarne JUTILA, PhD. Reviewer
Helsinki University of Technology, Finland
Prof. Nicolae POPA, PhD. Eng., Reviewer
Technical University of Civil Engineering, Bucharest

2007

PhD Thesis

ULTIMATE LIMIT STATE ANALYSIS AND DESIGN
OF A NEW TYPE OF ORTHOTROPIC STEEL PLATE
FOR COMPOSITE BRIDGES ACCORDING TO EUROCODES

Author

Miklos Ivanyi Jr.

Published by

“Politehnica” University of Timisoara

Faculty of Civil Engineering

All rights reserved. No part of this publication may be reproduced, stored in a retrieval systems or transmitted in any form or by any means, without prior permission in writing form of the Author.

Timisoara, 2007.

Acknowledgement

I would like to express my sincere gratitude to Professor Radu Bancila whose guidance, help and continuous interest was invaluable during this research.

I particularly wish to thank the help of Peter Ivanyi who continuously supported my numerical analysis research. I am also grateful for the useful discussions I have with all former and present members of the UVATERV Co.

I would like to express my gratitude to KÖZGÉP Co. to produce the test specimens and to University of Pécs, Pollack Mihály Faculty of Engineering for use the modern loading equipment.

This Thesis is dedicated to my parents who gave all their love and support to me.

Table of contents

CHAPTER 1 Introduction: Aims and Scope

1.1.	Aspects of “Structural Design Standards”	Ch.1-1
1.2.	Aspects of structural details	Ch.1-3
1.3.	Aspects of welding technology	Ch.1-4
1.4.	Aims and scope of the Thesis	Ch.1-5

CHAPTER 2 Composite Bridges

2.1.	Introduction	Ch.2-1
2.1.1.	Composite bridges – principal types	Ch.2-2
2.1.2.	Main advantages of composite bridges	Ch.2-6
2.2.	Structural action	Ch.2-8
2.2.1.	Positive “Bending Moment Regions”	Ch.2-8
2.2.2.	The behaviour of composite beams	Ch.2-9
2.2.2.1.	Component behaviour	Ch.2-9
2.2.2.2.	Description of a simply supported composite beam	Ch.2-11
2.2.2.3.	Practical load situations	Ch.2-17
2.2.2.4.	Creep and shrinkage	Ch.2-18
2.2.2.5.	Propped and unpropped composite beams	Ch.2-19
2.2.2.	Partial connection	Ch.2-22
2.2.3.	Continuous composite beams	Ch.2-22
2.2.4.	Design aspects of the concrete flange in compression	Ch.2-24
2.2.4.1.	Effective width	Ch.2-24
2.2.4.2.	Maximum longitudinal shear in the concrete slab	Ch.2-25
2.2.5.	Types and behaviour of shear connection	Ch.2-26
2.2.5.1	The forces applied to connectors	Ch.2-26
2.2.5.2	Basic forms of connection	Ch.2-29
2.3.	Aspects of the structural design and details	Ch.2-32
2.3.1.	Introduction	Ch.2-32
2.3.2.	The bridge at Oszlár over the river Tisza	Ch.2-32
2.3.3.	The bridge at Szekszard over the Danube	Ch.2-42
2.3.4.	The bridge over the Eastern Main Chanel	Ch.2-51
2.3.5.	The bridge over the river Mura	Ch.2-52
2.4.	Conclusion	Ch.2-53

CHAPTER 3 Experimental Test Program

3.1.	Test specimens	Ch.3-1
3.2.	Test procedures	Ch.3-6
3.2.1.	Load equipment	Ch.3-10
3.2.2.	Preparation for the experiments	Ch.3-10
3.2.3.	Measurement procedures	Ch.3-11
3.3.	Test for mechanical properties of the steel material of test girders	Ch.3-14
3.4.	Experimental behaviour of orthotropic plates	Ch.3-24
3.4.1.	Effect of sagging moment	Ch.3-24
3.4.2.	Effect of hogging moment	Ch.3-30

3.4.3.	Effect of shear loading	Ch.3-36
3.5.	The results of strain measurements	Ch.3-42
3.6.	Elastic behaviour of web with U-shaped holes	Ch.3-52
3.6.1.	Bending stress	Ch.3-52
3.6.2.	Vierendeel behaviour	Ch.3-54
3.6.3.	Shearing stress	Ch.3-55
3.7.	Ultimate strength of test girders	Ch.3-57
3.7.1.	Yielding of U-shaped sections	Ch.3-57
3.7.2.	Ultimate strength	Ch.3-58
3.8.	Conclusions	Ch.3-60

CHAPTER 4 Numerical Analysis

4.1	Linear 3D finite element analysis	Ch.4-1
4.1.1	The finite element model	Ch.4-2
4.1.2.	Results of the linear 3D finite element analysis for the shear load	Ch.4-6
4.1.3.	Results of the linear 3D finite element analysis for the sagging moment	Ch.4-8
4.1.4.	Results of the linear 3D finite element analysis for the hogging moment	Ch.4-8
4.2	Non-linear 3D finite element analysis	Ch.4-9
4.2.1	The imperfections according to EC 3 Part 1.5	Ch.4-14
4.2.2	Comparison of the experimental and numerical tests	Ch.4-14
4.3	Conclusions	Ch.4-18

CHAPTER 5 Behaviour and Design of Plated Steel Structures

5.1.	Introduction to plate behaviour and design	Ch.5-1
5.1.1.	Introduction	Ch.5-1
5.1.2.	Basic behaviour of a plate panel	Ch.5-2
5.1.2.1.	Geometric and boundary conditions	Ch.5-2
5.1.2.2.	In-plane Actions	Ch.5-3
5.1.2.3.	Out-of-plane Actions	Ch.5-4
5.1.2.4.	Determination of plate panel actions	Ch.5-5
5.1.2.5.	Variations in buckled mode	Ch.5-7
5.1.2.6.	Grillage analogy for plate buckling	Ch.5-10
5.1.2.7	Post buckling behaviour and effective widths	Ch.5-11
5.1.2.8	The influences of imperfections on the behaviour of actual plates	Ch.5-12
5.1.2.9.	Elastic behaviour of plates under lateral actions	Ch.5-14
5.1.3.	Behaviour of stiffened plate	Ch.5-16
5.2.	Behaviour and design of unstiffened plate	Ch.5-18
5.2.1.	Introduction	Ch.5-18
5.2.2.	Unstiffened plates under in-plane loading	Ch.5-19
5.2.2.1	Load distribution	Ch.5-19
5.2.2.1.1.	Distribution resulting from membrane theory	Ch.5-19
5.2.2.1.2	Distribution resulting from linear elastic theory using Bernoulli's hypothesis	Ch.5-19
5.2.2.1.3	Distribution resulting from finite element methods	Ch.5-20
5.2.2.2.	Stability of unstiffened plates	Ch.5-20

5.2.2.2.1	Linear buckling theory	Ch.5-20
5.2.2.2.2	Ultimate resistance of an unstiffened plate	Ch.5-25
5.2.3.	Unstiffened plates under out-of-plane actions	Ch.5-35
5.2.3.1.	Action distribution	Ch.5-35
5.2.3.1.1.	Distribution resulting from plate theory	Ch.5-35
5.2.3.1.2.	Distribution resulting from finite element methods (FEM)	Ch.5-37
5.2.3.2.	Deflection and ultimate resistance	Ch.5-37
5.2.3.2.1.	Deflections	Ch.5-37
5.2.3.2.2	Ultimate resistance	Ch.5-38
5.2.4.	Influence of the out-of-plane actions on the stability of unstiffened plates	Ch.5-38
5.3.	Behaviour and design of stiffened plates	Ch.5-39
5.3.1.	Introduction	Ch.5-39
5.3.2.	Stiffened plates under in-plane loading	Ch.5-41
5.3.2.1	Action distribution	Ch.5-41
5.3.2.1.1	Distribution resulting from membrane theory	Ch.5-41
5.3.2.1.2	Distribution resulting from linear elastic theory using Bernoulli's hypothesis	Ch.5-42
5.3.2.1.3	Distribution resulting from finite element methods	Ch.5-43
5.3.2.2	Stability of stiffened plates	Ch.5-43
5.3.2.2.1	Linear buckling theory	Ch.5-43
5.3.2.2.2	Ultimate resistance of stiffened plates	Ch.5-47
5.3.3.	Stiffened plates under out-of-plane action application	Ch.5-53
5.3.3.1	Action distribution	Ch.5-53
5.3.3.2	Deflection and ultimate resistance	Ch.5-54
5.4.	Planar orthotropic plated structures without transverse loading according to EC 3 (Part 1.5)	Ch.5-54
5.5.	Orthotropic buckling of compressed stiffened plates	Ch.5-62
5.6.	The analysis of elastically "layer" connected structures, The concept of the "ideal" cross section	Ch.5-71
5.7.	Application of an „ideal" cross section	Ch.5-77
5.7.1.	The inertia of the "ideal" (reduced) cross section for the experimental models	Ch.5-77
5.7.2.	Results of the numerical analysis and the experimental tests	Ch.5-78
5.7.3.	Structural details investigated by experimental models	Ch.5-80
5.7.4.	Case study of the floodplain bridge at Szekszárd over the Danube	Ch.5-81
5.7.5.	Study of the bottom flange at the middle pier in the floodplain bridge at Szekszárd over the Danube when an exponential function is used	Ch.5-83
5.7.6.	Study of the floodplain bridge at Szekszárd over the Danube	Ch.5-84
5.7.7.	"Supporting" effect of the cross girders	Ch.5-86
5.8.	Conclusions	Ch.5-90
 CHAPTER 6 Summary and Conclusions		
6.1.	Examining the design process	Ch.6-1
6.2.	Experiments	Ch.6-2
6.3.	Numerical simulation	Ch.6-2
6.4.	New Scientific Results	Ch.6-3

APPENDIX 1
APPENDIX 2
APPENDIX 3
APPENDIX 4
APPENDIX 5
APPENDIX 6

CHAPTER 1

Introduction: Aims and Scope

1.1. Aspects of “Structural Design Standards”

Structural Design Standards for bridges and structures influences greatly on the design process, design calculations and structural details. This influence can be observed even nowadays as the "Structural Eurocode" Standards are finalized. Beside changes in the standards the design strategy has also changed significantly:

- In the field of modern steel structures the increase in the variety of prefabricated components (e.g. hot-rolled and cold folded sections) brought significant changes in the design theory, design techniques and quality management.
- The developing welding techniques and fabricating processes in the past decades lead to structural details that differ from traditional solutions.
- The computational technology has been developed enormously in the past decades. This development helped that the design and research methodology can also go through an extensive transformation.

The Structural Eurocode Standards are the results of a long research and developing activity. The structure of the Eurocode system is well known:

EC-0	EN 1990 Eurocode : Basis of structural design
EC-1	EN 1991 Eurocode 1: Action on structures
EC-2	EN 1992 Eurocode 2: Design of concrete structures
EC-3	EN 1993 Eurocode 3: Design of steel structures
EC-4	EN 1994 Eurocode 4: Design of composite steel and concrete structures
EC-5	EN 1995 Eurocode 5: Design of timber structures
EC-6	EN 1996 Eurocode 6: Design of masonry structures
EC-7	EN 1997 Eurocode 7: Geotechnical design
EC-8	EN 1998 Eurocode 8: Design of structures for earthquake resistance
EC-9	EN 1999 Eurocode 9: Design of aluminium structures

In the rest of the thesis references to the section of the standard will be shortened, for example EC3 means EN1993-1.1-2005.

I have used the following Structural Eurocode:

EN 1993-1-1 (2005)	General rules and rules for buildings
prENV 1993-1-5 (1992)	General rules. Supplementary rules for planar plated structures without transverse loading
EN 1993-1-5 (2007)	
EN 1993-2 (2007)	Design of steel structures. Steel bridges
EN 1994-1-1 (2005)	General rules and rules for buildings
EN 1994-2 (2006)	Composite bridges

Out of the standards that are based on the limit-states principle EC 3 discusses plated structures. EC 3 contains the design methodology and structural details of planar plated structures. The design of planar plated steel structures is summarized in Fig. 1.1. It can be seen in the figure that two sections of the "Generic Code Side" deal with steel plated structures:

- EC-3-1.5 Planar plated structures without transverse loading: This class of stiffened planar plates will be called "orthotropic steel plate" in the following chapters.

- EC-3-1.7 Planar plated structures with transverse loading: This class of stiffened planar plates will be called "orthotropic steel deck" in the following chapters.

Fig. 1.1. also shows that on the "Structural Code Side" only one section of EC-3-2 Steel Bridges deals detailing in detail with the structural. The title of this section is "Annex G: Special Considerations for Structural Detailing of Orthotropic Decks".

Fig. 1.1 emphasizes strongly the currently used design practice that although the calculation of the two types of planar plated structures are significantly different, at the same time similar or the same structural details are used in the two types of planar plated structures.

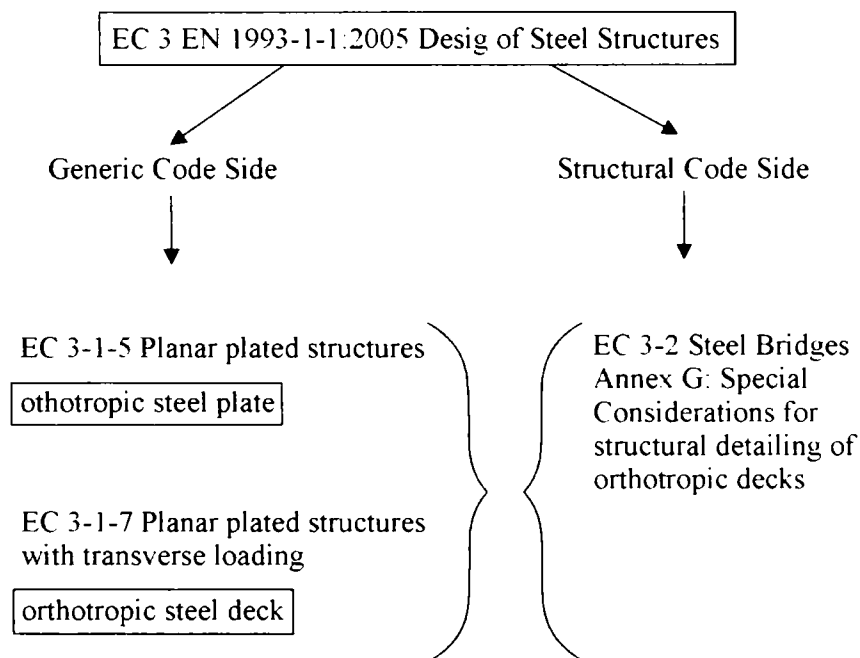


Fig. 1.1. Design of planar plated steel structures

1.2. Aspects of structural details

The most commonly used structural solution for bridges for orthotropic steel decks with different holes and closed cross section stiffeners is that a large U-shaped hole is cut into the top part of the web of the cross beams, which allows longitudinal U-shaped stiffeners to pass through. These U-shaped holes in the web of the cross beams reduce the cross section and thus cause weaknesses. Furthermore the overall structural behaviour is also affected by these holes.

Experimental results are available for orthotropic steel decks with U-shaped holes. The experimental and theoretical work of KUNERT (1967) and KUNERT and WAGNER (1968) must be mentioned, however in their study the longitudinal ribs have small open sections that pass through the cross beams. Another important work is due to FALKE (1983) (1984) who presented "an approximate method for calculating the reduction in the effective stiffness of a cross beam due to the cutting of a web". By performing experiments Falke also studied the collapse mechanism of the cross beam. In his study NARUSE (1975) emphasized that both ends of the slit shape under the ribs and the buckling strength of the web with large holes must be investigated. He has based his recommendations on the observation of higher than expected stress concentrations around the holes.

ITO, M. et al (1991) reported the "results of static loading tests on beams with U-shaped holes in the top part of the web", then presented "an evaluation of the bending and shearing stresses for such beams and the ultimate strength properties". They performed tests with simply supported beams loaded by a concentrated force, as they have regarded the cross beams as beams with holes in the top part of the web. Furthermore they designed the tests in such a way, that yielding will occur first rather than buckling.

WOLCHUK, R. and OSTAPENKO, A (1992) "attempted to assess the unexplored secondary local stresses in the rib walls, their relationship to the geometric parameters at the rib – floor-beam intersection and their effect on the level of combined stresses in the rib walls at the floor-beam cutouts".

1.3. Aspects of welding technology

Traditional structural details of steel plate girders with open cross-section stiffeners are not suitable for robotic welding. One of the most problematic part is the connection between the horizontal and vertical stiffeners. In the case of plates stiffened with open cross-section, horizontal and vertical stiffeners the modern welding technology requires the existence of a "gap" between the components, however in the design continuous stiffeners are assumed. This kind of connections has been investigated in a joint research project between the University of Osaka,

Japan and the Budapest University of Technology and Economics (BME), Hungary and the results have been summarized by IVANYI (2001).

In the framework of the joint research project static load tests of girders with different stiffener-end-gaps have been conducted (OKURA et al, 1997). On the basis of these experiments several numerical studies have been performed (OKURA et al, 1997; DUNAI et al, 1998; NÉZŐ et al, 1999; OKURA et al, 1999). First the influence of the aspect ratio of web panels and the initial out-of-plane deflection of webs on the ultimate behaviour of girders have been investigated (OKURA et al, 1997; DUNAI et al, 1998). Later the focus has been on the effects of bending stiffness of the horizontal stiffeners. The results has shown that the ultimate behaviour of girders with large gaps become independent from the bending stiffness of the horizontal stiffeners (NÉZŐ et al, 1999). In the last stages of the research a variety of gap sizes have been investigated to determine a limitation for the gap which would limit the reduction of the ultimate strength (OKURA et al, 1999).

1.4. Aims and scope of the Thesis

In the case of bridges with orthotropic steel girders one of the most sensitive structural component is the orthotropic deck, which is directly loaded by the wheels of the vehicles. Due to this sensitivity the behaviour of the orthotropic deck dictates the structural details of the other orthotropic plates such as stiffened web and flanges.

There is a completely different situation in the case of composite bridges, since the wheels of vehicles load the reinforced concrete plate directly. The other parts of the bridge are made out of steel and they are loaded only in their plane. The difference between the othotropic bridge and a composite bridge implies that the structural details must also be different.

Furthermore in the case of composite bridges different components must be designed according to different rules. "EC 4 Composite Structures Part 2" gives guidelines for the design of a composite bridge. The steel plate components (web and flanges) must be designed according to "EC 3 Generic Code Side" and the design of the structural details is described in "EC 3 Structural Code Side".

In Hungary the number of composite bridges is increasing as there is a possibility to use a new, simple and more easily fabricated structural detail for longitudinal stiffeners. This detail has several benefits compared to the structural detail used for orthotropic plates (Fig. 1.2). The new structural detail (“E” economic solution) has been proposed by Dr. István Szatmári (BME) and it has been utilised in several bridge designs by UVATERV Co. with some minor modifications. In these bridges I have designed the structural details of the steel parts.

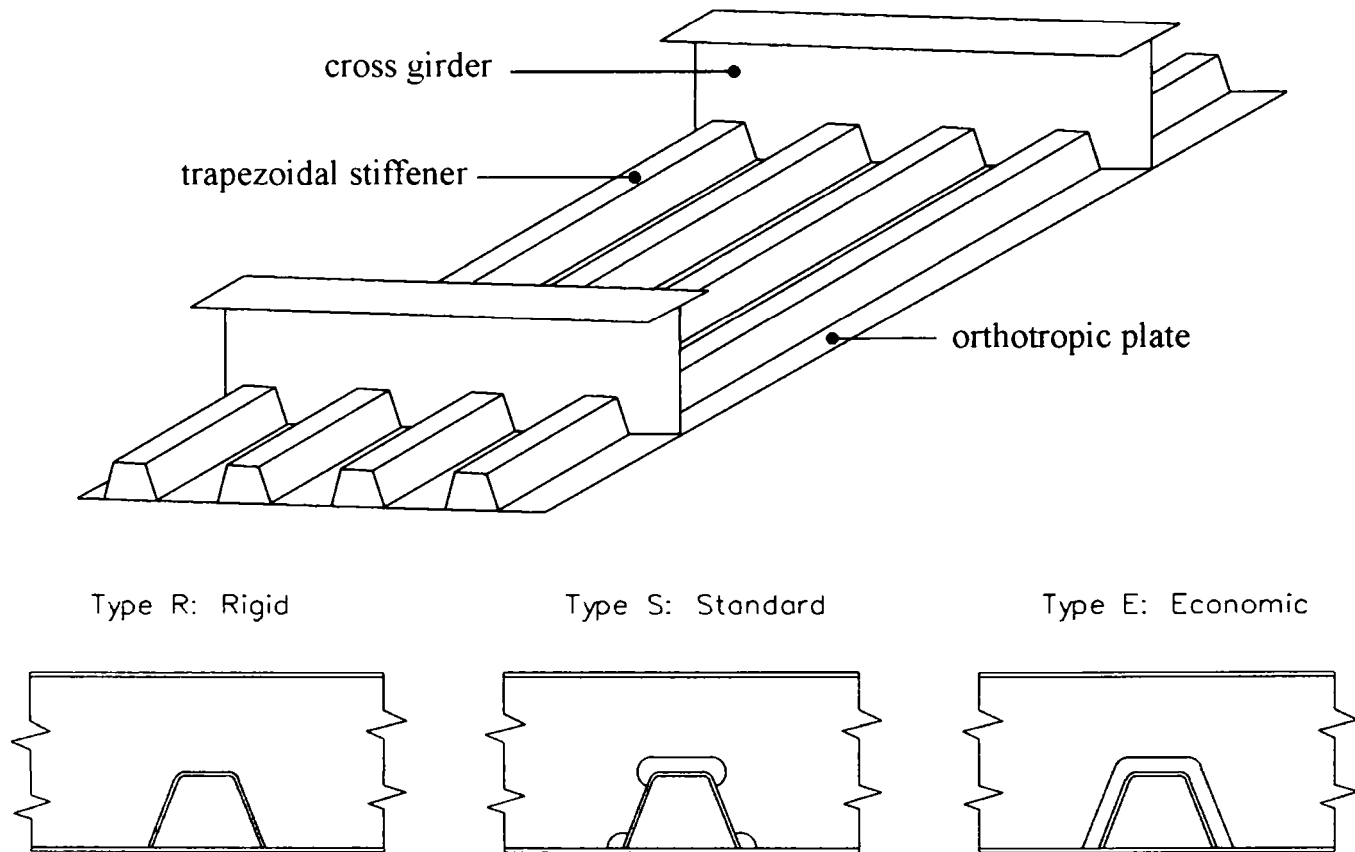


Fig. 1.2. Connections of trapezoidal stiffeners and cross beams

Since 2005 the Engineering Journal of “American Institute of Steel Construction” regularly publishes a column about steel research (Current Steel Structures Research). This column is edited by Prof. REIDAR BJORHOVDE. The volume of the second quarter in 2005 of the Engineering Journal presents my research in the following format: (ENGINEERING JOURNAL/ SECOND QUARTER /2005 p.117).

“Design of a New Type of Orthotropic Plate: Miklos Ivanyi Jr. directs this study for the company UvaterV in Budapest, Hungary with the cooperation of Professor Miklos Ivanyi of the Budapest University of Technology and Economics.

In traditional orthotropic plates the trapezoidal longitudinal stiffener is welded to the transverse girder web and to the bottom flange of the main girder, as shown in Fig. 1.3.a. In a recently developed orthotropic plate the stiffeners and the transverse girder web are not connected, as illustrated in Fig. 1.3.b.

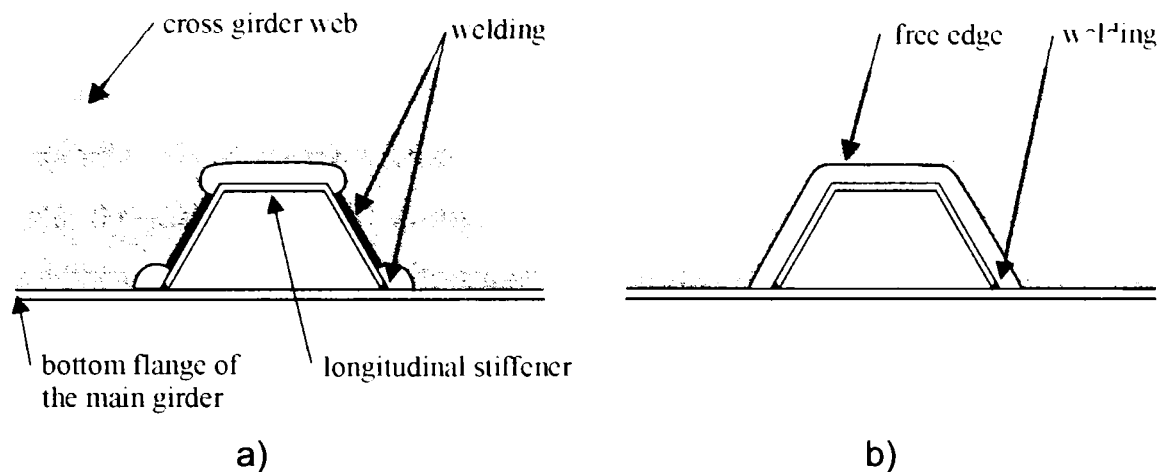


Fig. 1.3. Traditional and new orthotropic deck details.

This approach provides for a significant reduction in the amount of flame cutting and welding, but more importantly there is no longer a need to assess the fatigue condition of the weld between the stiffener and the web. On the other hand, the potential for local buckling of the free edge of the web near the trapezoidal stiffener must be considered. Finite element analyses of the new and traditional plates have been conducted, and a design guide is under development.”

The basis of my Doctoral Thesis is the study the new structural detail. During my research work I have investigated the "Ultimate Limit State" of orthotropic steel plates. The "Serviceability Limit State" and the "Fatigue Limit State" of orthotropic plates (although they are also very important) are not in the scope of this Doctoral Thesis. I have investigated the following problems:

- I have designed experiments to study the connection between a trapezoidal stiffener and a cross beam (Fig. 1.2). As a comparison study three geometric arrangements has been designed. In the first design the web of the cross beam is fully welded to the trapezoidal stiffener. This arrangement is called rigid (R). It must be emphasized that this geometric arrangement is not recommended and

not used due to its fatigue-sensitivity considering the current welding technology. The results performed with this geometric arrangement are used for comparison with the other two geometric arrangements. The other two geometric arrangements are the "standard" (S) and the economic (E).

- I have prepared 3D linear finite element models to study the elastic stiffness of the three geometric arrangements (R,S,E).
- I have also prepared 3D non-linear finite element models to investigate the behaviour of the three geometric arrangements (R,S,E) while the structural details go under plastic deformations. Furthermore the failure mode of the structural details could be observed.
- I have developed a design methodology for "orthotropic buckling" of compressed plates which considers the joint behaviour of several cross stiffeners and the structural detail (R,S,E). "Orthotropic buckling" means that the longitudinal and transversal stiffeners buckle at the same time.
- Finally I have also studied the experimental, numerical and analytical results with the emphasis on the economic (E) solution. In this study I have used the experience that was gained during the design and construction of the composite bridge over the floodplain of the Danube at Szekszárd.

The Doctoral Thesis contains the following chapters:

Chapter 1: Introduction: Aims and Scope. The chapter summarizes the conditions and aims of the research, it introduces the relevant aspects of the design standards, structural detailing and welding technologies. The chapter describes the new type of orthotropic plate with the new type of structural detail.

Chapter 2: Composite Bridges. This chapter reviews the different aspects of the design of composite bridges. Sections 2.1 and 2.2 have been written using the relevant sections of ESDEP "European Steel Design Education Programme" (1994) (www.esdep.com). Some of the composite bridges designed by the UVATERV Co. are also discussed in the chapter. The bridge over the floodplain of the Danube at Szekszard utilizes the new structural detail (connection type E) at the bottom flange

and at the web of the composite box girder. On the other hand the main bridge over the Danube at Szekszárd is an orthotropic steel bridge with the S type of connection in the deck and the plates.

Chapter 3: Experimental Tests. The chapter contains all the details about the design of the experiments, how the tests were performed and what kind of measurements have been taken.

Chapter 4: Numerical Analysis. This chapter discusses the linear and non-linear 3D finite element analysis of the structural details.

Chapter 5: Behaviour and Design of Plated Steel Structures. This chapter deals with the behaviour and design of stiffened plates and plates without stiffening. Sections 5.1-5.3 have been written using the relevant sections of ESDEP "European Steel Design Education Programme" (1994) (www.esdep.com). The chapter shows the design of the different connections (R, S, E) in an orthotropic plate according to EC 3-1-5. The concept and application of "ideal" cross section is also discussed.

Chapter 6: Summary and Conclusion. The chapter summarizes the results and draws conclusions.

The Doctoral Thesis is closed by a bibliography reference in the text.

Finally the Appendix contains the MathCAD program which was used in the calculation of the load bearing capacity of an orthotropic plate with stiffening.

1
2
3
4
5
6
7
8
9
10
11
12
13
14
15
16
17
18
19
20
21
22
23
24
25
26
27
28
29
30
31
32
33
34
35
36
37
38
39
40
41
42
43
44
45
46
47
48
49
50
51
52
53
54
55
56
57
58
59
60
61
62
63
64
65
66
67
68
69
70
71
72
73
74
75
76
77
78
79
80
81
82
83
84
85
86
87
88
89
90
91
92
93
94
95
96
97
98
99
100

CHAPTER 2

Composite Bridges

The advantages of composite bridges are outlined with emphasis on the use of this bridge type for normal spans. The different types of cross-sections applied in the technology are introduced, concentrating mainly on box and plate girders. Attention is drawn to the many different construction and erection stages with different "active" cross-sections and structural systems.

2.1. Introduction

Composite bridge construction has experienced considerable development since the first solutions in the 1940's using simple parallel beam grids over short spans (from 20 to 25 metres), to its present usage in large framed or cable stayed bridges, or in very important truss girders designed to meet the severe functional requirements of high speed trains. It is now commonly used for medium and large works, and also in cases of minor spans competing with prefabricated prestressed concrete systems, where, for example, problems of quick erection or slenderness arise.

It is neither possible, in this general chapter, to describe or to catalogue the complete range of actual solutions that composite construction offers for bridges, nor is it possible to outline the general problems of details, construction procedures, choices of analysis, etc. The chapter therefore concentrates on emphasising the advantages that the composite structure offers, dealing mainly with the systems and construction processes for medium span bridges. The chapter is completed with brief references

to other methods that can be useful in more important cases that require wider specialization and experience before they can be applied.

First an understanding of the nature of the inherent aspects of the bending of composite systems and the rheological interaction of the deck's construction materials is required. Starting from certain fundamental global considerations, an understanding of the phenomena that principally determine the functional performance, structural behaviour and execution problems of composite bridges can then be reached. (DOWLING et al, 1988, JOHNSON, 1975, 1979, PETERSEN, 1982, BONDARIUC, BANCILA 1987)

Therefore, the chapter analyses questions related to:

- Regions of dominant positive bending moments (sagging), i.e. simply supported decks or the central part of spans of continuous systems, with some consideration given to the transverse characteristics and the construction process.
- Regions of dominant negative bending moments (hogging), i.e. supports of continuous and cantilever systems, and their interaction with transverse shear and torsional effects, leading to the significant potential for double composite action in these zones.
- Shear connection of the composite systems and its influence on the analytical treatment, local effects at the beam ends, etc.

Fabrication and erection methods have a large influence on the detailed design of the steel structures. The supporting steel members must be designed so that they do not interfere with the placing of the concrete slab.

2.1.1. Composite bridges – principal types

The following general observations can be made concerning the principal types of composite bridge decks:

- For short spans, 25 to 45m approximately, solutions using multiple plate girders without any kind of transverse bracing are preferred with the concrete deck slab performing the total function of transverse distribution and stability (Fig. 2.1). The number of beams should be the least compatible with the transverse distribution capability of the concrete slab.

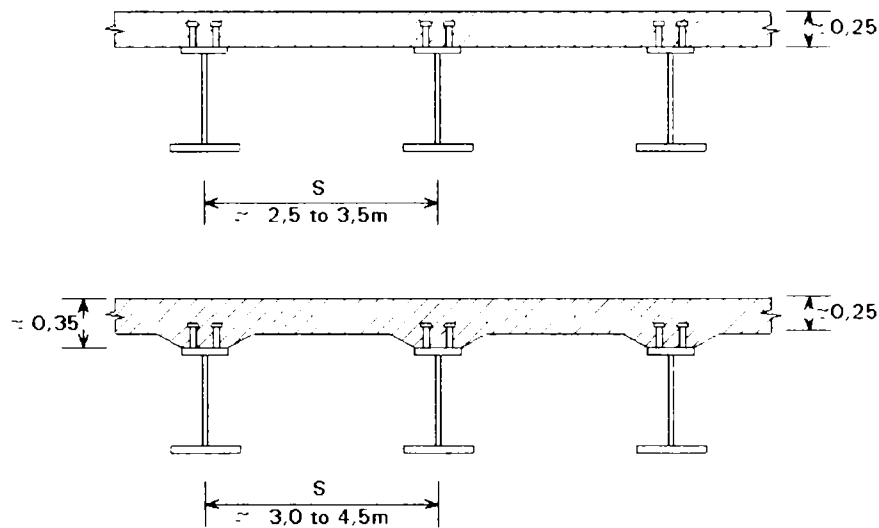


Fig. 2.1. Multiple plate girders

- Twin plate girders with haunched slab can be a very attractive solution for narrow bridges (Fig. 2.2).

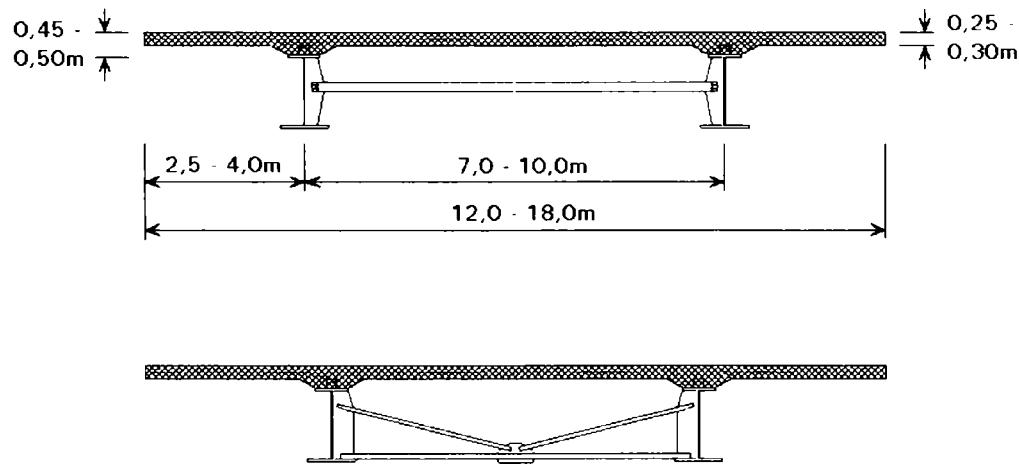


Fig. 2.2. Twin plate girders

- For longer spans (50 to 100m) the system of widely spaced twin girders (Fig. 2.3) joined with transverse composite beams, spaced at about 4 to 5 metres, is very suitable. Main and transverse girders can be plate girders or, in cases with very long spans or very severe deflection limits, trusses.

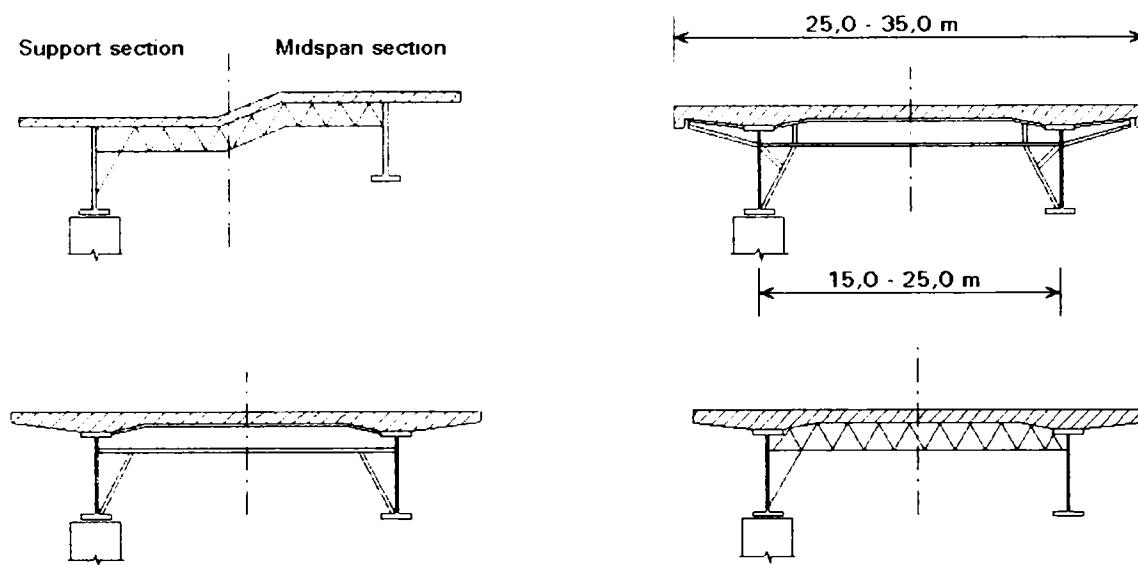


Fig. 2.3. Twin girders for wide and long-span bridges

- Box girders, preferably with trapezoidal semi-open cross-sections (Fig. 2.4a-b), also provide adequate solutions for all of the above mentioned cases, especially when curvatures exist in plan. Box girders become almost obligatory if the curvatures are very sharp.

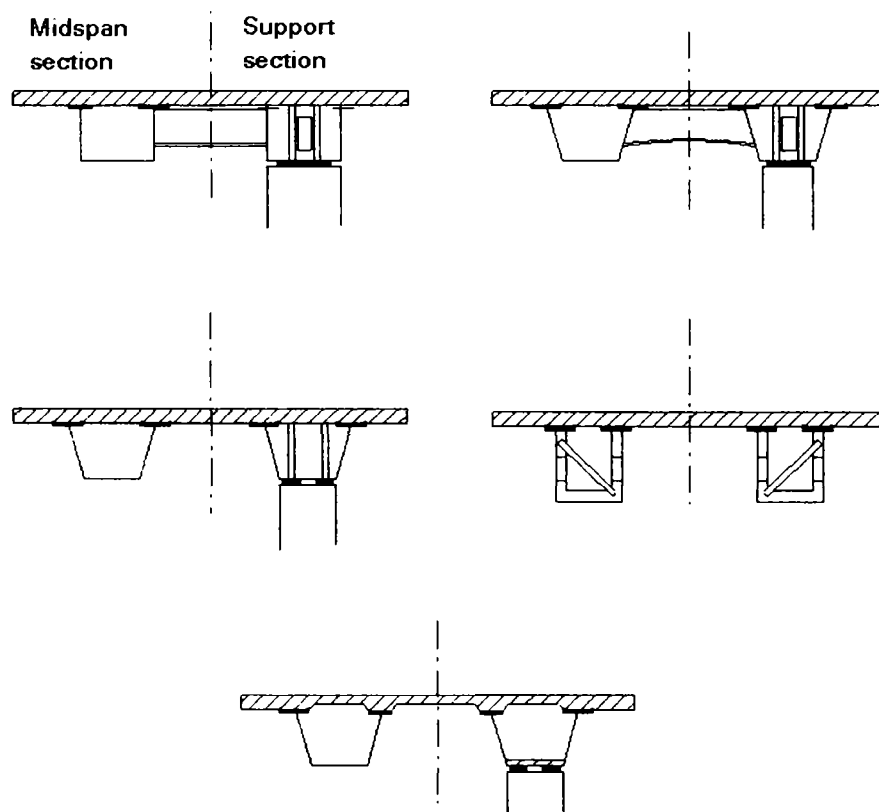


Fig. 2.4a. Twin box girders

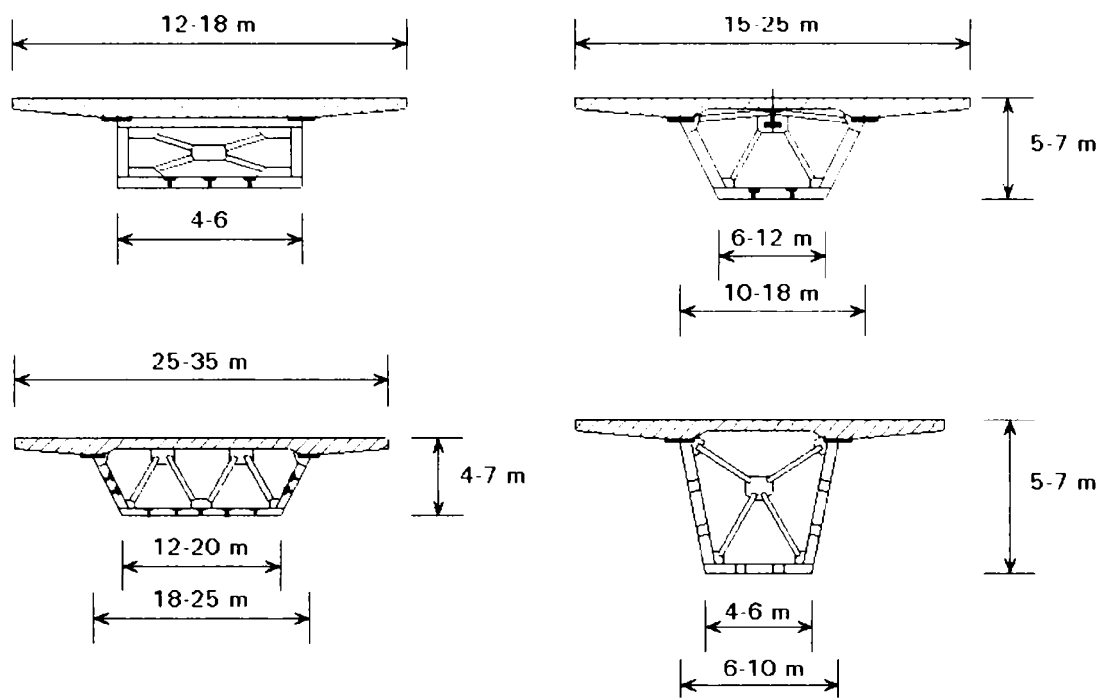


Fig. 2.4b. Large box girders

- For very large railway bridges, cross-sections formed by two large composite lattice girders (Fig. 2.5) and used with or without bottom concrete slabs, give very suitable solutions in terms of ease of construction, economy, serviceability and durability.

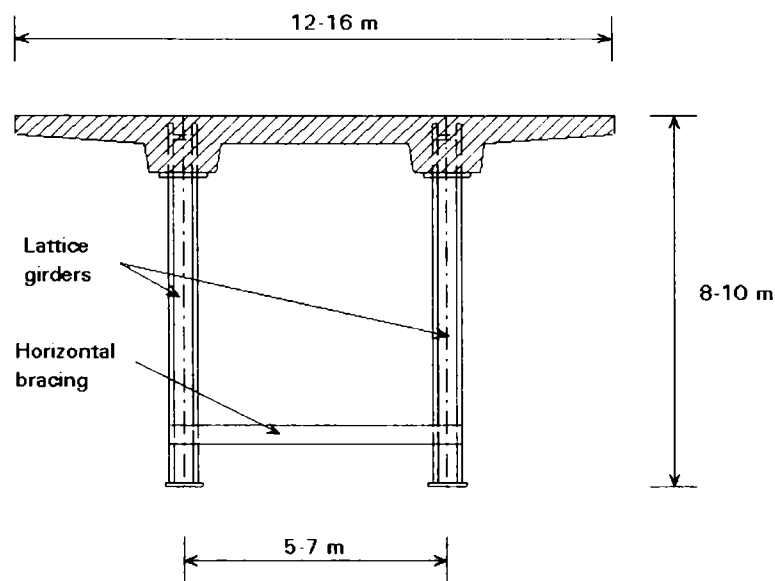


Fig. 2.5. Long span composite trusses

- Other solutions are based on the use of lattice webs joined to top and bottom concrete slabs (Fig. 2.6), or profiled steel sheet webs concreted to concrete filled and prestressed steel tubes (Fig. 2.7).

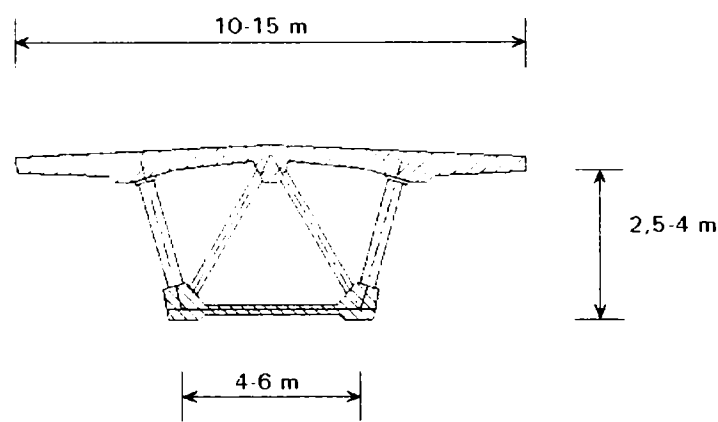


Fig. 2.6. Composite box girder with composite bottom flange

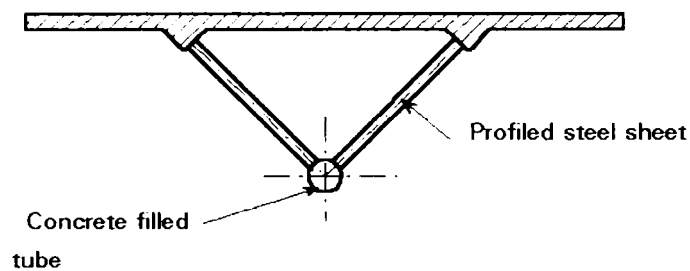


Fig. 2.7. Cross-section from le Viaduc de Maupre

2.1.2. Main advantages of composite bridges

By the appropriate combination of the two principal construction materials, structural steel and concrete (reinforced or prestressed), more efficient bridge construction can be achieved than is possible using the two materials independently. This advantage is gained particularly when the work specification is demanding in relation to short construction periods, functional conditions of high slenderness, the site topography, road or services complexity, or complex layouts in plan or elevation.

In particular, the use of self-supporting steel systems allows, in the same way as for steel bridge construction, the execution to proceed without shoring during the concreting of the deck slab thereby giving rapid execution even with difficult layouts, (strong curvatures in plan, complex transverse sections, etc.). Later the deck slab is used as an element of great inertia and resistance, which reduces the total amount of steel required, especially in the compression zones where its use reduces the need for additional stiffening and/or bracing.

This advantage, which is clear in the sagging regions, can be extended to the hogging regions through the correct use of prestressing methods, or to a least extent, with longitudinal reinforcement of the concrete slab, giving partial improvement to its properties. Likewise, an intelligent additional steel-concrete combination in double composite action could extend the global application of the composite solutions.

The resultant performance-structural-executional symbiosis of these two major materials improves the whole to a much greater extent than the simple juxtaposition of the two materials. The designer should carefully combine the steel and concrete in proportions that optimise the bridge performance in all the above-mentioned respects.

Essentially the principal advantages of composite bridges in comparison with others of similar dimensions are:

In comparison with concrete systems:

- Smaller depths and self weights.
- Greater simplicity and easy of execution, especially when the conditions are severe (high rises or plan curvature, etc.).
- Minimisation of environmental problems during execution.
- Favourable and simple use of continuous systems, including bottom concrete slabs in support regions.

In comparison with steel systems:

- Increased stiffness and better functional response.
- Better maintenance and durability characteristics.
- Reduction of secondary bracing systems.
- Lower costs because of a reduction in the total steel required, especially in continuous systems.

2.2. Structural action

2.2.1. Positive “Bending Moment Regions”

Irrespective of the type of bridge considered, maximum efficiency is achieved by adopting transverse cross-sections and execution processes that maximise the potential of the composite system.

This consideration in the past yielded rise to the use of propped construction of the partial steel section, or systems with pre-deformation (prestressed, precambered, preflexed). Alternatively, provisional continuity has been provided by temporary restraint of joints in the steel section, the effect being transferred to the whole composite system after the hardening of the slab. Today, this technique is no longer necessary due to the adoption of limit state methods or non-linear elastic-plastic analysis to establish the ultimate resistance of the cross-sections, together with adequate control of serviceability and functional conditions. In this way the total benefit of all the structural materials included in the section can be achieved without complicating the process of execution, but by taking into consideration some special aspects in the design of the section.

In current practice, by including a slightly larger top flange, a longitudinal web stiffener, and by giving the steel member a precamber of approximately $L/200$ in the workshop, ultimate and serviceability conditions for the non-propped steel beam can be obtained which are similar to those of the propped solution. Construction problems can thereby be reduced and/or sometimes solutions that are almost impossible to achieve in any other way are feasible.

The elastic-plastic behaviour of cross-sections, with the consequent redistribution of the internal stress pattern that allows the total usage of the materials in the ultimate state, begins earlier for the unpropped beam than in the propped beam. In the propped case it occurs much closer to the collapse, with a higher rate of transition to the plastic state.

The compact character of cross-sections which allows the development of a plastic hinge can be established from the criteria defined in EUROCODE 4. These criteria depend upon the steel quality and the compressed web regions. Given the variation of the neutral axis depth in the elastic or elastic-plastic ranges, the position of the neutral axis must be considered for the most unfavourable value that can occur.

In cases where, because of the large beam depth required, a compact section cannot be economically used, it is better to adopt semi-compact (Class 3) or slender (Class 4) cross-sections with elastic calculation methods. The procedures for propping and cambering, provisional restraints, preflexion or prestressing, etc. could then be of interest in order to obtain the most favourable solution.

When propped construction is used, the stability of the upper flanges of steel members during the non-composite work must be carefully considered because of the minimum sizes usually adopted. This aspect is especially important when decking is placed parallel to the beams.

2.2.2. The behaviour of composite beams

2.2.2.1. Component behaviour

Since a composite beam is formed from three components, steel, concrete and connection, it is necessary to review the behaviour of each before describing the overall behaviour of the combination.

Under both tension and compression, **steel** behaves in a linearly elastic fashion until first yield of the material occurs. Thereafter it deforms in a perfectly plastic manner until strain hardening occurs. This behaviour is shown in Fig. 2.8a together with the idealisation of steel behaviour which is assumed for design. In general, most of the steel section is in tension for simple sagging bending and local buckling of slender sections is not a problem. However, for continuous beams, significant parts of the steel section are subject to compression and local buckling has to be considered.

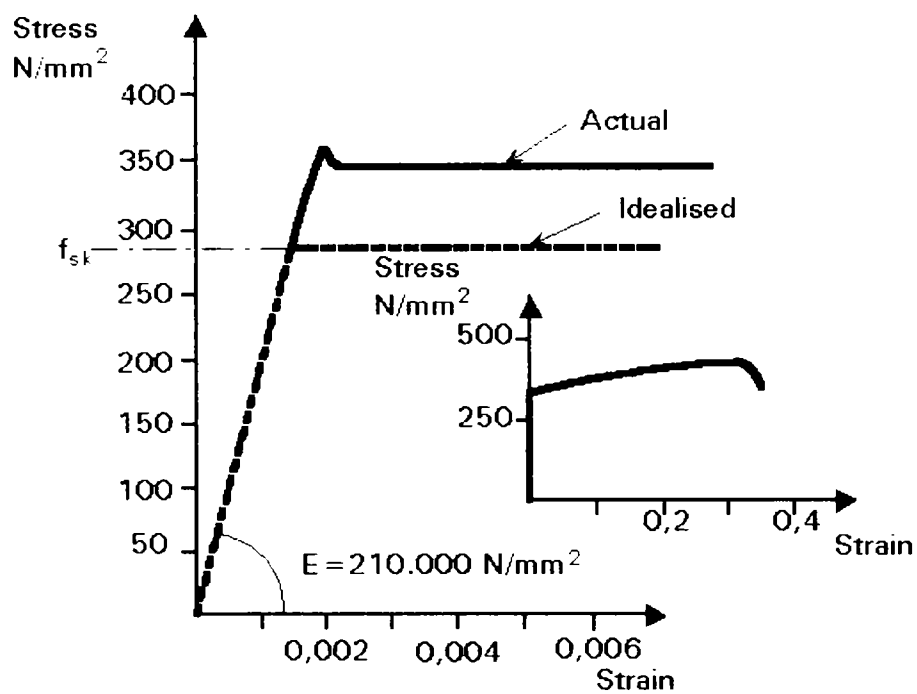


Fig. 2.8a. Mechanical properties of steel

The behaviour of **concrete** is more complex. Two situations have to be considered. Concrete in compression follows a non-linear stress/strain curve. This behaviour is shown in Fig. 2.8b together with the two idealisations used in design. The parabolic stress block is often used in reinforced concrete design but the rectangular block is normally assumed in composite beam design. The non-linear material behaviour gives rise to an inelastic response in the structure. Concrete in tension cracks at very low loads and it is normally assumed, in design, that concrete has no tensile strength.

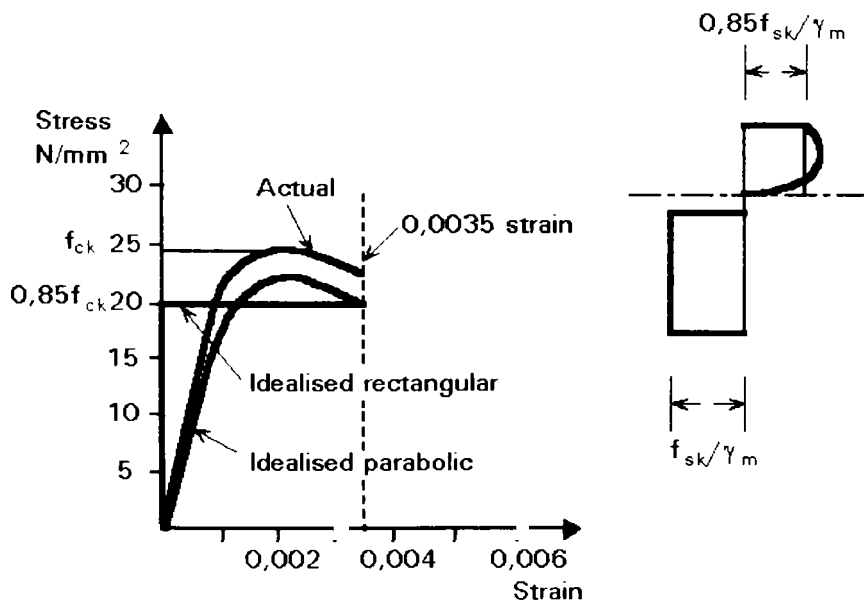


Fig. 2.8b. Mechanical properties of concrete

The **connection** behaviour (see Fig. 2.8c) is sufficient, here, to say that it is also non-linear. This behaviour adds to the complexity of design.

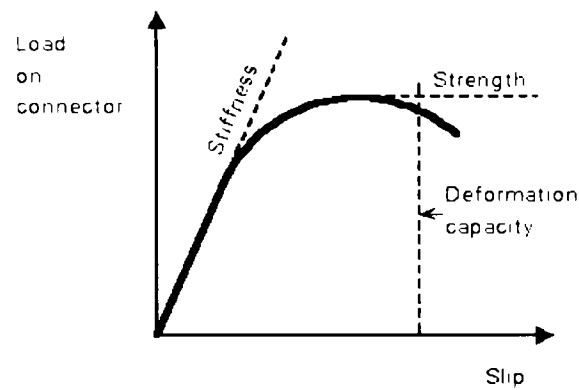


Fig. 2.8c. Mechanical properties of shear connectors

2.2.2.2. Description of a simply supported composite beam

Composite beams are formed with a solid, composite or precast concrete slab spanning between, and connected to, the steel sections.

The slab usually spans between parallel steel sections and its design is normally dictated by this transverse action. Consequently the span, depth and concrete grade are determined separately and are known prior to the beam design.

For non-composite construction, the steel sections alone are designed to carry the load acting on the floor plus the self weight of the slab, as shown in Fig. 2.9. The steel section is symmetric about its mid depth and has a neutral axis at this point. The section strains around this neutral axis and both the outer fibre tensile and compressive stresses are identical. The stresses (σ) in tension (τ) and in compression (c) in the steel section may be evaluated using simple bending theory.

The concrete slab is not connected to the steel section and therefore behaves independently (Fig. 2.9). As it is generally very weak in longitudinal bending it deforms to the curvature of the steel section and has its own neutral axis. The bottom surface of the concrete slab is free to slide over the top flange of the steel section and considerable slip occurs between the two parts. The bending resistance of the slab is often so small that it is ignored.

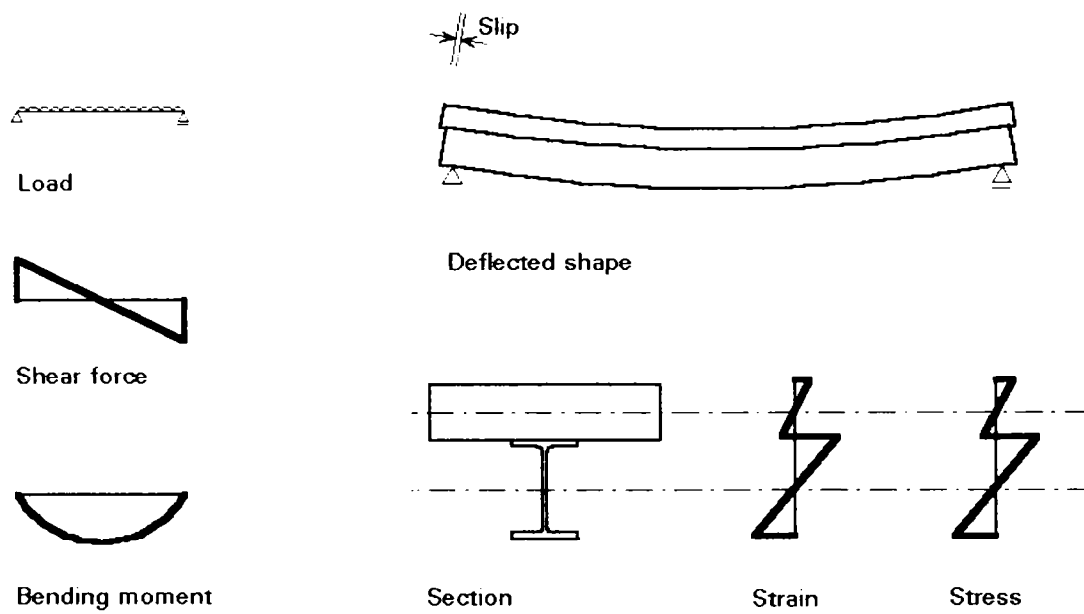


Fig. 2.9. Non-composite beam

Stage 1 Fig. 2.10.

Alternatively, if the concrete slab is connected to the steel section, both act together in carrying the service load as shown in Fig. 2.10. Slip between the slab and steel section is now prevented and the connection resists a longitudinal shear force similar in distribution to the vertical shear force shown.

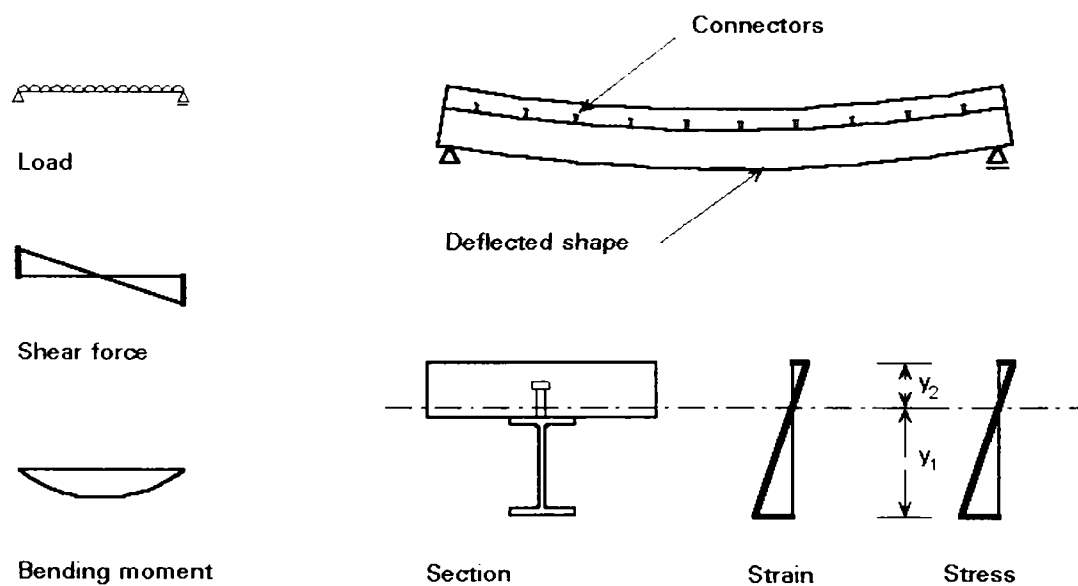


Fig. 2.10. Composite beam -stage 1

The composite section is non-symmetric and shown a single neutral axis often close to the top flange of the steel section. The tensile and compressive stresses at the outer fibres are therefore dependent upon the overall moment of inertia (I) of the

composite section and their distance from the single neutral axis. Assuming that the loading causes elastic deformation the stresses generated in the section may be determined using simple bending theory. The stresses for the service load condition may be obtained (Fig. 2.10). The I value of the composite section is normally several times that of the steel section. It can therefore be seen that, for a similar load, the extreme fibre stresses generated in the composite section will be much smaller than those generated in the non-composite beam.

This difference also has an effect on the stiffness of the beams. The stresses developed in the slab as it spans transversely to the length of the beam are assumed not to affect the longitudinal behaviour. They are generally ignored when designing the composite beam. However, the span of the beam often dictates how much of the slab may be assumed to help in the longitudinal bending action.. Here half the transverse span, each side of the steel section, is assumed to be effective in carrying the longitudinal compression.

The connection between the slab and steel section may be made in many ways. In general it is formed using a series of discrete mechanical keys. This stage corresponds to the service load situation in the sagging moment region of most practical composite beams.

Stage 2 Fig. 2.11.

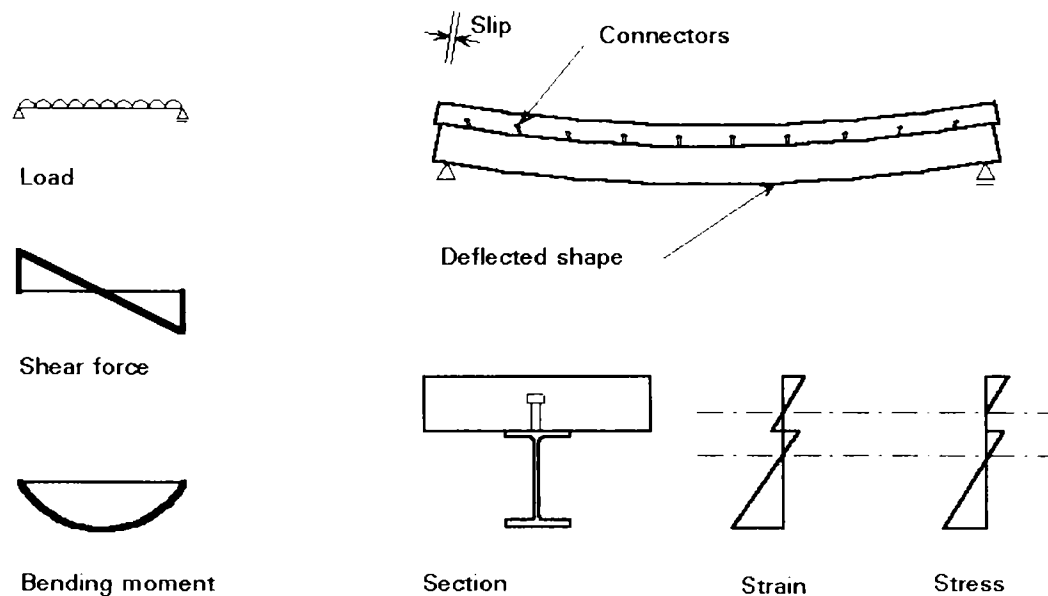


Fig. 2.11. Composite beam –stage 2

As the load increases the shear stress between the slab and steel section gives rise to deformation in the connection. This deformation is known as 'slip' and contributes to the overall deformation of the beam. Fig. 2.11 shows the effect of slip on the strain and stress distribution. For many composite beams slip is very small and may be neglected.

This stage corresponds to the service load stage for that class of composite beams which has been designed as partially connected.

Stage 3 Fig. 2.12 and Fig. 2.13.

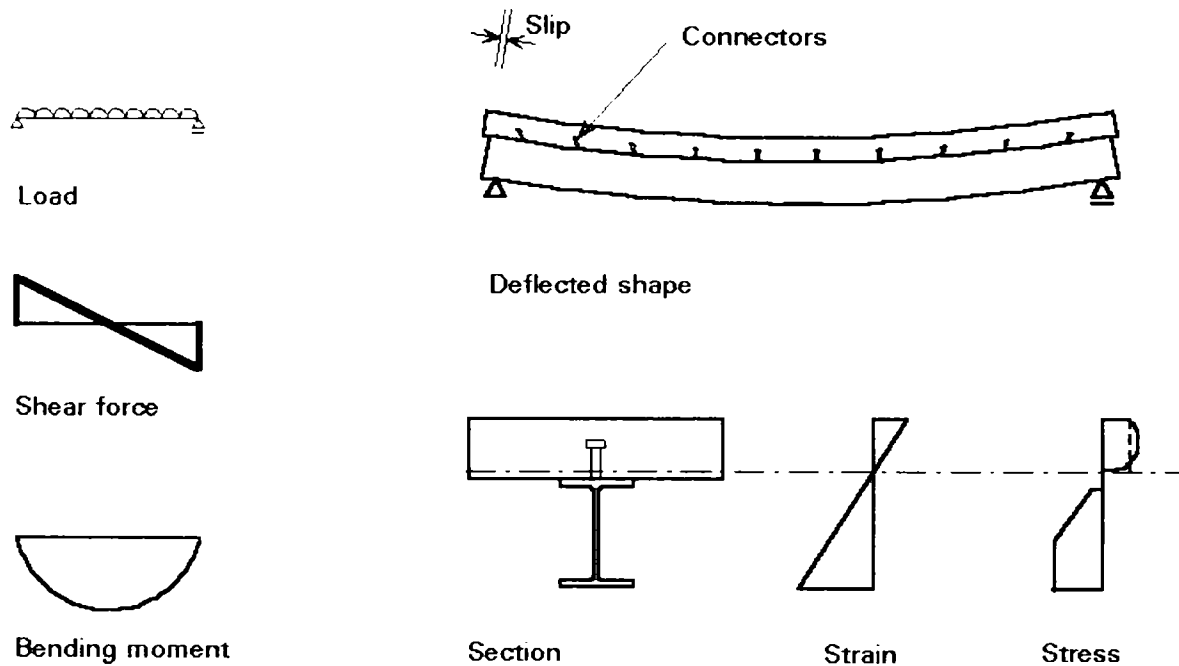


Fig. 2.12. Composite beam –stage 3

Eventually the load becomes sufficient to cause yield strains in one or more of the materials.

Stage 3a

In the case of yield occurring in the steel, plasticity develops and the stress block develops as it is shown in Fig. 2.12. It is normally assumed that, for the ultimate limit state, the plastic stress block develops such that the whole steel section may eventually reach yield as it is shown by the dotted line in Fig. 2.12.

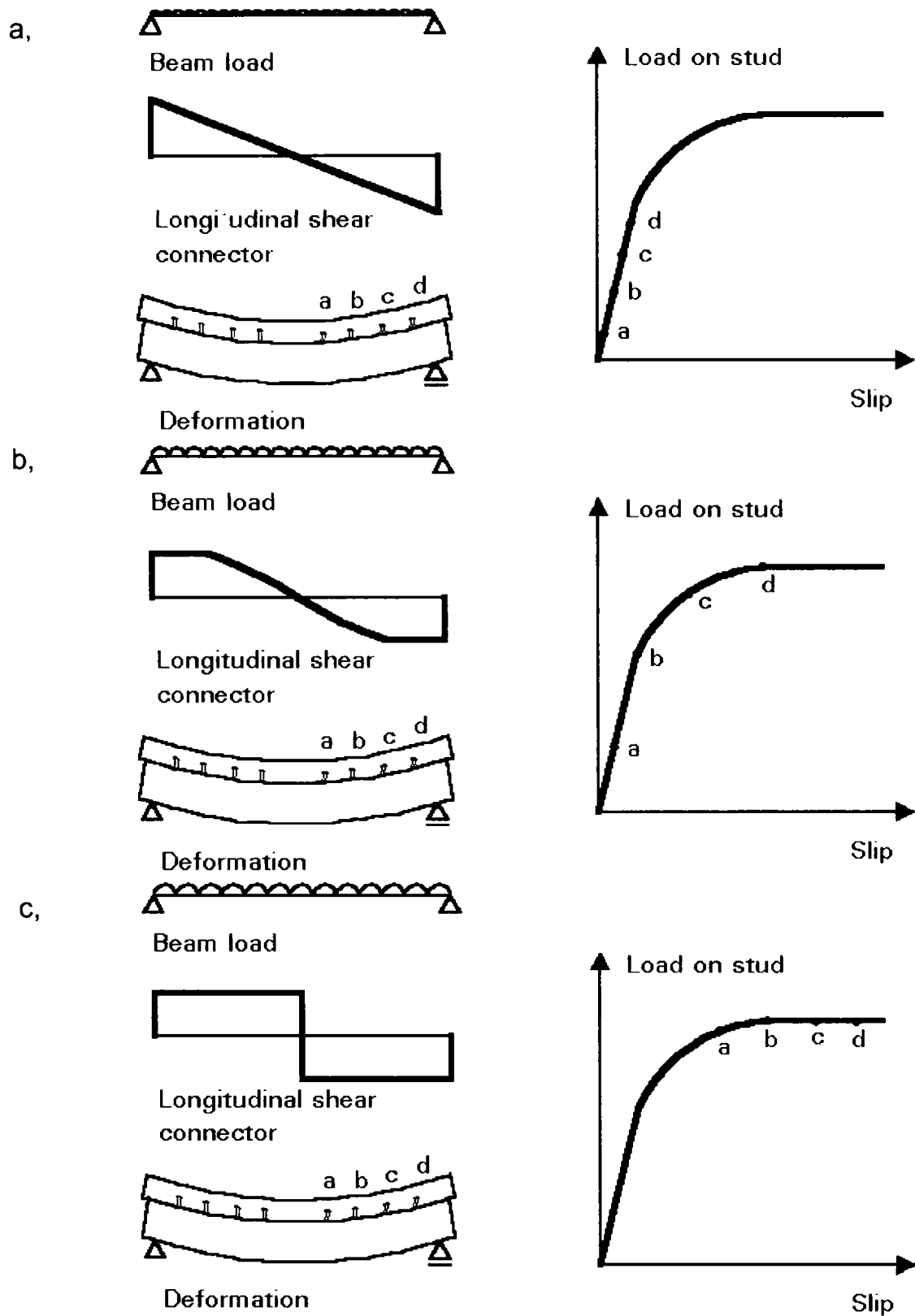


Fig. 2.13. Longitudinal shear connectors

Stage 3b

Concrete is not a plastic material. If strains develop such as to cause overstress it is potentially possible that explosive brittle failure of the slab would occur. This behaviour would be similar to the brittle failure expected in an over-reinforced

concrete beam. The volume of concrete in most practical slabs means that it is unlikely that this situation could ever arise in practice.

With increase in stress within the concrete, induced by increasing strain, the stress block changes from the triangular shape shown in Fig. 2.11 to the shape shown in Fig. 2.12. For design this shape is difficult to represent in mathematical form and approximations are used. For composite beams the most common approximation is the rectangular stress block shown by the dashed line in Fig. 2.12 and in more detail in Fig. 2.8b.

Stage 3c

The remaining components of the composite beam that may fail before the steel yields or the concrete crushes are the connectors. As the load increases the shear strain, and therefore the longitudinal shear force between the concrete slab and steel section, increases in proportion.

Since the longitudinal shear force is directly proportional to the applied vertical shear force, the force on the end connectors is the largest. For low loads the force acting on a connector produces elastic deformations. This the slip between the slab and the steel section will be greatest at the end of the beam. The longitudinal shear and deformation of a typical composite beam, at this stage of loading, are shown in Fig. 2.13a.

If the load is increased the longitudinal shear force increases, and the load on the end stud may well cause plastic deformation. A typical load slip relationship for the connectors is shown in Fig. 2.13. The ductility of the connectors means that the connectors are able to deform plastically whilst maintaining resistance to longitudinal shear force. Fig. 2.13b shows the situation when the two end connectors are deforming plastically.

Increasing applied load will produce increasing longitudinal shear and connector deformation. In consequence, connectors nearer to the beam centreline also begin sequentially to deform plastically. Failure occurs once all of the connectors have

reached their ultimate resistance as shown in Fig. 2.13c. This sequence of shear load and connector straining is shown in an exaggerated manner in Fig. 2.13a, b, and c.

This failure pattern is dependent upon the connectors being able to deform plastically. The end connector in Fig. 2.11 must be able to deform to a considerable extent before the connector close to the beam centreline even reaches its ultimate capacity.

It can be seen that the failure of the composite beam is dictated by the resistance of its three main components. As the elastic interaction of these components is very complex it is normal to design these sections assuming the stress distribution shown in Fig. 2.8b.

Composite beams designed to fail when the steel yields, the concrete just reaches a failing strain and all of the connectors deform plastically would appear to be the ideal situation. There are however several reasons why this situation rarely occurs.

2.2.2.3. Practical load situations

It has been assumed so far that the loading on the beam is uniformly distributed and gives rise to a parabolic bending moment diagram. This is a common situation but it is also equally possible to find situations where concentrated loads act on beams.

In the case of uniform loading the maximum bending moment occurs at mid span. This section is then termed the critical section in bending. The stress block at the critical section is that described in Fig. 2.12. It results in a longitudinal shear distribution to the shear connectors shown in Fig. 2.13c. It can be seen that the longitudinal shear developed at the critical section must be resisted by the connectors between this point and the end of the beam. It can be deduced that, if the critical section is closer to the beam end, as would be the case for a single point load close to the support, the number of connectors between this point and the support needs to increase.

657.143
1914
ANICA
ARA
BIBLIOTECA CENTRALA

In practice the number of connectors between each load point on a beam subject to multiple point loads must be determined. This calculation often gives rise to variable spacing of connectors along the span length.

Point loads may also give rise to high vertical shear force. Although some of the vertical shear may be carried by the slab and beam flanges, it is common practice to ignore that and assume all the vertical shear is carried by the web of the steel section.

For continuous beams, there is a possibility of high shear and bending occurring together. In this case the moment resistance of the section is reduced.

2.2.2.4. Creep and shrinkage

Concrete is subject to two phenomena, which alter the strain and therefore the deflection of the composite beam.

During casting the wet concrete gradually hardens through the process of hydration. This chemical reaction releases heat causing moisture evaporation, which in turn causes the material to shrink. As the slab is connected to the steel section through the shear connectors, the concrete shrinkage forces are transmitted into the steel section. These forces cause the composite beam to deflect. For small spans this deflection can be ignored, but for very large spans it may be significant and must be taken into account.

Under stress, concrete tends to relax, i.e., to deform plastically under load even when that load is not close to the ultimate. This phenomenon is known as creep and is of importance in composite beams. The creep deformation in the concrete gives rise to additional, time dependent, deflection which must be allowed for in the analysis of the beam at the service load stage.

2.2.2.5. Propped and unpropped composite beams

The geometry of most composite beams is often predetermined by the slab size, as previously discussed, and by the capability of the steel section to carry the load of wet concrete during construction. This construction limitation gives rise to two composite beam types, the propped and the unpropped composite beam.

Consider first the case of the propped beam shown in Fig. 2.14. During construction the steel section is supported on temporary props. It does not have to resist significant bending moment and is therefore unstressed and does not deflect. Once the concrete hardens the props are removed. Each of the component parts of the beam then takes load from the dead weight of the materials. However, at this stage, the beam is acting as a composite element and its stiffness and resistance are very much higher than that of the steel section alone. The deformation due to dead loads is, therefore, small. Any further live loading causes the beam to deflect. The total stresses present in the beam can be found by summing the stresses due to dead and live loads.

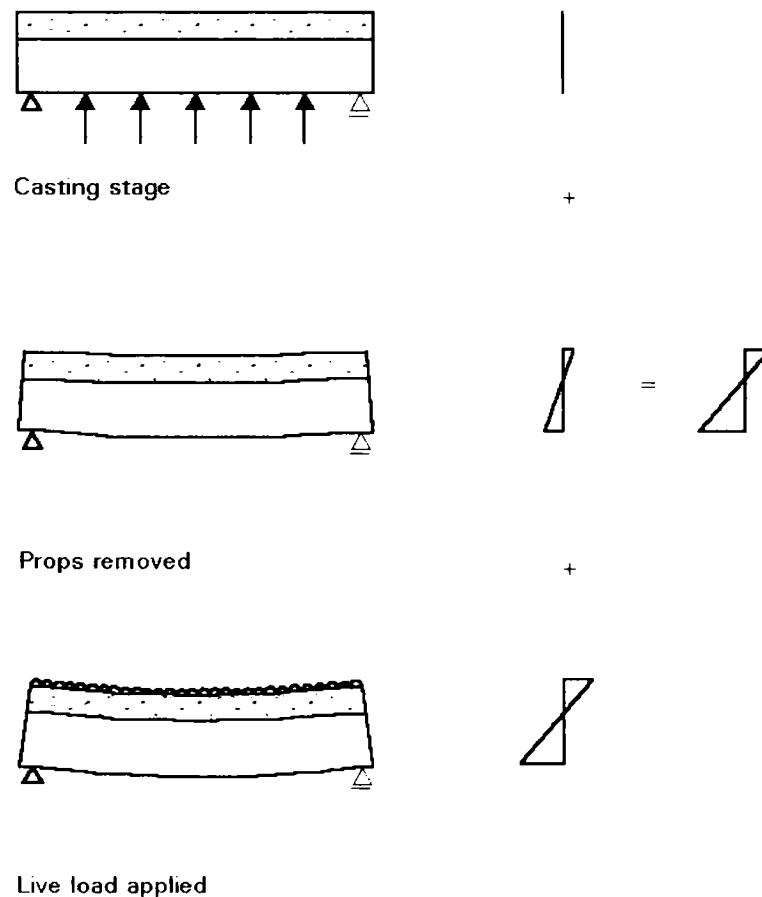


Fig. 2.14. Propped composite beams

Consider now the unpropped beam shown in Fig. 2.15. During construction the steel section is loaded with the dead weight of wet concrete. The steel section is stressed and deforms. The concrete and the connectors remain largely unstressed, apart from the shrinkage stresses developed within the hardened concrete. It can be seen, in Fig. 2.15, that the wet concrete ponds, i.e. the top surface of the concrete remains level and the bottom surface deforms to the deflected shape of the steel section. The dead load due to the weight of wet concrete is a substantial proportion of the total load and the stresses developed in the section are often high.

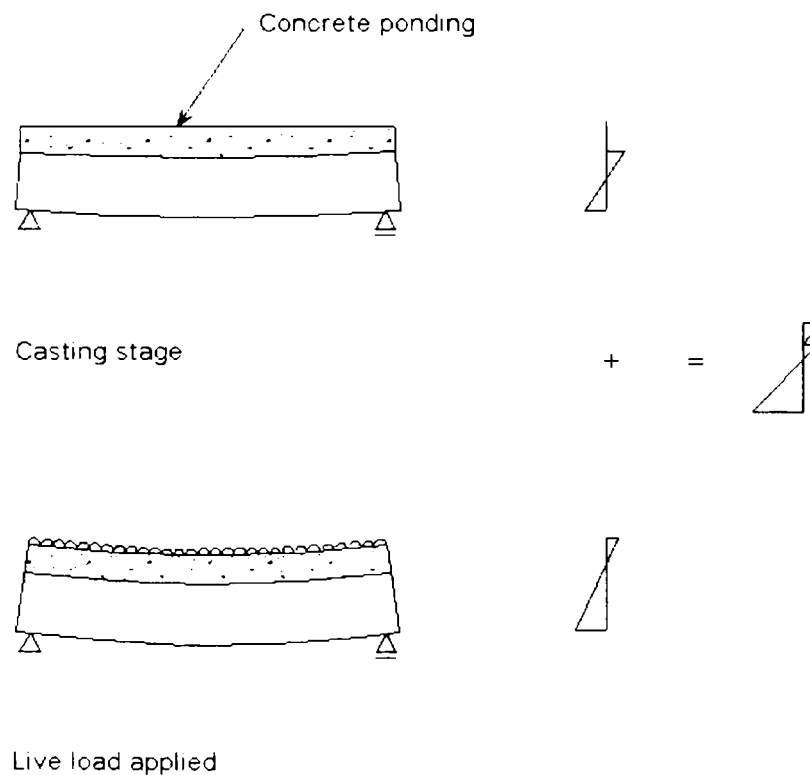


Fig. 2.15. Unpropped composite beams

Additional live loads are carried by the composite section, which has almost the same stiffness as that of the propped beam. The stresses present in the unpropped section can therefore be obtained by summing the wet concrete stresses and the composite stresses. This calculation leads to a different stress distribution in the section to that present in the propped composite beam. However, the yield stresses developed in the steel and concrete are the same in both cases and both unpropped and propped composite beams carry the same ultimate load.

The steel section of an unpropped composite beam often needs to be substantial so that the weight of wet concrete can be carried. The section is, in fact, often substantially larger than would be required if the beam had been propped.

The load deflection response of a steel section alone and of a composite beam, both propped and unpropped, is shown in Fig. 2.16. The strains present and stresses developed are shown in sequence with the section upon, which they act. In the unpropped case the steel section alone takes the load of wet concrete and the strains due to this wet concrete load are added to the strains caused by the subsequently applied service loads. The resulting stresses are shown in the stress block. Whilst the overall deflection of the unpropped beam may be larger than the propped beam at the working load stage, that is often not important as the deflection occurring during construction, which can be hidden by the finishes.

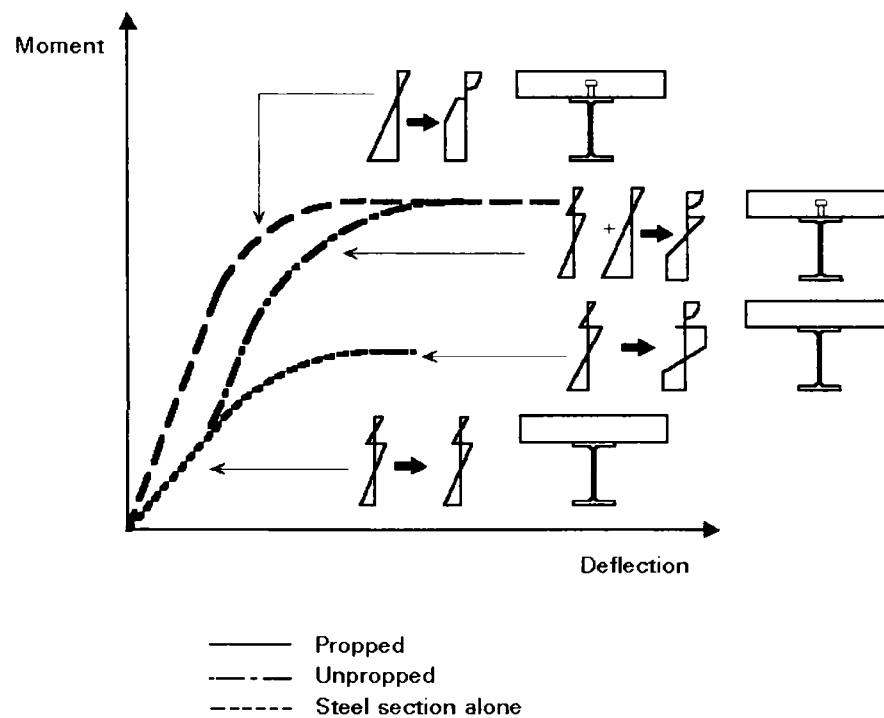


Fig. 2.16. Load deflection response for a steel section alone and a composite beam, propped and unpropped

Despite the drawbacks discussed above, unpropped construction is often preferred for the following reasons:

- The extra cost involved in providing props.
- The restricted working space available in propped areas.
- The adverse effect on speed of construction.

2.2.2. Partial connection

In unpropped construction the size of the steel section is often determined by the weight of wet concrete, and the size of the slab is determined independently by its transverse span. If sufficient connectors are provided to transfer the maximum longitudinal force in the steel section or concrete slab, the resistance of the unpropped composite beam becomes very high. Indeed composite beams so formed are often capable of carrying several times the required live load. To avoid providing such excess resistance the partially connected composite member is used.

It has been assumed so far that the connection will carry all the shear force in the beam up to the time when the steel section has fully yielded. However, because the resistance of the unpropped beam is so high, it is often possible to reduce the number of connectors. This reduction results in a beam where the failure mode would be by connector failure prior to the steel having fully yielded or the concrete having reached its crushing strength. (STARK, HOVE 1990)

Such beams require fewer connectors thereby reducing the overall construction cost. They are, however, less stiff since fewer connectors allow more slip to occur between the slab and steel section.

2.2.3. Continuous composite beams

Although simply supported beam design is most common there may be situations where use of continuous beams is appropriate.

The mid span regions of continuous composite beams behave in the same way as the simple span composite beam. However, the support regions display a considerably different behaviour. This behaviour is shown diagrammatically in Fig. 2.17.

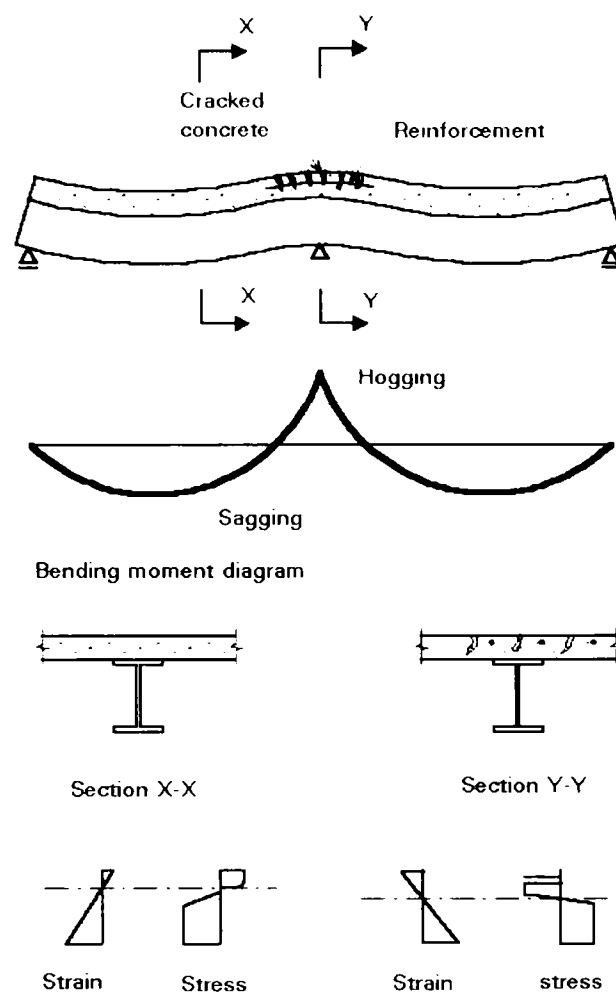


Fig. 2.17. Continuous composite beams

The concrete in the mid span region is generally in compression and the steel in tension. Over the support this distribution reverses as the moment is now hogging. The concrete cannot carry significant tensile strains and therefore cracks, leaving only the embedded reinforcement as effective in resisting moment.

The steel section at the support then has to carry compressive strains throughout a considerable proportion of its depth. Slender sections are prone to local buckling in this region and any intervening column section may need to be strengthened to absorb the compression across its web.

As well as local buckling it is possible that lateral-torsional buckling of the beam may occur in these regions.

2.2.4. Design aspects of the concrete flange in compression

2.2.4.1. Effective width

A typical form of composite construction consists of a slab connected to a series of parallel steel members.

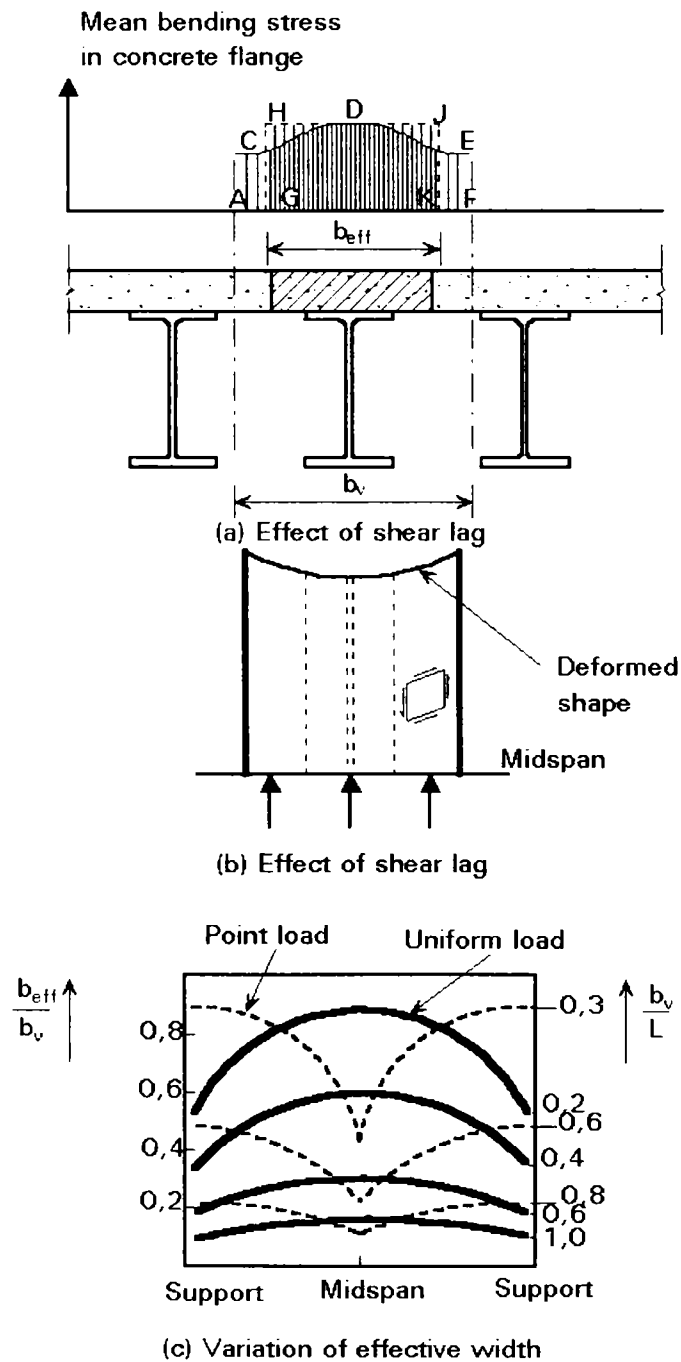


Fig. 2.18. Concrete flange

The construction is essentially a series of interconnected T-beams with wide, thin flanges, as shown in Fig. 2.18a. In such a system "shear lag" may cause the flange

width to be not fully effective in resisting compression (DOWLING, et. al, (1988)). This phenomenon can be explained by reference to a simply supported member, part of whose length is shown on plan in Fig. 2.18b.

The maximum axial force in the slab is at midspan, while the force at the ends is zero. The change in longitudinal force is associated with shear in the plane of the slab. The resulting deformation, shown in Fig. 2.18b is inconsistent with simple bending theory, in which initially plane sections are assumed to remain plane after bending. The edge regions of the slab are effectively less stiff, and a non-uniform distribution of longitudinal bending stress is obtained across the section. Simple theory gives an effective value for width, b_{eff} , such that the area GHJKG equals the area ACDEFA.

The ratio b_{eff}/b_v depends not only on the relative dimensions of the system, but also on the type of loading, the support conditions and the cross-section considered; Fig. 2.18c shows the effect of the ratio of the beam spacing to span length, b_v/L , and the type of loading, on a simply supported span.

In most codes of practice very simple formulae are given for the calculation of effective widths, although this may lead to some loss of economy. According to EUROCODE 4, for simply supported beams, the effective width on each side of the steel web should be taken as $I_0/8$, but not greater than half the distance to the next adjacent web, nor greater than the projection of the cantilever slab for edge beams.

The length I_0 is the approximate distance between points of zero bending moment. It is equal to the span for simply supported beams. A constant effective width may be assumed over the whole of each span. This value may be taken as the midspan value for a beam.

2.2.4.2. Maximum longitudinal shear in the concrete slab

In the concrete slab, a complex (three-dimensional) force distribution occurs in the region of the connector. The reason for this behaviour is that bending moments and vertical shear forces act parallel as well as perpendicular to the beam. It is difficult to

find a physical design model for this complex stress distribution, and therefore, most design rules are empirical. Two design criteria can be identified:

- Longitudinal shear in the concrete slab, along the shear planes indicated in Fig. 2.19.
- Splitting of the concrete.

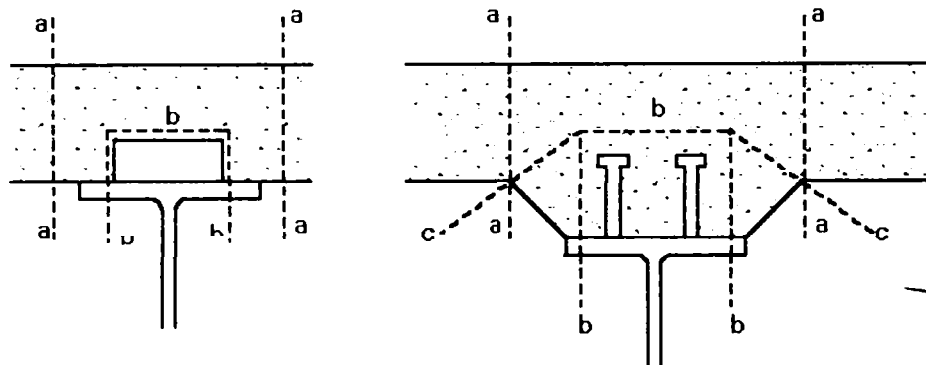


Fig. 2.19. Planes of shear failure

It is possible to avoid these failure modes by providing sufficient transverse reinforcement and choosing the correct distance between the connectors. In some cases, satisfying these criteria may lead to an increase in concrete slab thickness or resistance.

If the connectors are welded or shot fired through a continuous profiled steel sheet of a composite slab, the cross-section of the steel sheet can also be considered as transverse reinforcement.

2.2.5. Types and behaviour of shear connection

2.2.5.1 The forces applied to connectors

It has been assumed that the concrete and steel were fully connected together (full connection). If there is no connection then the concrete slab and steel section slide relative to one another and the bending stresses in the section are as shown in Fig 2.20.

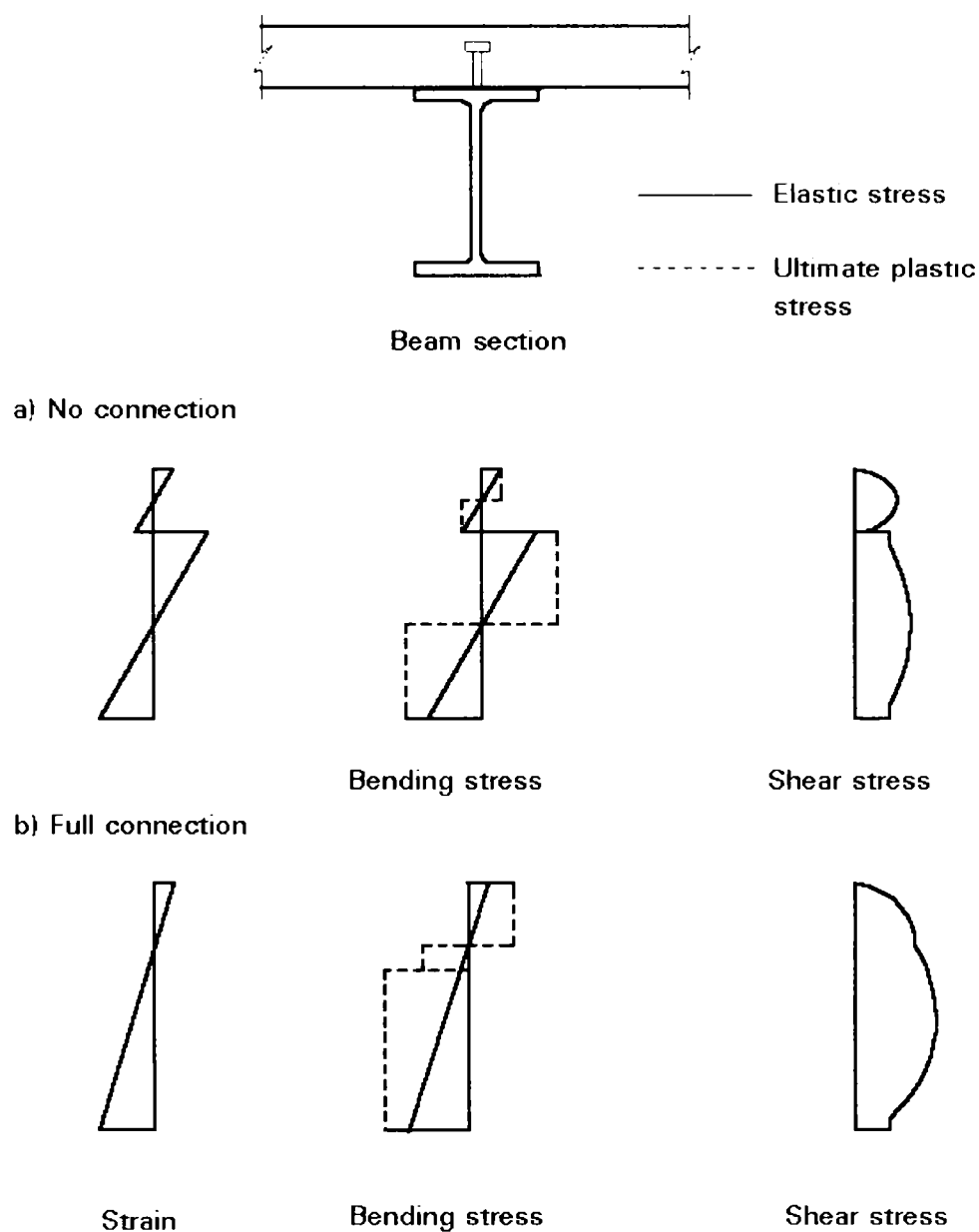


Fig. 2.20. Strain, bending and shear stresses for no connection and full connection

Clearly, if longitudinal shear resistance is provided by some form of connection, so that the stresses at the interface of the two materials are coincident, then the beam acts as a fully composite section. If it is assumed that the fully connected composite beam acts in an elastic way then the shear flow (shear force per unit length) between the concrete slab and the steel section may be calculated.

Fig. 2.20 also shows the elastic shear stress developed in the section for the conditions of both full and zero connection.

It can be seen, that the longitudinal shear forces, that must be carried by the connection, will vary depending upon the vertical shear present. Fig. 2.21a shows the

distribution of longitudinal shear, along the interface between the steel section and slab, for a beam that has a rigid full connection. It must be remembered, however, that this applies only when the beam is assumed to be behaving in an elastic manner. As the ultimate moment of resistance is reached, the steel section or concrete slab will yield or crush and a plastic hinge will form at the critical section. The bending stresses in the beam are as shown in the dashed lines in Fig. 2.20. the distribution of longitudinal shear in the beam also changes and the connectors close to the hinge are subject to higher loads. The dashed line, in Fig. 2.21a, shows the plastic distribution of shear force along a uniformly loaded beam.

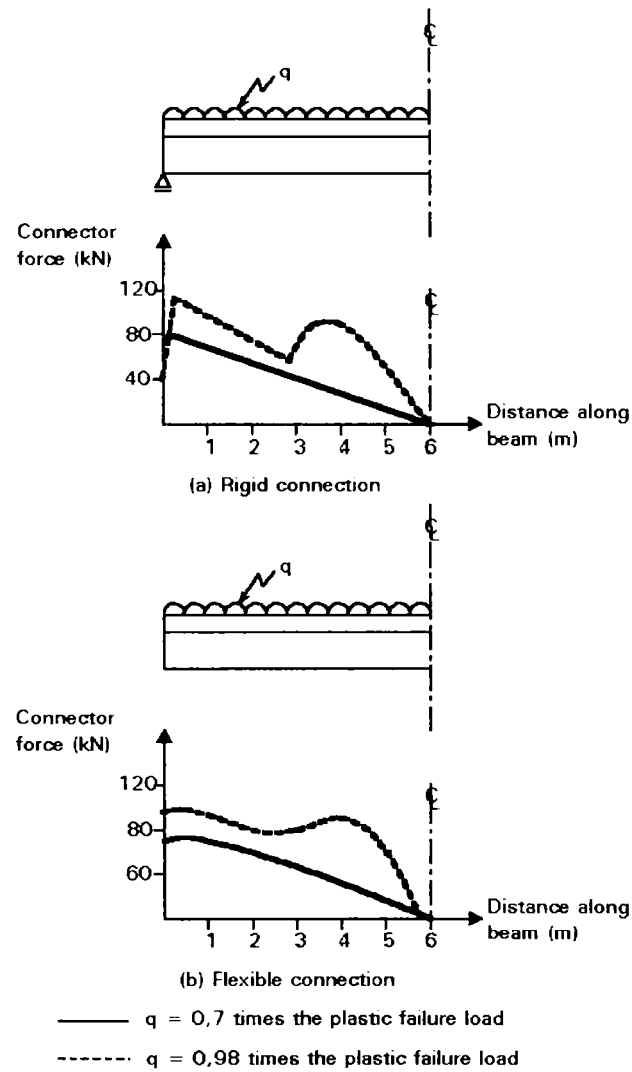


Fig. 2.21. Connector loads for rigid and flexible connectors

In practice, connectors are never fully rigid, and there is always some slip between the slab and the steel section. The flexibility of the connectors allows more ductility and a variation in the distribution of longitudinal shear between slab and steel section. The longitudinal shear force present in a composite beam with flexible connection it is shown in Fig. 2.21b (YAM, CHAPMAN, 1968).

The major force resisted by the concrete is one of bearing against the leading edge of the connector. It has already been mentioned that the concrete in this region is likely to crush allowing bending deformation to occur in the connector. The bearing resistance of the concrete in this region is dependent upon its volume as well as strength and stiffness. In fact, where there is sufficient concrete around the connector, the bearing stress may reach several times the unconfined crushing strength of the concrete (ARIBERT, ABDEL, 1985, ARIBERT, 1990).

There is also likely to be direct tension in the connector. The different bending stiffnesses of the slab and the steel section, coupled with the deformed shape of the connectors, gives rise to the tendency for the slab to separate from the steel section. It is, therefore, usual for connectors to be designed to resist this tensile force.

In most composite beams the connectors are spaced along the steel section and, therefore, provide a resistance to longitudinal shear only locally to the top flange. The longitudinal shear force must, therefore, be transferred from the narrow steel section into the much wider slab. This transfer is normally achieved using bar reinforcement that runs transverse to the beam line. These bars are normally placed below the head of the stud and extend into the slab.

2.2.5.2 Basic forms of connection

Early forms of shear connector were shop welded, using conventional arc welding. The most common types are the hoop connector and T connector which serve to show the complexity of the forming and welding operation necessary. The popularity of composite beam construction has led manufacturers to develop very simple forms of shear connector (ANDRA, 1990).

Despite the plethora of connection types available, the shear stud connector has now become the primary method of connection for composite beams. The stud can be forge welded to the steel section in one operation, using micro-chip controlled welding equipment. These machines, operating at current settings of up to 2000 Amps allow operators to weld approximately 1000 studs per day. The most advanced

machines allow studs to be welded through galvanised steel sheeting. This ability has enabled the economic advantages of composite floor decks to be fully exploited. Fig. 2.22 shows a typical shear stud before and after welding and the sequence of weld current required (ANSI/AWS,1985).

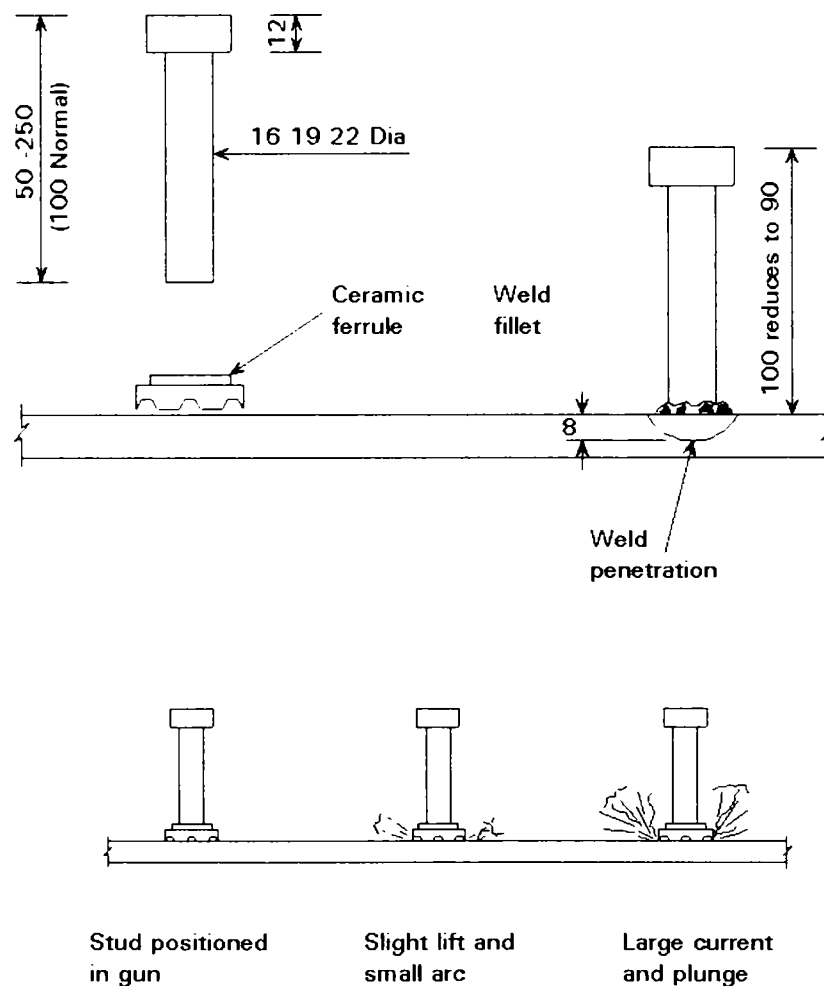


Fig. 2.22. Stud connector welding

Such complex welding technology does have disadvantages when used on construction sites. The weld relies on the two surfaces being clean, free of mill-scale and, above all, dry. These conditions are often difficult to achieve especially when the studs are welded through a galvanised steel sheet; in this case, the weld current is maintained for a sufficient period to burn away the zinc galvanising, which would otherwise cause imperfect welds. Welding 22mm, rather than the more common 19mm studs, through deck also demands care. An alternative to through deck welding is to punch holes in the steel deck and then weld the studs directly to the steel section. A more reliable weld is obtained in this way but the construction process is made more complex.

The designer may also obtain stud resistance values from tests. Full beam tests are expensive and a model test known as the "push-out" test is often used. This test is shown in Fig. 2.23, together with a typical graphs of load against slip from the test. The resistance is, of course, dependent upon the concrete cube strength and is also reduced if the concrete is made from lightweight aggregate.

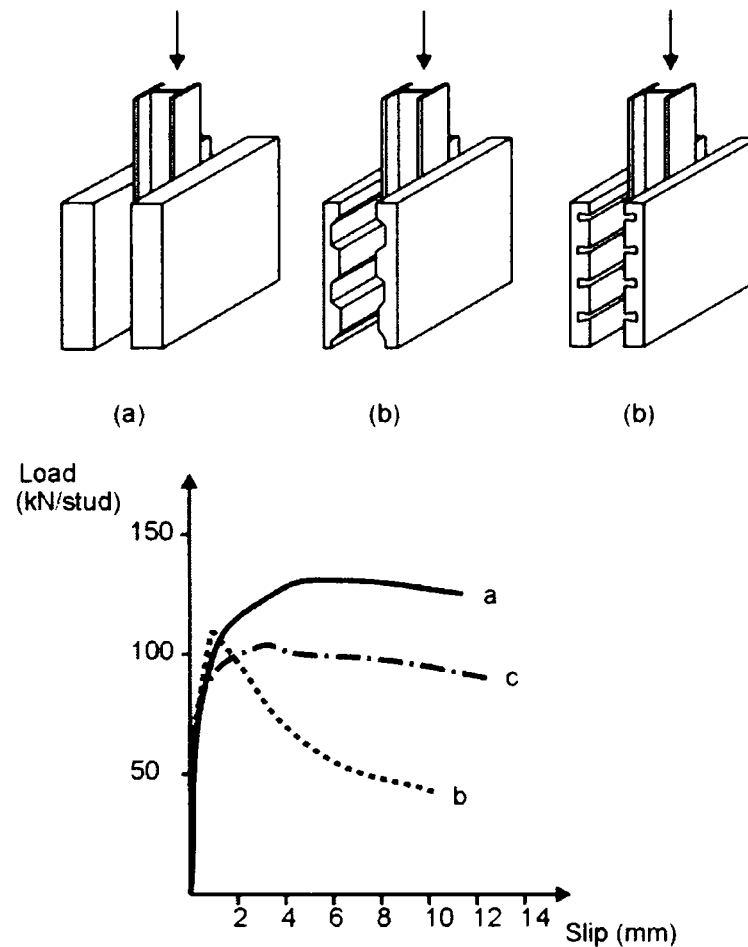


Fig. 2.23. Push-out test and load slip curves

Shear studs carry very high loads and are normally made from drawn steel rod. Most codes quote steel properties for stud shear connectors; in addition to a high yield value the studs must be ductile and a minimum elongation is often specified. The necessity for ductility has already been explained (DOWLING et al, 1988).

2.3. Aspects of the structural design and details

2.3.1. Introduction

In recent years the development of network of motorways and highways of Hungary is flourishing. There are several construction sites throughout the country (KOVÁCS, 2002, IVÁNYI, IVÁNYI Jr, 2005, IVÁNYI Jr. 2004, IVÁNYI Jr. 2005). This section introduces some bridges connected with these road constructions. Some of these bridges have already been finished and other bridges exist only in the planning phase. The structures are composite bridges. This structural system of the bridges is partly dictated by the requirement of the commission and partly by economic reasons as these composite bridges provide the most competitive solution for short and middle span. It must be noted that during the design of the bridges discussed in this section the ÚT 2-3.401, ÚT 2-3.413, ÚT 2-3.414. Standard was used and not Eurocode.

2.3.2. The bridge at Oszlár over the river Tisza

The highway road (M3) towards Ukraina crosses the river Tisza at Oszlár. The width of the road is 26.50m which requires two bridges placed next to each other. One bridge has three parts. The superstructure over the flood area is precasted, prestressed reinforced concrete beam. The arrangement of the spans is symmetrical on both banks and the distribution of the spans is: 24.00+24.20+23.95m.

The middle section of the bridge over the river bed has also three spans: 72.00+112.00+72.00m. The structural system of the bridge is composite with steel haunched main girders. The width of the deck is $12.35+0.87+12.35=25.57$ m, which supports in both directions a two lane road with a safety lane. The distance between the main girders is 6400mm. The height of the web plate is 2565mm at the end cross girders, 5600mm at the middle supports and 3000mm along the span. The thickness of the web plate is 16mm which increases to 20mm around the middle supports. The width of the upper flange is 800mm and the thickness varies between 30-100mm. However the width of the bottom flange is 1200mm and the width changes between 30-150mm.

The web plate is stiffened by closed-section trapezoidal stiffeners in the longitudinal direction, while there are cross-girders at every 4000mm. The concrete deck slab has varying depth and it is connected to the main girders by shear connectors. These features are shown in Fig. 2.24, Fig. 2.25.

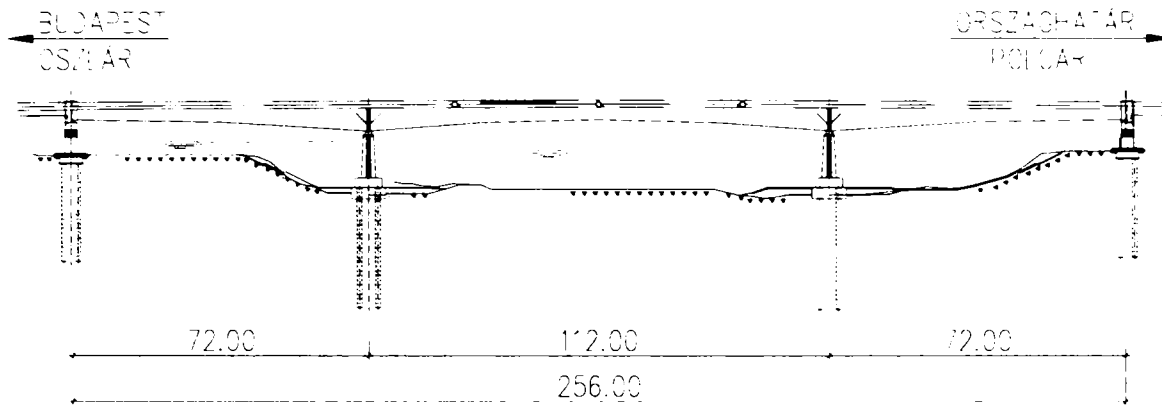


Fig. 2.24. The elevation drawing of the main bridge at Oszlár over the river Tisza

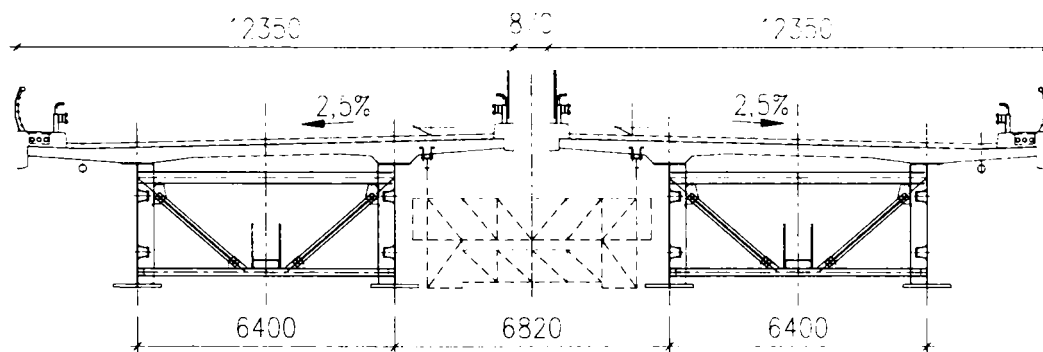


Fig. 2.25. The cross section drawing of the main bridge over the river Tisza

The fabricated units of the main girder has been assembled in the factory to try their fitting, then they have been transported to the on-site workshop by trucks. The pieces have been reassembled and painted on site. The finished superstructure has been lifted to its final position by floating barges. The self weight of one bridge is approximately 1050 tons. The most important aspect of this bridge design is that in Hungary probably this is the first bridge structure where on-site welding was used for 100-150mm flanges. These features are shown in Fig. 2.26-2.44. Figure 2.30-2.33 show the stiffeners of the plates and show the economic (E) structural detail for the longitudinal and transversal stiffeners.

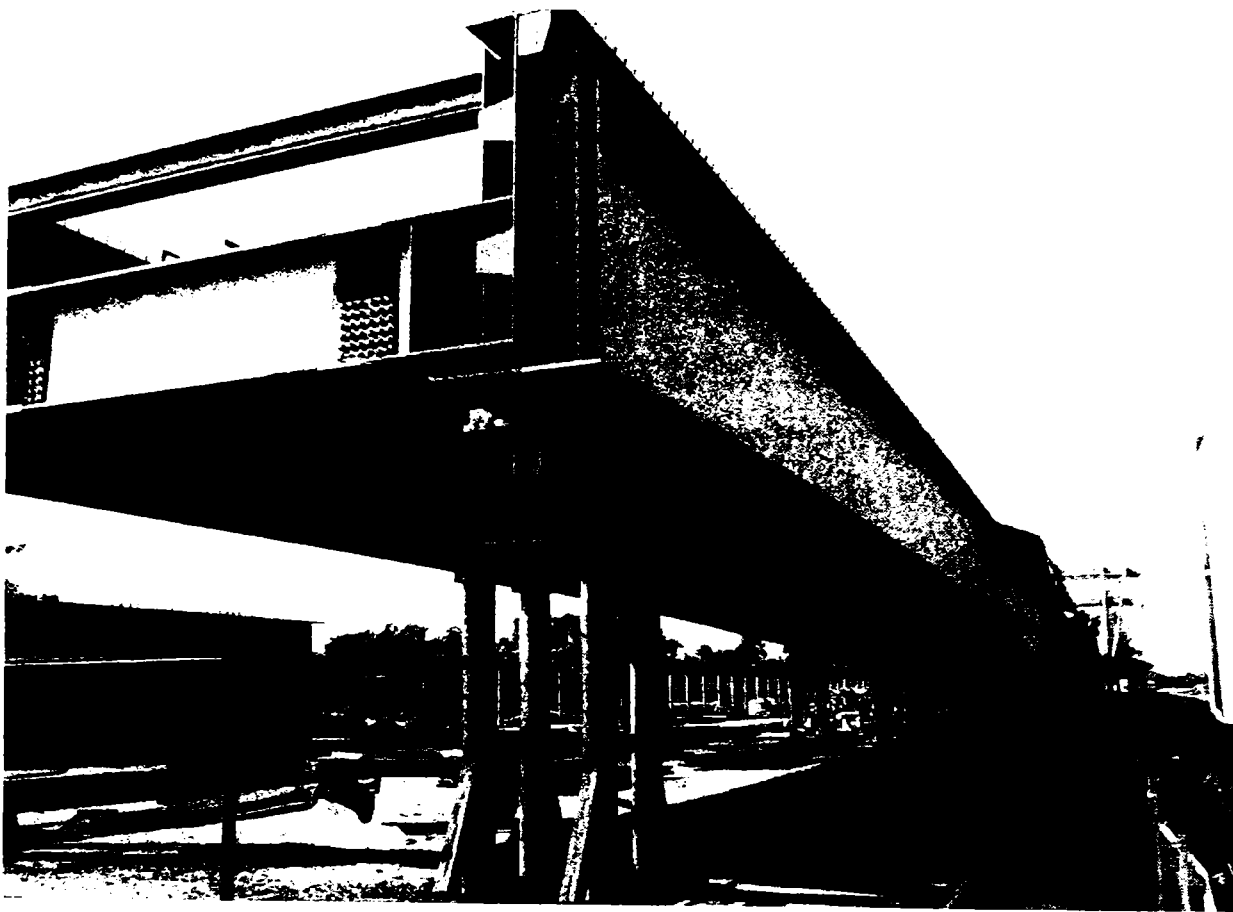


Fig. 2.26. Main girder

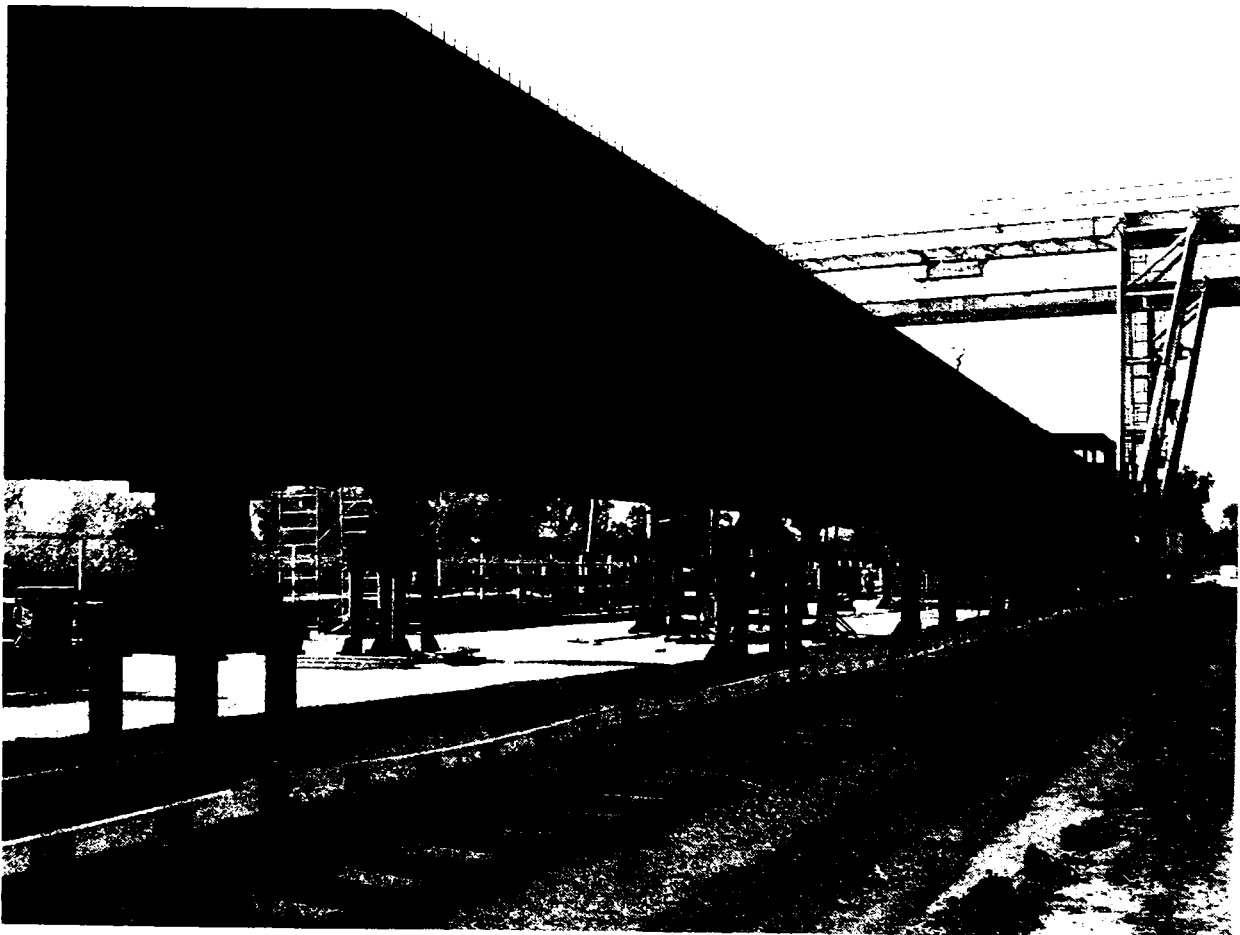


Fig. 2.27. Middle of the main girder

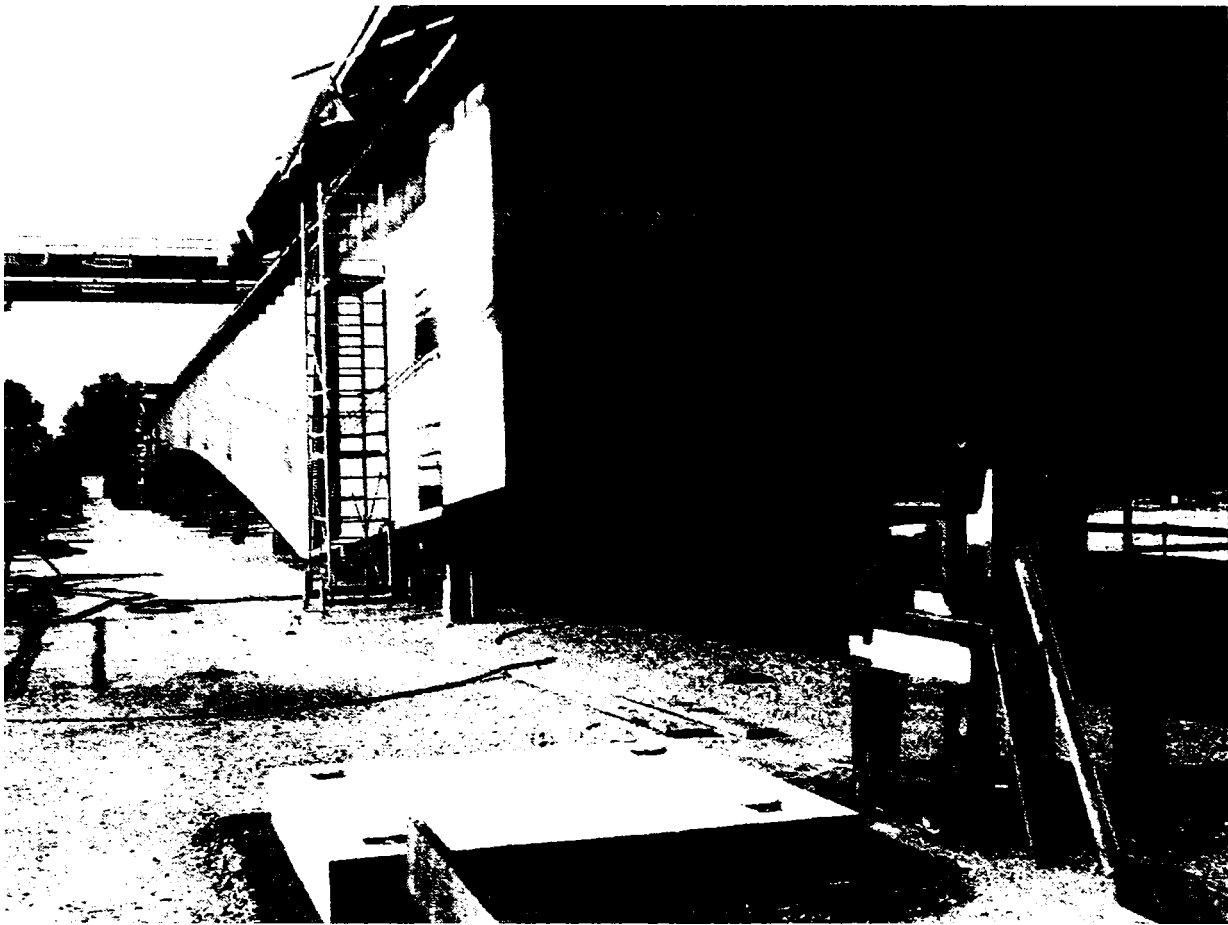


Fig. 2.28. Main girder around the support



Fig. 2.29. Welding of the bottom flange



Fig. 2.30. Transversal stiffeners



Fig. 2.31. Stiffeners from inside

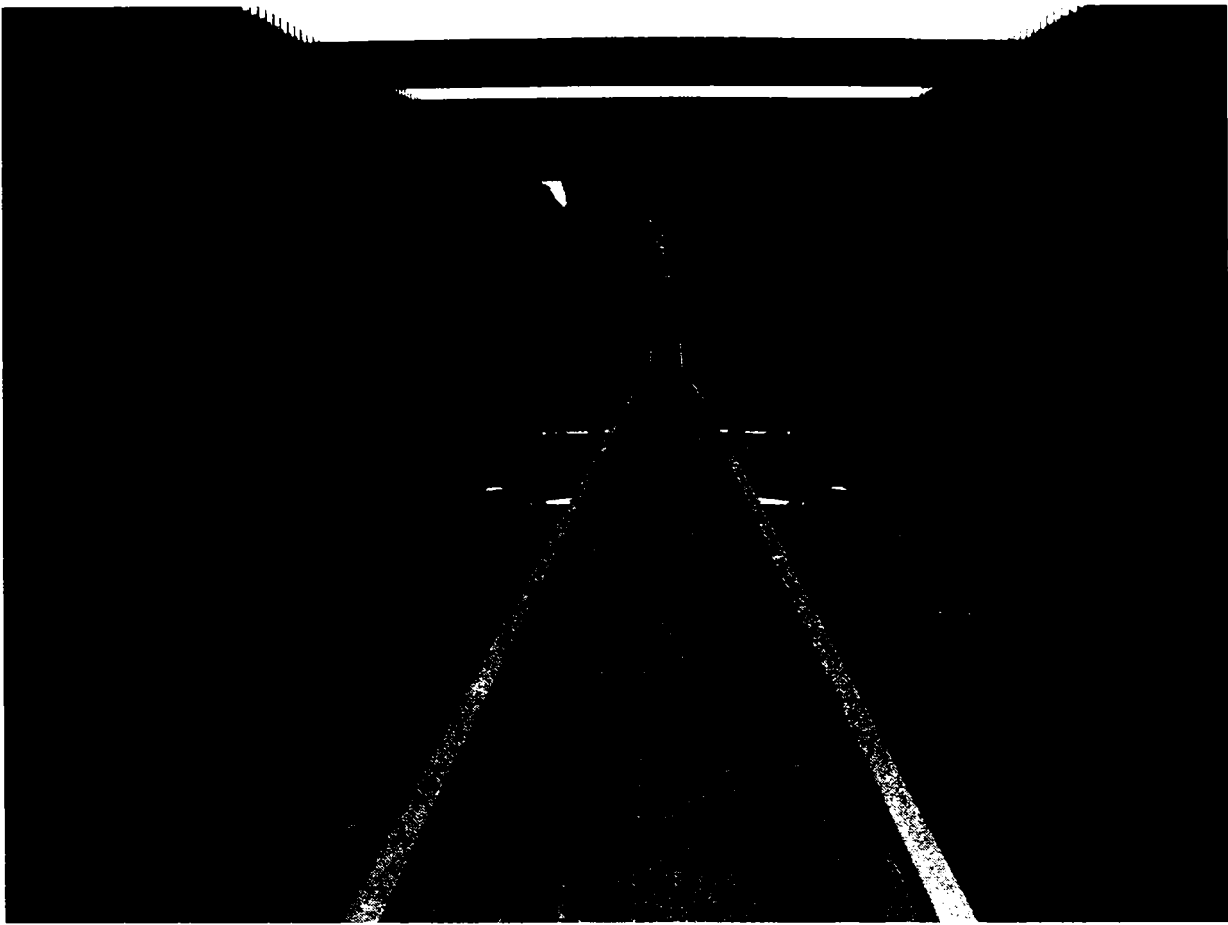


Fig. 2.32. Support cross girder



Fig. 2.33. Constructed bridge on site

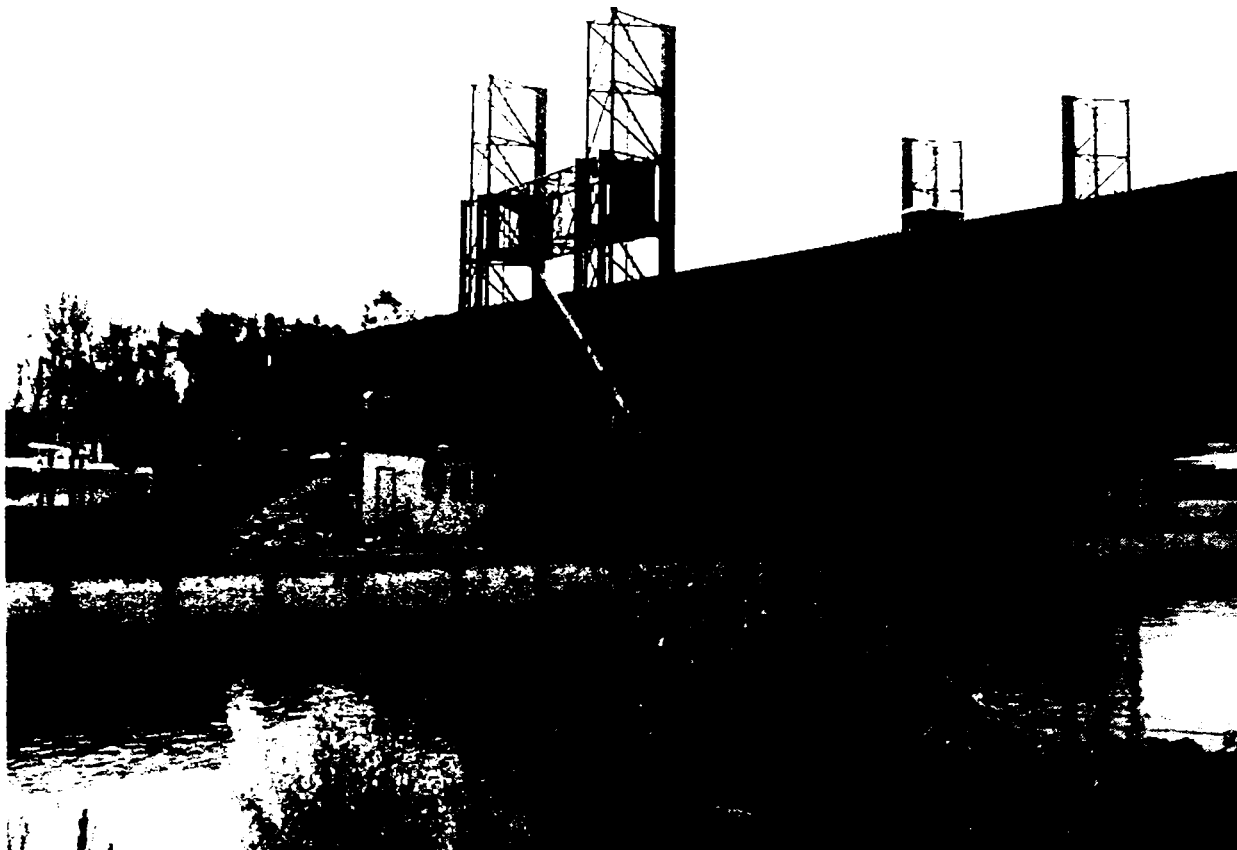


Fig. 2.34. Part of the bridge on a barrage



Fig. 2.35. Putting the bridge in place

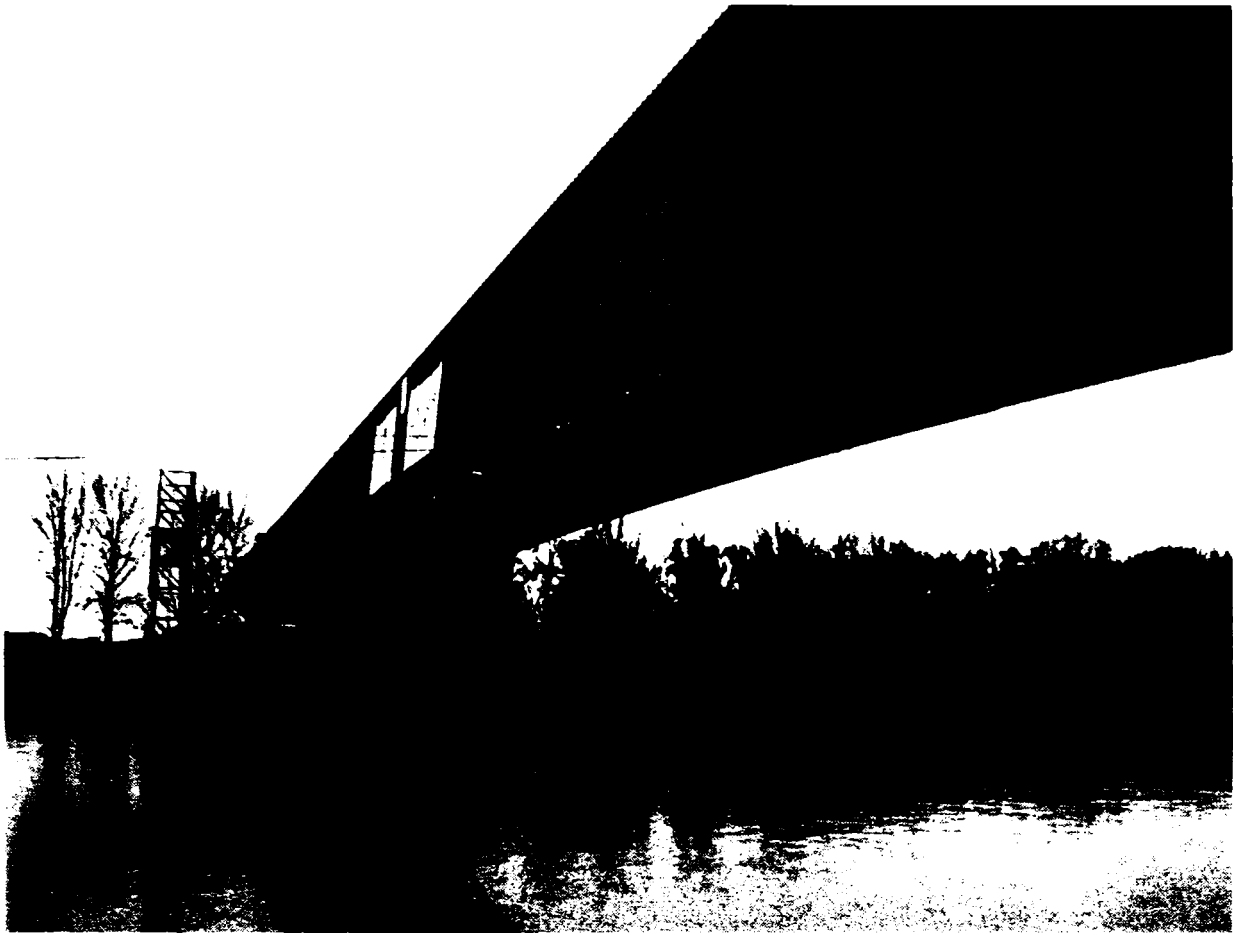


Fig. 2.36. Positioning the bridge



Fig. 2.37. Next stage in positioning



Fig. 2.38. Same stage in positioning



Fig. 2.39. Lifting the bridge

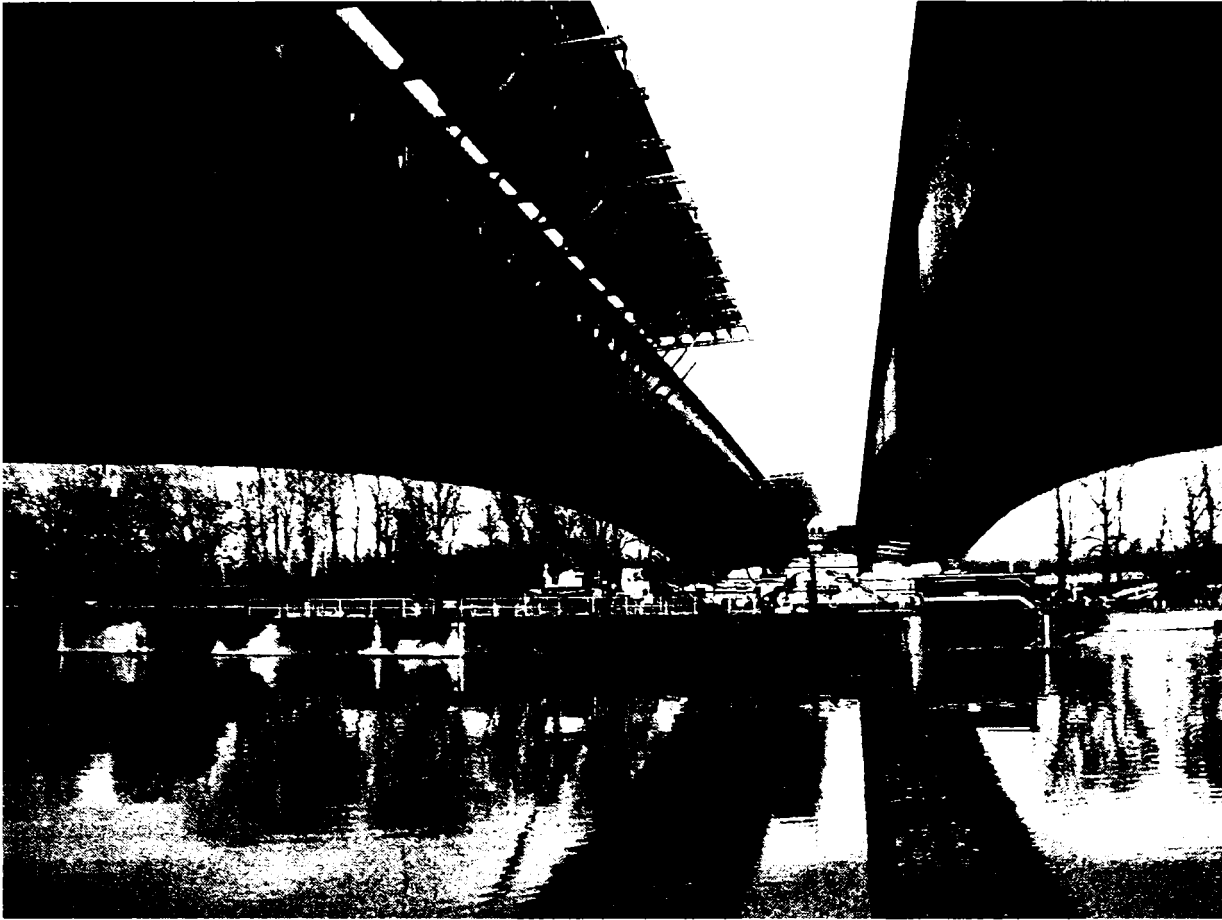


Fig. 2.40. Building the framework for the concrete deck

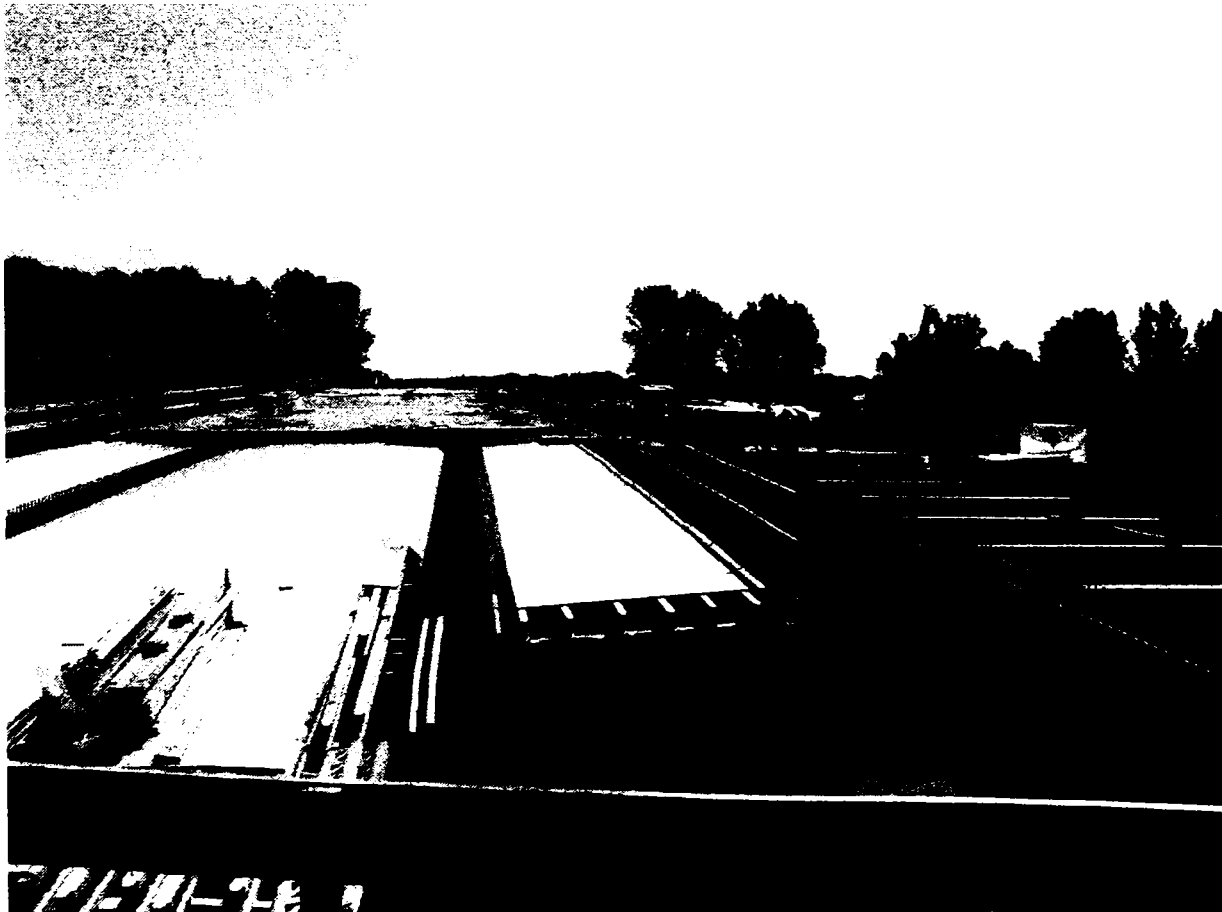


Fig. 2.41. First stage of the concrete slab



Fig. 2.42. Creating the curbs

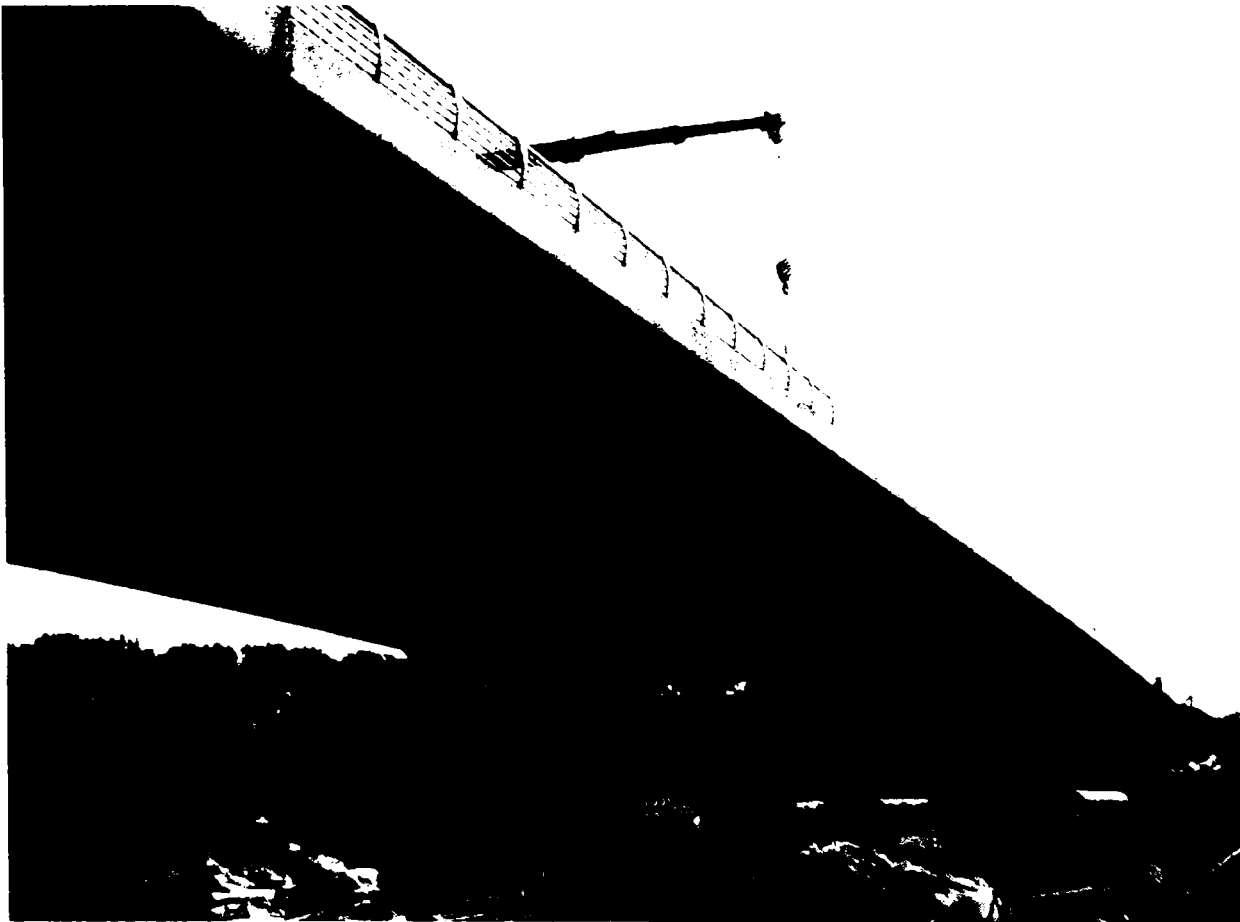


Fig. 2.43. Placing the fences



Fig. 2.44. The finished bridge

2.3.3. The bridge at Szekszárd over the Danube

In the southern part of Hungary the connection between the east and the west part of the country is partly ensured by the new M9 road which can be developed into a highway. The road has a single lane in both directions and its width is 12.00m. A part of the development project is the bridge at Szekszárd over the Danube. The total length of the bridge is 916m which is divided into two bridges over the floodplain (196.5m) and a bridge over the river bed (520m).

The structure of the bridge over the river bed is orthotropic box girders with inclined webs. The two bridges over the floodplain follows the structure of the bridge over the river bed and they are composite box girders (SZATMÁRI, FARKAS, 2003). The distance between the supports for the floodplain bridges is three times 65.50m. The width of the bridge is 14.00m which has two, 3.75m wide lanes with safety lanes. On one side there is sidewalk and a bicycle road. This feature is shown in Fig. 2.45.

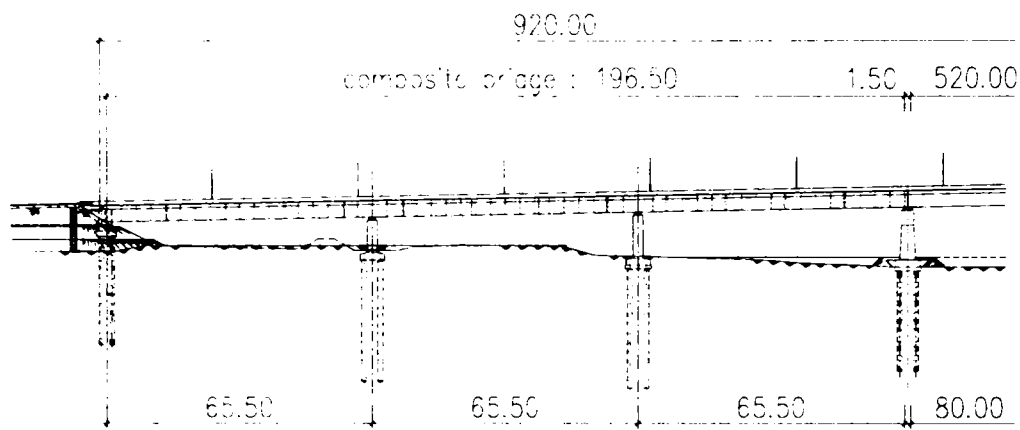


Fig.2.45. The elevation drawing of the floodplain bridge at Szekszárd over the Danube

The box girder has inclined webs which are 5500mm apart at the bottom plate while they are 7500mm apart at the top plate. The width of the web is 12mm which increases to 16 and 20mm at the supports. The width of the bottom plate changes between 12 and 30mm. The web and bottom plate is stiffened by closed section trapezoidal stiffeners and there are cross girders at every 3640mm. This feature is shown in Fig. 2.46.

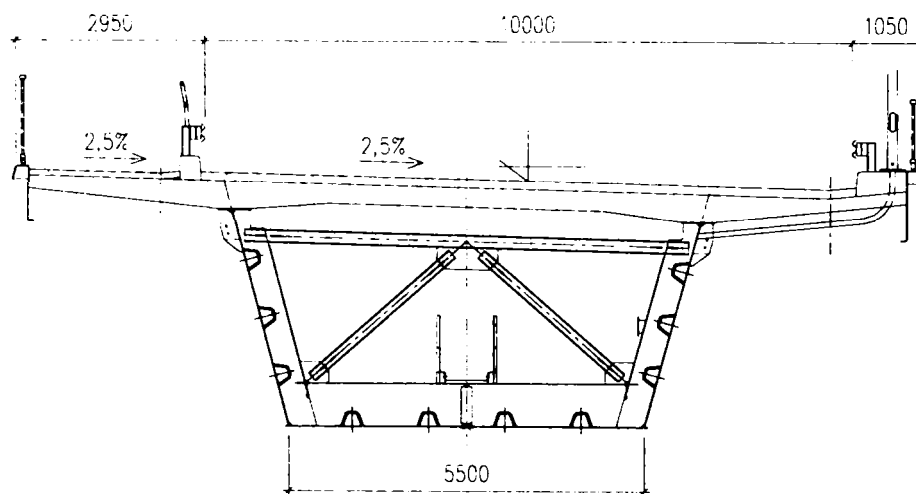


Fig. 2.46. The cross section of the floodplain bridge at Szekszárd over the Danube

The concrete deck slab has varying depth and it is connected to the box girders by shear connectors.

The prefabricated units of the structure is assembled on site on temporary supports, then the monolithic concrete slab is casted. The important feature of the bridge is that the stiffeners of the web and the bottom plates are not connected to the cross girders

as it is expected in the classical bridge design. These features are shown in Fig. 2.47- 2.57. The correctness of this arrangement was verified on the structure by experiments.



Fig. 2.47. First stages in the construction of the box girder

Fig. 2.50 and 2.51 show the structural details (connection type E) of the longitudinal and transversal stiffeners on the web and on the bottom flange.

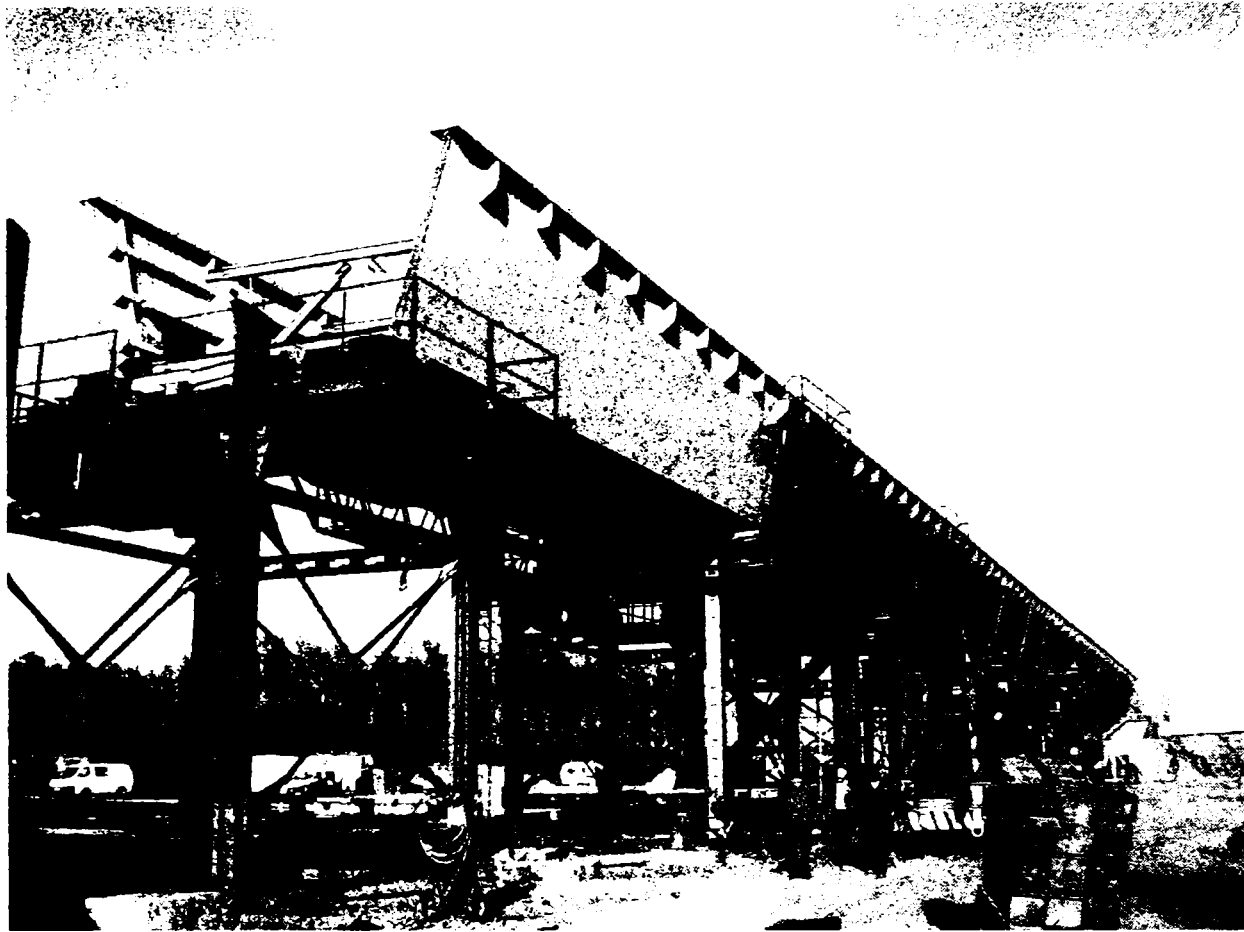


Fig. 2.48. Construction of the box girder



Fig. 2.49. Finished section of the box girder



Fig. 2.50. Inside view of the box girder



Fig. 2.51. Stiffeners of the box girder



Fig. 2.52. Framework for the concrete deck



Fig. 2.53. View of the propped box girder

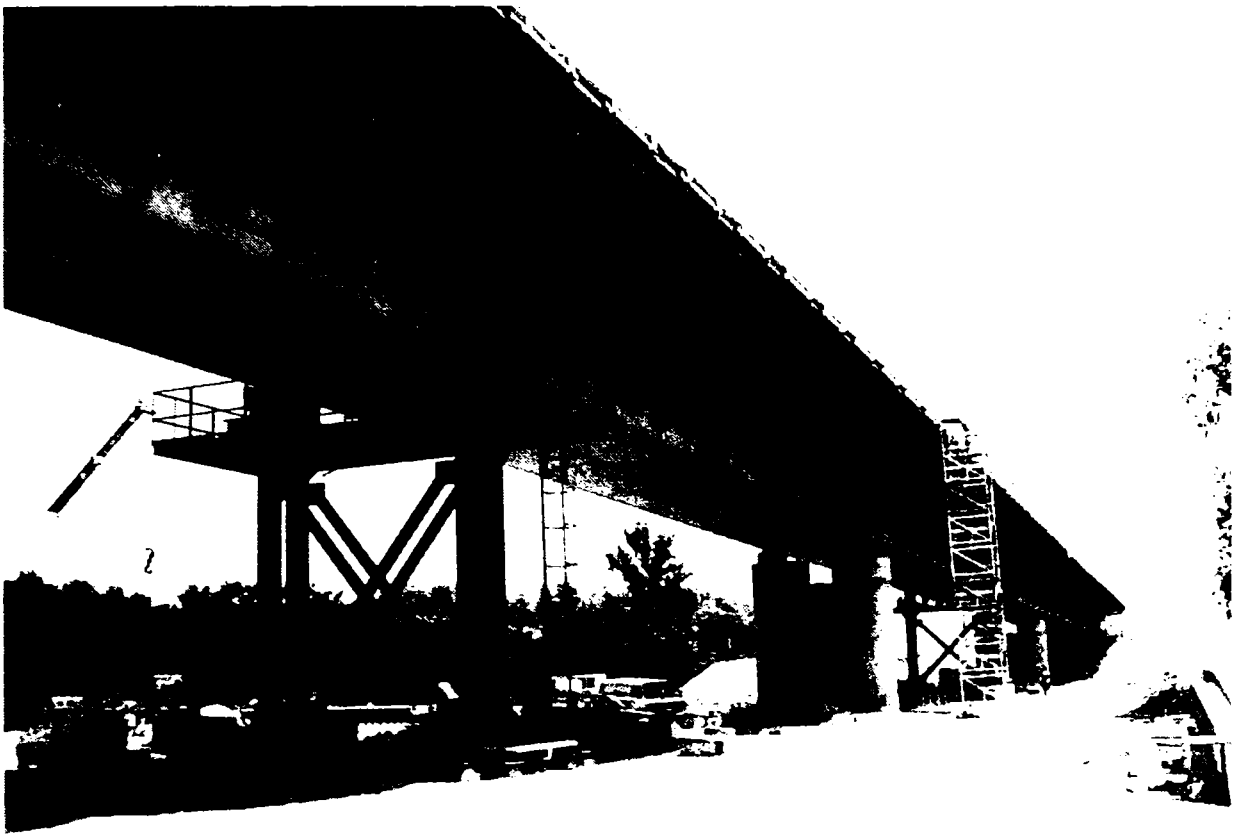


Fig. 2.54. Before pouring the concrete



Fig. 2.55. Finished bridge



Fig. 2.56. View of the full bridge



Fig. 2.57. Another view of the full bridge

2.3.4. The bridge over the Eastern Main Chanel

The M35 road towards Debrecen, which is a part of the M3 highway, joins the eastern regions to the heart of the country. The highway crosses the Eastern Main Channel before Debrecen with the finished bridge described in this section.

The width of the road is 28.73m that in both directions has 2 lanes with a safety lane. The distances between supports are 44.00+60.00+44.00m. The 60.00m middle span will be passable by ships, while on top of the the two embankments service roads and wildroads are planned. The angle between the axis of the road and the line of the supports is 70 degrees. This feature is shown in Fig. 2.58.

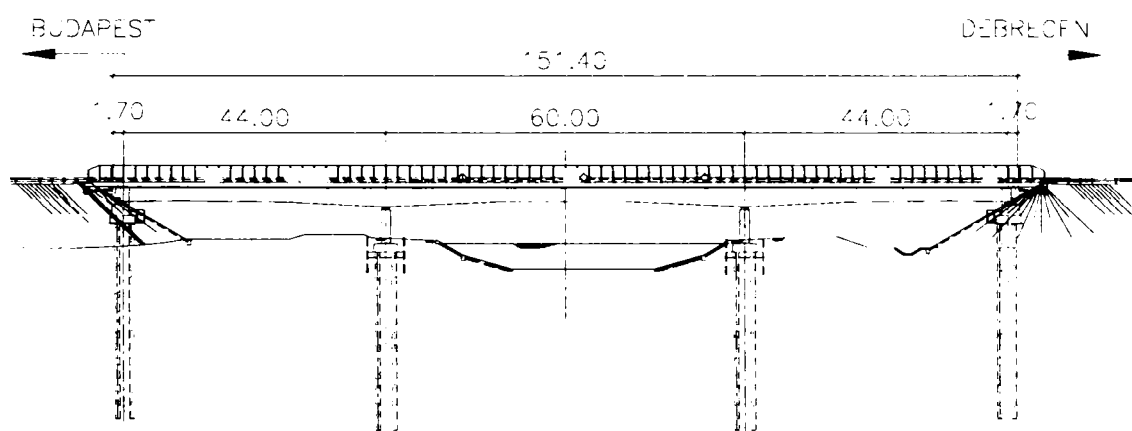


Fig. 2.58. The elevation drawing of the bridge over the Eastern Main Channel

The distance between the open main girders is 7300mm. The height of the web plate is 2100mm at the end cross girders, 3000mm at the supports and 2100mm along the span. The thickness of the web plate is 12mm, which increases to 20mm around the supports. The width of the top plate is 600mm and the thickness is 20-60mm. The width of the bottom plate is 800mm while the thickness varies between 30-100mm.

The web and bottom plate is stiffened by closed section trapezoidal stiffeners and there are cross girders at every 3000mm. The concrete deck slab has varying depth and it is connected to the girders by shear connectors. The cross-slope of the deck is 3.5%. This feature is shown in Fig. 2.59.

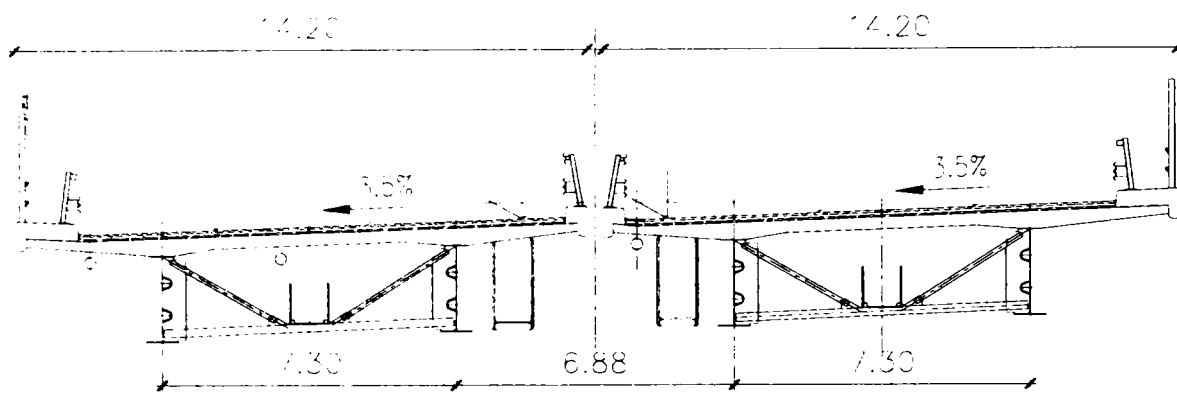


Fig.2.59. The cross section of the bridge over the Eastern Main Channel

This bridge is similar to the bridge at Szekszárd over the Danube where the stiffeners of the web and the bottom plates are not connected to the cross girders. This bridge design unites all the advantages of the experience gained during the construction of the previously described bridges.

2.3.5. The bridge over the river Mura

The M7 highway ensures the road connection to Croatia. Croatia has made large scale road infrastructure development, which has already reached the borders of the two countries. This also means that now Hungary must make the investment to connect the two highways. Furthermore, it also makes a constraint on the design of the bridge, since the line of the road is fixed.

This composite bridge has six supports where the total length of the bridge is 216m. Under the concrete deck slab there are two main box girders. A box girder has parallel, vertical web plates. The height of the web plate is 2000mm, its thickness is 12mm upto 20mm around the supports. The web plates, the top and bottom plates are stiffened by trapezoidal longitudinal stiffeners and at every 4000mm there are 400mm high cross girders. The two main box girders are identical, which helps the manufacturing of the structure. The angle between the axis of the road and the line of the supports is 70 degrees. These features are shown in Fig. 2.60, Fig. 2.61.

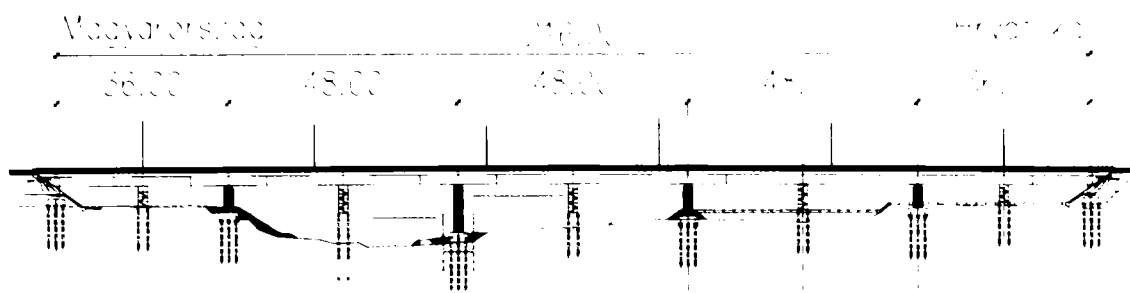


Fig.2.60. The elevation drawing of the bridge over the river Mura

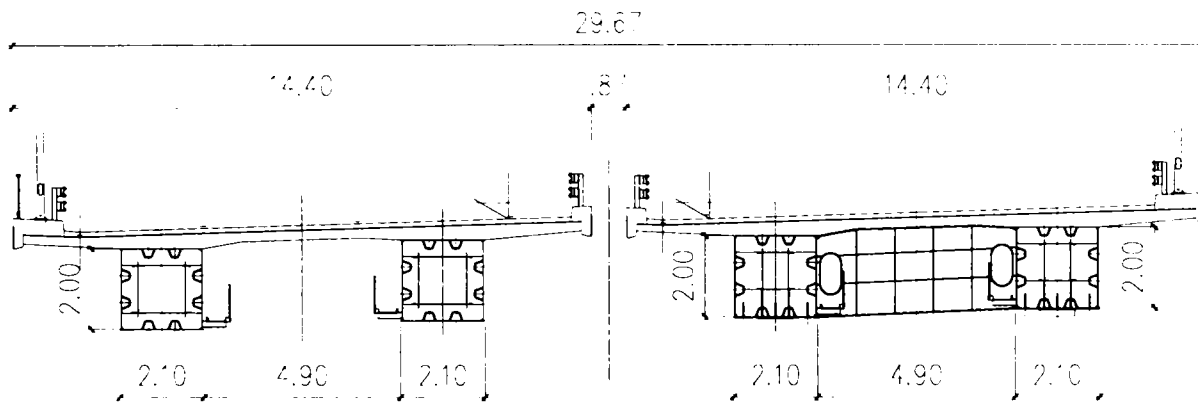


Fig.2.61. The cross section of the bridge over the river Mura

The components of the structure are assembled on top of the embankment and the structure is sliding into position with the help of hydraulic jacks. For this construction process special temporary supports have been constructed.

2.4. Conclusion

The system of composite bridges is used for new road and railway bridges in Hungary. Considering the different aspects of design and fabrication a new type of connection (E, economic) for the stiffeners has been developed and it has been used in the bridges designed by the UVATERV Co with some minor modifications (IVÁNYI Jr, 2004).

CHAPTER 3

Experimental Test Program

I will study the effect of the different structural details between the trapezoidal stiffener and the open cross section cross girder. Three models will be investigated:

- a continuous welded connection (R-rigid type)
- a standard connection (S type)
- a new type of connection, proposed in this thesis (E-economic type).
(IVÁNYI, Jr., BANCILA 2006, IVÁNYI, Jr. et al 2006/a, 2006/b, 2006/c)

It should be emphasized again, that the rigid (R) type of structural detail is never used in practice due to fatigue sensitivity. The rigid type of connection only serves as a basis for the comparison with the other two (S and E) type of solutions and only the ultimate limit state solution of the rigid type of connection is used.

The experiments were conducted in the Structural Laboratory of Pollack Mihály Faculty of Engineering, University of Pécs. The machine in this laboratory is enabled me to perform half scale experiments. The structures for the experiments were constructed by the KÖZGÉP Company.

3.1. Test specimens

Nine welded, simply supported beams were tested. The beams were classified as follows: type R (rigid), type S (standard) and type E (economic). Each beam was

assembled from steel plates, as shown in Fig. 3.1. The dimensions of the U-shaped holes around the trapezoidal stiffener were determined so they would permit the passage of U-shaped stiffeners with the standard size of 153/75x100 mm. The depth of the slit is 20 mm. The form of the U-shaped hole was kept as simple as possible (Fig. 3.2, Fig. 3.3, Fig. 3.4). It must be noted that due to easier fabrication the quarter circle hole in the web of the cross girder at the corner of the trapezoidal stiffener is not cut out. The experimental specimens were prepared for the study of the ultimate limit state thus this modification is acceptable. On the other hand the numerical models contain this cut out hole in the web of the cross girder.

The problem of the effective width of the stiffened plates for the steel deck is beyond the scope of this test since this study is intended to evaluate the normal and shear stresses for a web with holes.

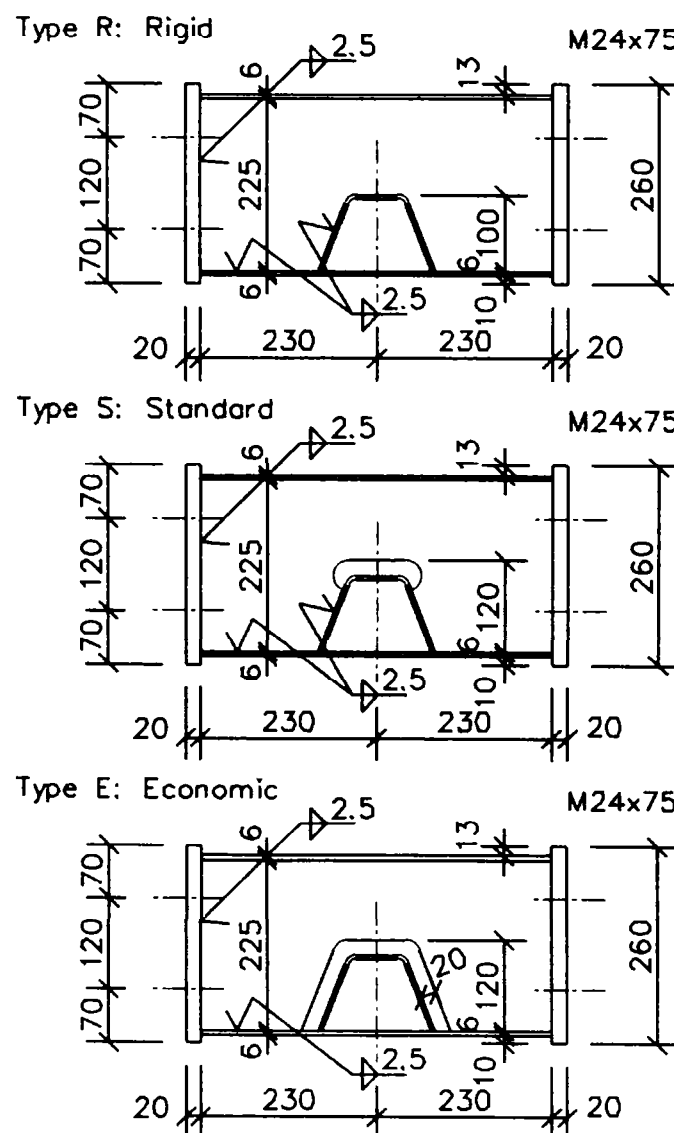


Fig. 3.1. Test specimens

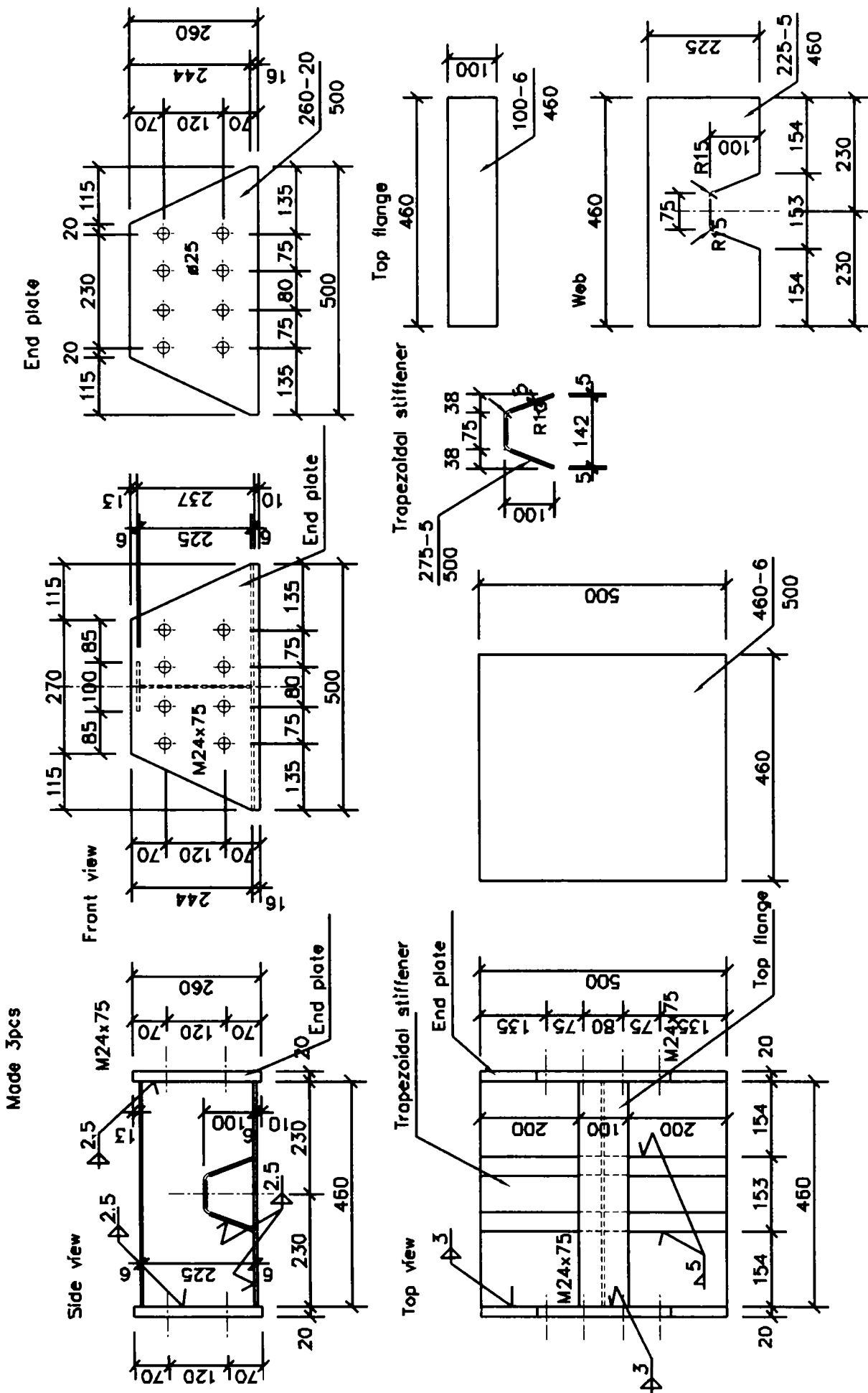


Fig. 3.2. "R" Rigid joint fabrication drawing

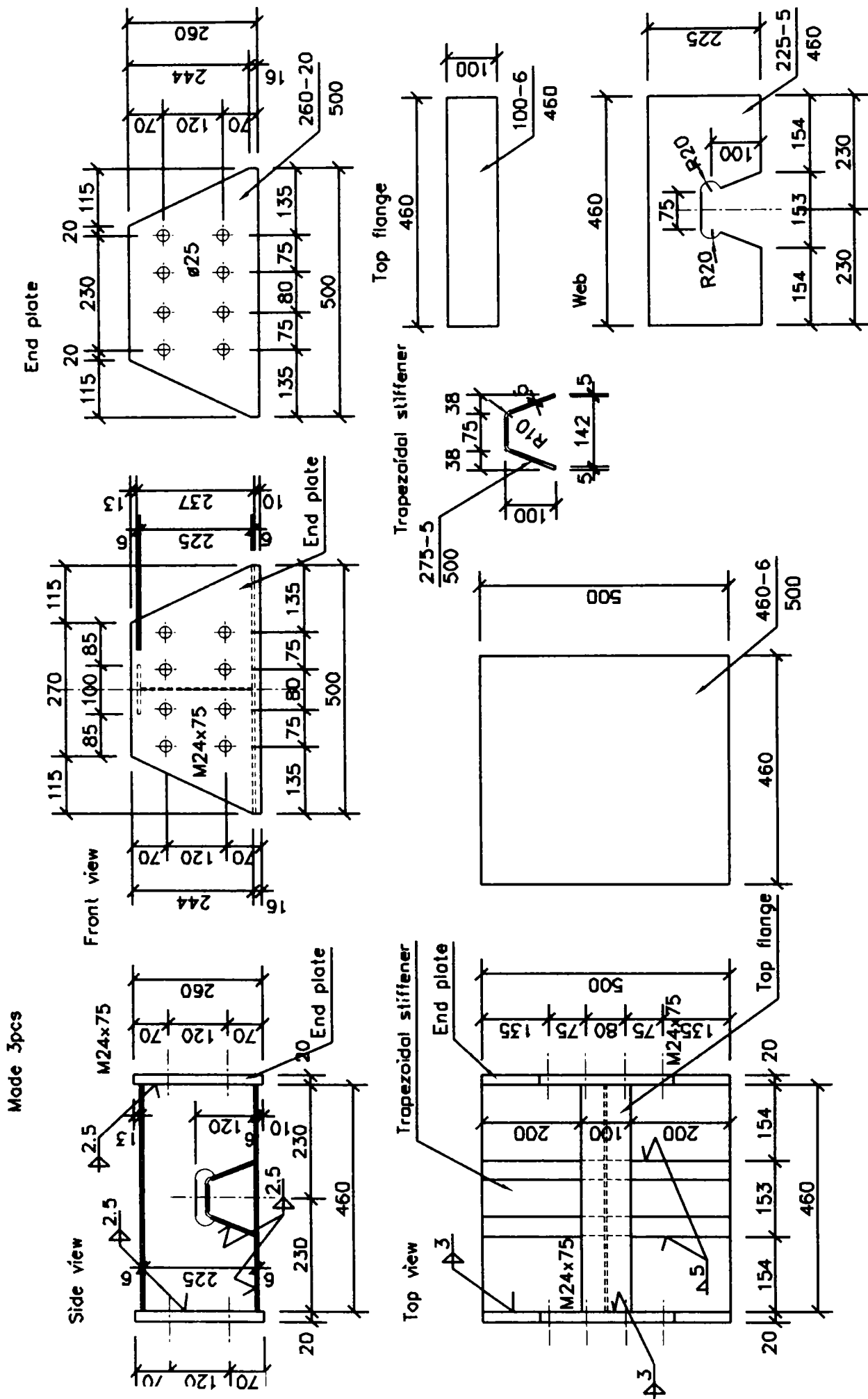


Fig. 3.3. "S" Standard joint fabrication drawing

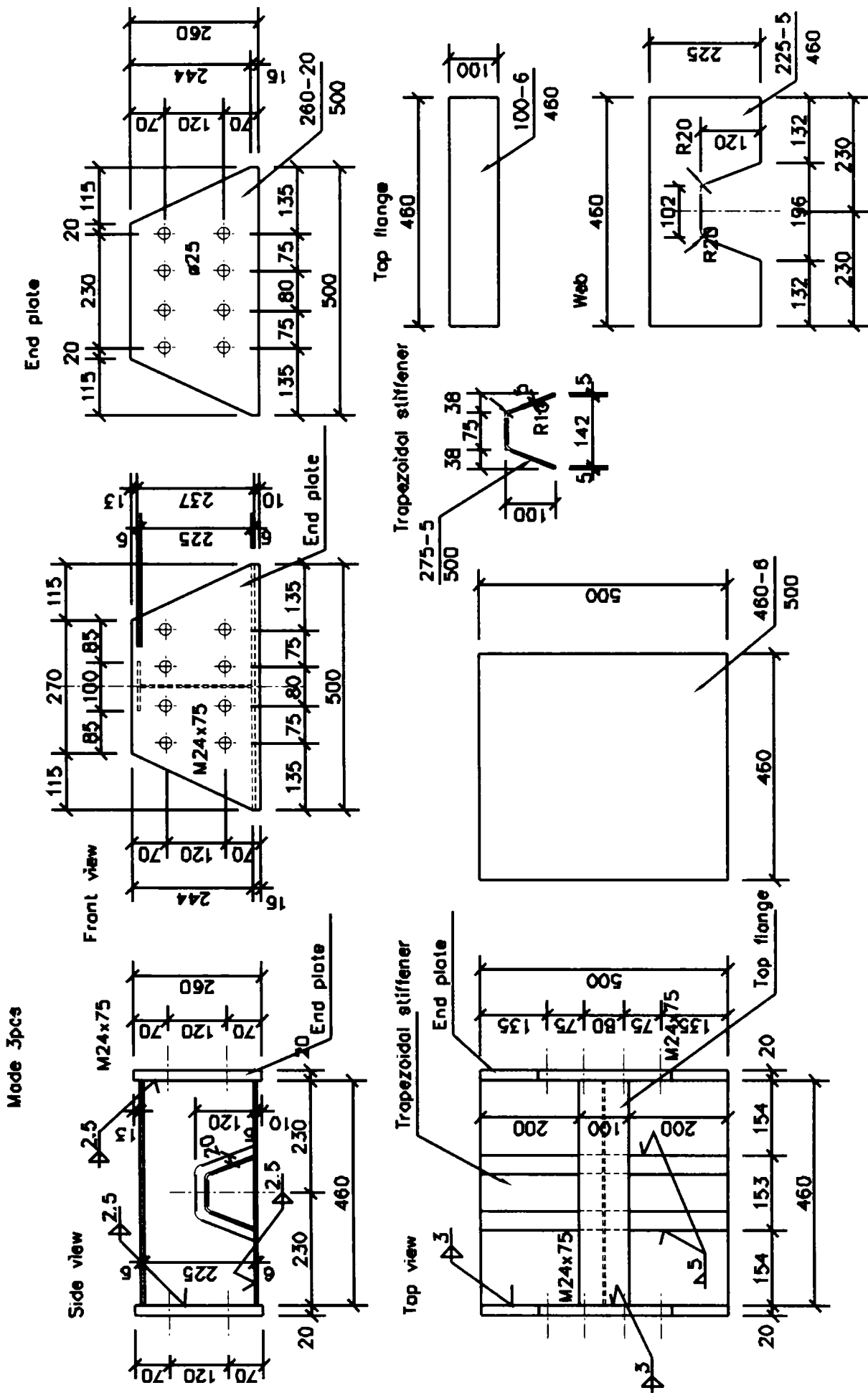
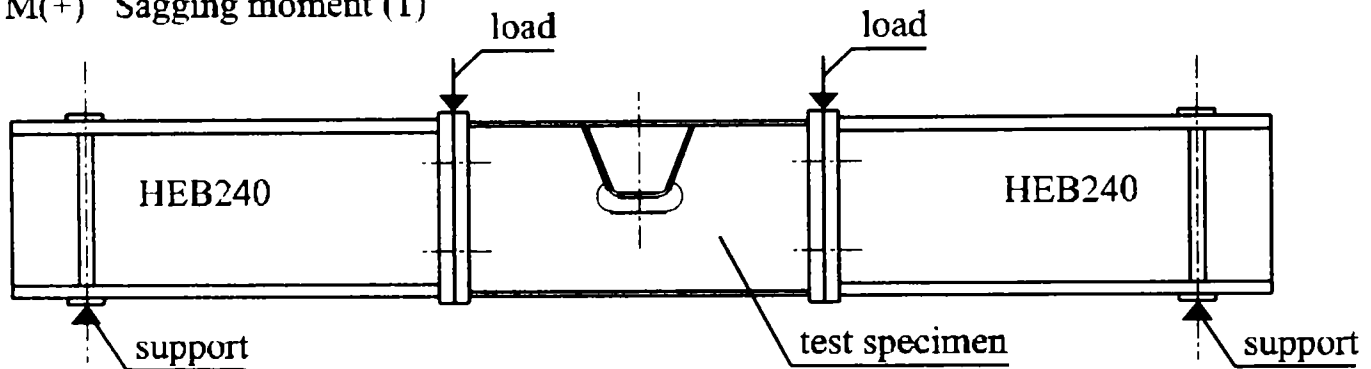


Fig. 3.4. "E" Economic joint fabrication drawing

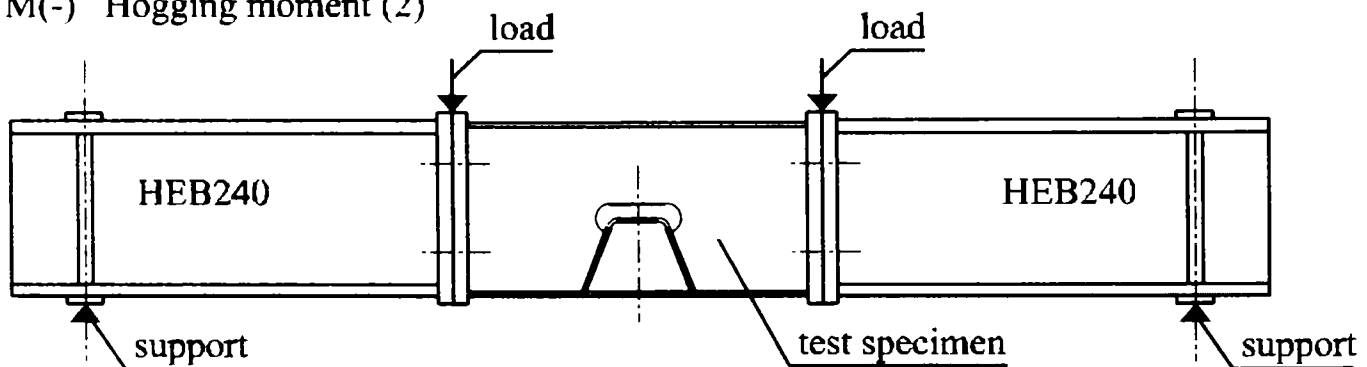
3.2. Test procedures

The other parts of the beam specimens were reinforced by cover plates and vertical stiffeners. Fig. 3.5 shows the loading systems: sagging moment (M^+), hogging moment (M^-), shear force (V). Fig. 3.6 shows the geometrical arrangement with the loading beam and annex beams (Fig. 3.7, Fig. 3.8).

M^+ Sagging moment (1)



M^- Hogging moment (2)



V Shear force (3)

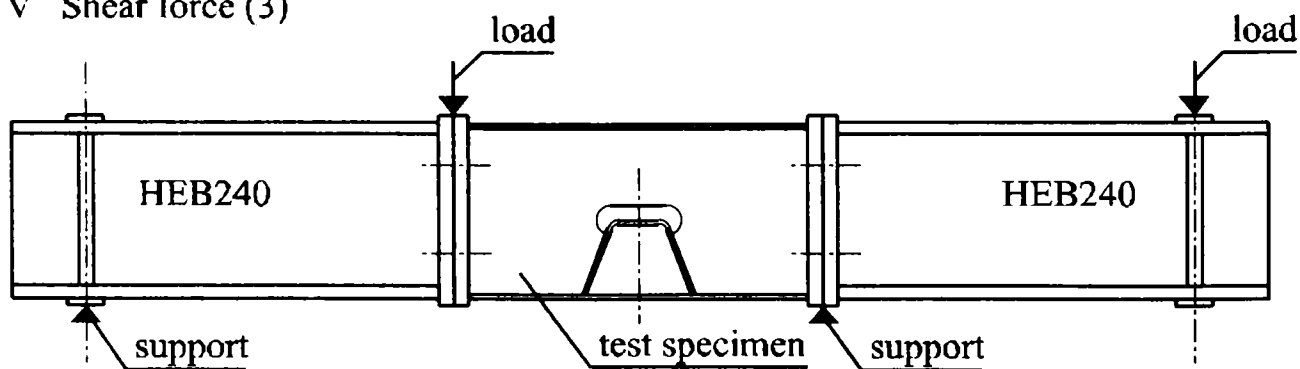


Fig. 3.5. The loading system

The notation used in the experiments:

- TR : Trapezoidal stiffener.
- R-S-E : different connection type between the stiffener and the cross girder.

- 1-2-3 : type of internal force in the structure.

1 : sagging moment,

2 : hogging moment,

3 : shear force.

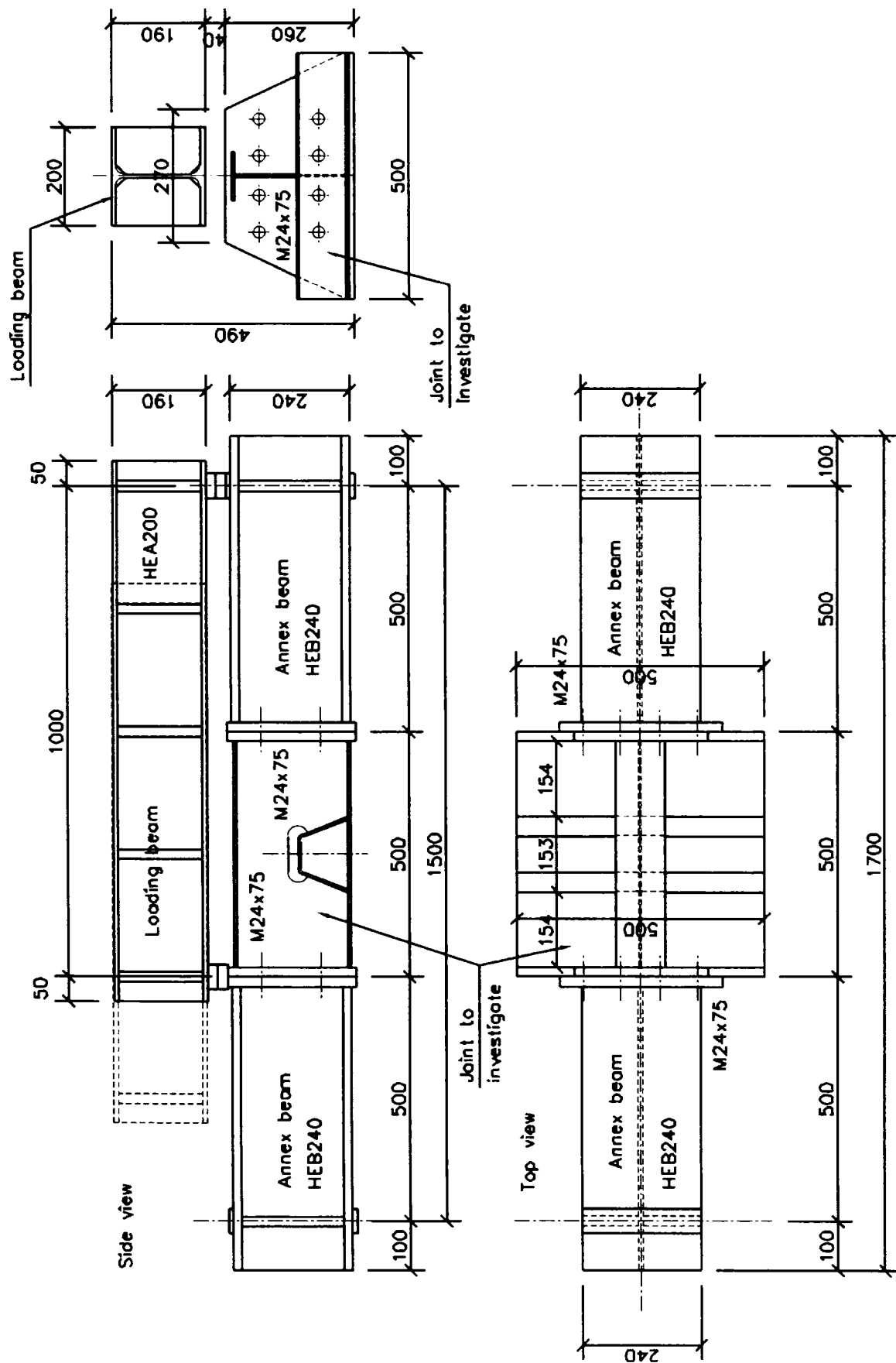
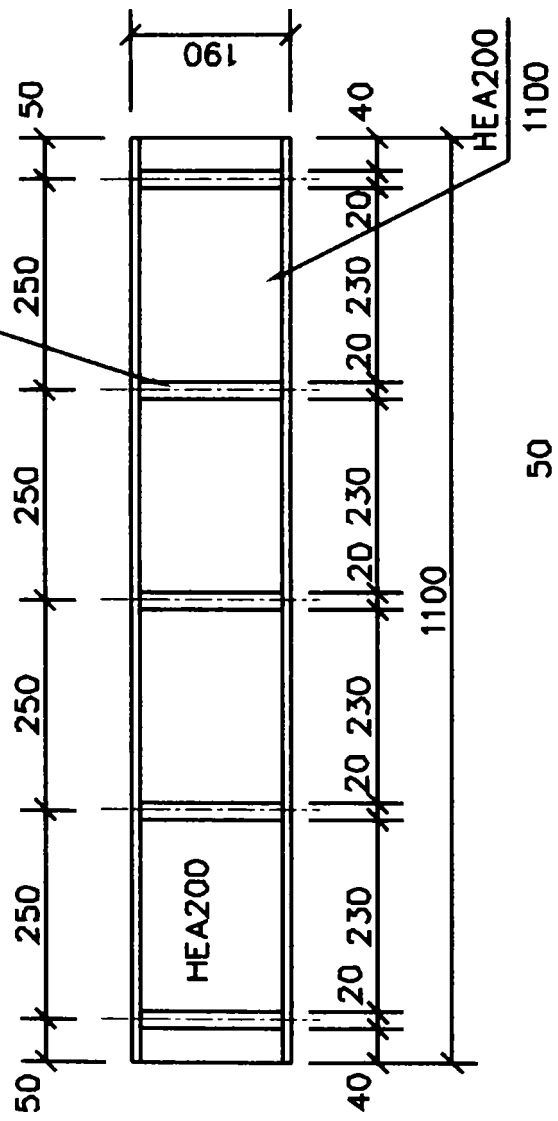


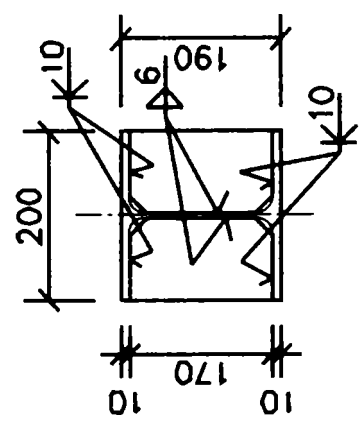
Fig. 3.6. Geometric arrangement

Made 1pc

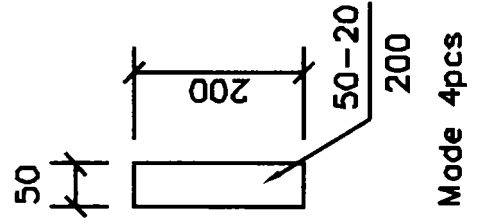
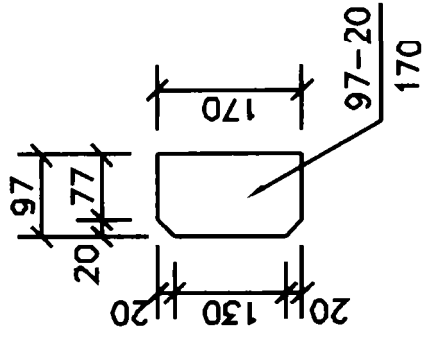
Side view



Section



Stiffener
Made 5x2=10pcs



Made 4pcs

Fig. 3.7. Loading beam

Made 2pcs

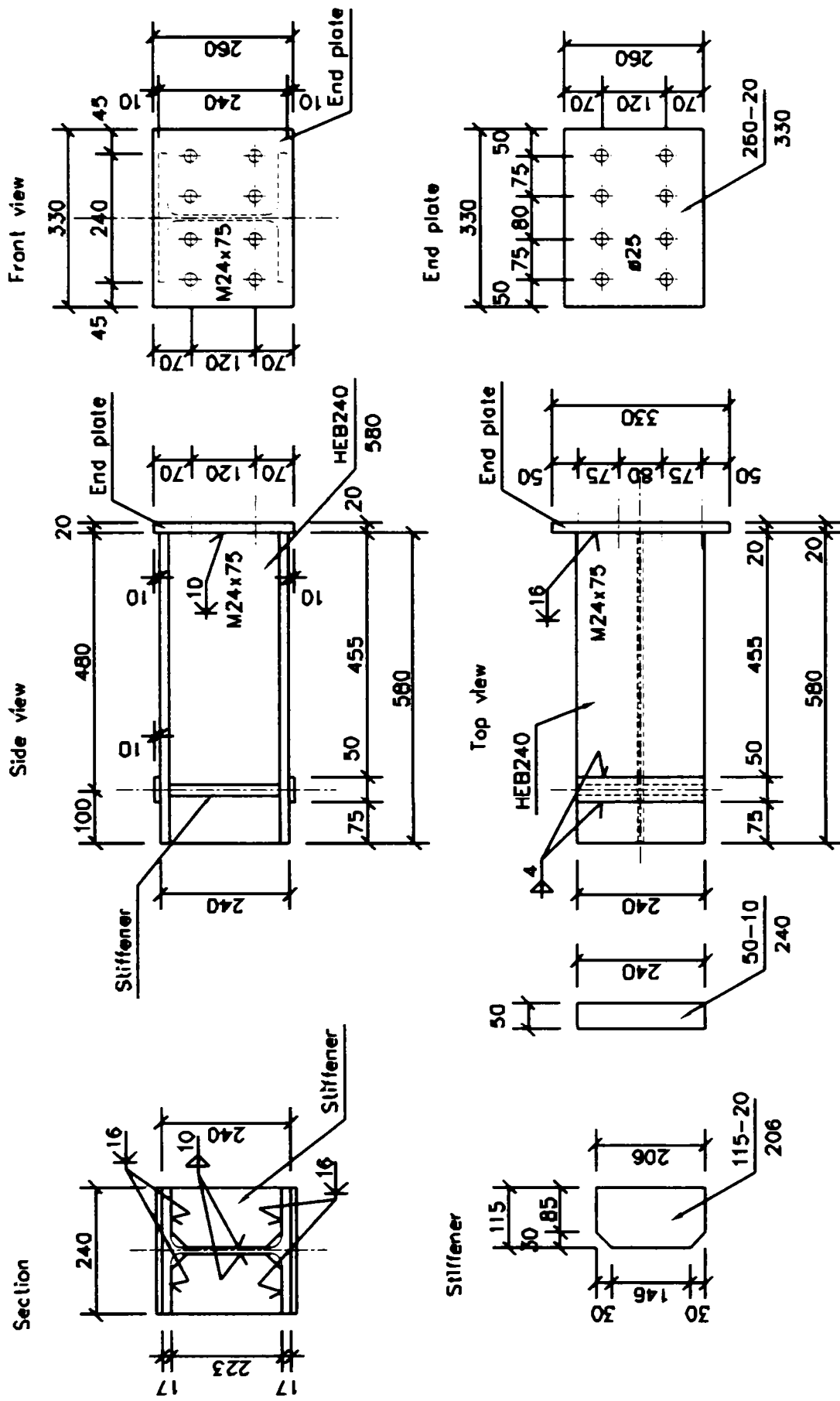


Fig. 3.8. Annex beam

3.2.1. Load equipment

The test procedures were in the laboratory of Department of Structural Engineering Pollack Mihály Faculty of Engineering, University of Pécs. Fig. 3.9 shows the loading equipment.

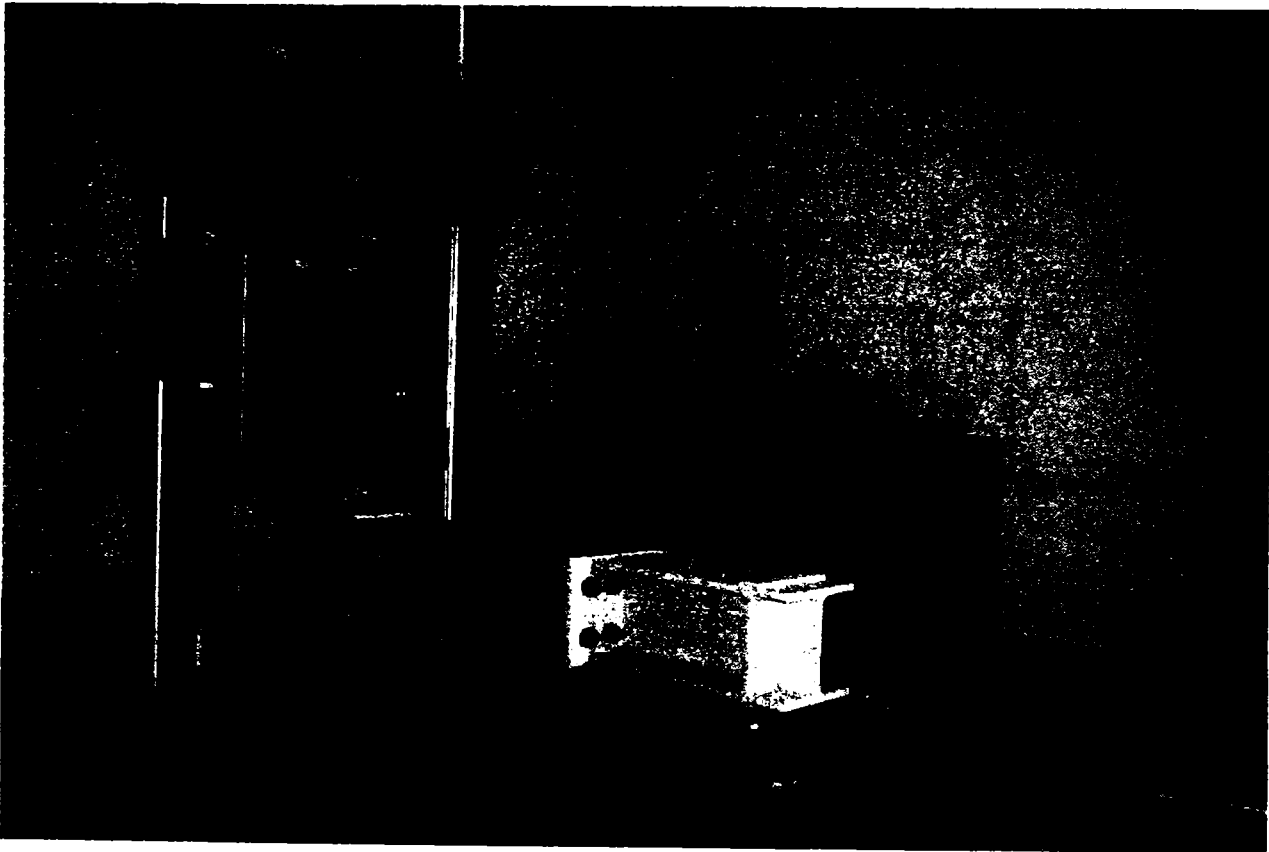


Fig. 3.9. Loading equipment

3.2.2. Preparation for the experiments

Special annex beams have been attached to the experimental structure to be able to produce the required internal forces. The connection between the parts has been made with high strength bolts. To reduce the deformation of the connections the bolts are tensioned to the required level.

A special track has also been constructed to be able to roll the experimental pieces under the machine. In this way the experiments could be conducted without any power lifting machine or crane. This track structure is shown in Fig. 3.10. This track can be easily disassembled and therefore it was not present in the experiments during the loading stage.

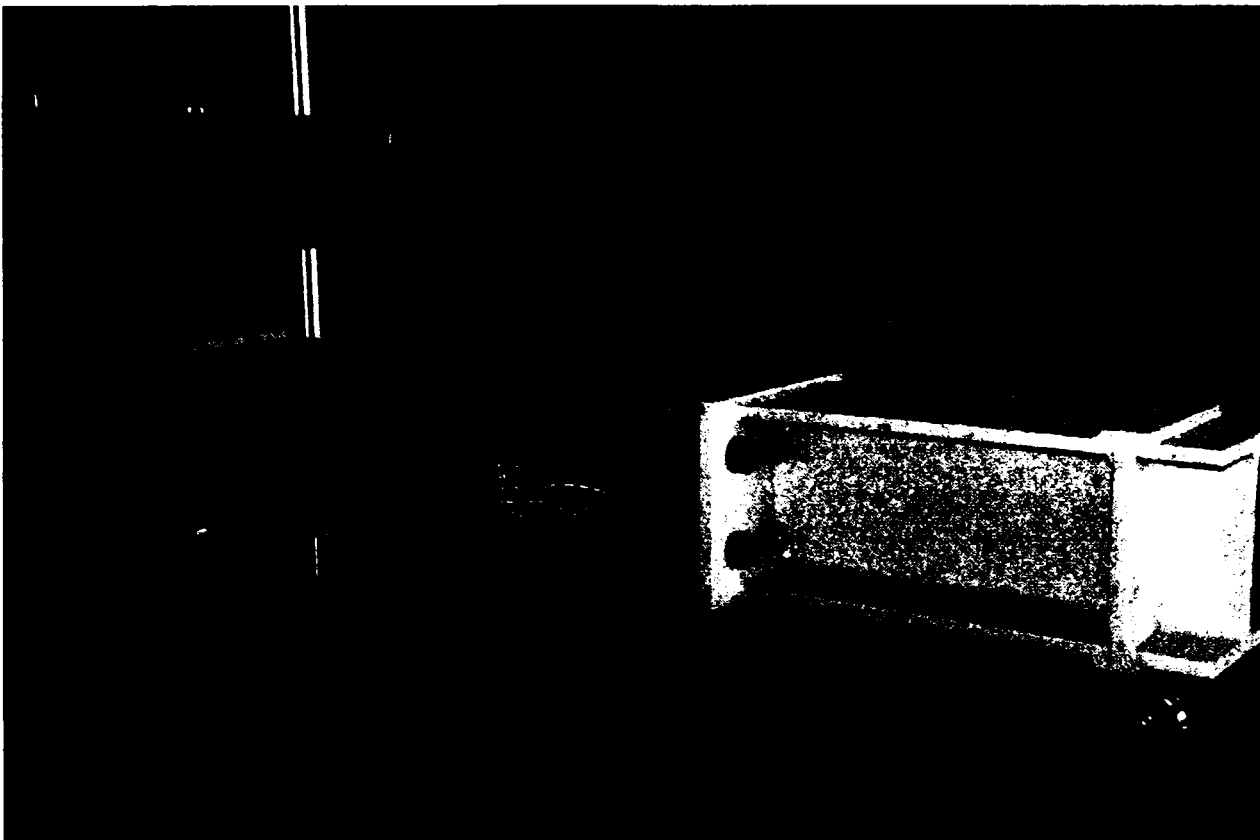


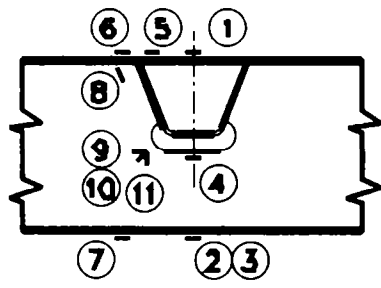
Fig. 3.10. Special track for the specimens

3.2.3. Measurement procedures

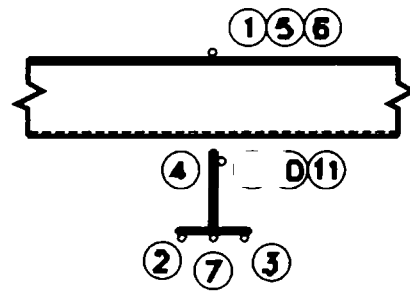
A rosette strain gage and several single strain gages around the U-shaped holes were placed to obtain the web buckling behavior. The single strain gages were placed in such a way as to obtain primarily bending stresses. The locations of the strain gages in the vicinity of the U-shaped hole, but closest to the loading point are shown in Fig. 3.11 and Fig. 3.12. The rosette strain gage was placed to obtain principal stresses of the web section.

The vertical displacements were measured at the middle of the specimens by using deformation gages. All data of strains, displacements and loads were measured at each of the loading stages simultaneously.

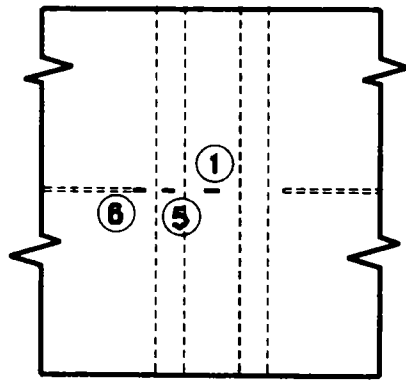
Side view



Section



Top view



Bottom view

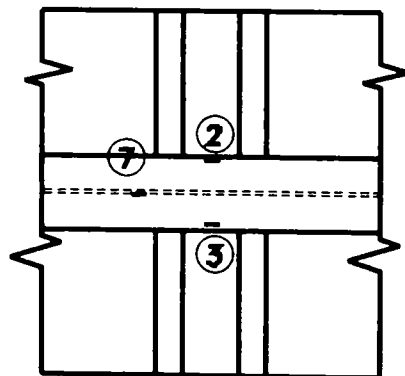


Fig. 3.11. Geometric arrangement of strain gauges

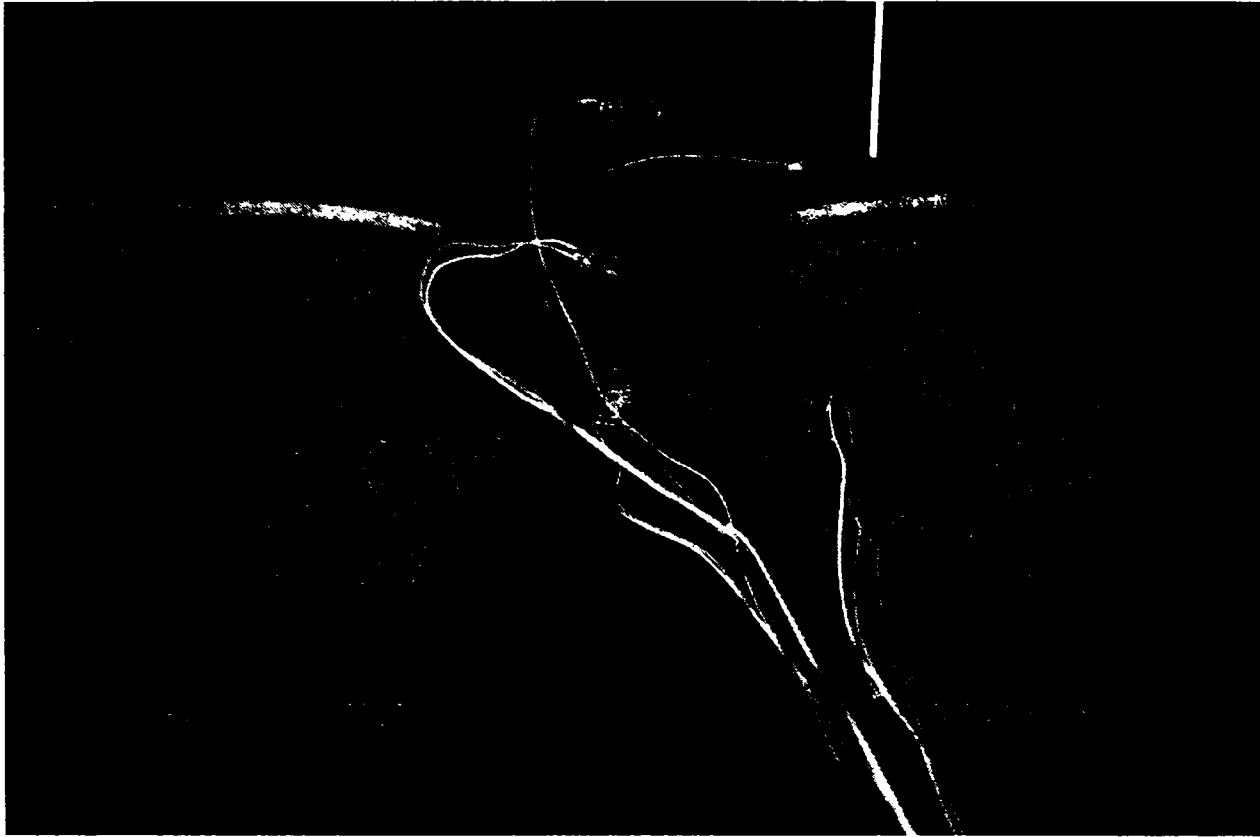


Fig. 3.12. Arrangement of the strain gauges

Special measurement of strains was used when the specimen was loaded by shear forces. The measurements were performed between point A and D (Fig. 3.13). This measurement result in a so called “push out” test.

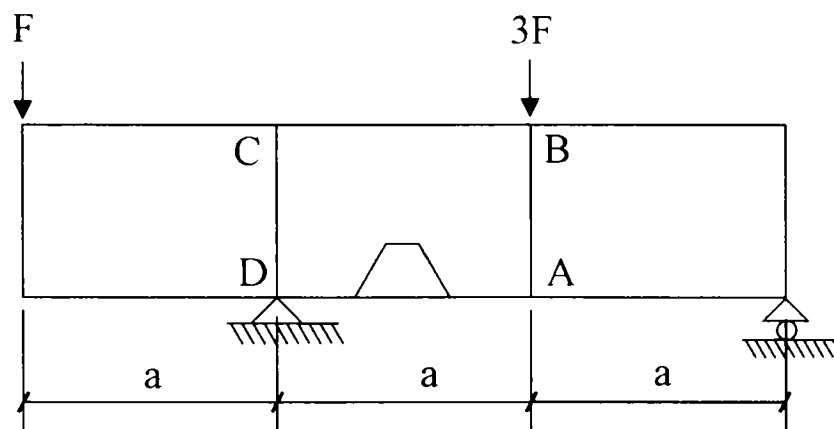


Fig. 3.13. Relative displacement measurement point “A” and “D”

3.3. Test for mechanical properties of the steel material of test girders

The mechanical properties of the steel material have been determined by standard tensile tests, see Fig. 3.14.

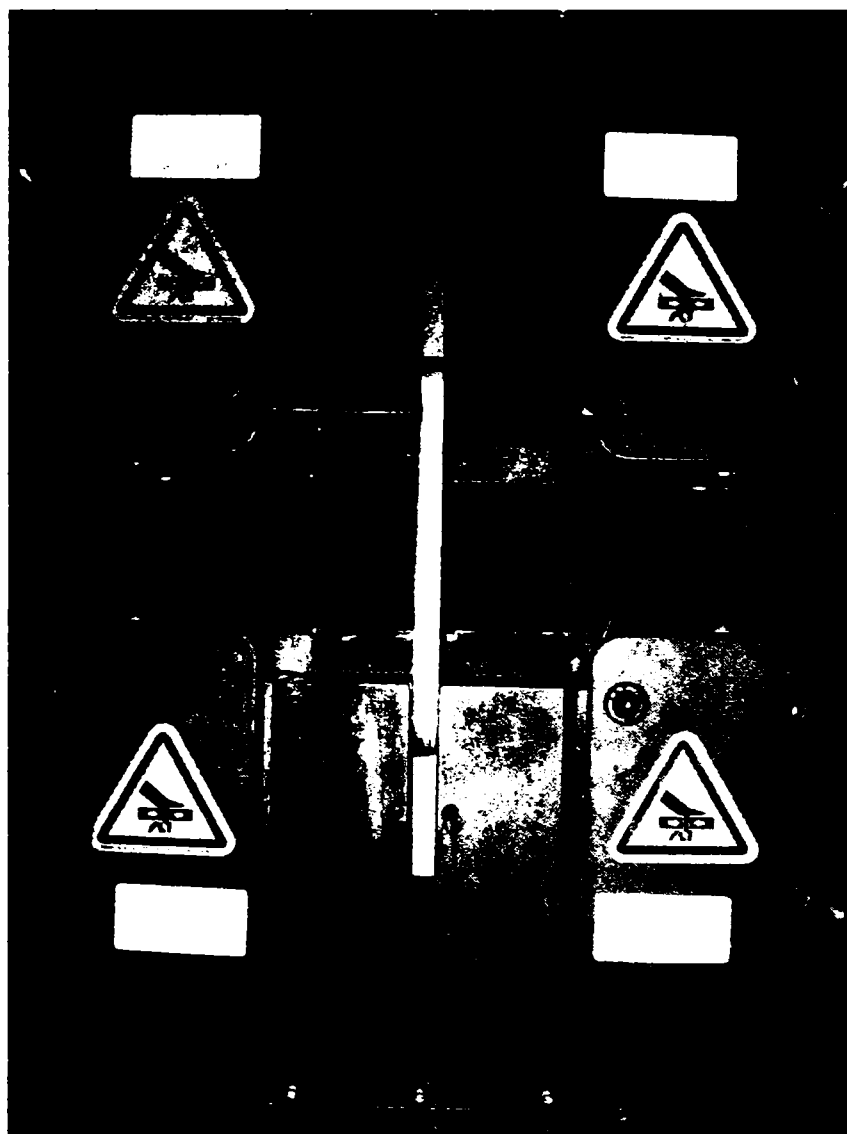
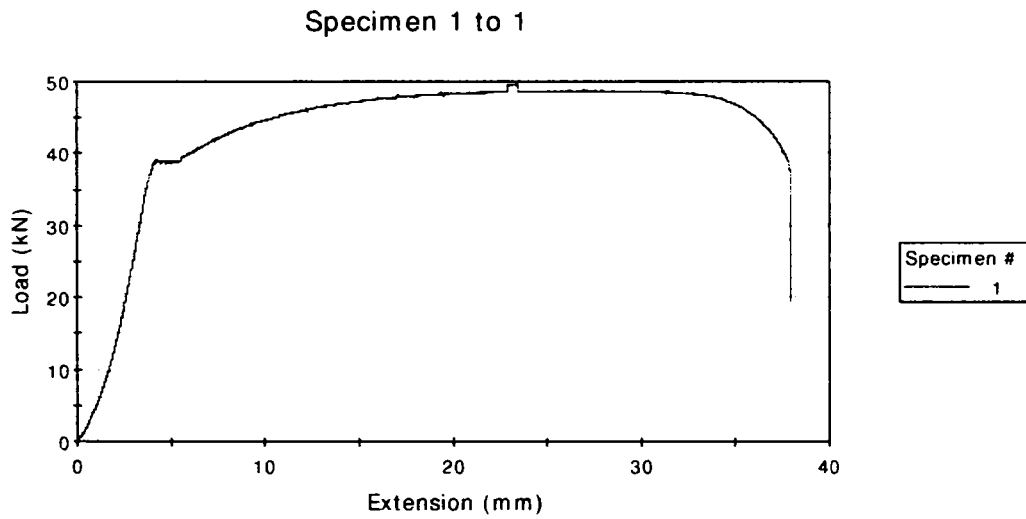


Fig. 3.14. Standard tensile test

The results of the tensile material test can be seen in Fig. 3.15 - Fig. 3.22.



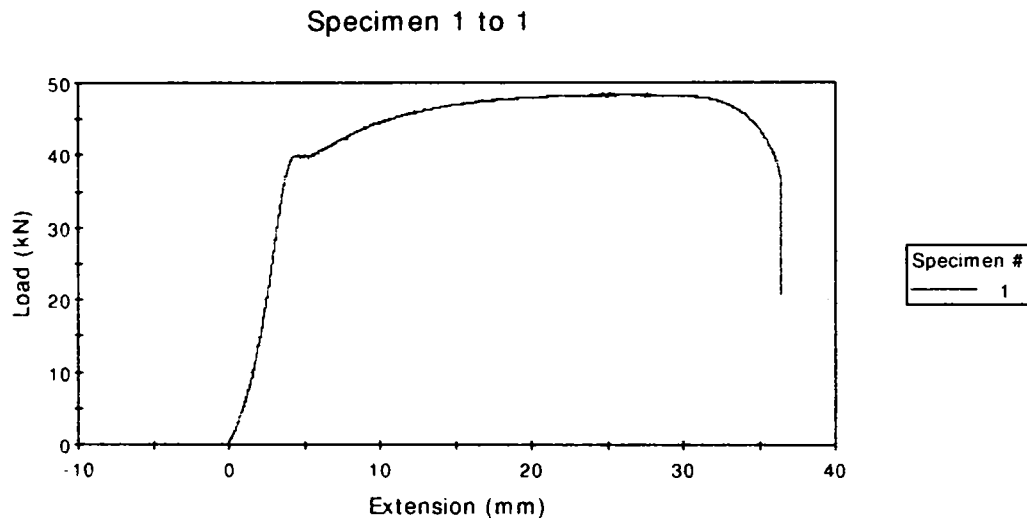
	Maximum Load (kN)	Tensile extension at Maximum Load (mm)	Tensile strain at Maximum Load (mm/mm)
1	49,662	23,41	0,23
	Load at Yield (Zero Slope) (kN)	Tensile extension at Yield (Zero Slope) (mm)	Tensile strain at Yield (Zero Slope) (mm/mm)
1	49,662	23,415	0,234
	Final length (mm)	Start Date	End Date
1	100,000	2005.10.06. 15:48:08	2005.10.06. 16:07:08
	Specimen label		
1	13-as próbatest		

A=1.0 cm²

$f_y=39,0 \text{ kN/cm}^2$

$f_u=49,66 \text{ kN/cm}^2$

Fig. 3.15. Load-extension curve



	Maximum Load (kN)	Tensile extension at Maximum Load (mm)	Tensile strain at Maximum Load (mm/mm)
1	48.411	27.02	0.27
	Load at Yield (Zero Slope) (kN)	Tensile extension at Yield (Zero Slope) (mm)	Tensile strain at Yield (Zero Slope) (mm/mm)
1	48.411	27.016	0.270
	Final length (mm)	Start Date	End Date
1	100,000	2005.10.13. 15:36:28	2005.10.13. 15:48:38
Specimen label			
1	14-es próbatest		

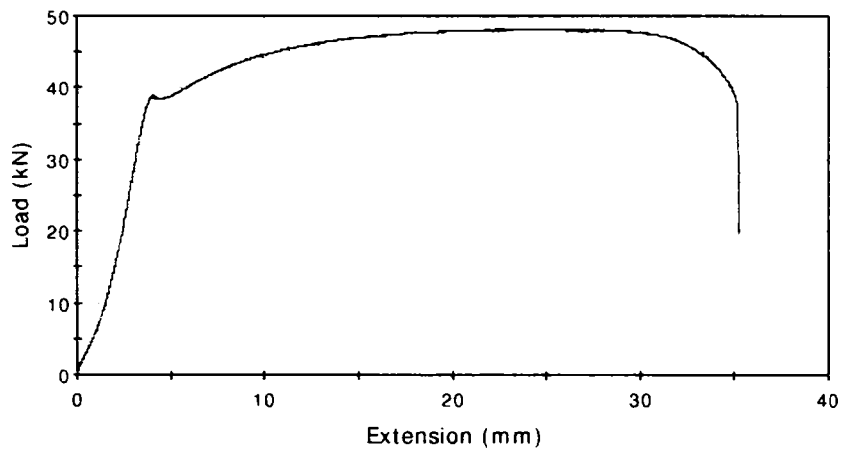
A=1,0 cm²

f_y=40,0 kN/cm²

f_u=48,4 kN/cm²

Fig. 3.16. Load-extension curve

Specimen 1 to 1



Specimen #	1
------------	---

	Maximum Load (kN)	Tensile extension at Maximum Load (mm)	Tensile strain at Maximum Load (mm/mm)
1	48.168	21.86	0.22
	Load at Yield (Zero Slope) (kN)	Tensile extension at Yield (Zero Slope) (mm)	Tensile strain at Yield (Zero Slope) (mm/mm)
1	48.168	21.856	0.219
	Start Date	End Date	Specimen label
1	2005.10.13. 15:58:03	2005.10.13. 16:09:48	15-ös próbatást

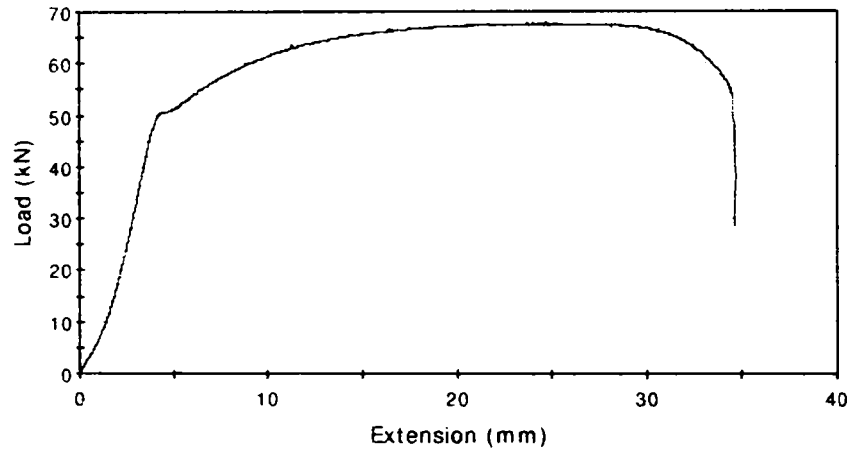
A=1,0 kN/cm²

f_y=38,5 kN/cm²

f_u=48,17 kN/cm²

Fig. 3.17. Load-extension curve

Specimen 1 to 1



Specimen #
1

	Maximum Load (kN)	Tensile extension at Maximum Load (mm)	Tensile strain at Maximum Load (mm/mm)
1	67.550	24.54	0.25
	Load at Yield (Zero Slope) (kN)	Tensile extension at Yield (Zero Slope) (mm)	Tensile strain at Yield (Zero Slope) (mm/mm)
1	67.550	24.540	0.245
	Final length (mm)	Start Date	End Date
1	100,000	2005.10.06. 16:22:21	2005.10.06. 16:33:54
	Specimen label		
1	16-os próbatest		

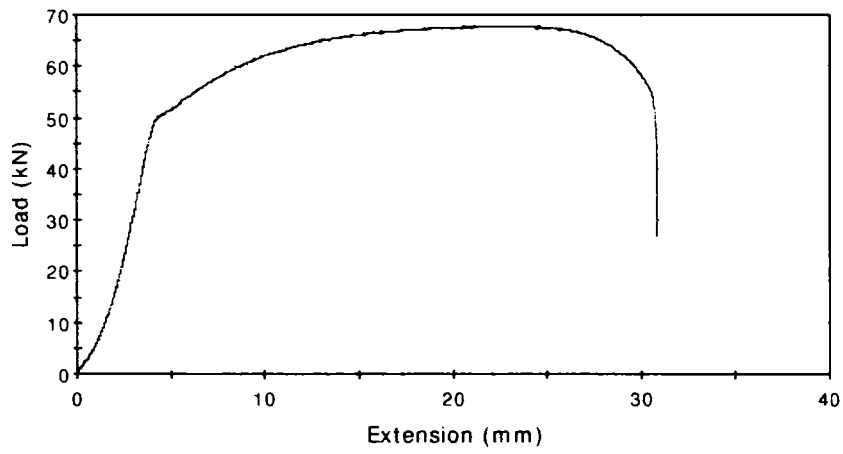
A=1,2 cm²

$f_y=41,66 \text{ kN/cm}^2$

$f_u=56,29 \text{ kN/cm}^2$

Fig. 3.18. Load-extension curve

Specimen 1 to 1



Specimen #	1
------------	---

	Maximum Load (kN)	Tensile extension at Maximum Load (mm)	Tensile strain at Maximum Load (mm/mm)
1	67.692	24.69	0.25
	Load at Yield (Zero Slope) (kN)	Tensile extension at Yield (Zero Slope) (mm)	Tensile strain at Yield (Zero Slope) (mm/mm)
1	67.673	22.854	0.229
	Start Date	End Date	Specimen label
1	2005.10.13. 16:20:14	2005.10.13. 16:30:29	17-es próbatest

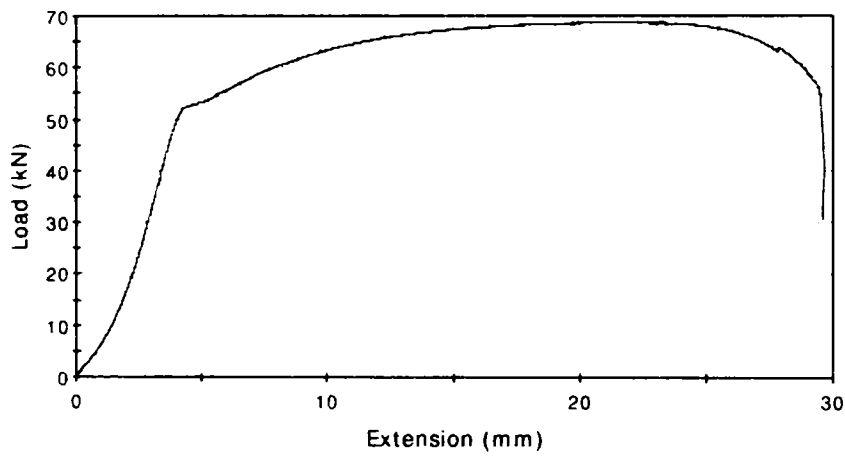
A=1,2 cm²

f_y=41,5 kN/cm²

f_u=56,41 kN/cm²

Fig. 3.19. Load-extension curve

Specimen 1 to 1



Specimen #	1
------------	---

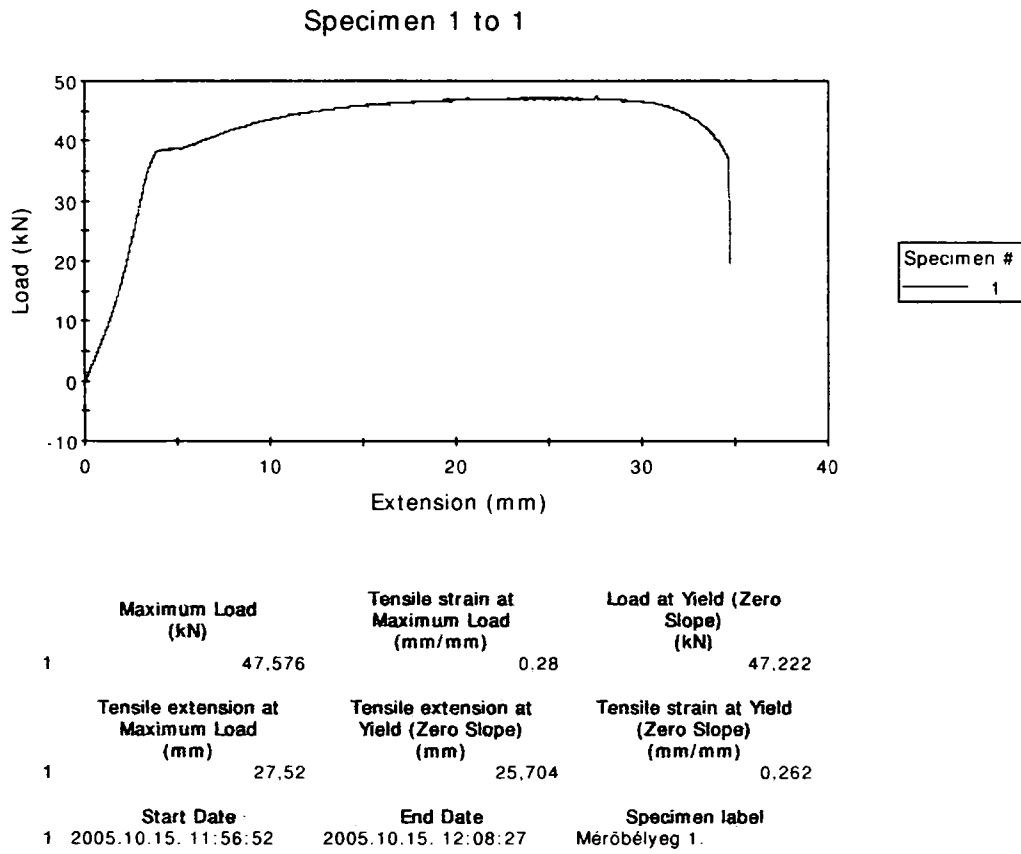
	Maximum Load (kN)	Tensile extension at Maximum Load (mm)	Tensile strain at Maximum Load (mm/mm)
1	68.818	21.26	0.21
	Load at Yield (Zero Slope) (kN)	Tensile extension at Yield (Zero Slope) (mm)	Tensile strain at Yield (Zero Slope) (mm/mm)
1	68.818	21.263	0.213
	Start Date	End Date	Specimen label
1	2005.10.13. 16:37:06	2005.10.13. 16:46:59	18-as próbatest

A=1,2 cm²

$f_y=43.75 \text{ kN/cm}^2$

$f_u=57,35 \text{ kN/cm}^2$

Fig. 3.20. Load-extension curve



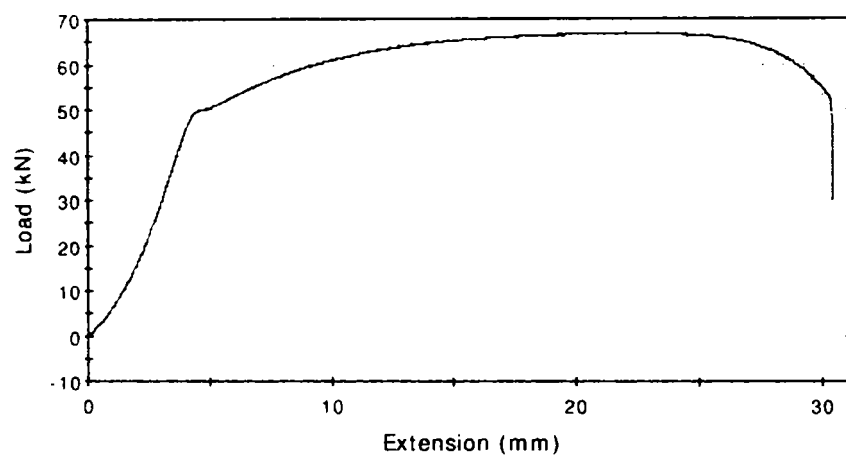
A=1.0cm²

$f_y=38,5 \text{ kN/cm}^2$

$f_u=47,58 \text{ kN/cm}^2$

Fig. 3.21. Load-extension curve

Specimen 1 to 1



Specimen #
1

	Maximum Load (kN)	Tensile strain at Maximum Load (mm/mm)	Load at Yield (Zero Slope) (kN)
1	66,871	0,22	66,871
	Tensile extension at Maximum Load (mm)	Tensile extension at Yield (Zero Slope) (mm)	Tensile strain at Yield (Zero Slope) (mm/mm)
1	21,97	21,975	0,220
	Start Date	End Date	Specimen label
1	2005.10.15. 12:56:20	2005.10.15. 13:06:29	Mérőbélyeg 2. - 20

A=1,2cm²

f_y=42,08 kN/cm²

f_u=55,73 kN/cm²

Fig. 3.22. Load-extension curve

The results of the experiments for mechanical properties of steel material are summarized by Table 3.1.

	A [cm ²]	f _y [kN/cm ²]	f _u [kN/cm ²]
13	1,0	39,00	49,66
14	1,0	40,00	48,40
15	1,0	38,50	48,17
16	1,2	41,66	56,29
17	1,2	41,50	56,41
18	1,2	43,75	57,35
M1-19	1,0	38,50	47,58
M2-20	1,2	42,08	55,73
average		40,62	52,44

Table 3.1.

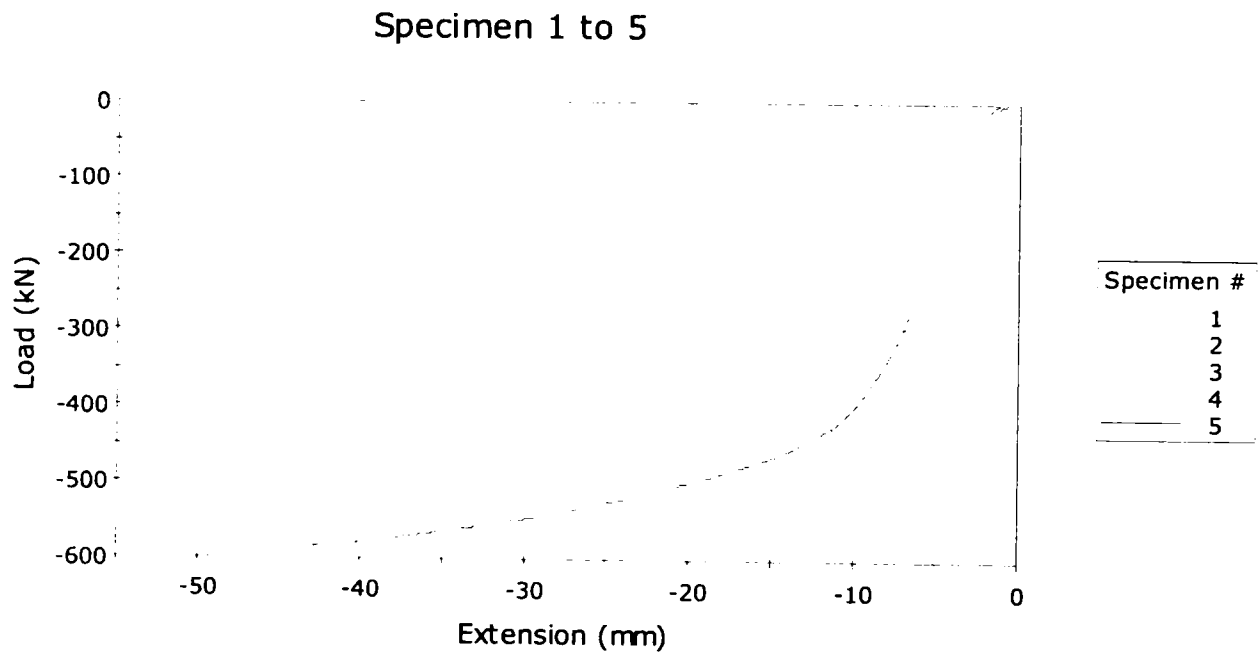
Young's modulus: $E=210000 \text{ N/mm}^2$

Poisson ratio: $\nu=0,3$

3.4. Experimental behaviour of orthotropic plates

3.4.1. Effect of sagging moment

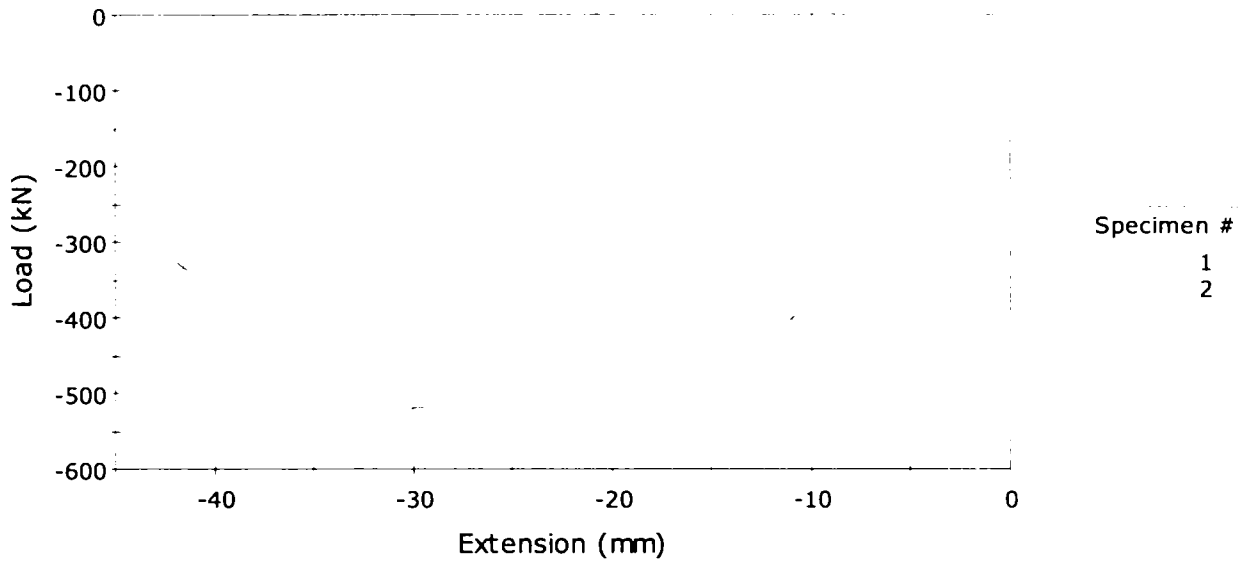
Fig. 3.23-Fig.3.25 show the experimental test results for the effect of sagging moment. (R-1, S-1,E-1)



	Specimen label	Maximum Load (kN)	Extension at Maximum Load (mm)
1	TR1-1	0,137	0,01
2	TR1-1	0,243	-0,05
3	TR1-1	-208,330	-5,01
4	TR1-1	0,242	-0,17
5	TR1-1	0,236	-0,30
	Load at Maximum Time (kN)	Maximum Time (sec)	Start Date
1	-212,571	601,91	2006.01.20. 15:04:38
2	-209,914	604,88	2006.01.20. 15:18:09
3	-302,167	241,11	2006.01.20. 15:29:14
4	-0,943	131,70	2006.01.20. 15:45:25
5	-335,067	6424,40	2006.01.20. 15:49:35
	End Date	Time at Maximum Load (sec)	Load at Maximum Extension (kN)
1	2006.01.20. 15:14:40	0,20	0,137
2	2006.01.20. 15:28:14	9,10	0,227
3	2006.01.20. 15:33:16	0,00	-208,330
4	2006.01.20. 15:47:37	20,10	0,221
5	2006.01.20. 17:36:39	36,40	0,212

Fig. 3.23. Load-extension curve for TR R-1

Specimen 1 to 2



	Specimen label	Load at Maximum Time (kN)	Maximum Time (sec)
1	TR2-1	-219,759	669,98
2	TR2-1	-321,422	5087,55

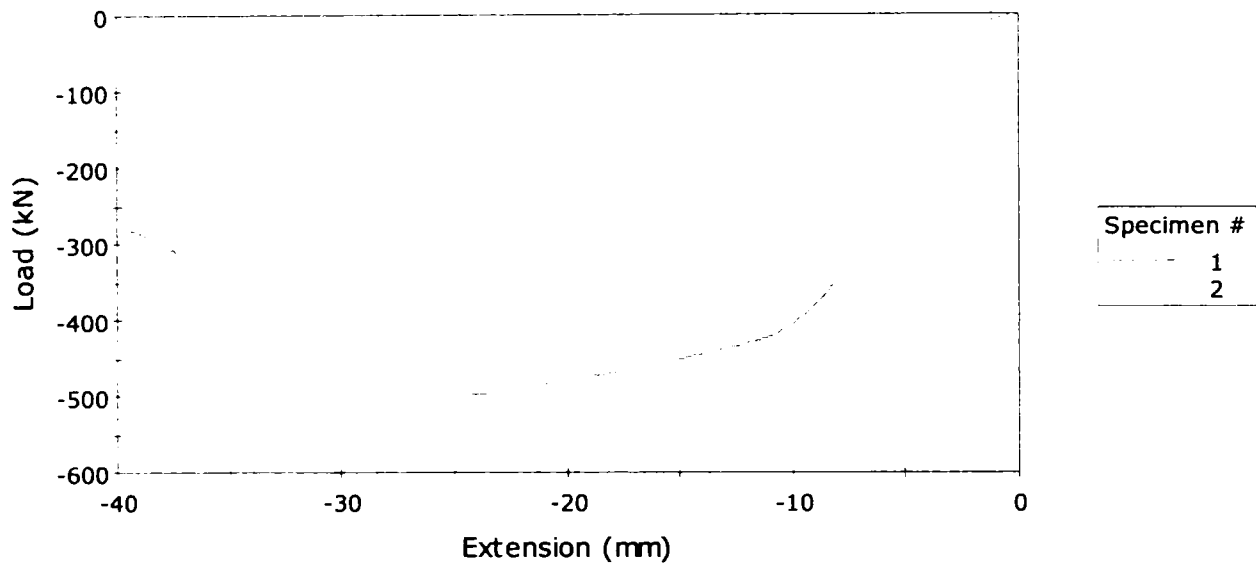
	Start Date	End Date	Time at Maximum Load (sec)
1	2006.02.03. 08:30:55	2006.02.03. 08:42:05	0,10
2	2006.02.03. 08:42:31	2006.02.03. 10:07:19	0,10

	Load at Maximum Extension (kN)	Time at Maximum Extension (sec)	Loading span (mm)
1	0,005	0,1	500,0
2	0,223	0,0	500,0

	Support span (mm)	Minimum Load (kN)	Extension at Minimum Load (mm)
1	1500,0	-219,759	-5,587
2	1500,0	-542,403	-37,766

Fig. 3.24. Load-extension curve for TR S-1

TR 3 - 1



	Specimen label	Minimum Load (kN)	Extension at Minimum Load (mm)
1	TR3-1	-221,392	-5,106
2	TR3-1	-524,238	-34,211

	Load at Maximum Time (kN)	Extension at Maximum Time (mm)	Load at Minimum Extension (kN)
1	-221,392	-5,106	-221,392
2	-274,234	-40,017	-274,267

	Start Date	End Date	Maximum Time (sec)
1	2006.02.03. 12:01:05	2006.02.03. 12:11:17	612,53
2	2006.02.03. 12:11:32	2006.02.03. 13:31:38	4806,11

	Time at Minimum Load (sec)	Time at Minimum Extension (sec)
1	612,53	612,53
2	4109,30	4805,75

Fig. 3.25. Load-extension curve for TR E-1

Fig. 3.26. shows the load-displacement curves for specimens R-1, S-1 and E-1.

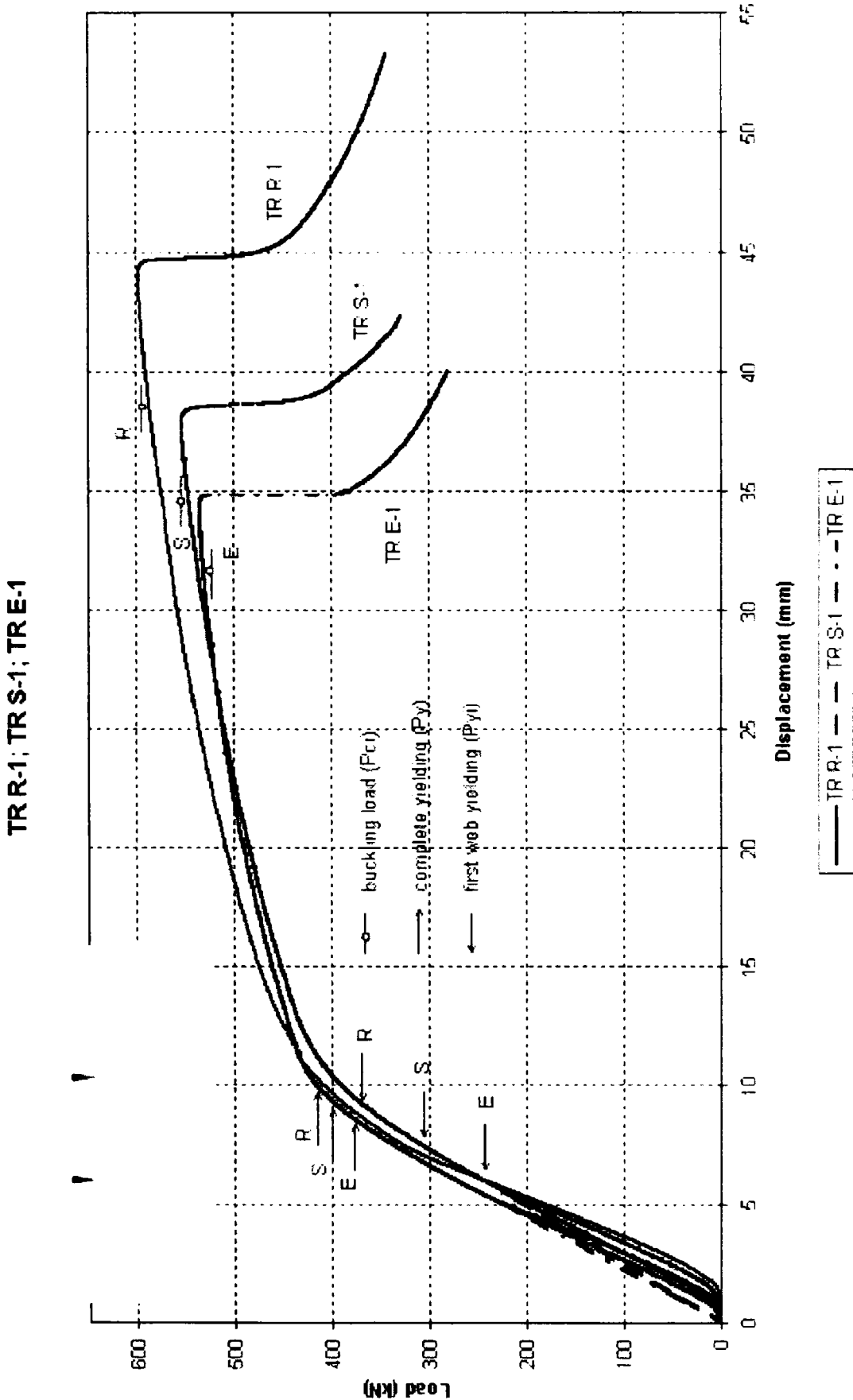


Fig. 3.26. Load-displacement curves at sagging moment (M+)

The specimens have been loaded by a sagging moment, which causes compression in the plate that is stiffened by the trapezoidal stiffener. The load carrying capacity under the sagging moment does not change significantly for the different arrangements of the connection between the trapezoidal stiffener and the web of the cross girder. The failure mode (Fig. 3.27, Fig. 3.28 and Fig. 3.29) was similar for all three specimens, specifically the stiffened plate buckled out of the plane between the two points where the trapezoidal stiffener is attached to the stiffened plate.



Fig. 3.27a. Type R test after sagging moment (M+)

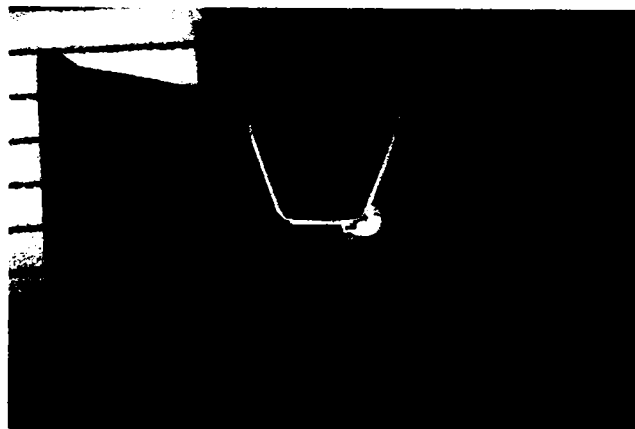


Fig. 3.27b. Type R test after sagging moment (M+)



Fig. 3.28a. Type S test after sagging moment (M+)

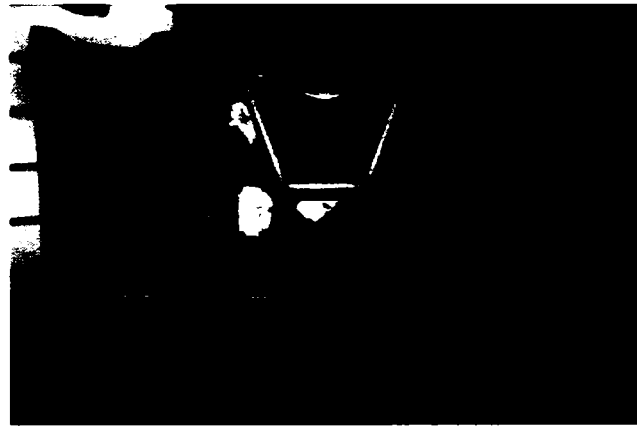


Fig. 3.28b. Type S test after sagging moment (M+)



Fig. 3.29a. Type E test after sagging moment (M+)

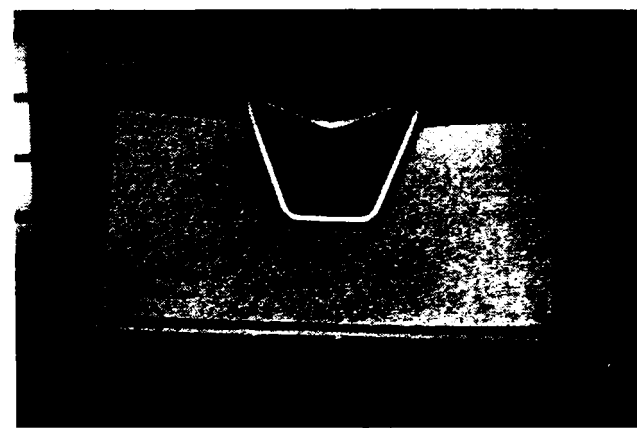
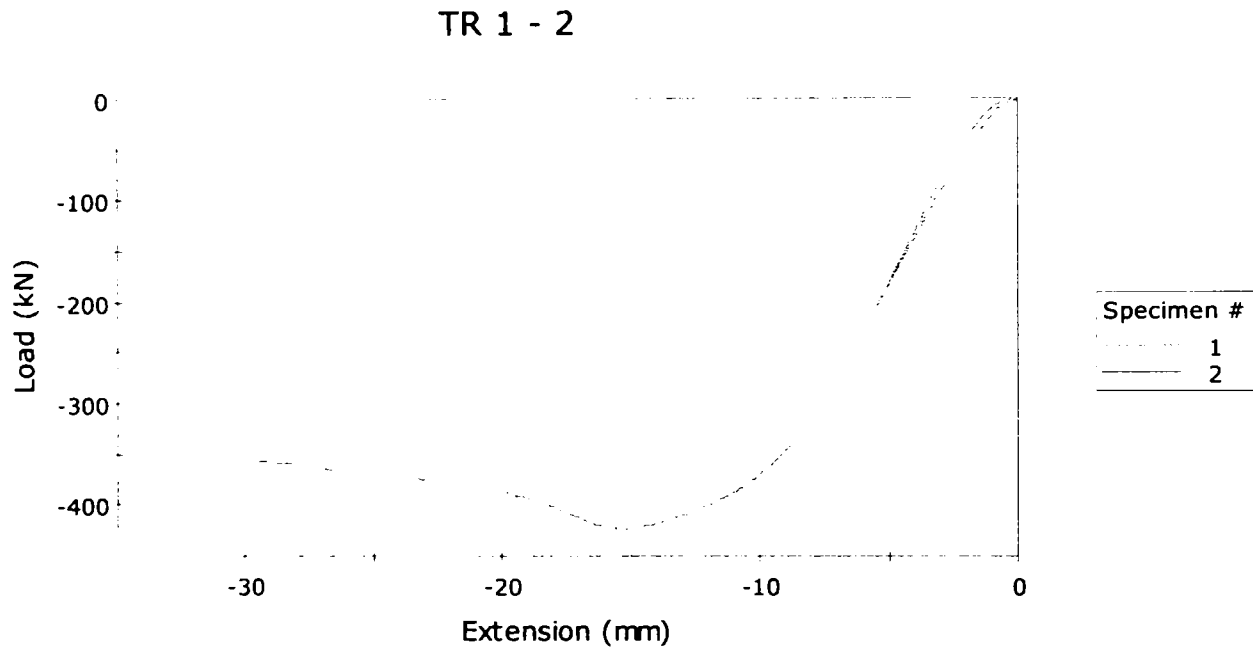


Fig. 3.29b. Type E test after sagging moment (M+)

3.4.2. Effect of hogging moment

Fig. 3.30-Fig. 3.32 show the experimental test results for the effect of hogging moment. (R-2, S-2, E-2)



	Specimen label	Minimum Load (kN)	Extension at Minimum Load (mm)
1	TR1-2	-185,862	-5,028
2	TR1-2	-422,982	-15,243

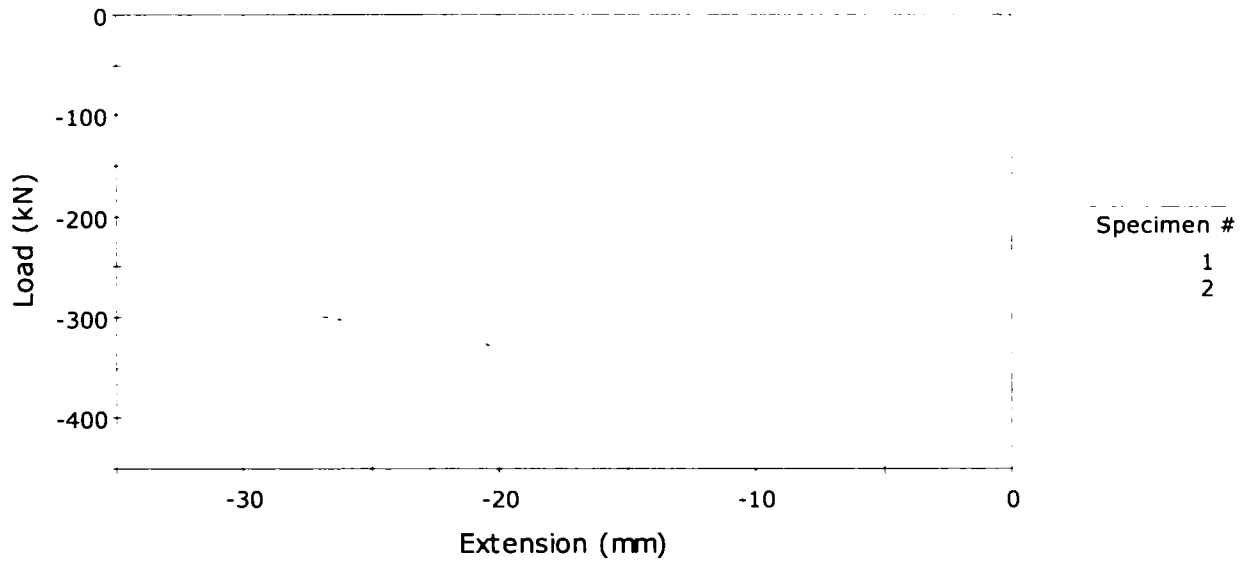
	Load at Maximum Time (kN)	Extension at Maximum Time (mm)	Load at Minimum Extension (kN)
1	-185,862	-5,028	-185,837
2	-344,657	-32,566	-344,678

	Start Date	End Date	Maximum Time (sec)
1	2006.02.03. 15:09:02	2006.02.03. 15:19:05	603,25
2	2006.02.03. 15:19:23	2006.02.03. 16:24:35	3911,80

	Time at Minimum Load (sec)	Time at Minimum Extension (sec)
1	603,25	603,20
2	1832,60	3911,60

Fig. 3.30. Load-extension curve for TR R-2

TR 2 - 2



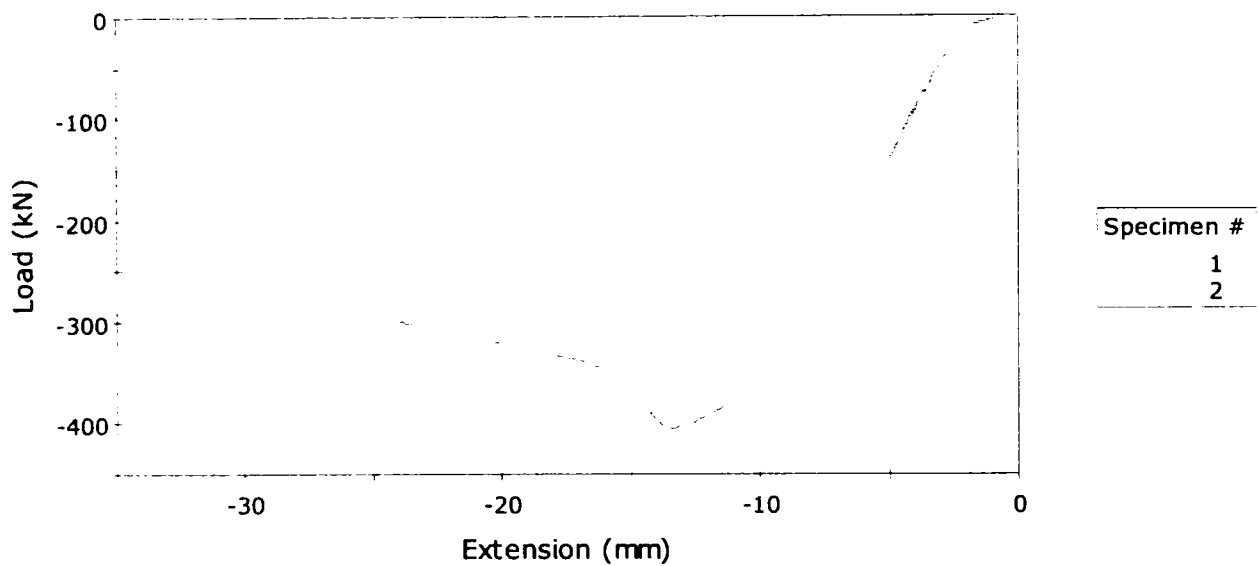
	Specimen label	Minimum Load (kN)	Extension at Minimum Load (mm)
1	TR2-2	-180,316	-5,017
2	TR2-2	-404,243	-13,032

	Load at Maximum Time (kN)	Extension at Maximum Time (mm)	Load at Minimum Extension (kN)
1	-180,316	-5,017	-180,303
2	-275,368	-32,560	-275,368

	Start Date	End Date	Maximum Time (sec)
1	2006.02.04. 08:50:00	2006.02.04. 09:00:02	601,83
2	2006.02.04. 09:00:18	2006.02.04. 10:05:29	3910,93

Fig. 3.31. Load-extension curve for TR S-2

TR 3 - 2



	Specimen label	Minimum Load (kN)	Extension at Minimum Load (mm)
1	TR3-2	-142,636	-5,013
2	TR3-2	-404,934	-13,423

	Load at Maximum Time (kN)	Extension at Maximum Time (mm)	Load at Minimum Extension (kN)
1	-142,636	-5,013	-142,579
2	-257,771	-32,558	-257,771

	Start Date	End Date	Maximum Time (sec)
1	2006.02.04. 11:32:52	2006.02.04. 11:42:54	601,69
2	2006.02.04. 11:43:09	2006.02.04. 12:48:20	3910,77

Fig. 3.32. Load-extension curve for TR E-2

Fig. 3.33 shows the load–displacement curves for specimens R–2, S–2 and E–2. In these cases the hogging moment causes tension in the stiffened plate.

The shape of the load–deflection curves and the load carrying capacity are similar, however the softening part of curve R–2 is higher than the softening part of curves S–2 and E–2. On the other hand the failure mode of the specimens is quite different (Fig. 3.34. Fig. 3.35 and Fig. 3.36).

TR R-2; TR S-2; TR E-2

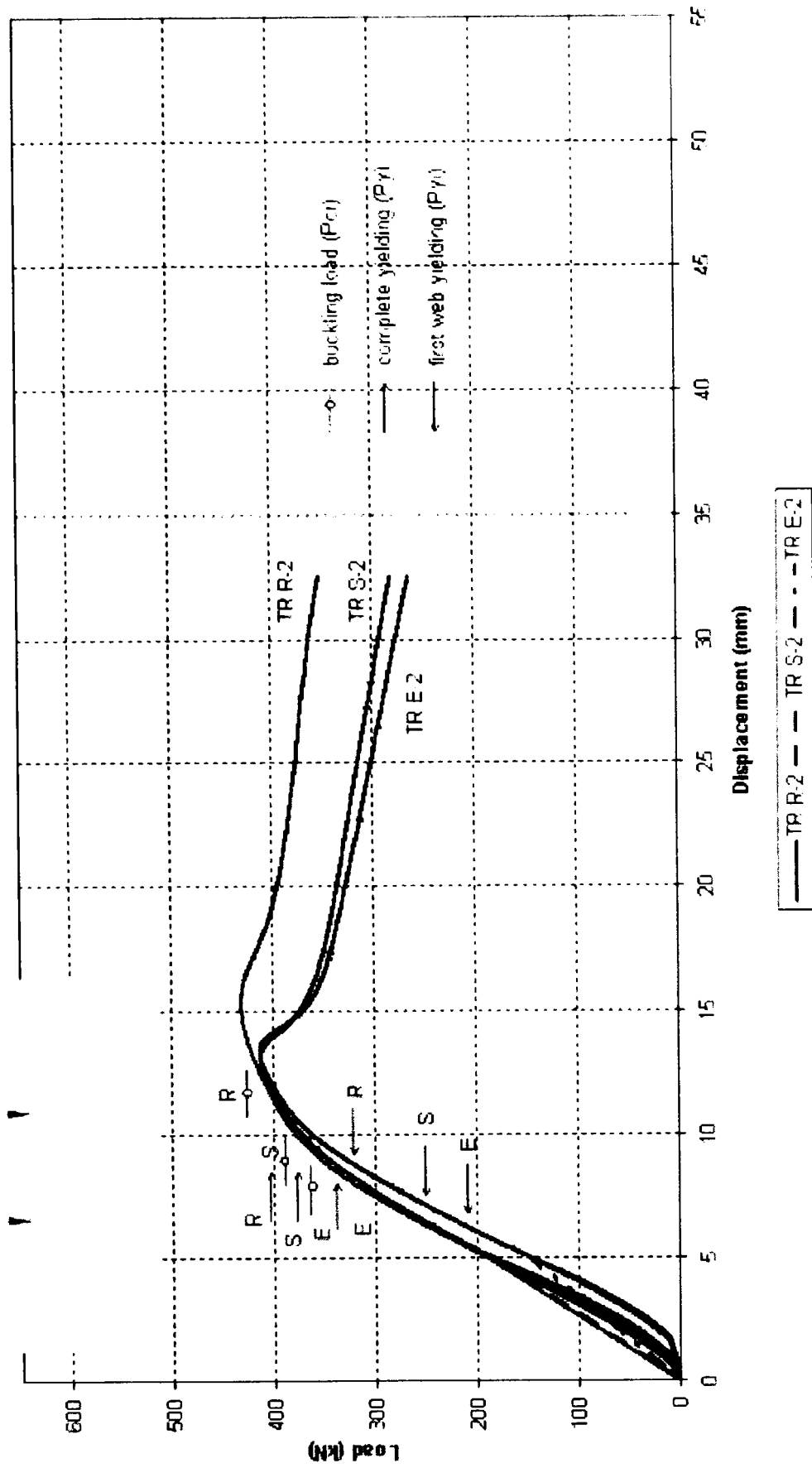


Fig. 3.33. Load-displacement curves at hogging moment (M-)

In the case of specimen R-2 the web and the flange of the cross-girder near to the trapezoidal stiffener have buckled out together. However the trapezoidal stiffener and the plate between the two points where the trapezoidal stiffener is attached to the plate are unbuckled. In the case of specimen S-2 the web of the cross girder has buckled between the top edge of the hole and the flange of the cross girder.

Moreover, the part of the flange has also buckled out in the region of the buckled web. In the case of specimen E-2 the web of the cross girder has also buckled, but in a larger region, between the stiffened plate and the flange of the cross girder. Similarly to the previous case the flange of the cross girder has also buckled.



Fig. 3.34a. Type R test after hogging moment (M-)

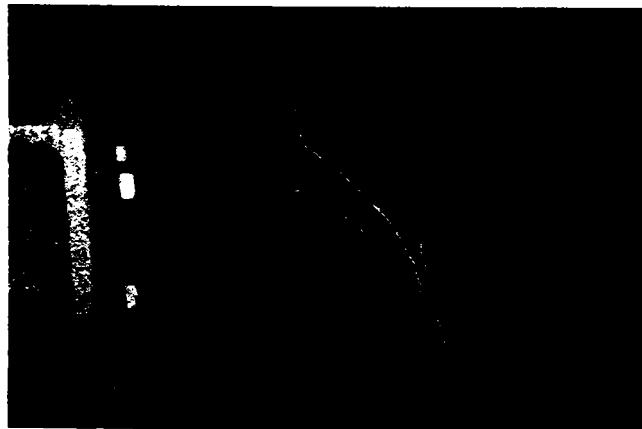


Fig. 3.34b. Type R test after hogging moment (M-)

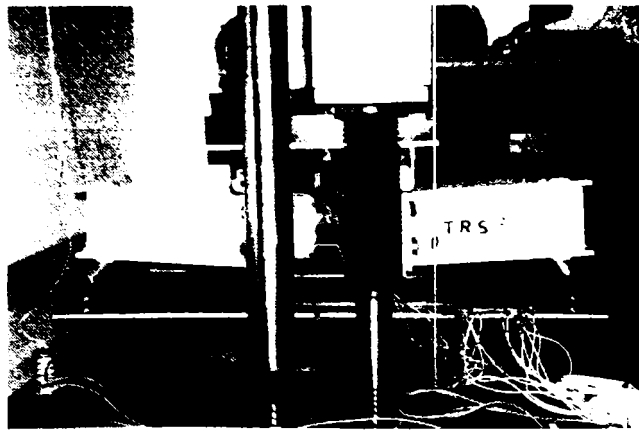


Fig. 3.35a. Type S test after hogging moment (M-)



Fig. 3.35b. Type S test after hogging moment (M-)



Fig. 3.36a. Type E test after hogging moment (M-)

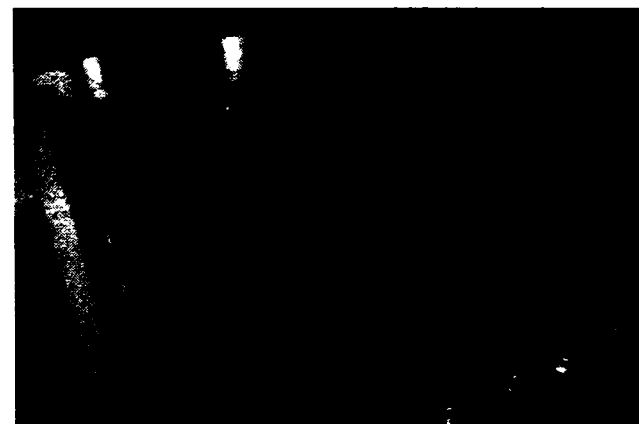
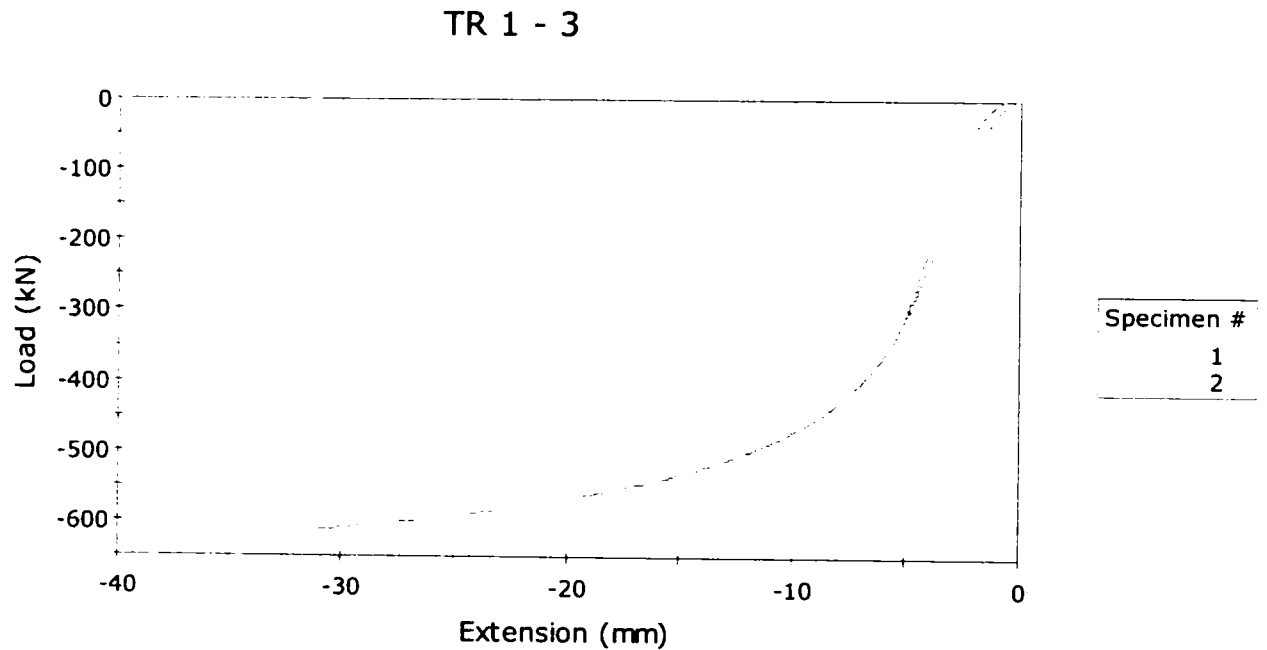


Fig. 3.36b. Type E test after hogging moment (M-)

3.4.3. Effect of shear loading

Fig. 3.37- Fig. 3.39 show the experimental tests results for effect of shear loading.



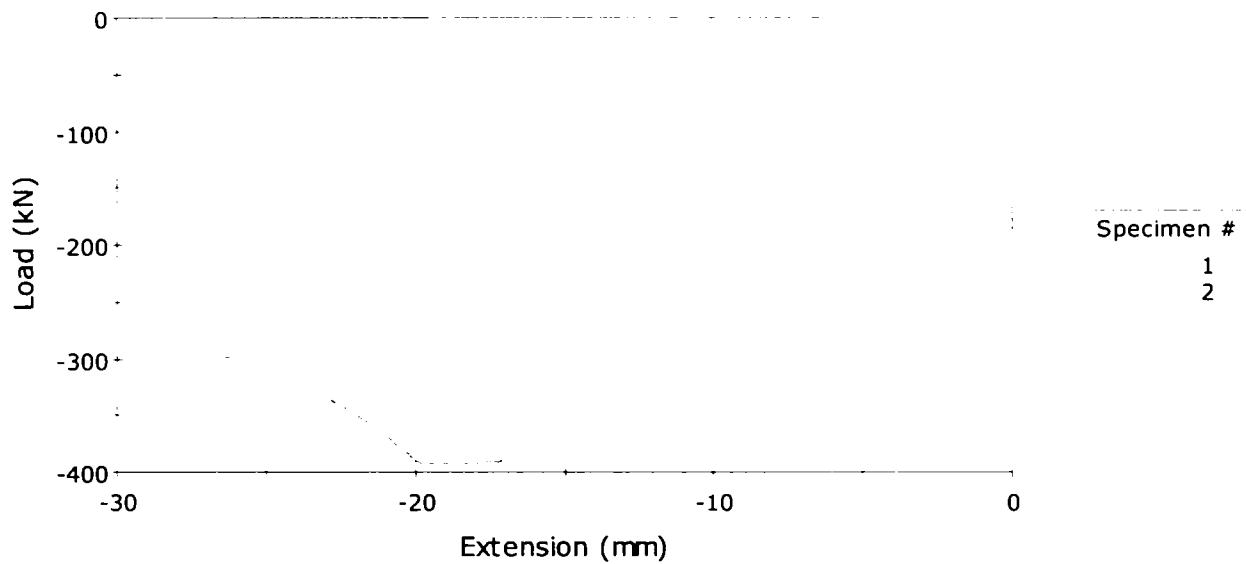
	Specimen label	Minimum Load (kN)	Extension at Minimum Load (mm)
1	TR1-3	-307,876	-5,004
2	TR1-3	-623,494	-35,532

	Load at Maximum Time (kN)	Extension at Maximum Time (mm)	Load at Minimum Extension (kN)
1	-307,876	-5,004	-307,847
2	-623,458	-35,534	-623,461

	Start Date	End Date	Maximum Time (sec)
1	2006.02.04. 15:34:08	2006.02.04. 15:44:10	601,25
2	2006.02.04. 15:44:24	2006.02.04. 16:55:32	4268,01

Fig. 3.37. Load-extension curve for TR R-3

TR 2 - 3



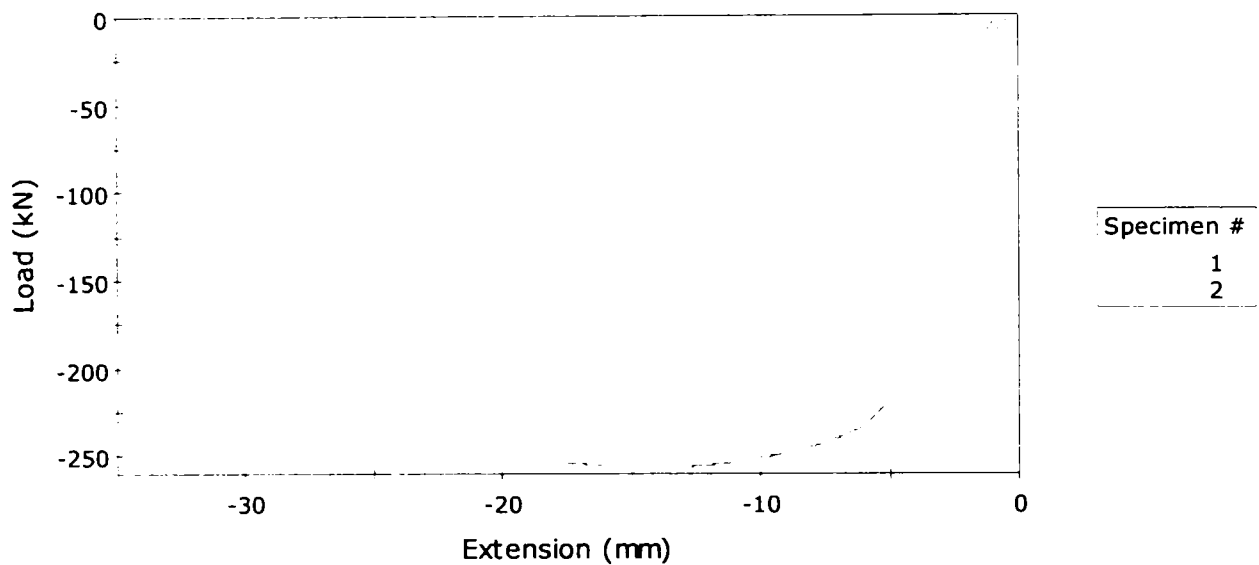
	Specimen label	Minimum Load (kN)	Extension at Minimum Load (mm)
1	TR2-3	-163,902	-4,007
2	TR2-3	-392,586	-18,535

	Load at Maximum Time (kN)	Extension at Maximum Time (mm)	Load at Minimum Extension (kN)
1	-163,902	-4,007	-163,837
2	-294,571	-27,131	-294,571

	Start Date	End Date	Maximum Time (sec)
1	2006.02.04. 18:48:18	2006.02.04. 18:56:19	481,03
2	2006.02.04. 19:02:50	2006.02.04. 19:57:09	3259,36

Fig. 3.38. Load-extension curve for TR S-3

TR 3 - 3



	Specimen label	Minimum Load (kN)	Extension at Minimum Load (mm)
1	TR3-3	-173,163	-4,023
2	TR3-3	-256,990	-14,200

	Load at Maximum Time (kN)	Extension at Maximum Time (mm)	Load at Minimum Extension (kN)
1	-173,163	-4,023	-173,127
2	-167,095	-30,104	-167,121

	Start Date	End Date	Maximum Time (sec)
1	2006.02.05. 08:40:46	2006.02.05. 08:48:49	483,12
2	2006.02.05. 08:49:06	2006.02.05. 09:49:23	3616,07

Fig. 3.39. Load-extension curve for TR E-3

Fig. 3.40 shows the load-deflection curves for specimens R-3, S-3 and E-3. The loading for these specimens was shear force. The load-deflection curves are significantly different. In the case of specimen R-3 there is no softening in the curve even for large displacements. The curves for specimens S-3 and E-3 exhibit softening behavior, but there are significant differences between these softening behaviors.

The failure modes for these specimens are also different (Fig. 3.41, Fig. 3.42 and Fig. 3.43). In the case of specimen R-3 diagonal buckled waves appear in the web,

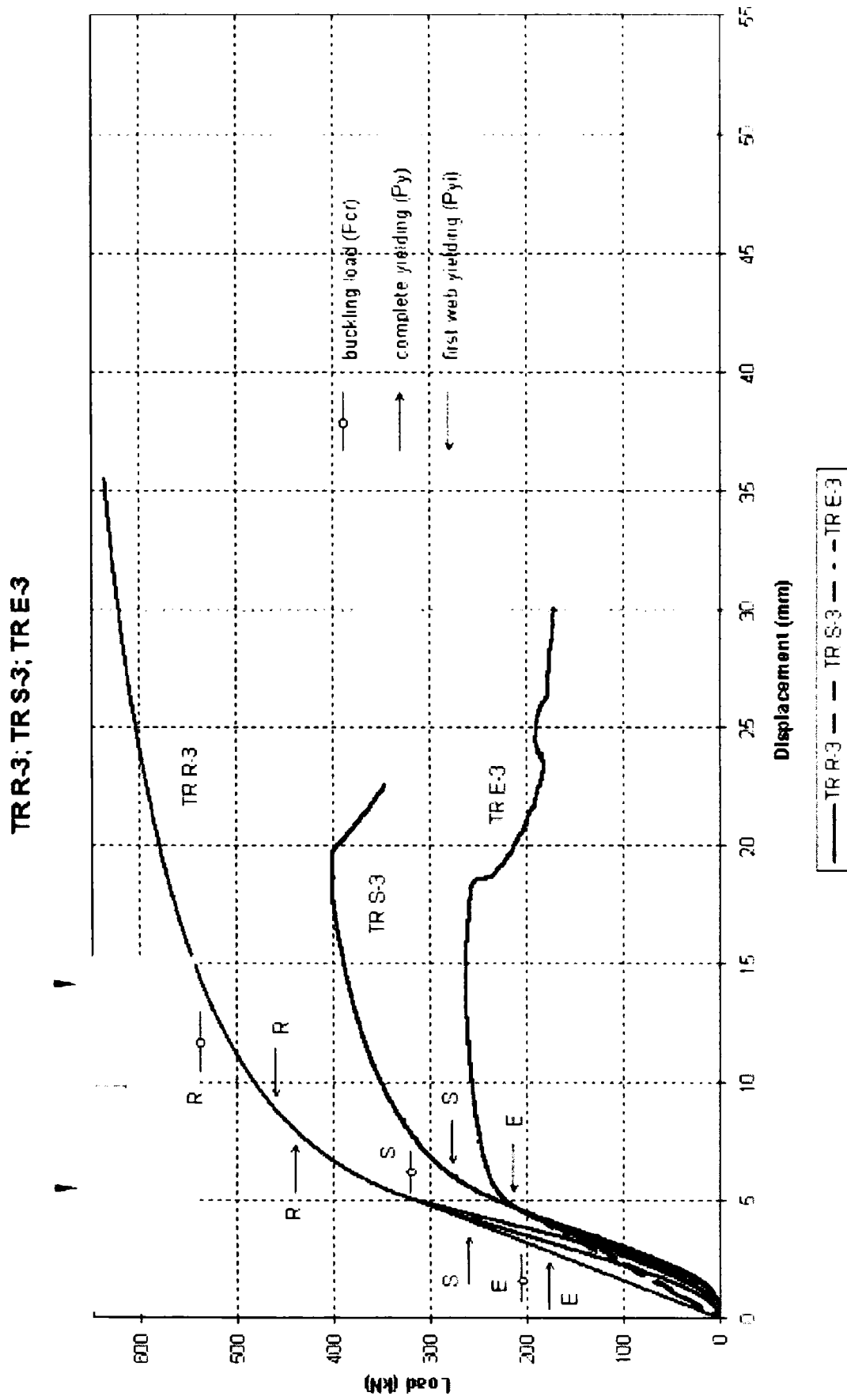


Fig. 3.40. Load-displacement curves at shear force (V)

however they are not significant at the ultimate failure state. In the case of specimen S-3 apparent compressed and tensioned zones are formed at two ends of the hole. In the compressed zone the diagonal waves are more significant than in the case of specimen R-3.

Furthermore in the tensioned zone as a result of the large tension force the web plate is fractured. The failure mode for specimen E-3 is similar to the failure mode for specimen S-3. However the tension is so high at one end of the hole that the weld between the web of the cross girder and the stiffened plate is also fractured.

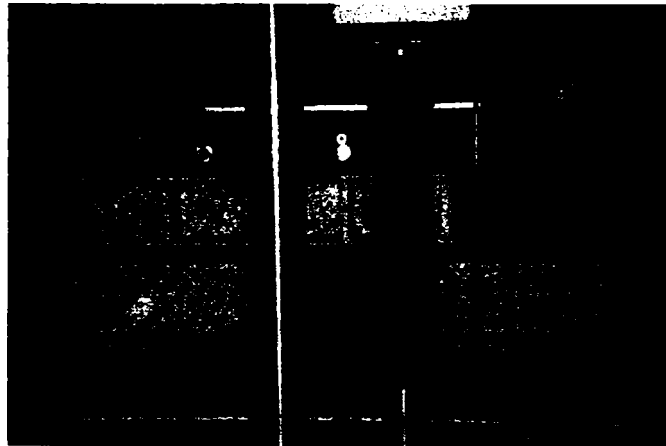


Fig. 3.41a. Type R test after shear force (V)

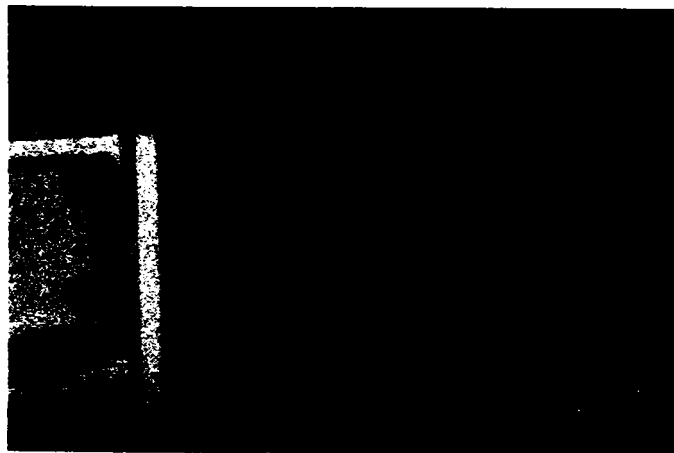


Fig. 3.41b. Type R test after shear force (V)



Fig. 3.42a Type S test after shear force (V)

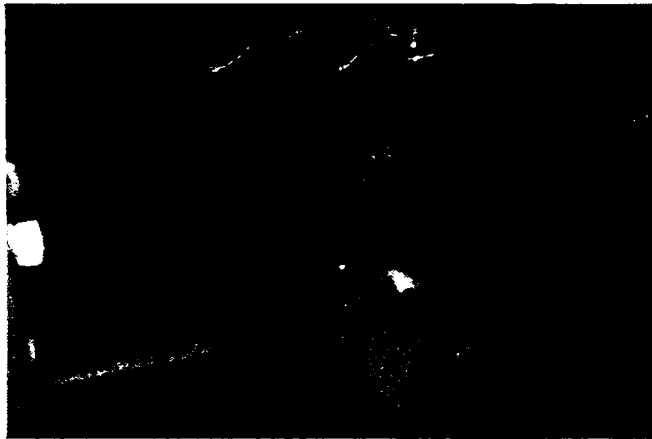


Fig. 3.42b Type S test after shear force (V)

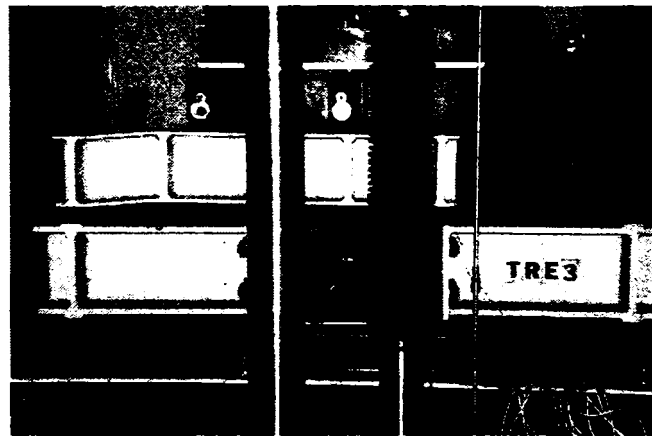


Fig. 3.43a Type E test after shear force (V)



Fig. 3.43b Type E test after shear force (V)

3.5. The results of strain measurements

In Fig. 3.11 the geometric arrangements of the strain gauges is shown. The strain gauges were connected to a device (Spider) to collect the measurements. Fig. 3.44- Fig. 3.52 shows the measured values in relation to loading. In the figures the uncertainties are still visible, which are mostly specific to the plastic state. During the experiments the strain was measured directly, however in the figures – to be able to display in a more meaningful way – the strain multiplied by the Young's modulus is shown. This value can be called as stress, but after yielding this can be called only "formally" as stress.

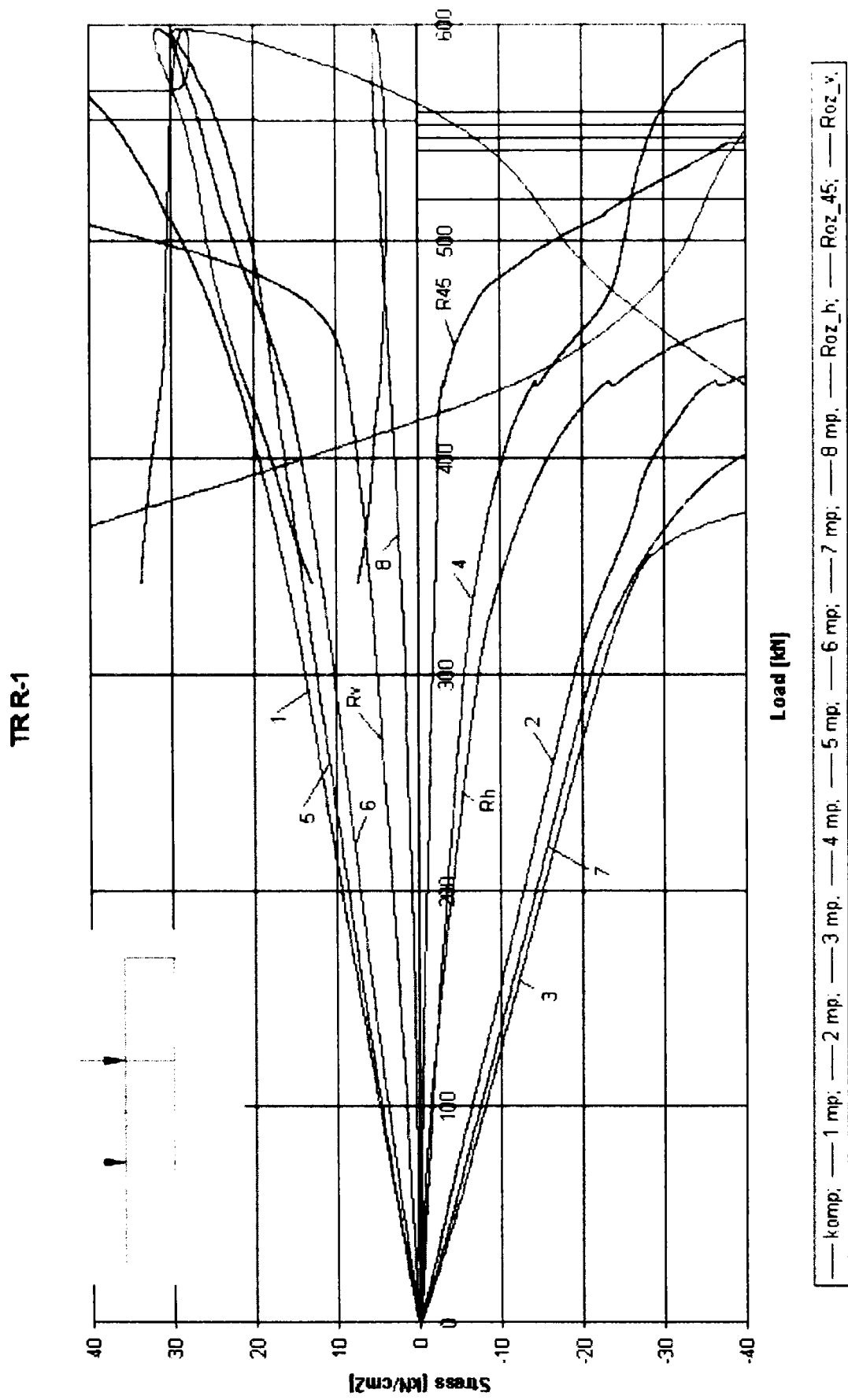


Fig. 3.44. TR R-1 Load - Stress curves

TR S-1

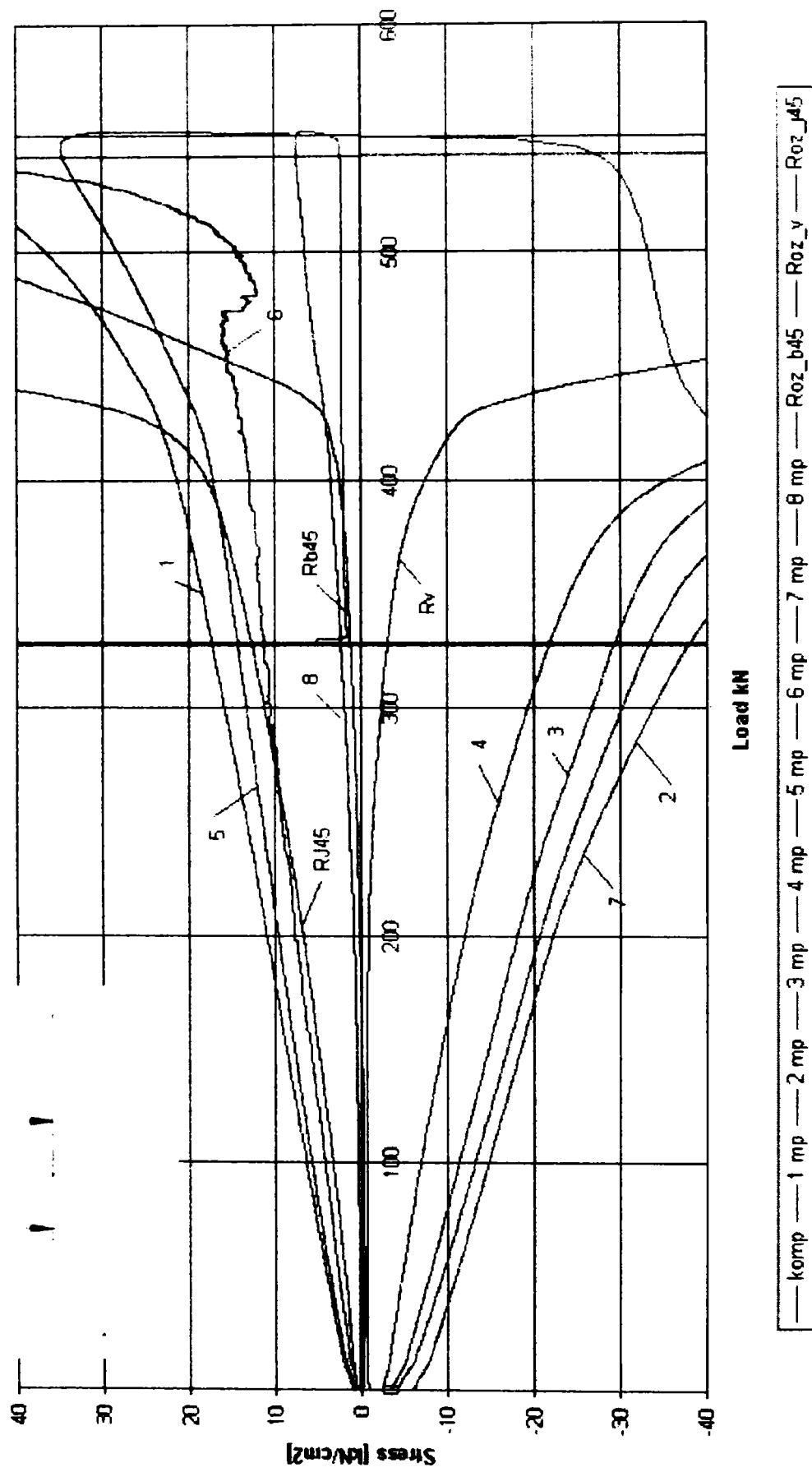


Fig. 3.45. TR S-1 Load - Stress curves

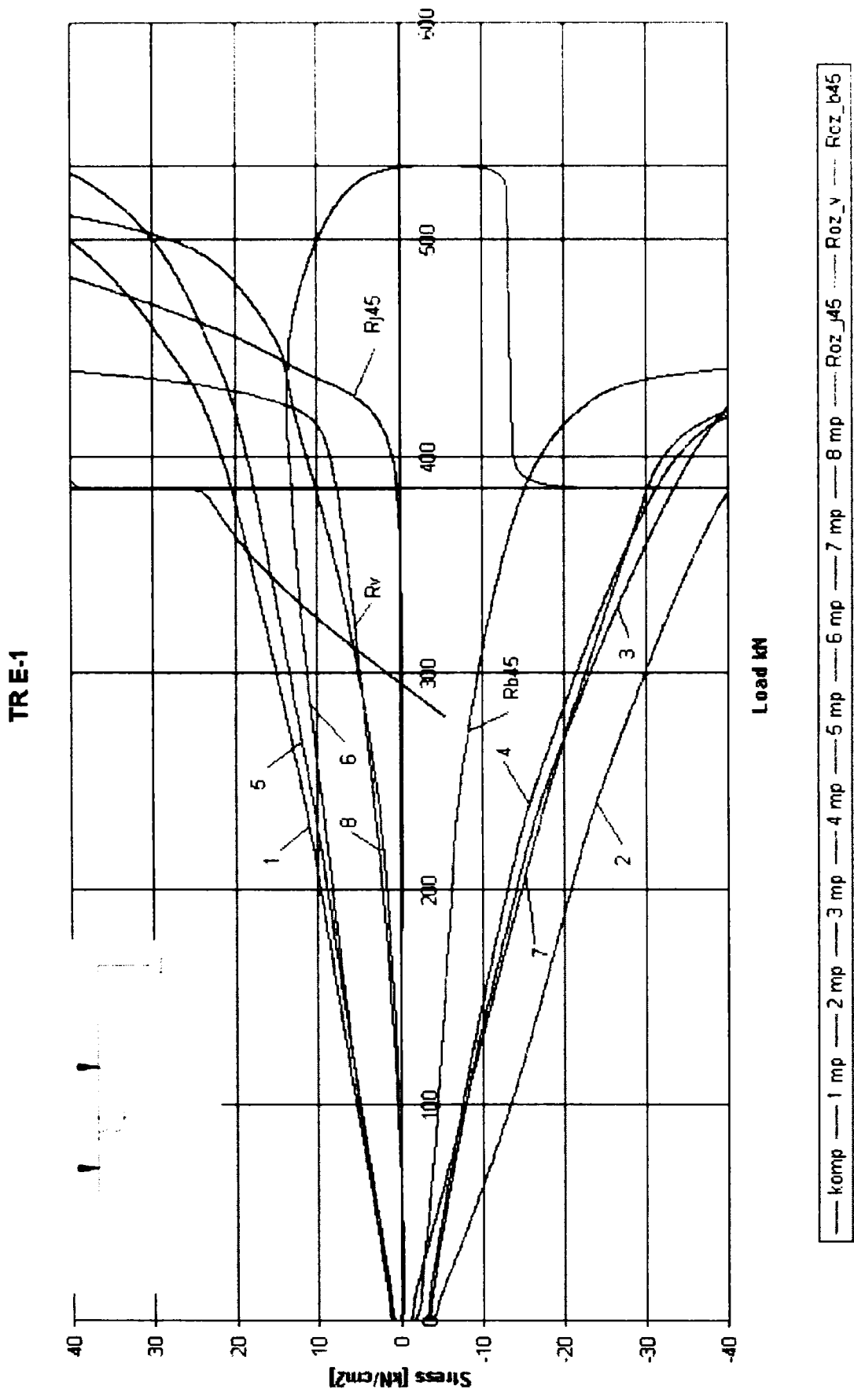


Fig. 3.46. TR E-1 Load - Stress curves

TR R-2

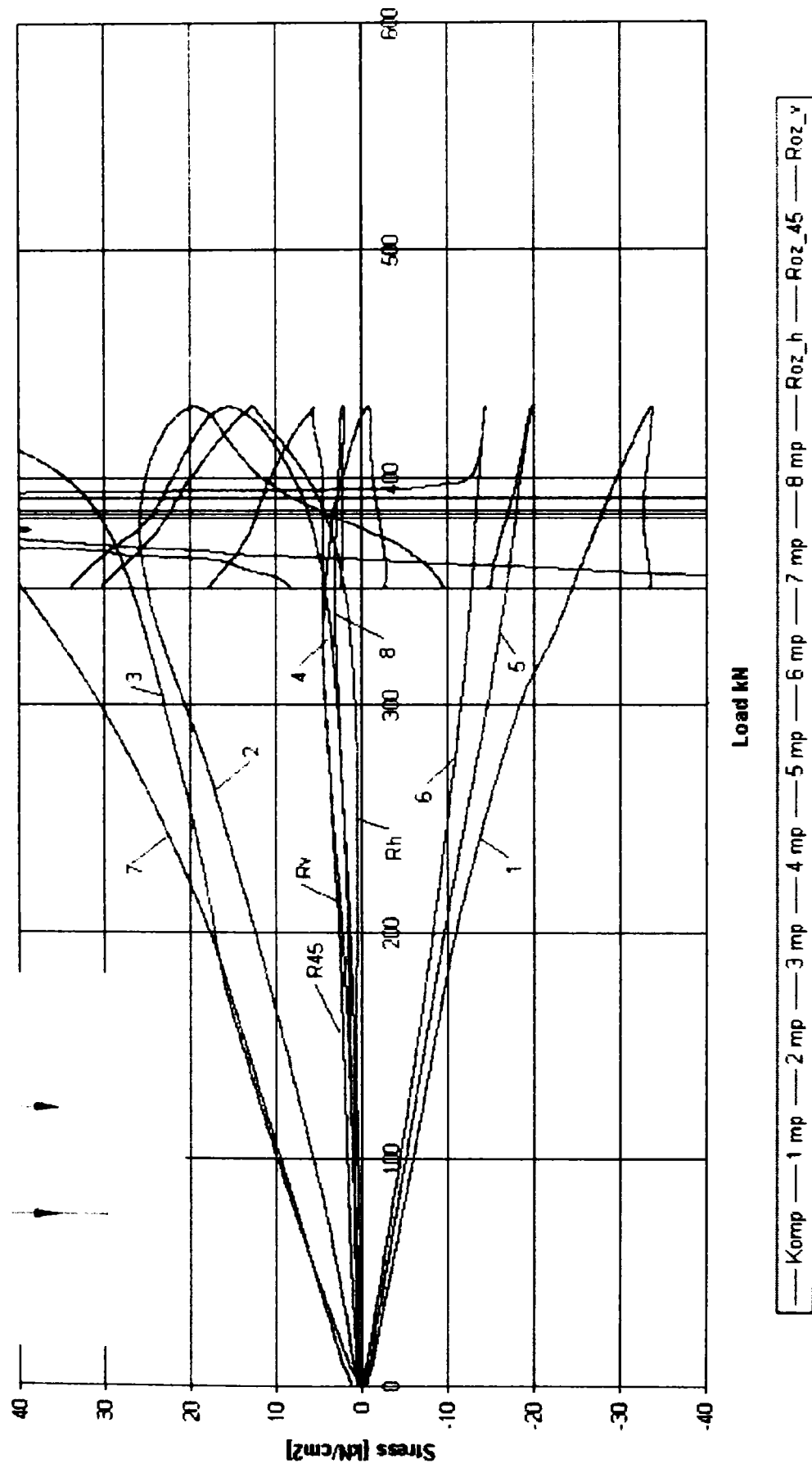


Fig. 3.47. TR R-2 Load - Stress curves

TR S-2

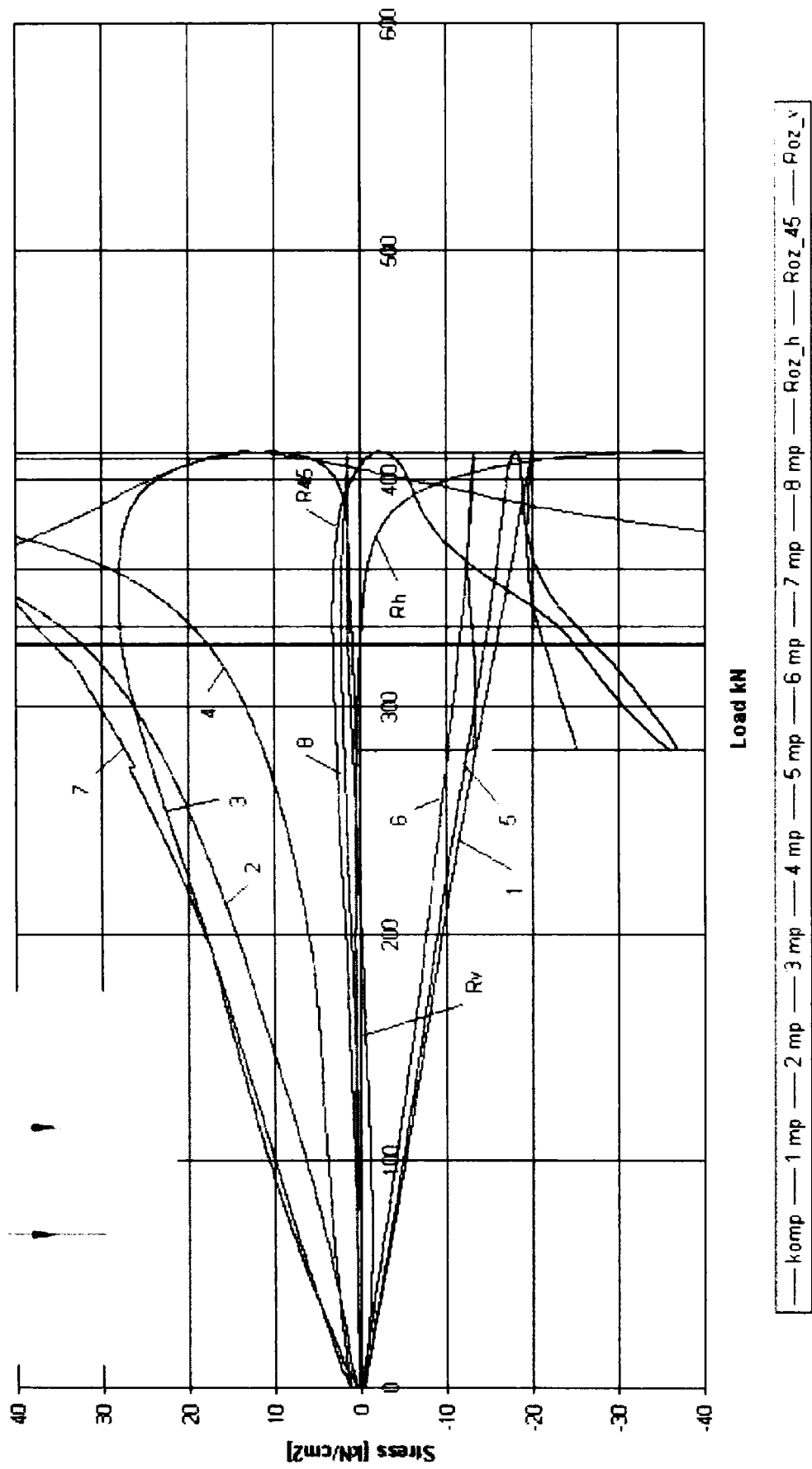


Fig. 3.48. TR S-2 Load - Stress curves

TR E-2

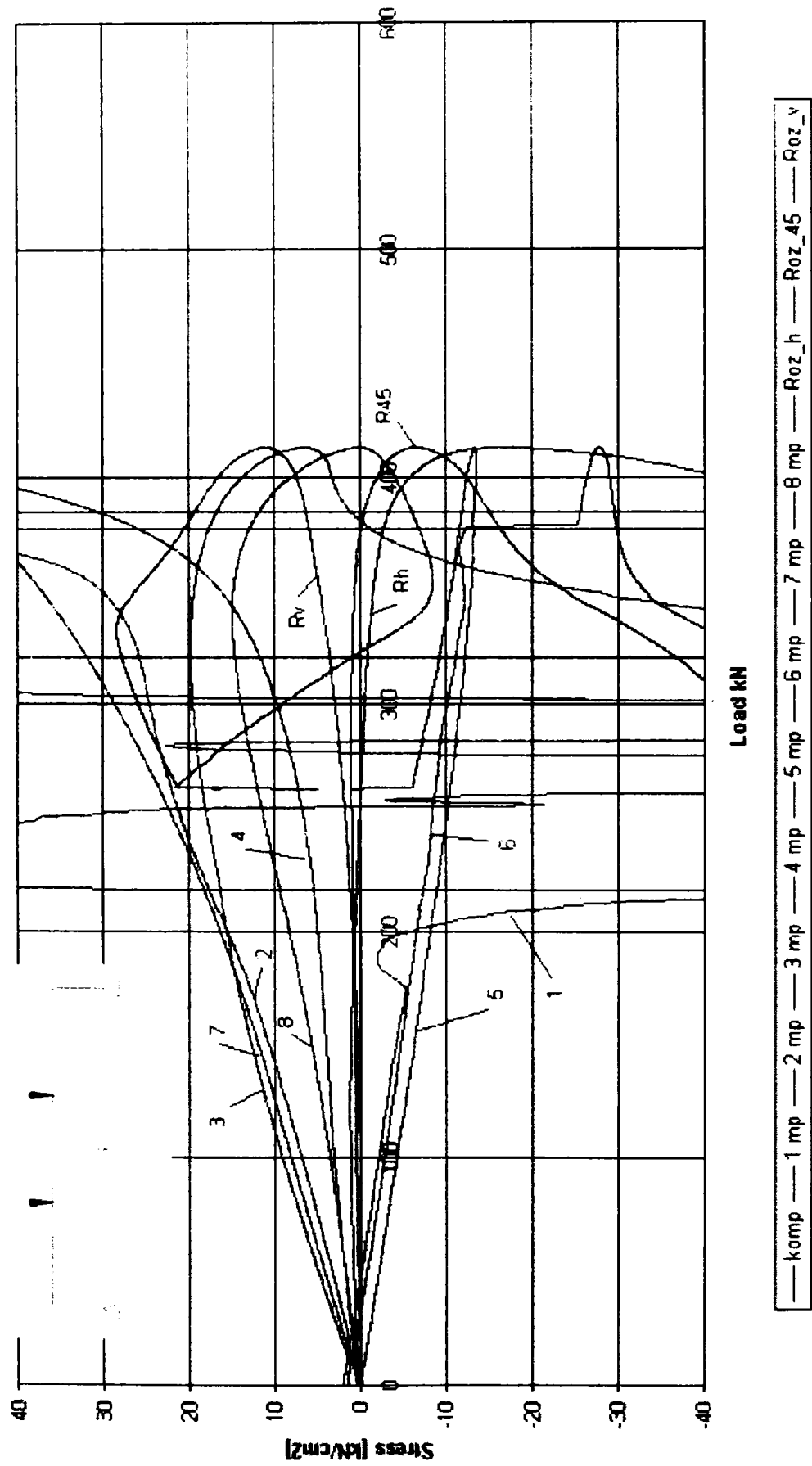


Fig. 3.49. TR E-2 Load - Stress curves

TR R-3

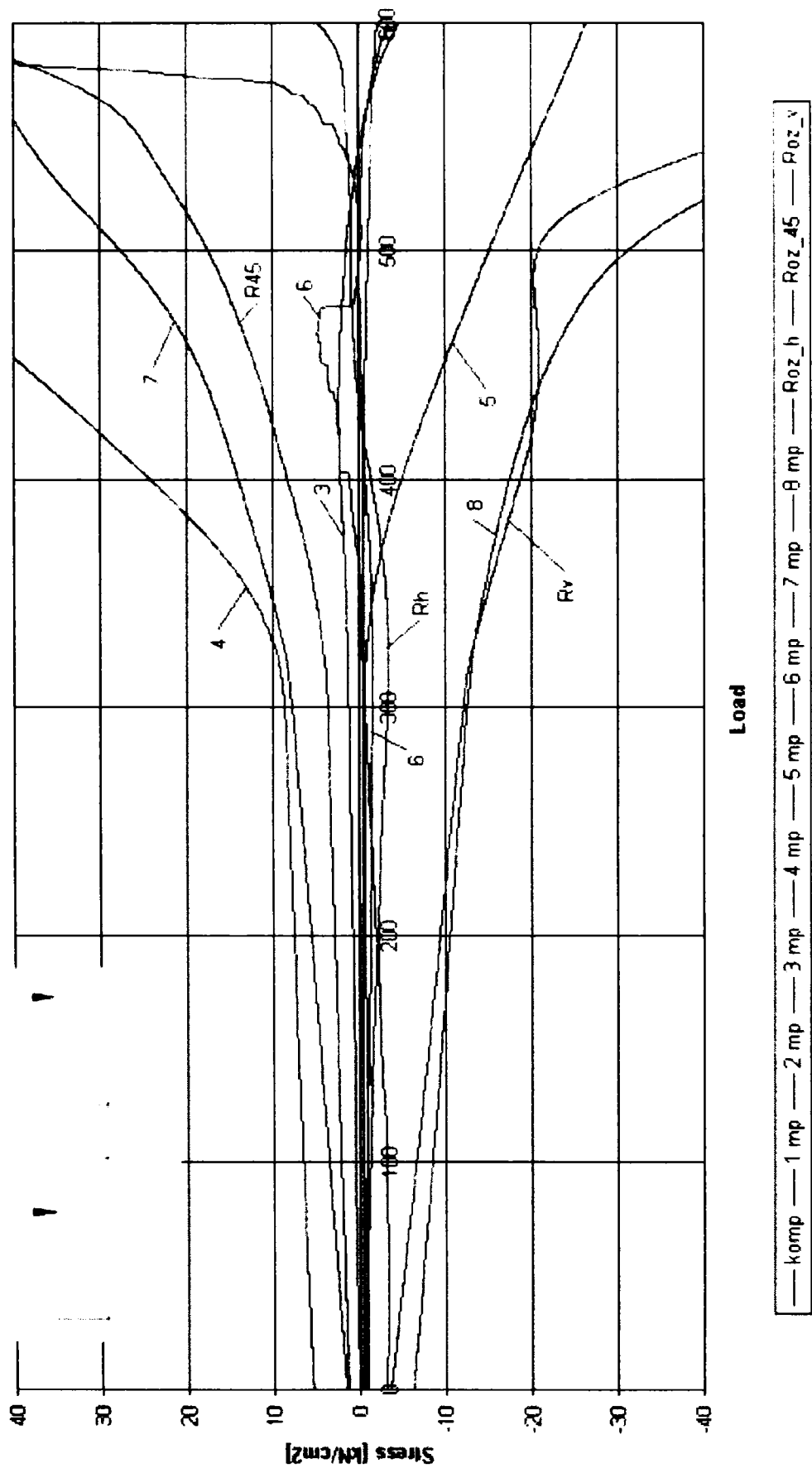


Fig. 3.50. TR R-3 Load - Stress curves

TR S-3

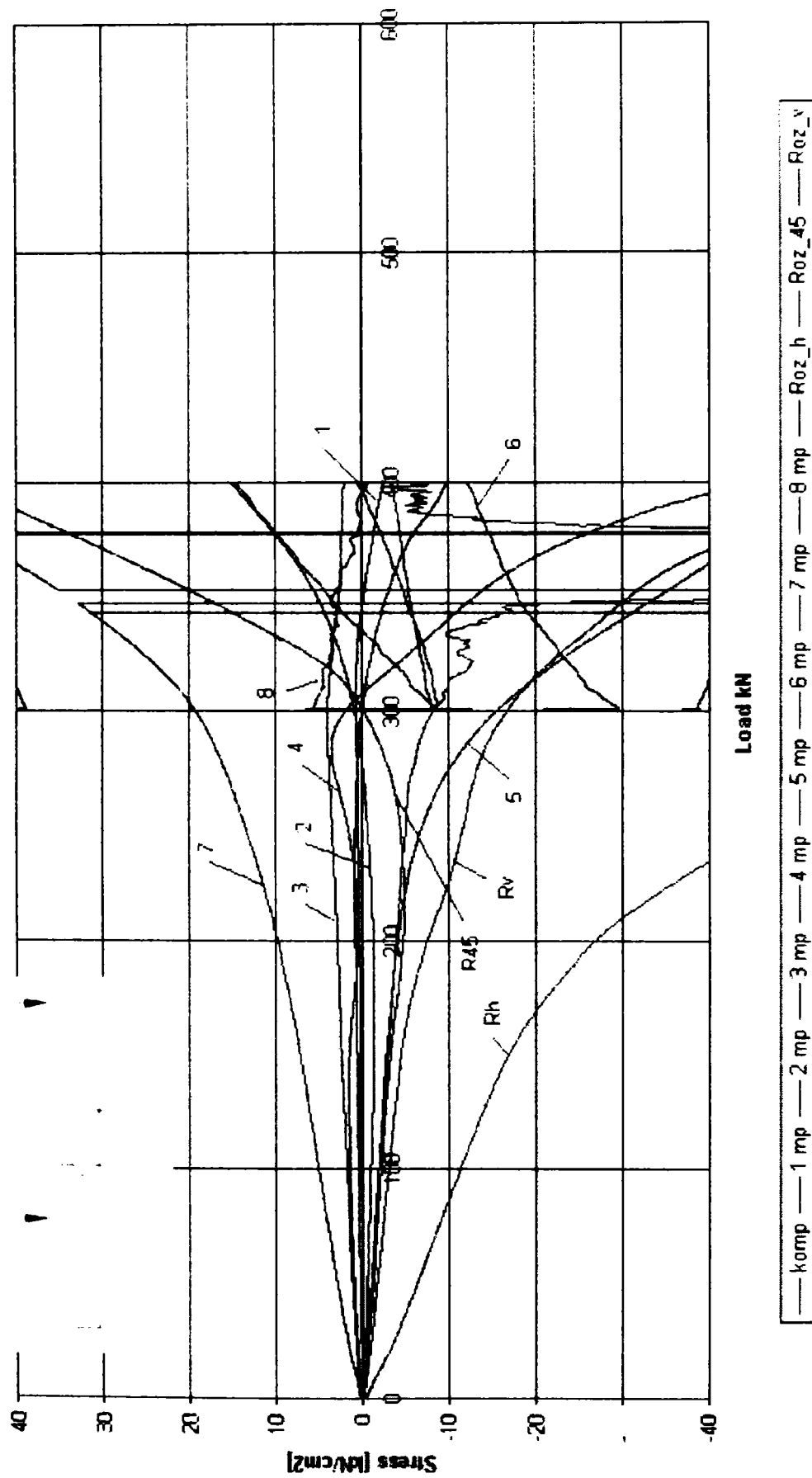


Fig. 3.51. TR S-3 Load - Stress curves

TRE3

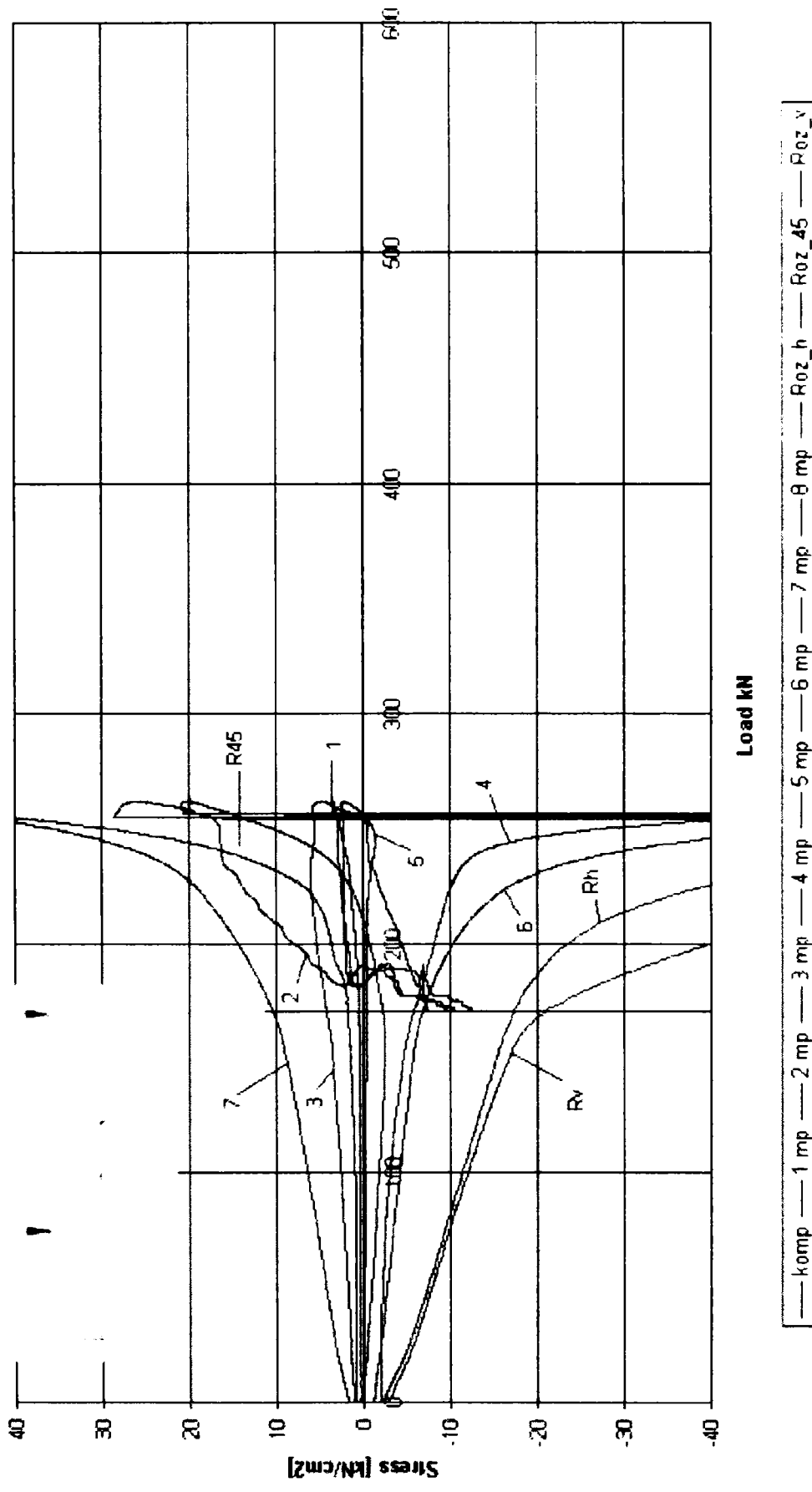


Fig. 3.52. TR E-3 Load - Stress curves

3.6. Elastic behaviour of web with U-shaped holes

3.6.1. Bending stress

The bending stress distributions of the web cross section are shown in Fig. 3.53- Fig. 3.55 for specimens respectively. Strain gauges 1 – 4 provide the stress through the measured strain at the middle of the U-shaped hole at the load level $F=200\text{kN}$. Strain gauges 6 and 7 provide the stress at the edge of the U-shape hole at the load level $F=200\text{kN}$. The stresses can be determined from the measurement of strain gauge 8 at the point where the U-shape hole starts in the web of the cross girder. The rosette of strain gauges 9 – 11 at the corner of the U-shape hole as shown in Fig. 3.11.

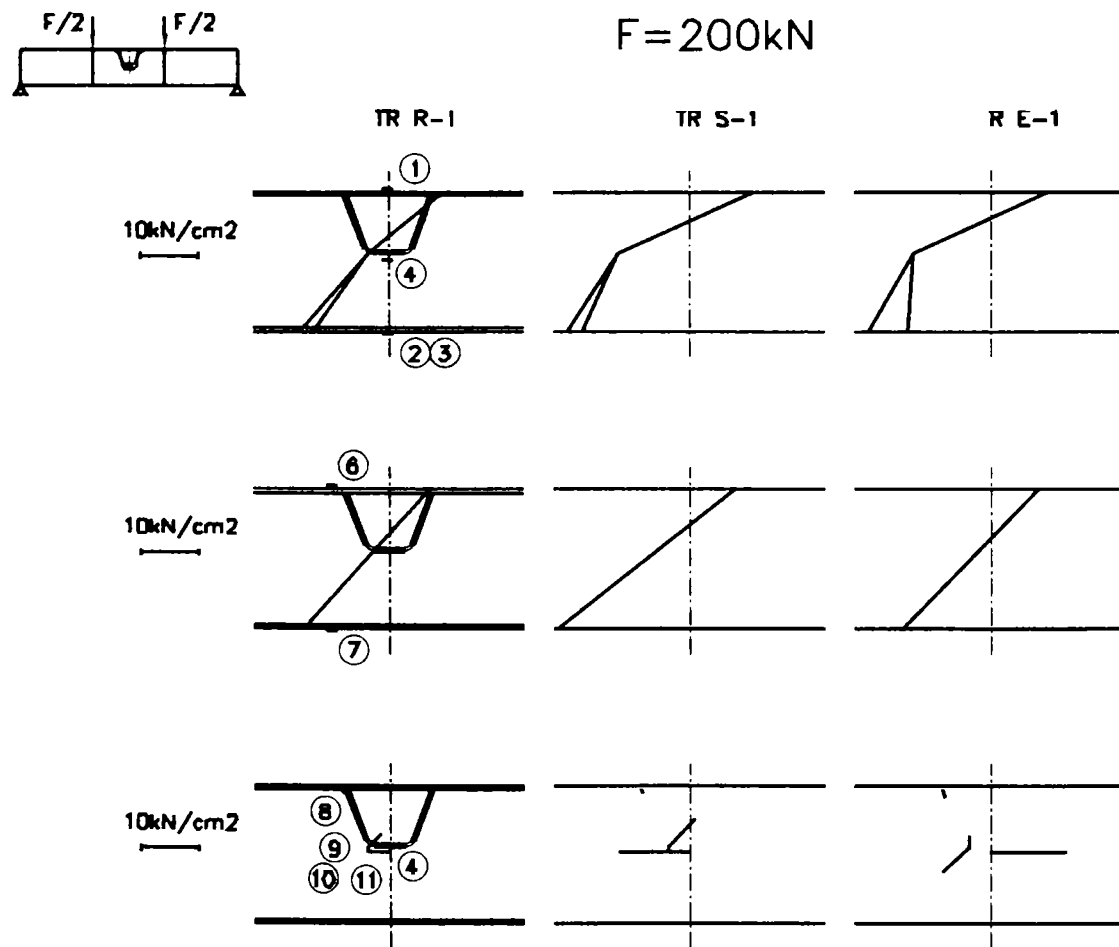


Fig. 3.53. Effect of sagging moment for the distribution of stresses

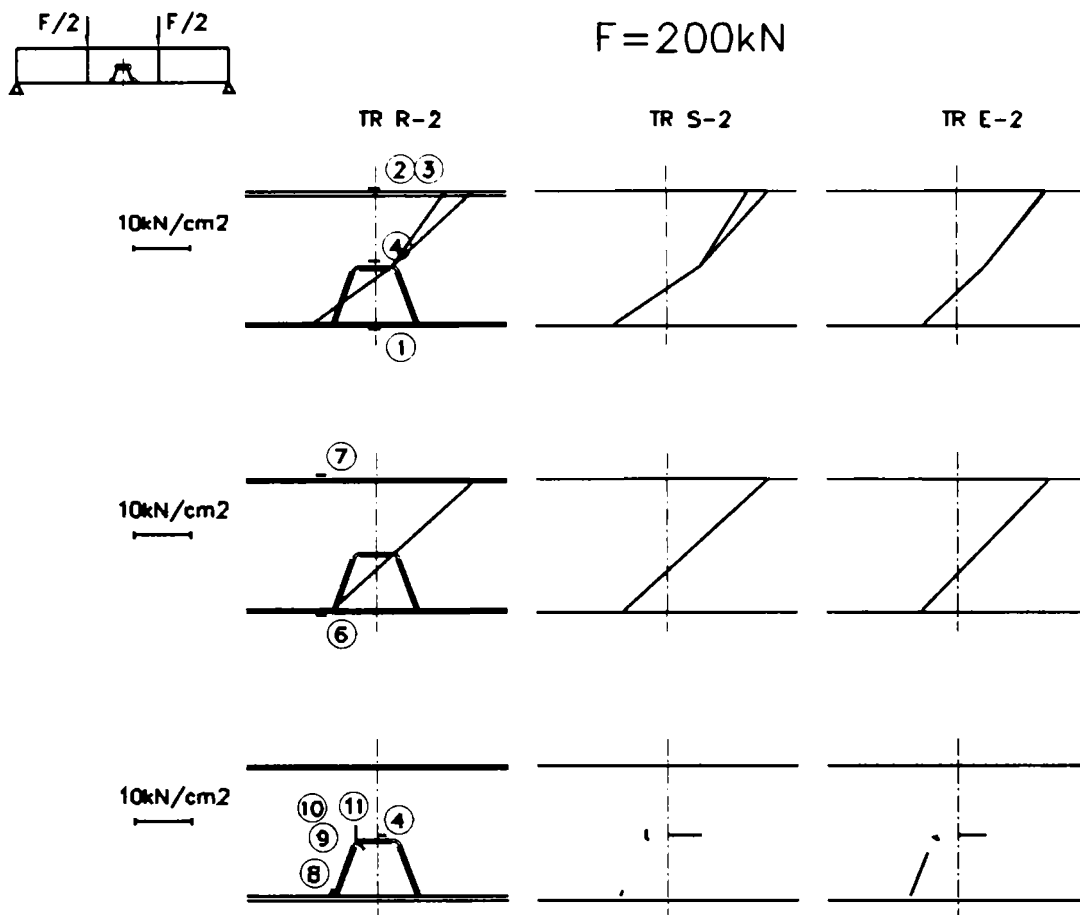


Fig. 3.54. Effect of hogging moment for the distribution of stresses

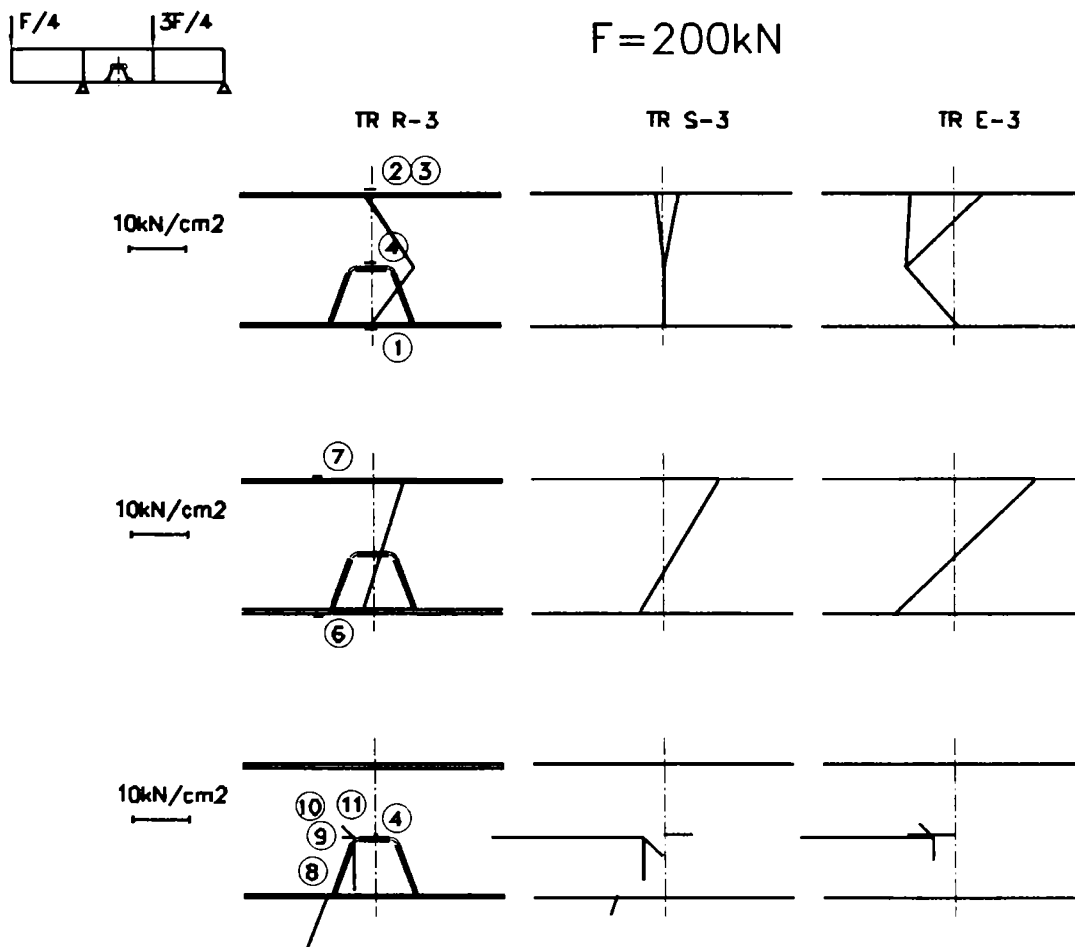


Fig. 3.55. Effect of shear loading for the distribution of stresses

3.6.2. Vierendeel behaviour

Beams with U-shaped holes in the web as used in this test are predicted to behave differently from standard beams without openings in the web.

This different behaviour is explained as follows in Fig. 3.56, ITO M. et al (1991). The bending moment $M=Rx$, where R -reactions, x -distance from the support, and the shearing force $V=V_1+V_2$ are assumed to act on the section of the center part for beams with U-shaped holes, where V_1 and V_2 - the shearing forces acting upon the T-shaped sections that correspond to the section under the U-shaped holes and the upper flange, respectively. The V_1 and V_2 values are assumed to be distributed according to ratios of the moments of inertia of the T-shaped sections and the upper flanges.

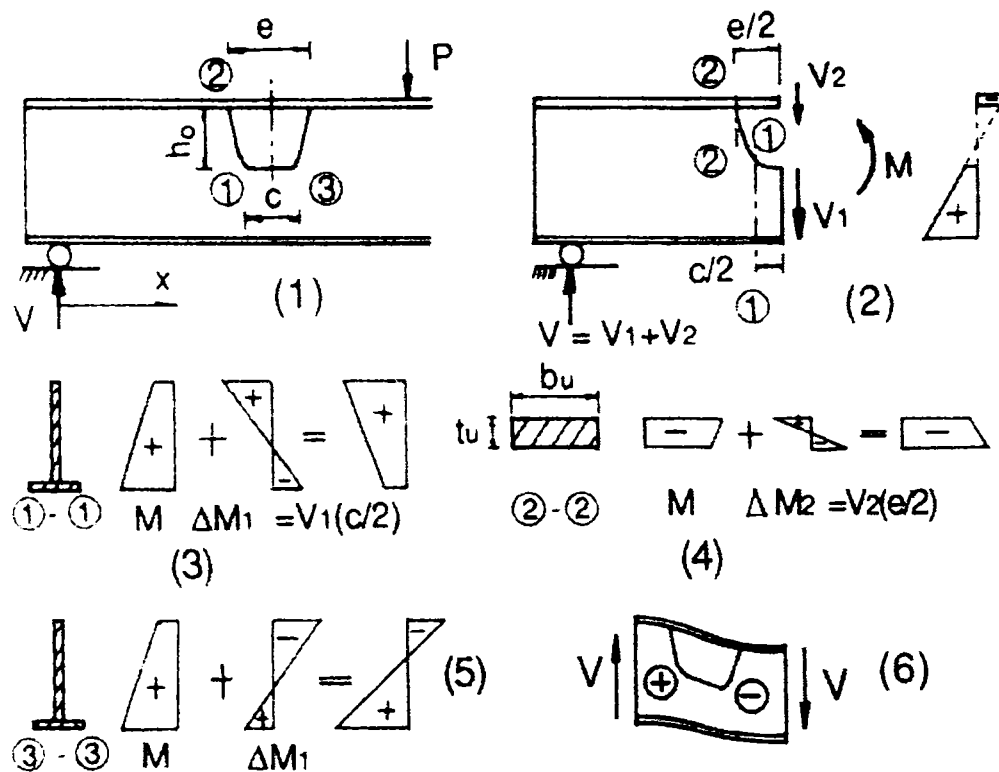


Fig. 3.56. Vierendeel action of U-shape holes, ITO M. et al (1991)

The V_1 and V_2 values are calculated as follows:

$$V_1 = \frac{V}{1 + \left(\frac{I_e}{I_c}\right)\left(\frac{c}{e}\right)^3}, \quad V_2 = \frac{V}{1 + \left(\frac{I_c}{I_e}\right)\left(\frac{e}{c}\right)^3},$$

where I_c and I_e – the moments of inertia of the T-shaped sections and the upper flange sections and c and e – the upper and bottom widths of the U-shaped holes Fig. 3.56, respectively.

In Fig. 3.56, the additional moments $\Delta M_1 = V_1(c/2)$ and $\Delta M_2 = V_2(e/2)$ produced at the sections 1-1 and the sections 2-2 by each of the shearing forces are shown in Fig. 3.56.

The tensile and compressive forces act on the sections of the right and left sides under the U-shaped holes. Such actions produce additional moments because of these shearing forces, which are called the Vierendeel action [e.g., BOWER(1966) and REDWOOD (1969)].

Overall, the theoretical values shown good agreement with the experimental values. Where they do diverge, it seems that the differences between the theoretical values and the experimental values were caused by the stress concentrations. Apparently, Vierendeel analysis is not limited to beam with circular or rectangular holes in the center part of the web, but may also be applied to beams with U-shaped holes in the top part of the web.

The magnitudes and directions of the principal stresses for the different specimens are shown in Fig. 3.53, – 3.55. The stress concentrations are considerably greater at the corner section of both sides of the right and left corners under the U-shaped holes.

3.6.3. Shearing stress

Assuming that the bending moments M_1 and M_2 , and the shearing forces $V = V_1 + V_2$ act between the center section of the U-shaped holes, as shown in Fig. 3.57a, ITO M. et al (1991), the arm length z of the resisting moments is $z = I_n / w_c$, where I_n – the moment of inertia in reference to the neutral axis, and w_c – the geometrical moment of area for the upper flange in reference to the neutral axis.

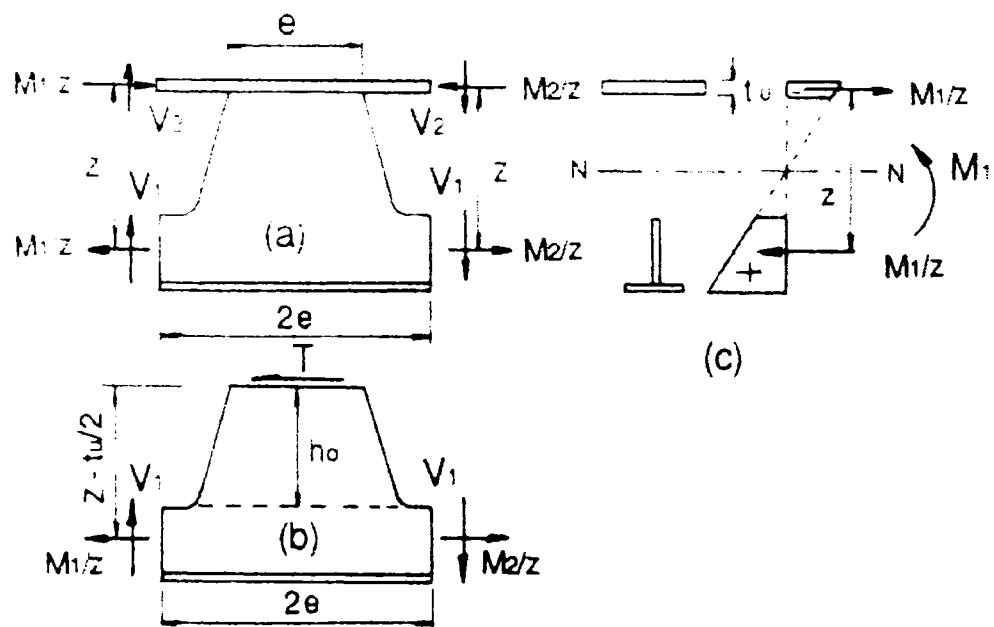


Fig. 3.57. Longitudinal shearing force, ITO M. et al (1991)

If it is now assumed that the axis force M_1/z acts at the center of the upper flange, since the thickness of the upper flange is small, the longitudinal shearing force V_H shown in Fig. 3.57b is obtained as follows:

$$V_H = \frac{4e}{2z - t_u} V_1.$$

Therefore, the longitudinal shearing stresses τ_V is obtained as $\tau_V = V_H / (e t_w)$, where e and t_w – the upper width of the U-shaped holes and the web thickness, respectively. It appears that the longitudinal shearing stresses acting on the web sections between the U-shaped holes can be predicted by ITO et al (1991).

3.7. Ultimate strength of test girders

3.7.1. Yielding of U-shaped sections

Fig. 3.26, Fig. 3.33, Fig. 3.40 show the load-deflection curves for the different specimens. The deflections of the beams with respect to the center part of the U-shaped holes in the vicinity of the loading point are shown as the abscissa. In these figures, the initial yield loads P_{yi} , when the experimental values showed that the corner edge of the U-shaped holes yielded first, are obtained. Further, the yield load P_y , at which it was predicted that both the web and the flange sections would yield completely, are obtained.

In general, the full plastic states of the experiment were predicted from the load-deflection curves or the moment-curvature curves. However, in such cases, it is difficult to determine exactly the full plastic state of the steel beams, because steel beams have strain-hardening properties and the yield stresses are different in different parts of the cross section.

The complete yield state of the U-shaped sections of this experiment is defined as the yield load P_y , obtained from the elastic curves in the foregoing load-deflection curves (Fig. 3.26, Fig. 3.33 and Fig. 3.40).

Table 3.2 shows each test load for all specimens. From Table 3.2 it can be seen that yielding, rather than buckling, has taken precedence. The maximum loads P_{max} in Table 3.2 show the loads obtained when the peak load in the load-deflection curve is reached, which occurs when buckling of the compression flange at the U-shaped holes in the vicinity of the loading points is observed.

The initial yield loads P_{yi} are smaller than P_y , P_{cr} , and P_{max} in Table 3.2 because the corner edges of the U-shaped holes carry both additional moments by Vierendeel action and the longitudinal shearing forces V_H in addition to the usual bending moment and shearing force. Therefore, it seems that this local yielding of the corner edges is not directly related to the ultimate strength of the beams. Accordingly, it is not necessary to consider this local yielding in the design of such beams.

Specimens	Loading	Initial yield load P_{yi} [kN]	Yield load P_y [kN]	Buckling load P_{cr} [kN]	Maximum load P_{max} [kN]
TR R-1	Sagging moment	381,0	420,1	580,1	595,0
TR S-1		310,0	400,5	530,2	542,4
TR E-1		245,1	385,0	510,5	524,2
TR R-2	Hogging moment	310,0	405,0	410,0	422,9
TR S-2		255,2	375,0	390,0	404,2
TR E-2		220,7	330,6	370,1	404,9
TR R-3	Shear load	450,3	475,2	508,0	623,5 *
TR S-3		272,4	317,1	315,4	392,6
TR E-3		186,2	210,7	196,2	256,9

* Load limit of the loading system has been reached

Table 3.2. Experimental beam load

3.7.2. Ultimate strength

In general, the ultimate strength analysis method (BOWER (1966), REDWOOD (1969)), taking account of Vierendeel action, as applied to rolled beams or welded beams with circular or rectangular holes in the center part of the web also appropriate for these beams.

In this study, BOWER's (1966) method is applied to test beams with U-shaped holes in the top part of the web. In this analysis the stress distribution at the ultimate load was assumed to be as shown in Fig. 3.58. In this case, it is assumed that the additional moment caused by Vierendeel action acts on the T-shaped section under the U-shaped holes and that the shearing stress is carried uniformly by the web. The combined stress of the bending stress and the shearing stress satisfy Von Mises' yield condition.

For the assumed stress distribution as shown in Fig. 3.58 the equilibrium equations (1)-(4) for the applied bending moment M and the shearing force V are able to predict behaviour as well as the solution of BOWER (1968), i.e.

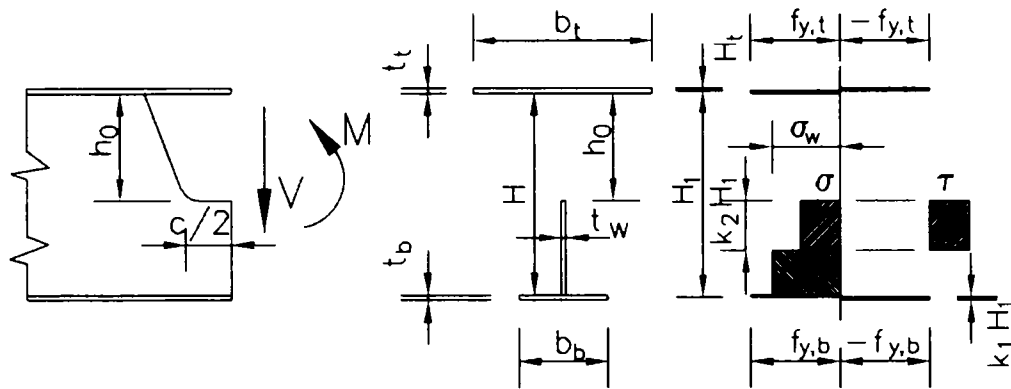


Fig. 3.58. Assumed stress distribution at Ultimate load, BOWER (1968)

$$M = \frac{f_{y,t} b_t \left[H_t^2 - (H_1 - H - t_b)^2 \right]}{2} +$$

$$+ \sigma_w t_w (H - h_0 - k_2 H_1) \left[H_1 - t_b - \frac{(H - h_0 - k_2 H_1)}{2} \right] +$$

$$+ f_{y,b} b_b (t_b - k_1 H_1) \left[\left(1 - \frac{k_1}{2} \right) H_1 - \frac{t_b}{2} \right], \quad (3.1)$$

$$V = \sigma_w k_2 H_1, \quad (3.2)$$

$$\frac{Vc}{2} = f_{y,b} b_b k_1 H_1 \left[H + t_b - h_0 - \frac{(k_1 + k_2) H_1}{2} \right], \quad (3.3)$$

$$f_{y,b} k_1 b_b = \sigma_w k_2 t_w, \quad (3.4)$$

where $k_2 H_1 \leq H - h_0$, $f_{y,t}$ and $f_{y,b}$ – the yield stress of the upper and the bottom flange, respectively, and σ_w – the yield stress of the web. H_t and H_1 – the distance from the neutral axis to the top surface of the upper flange and the bottom surface of the bottom flange, respectively, $k_2 H_1$ – the depth of the web after yielding in bending and shearing, and $k_1 H_1$ – the depth of the bottom flange reversed by Vierendeel action.

The interaction diagrams for each test beam obtained by using Eq. 3.1 – Eq. 3.4 are shown in Fig. 3.59. The M and V of the ordinate and the abscissa are nondimensionalized by the full plastic moment M_p of the net section without holes and by the full shearing force $V_p = \frac{A_w f_{y,w}}{\sqrt{3}}$, respectively. They were used for the ordinate and the abscissa.

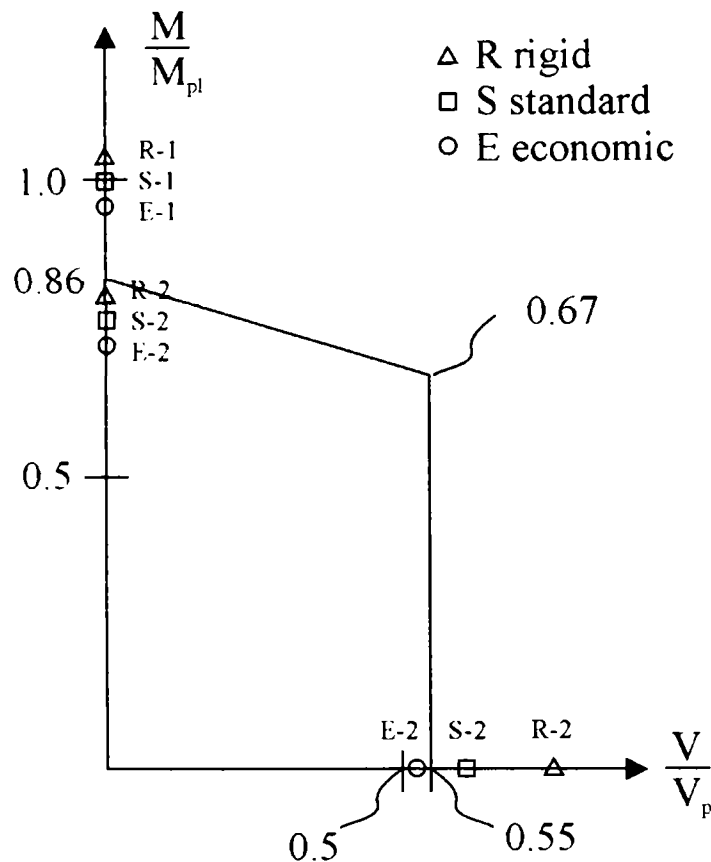


Fig. 3.59. Theoretical and experimental ultimate loads

3.8. Conclusions

The ultimate strength of test specimens with trapezoidal stiffeners was experimentally investigated. The specimens were constructed from three components, the stiffened plate, the trapezoidal stiffener and the cross girder. In the experiments three arrangements were considered where the hole around the trapezoidal stiffener had three different shapes providing different connection between the trapezoidal stiffener and the web of the cross girder. Specifically when the components are fully welded to each other then the connection is rigid (R). When there is a hole in the web of the cross girder around the flange of the trapezoidal stiffener the connection is considered as standard (S). Finally when the trapezoidal

stiffener is fully cut around in the web of the cross girder the connection is economical (E).

With the aid of these experiments it was possible to determine the behavior of the components under sagging and hogging moment and shear force.

The experiments investigated the elastic and the plastic behavior of the specimens; they determined the load carrying capacity and the failure mode (IVÁNYI, Jr., BANCILA, 2006, IVÁNYI, Jr., et al., 2006/a, IVÁNYI, Jr., et al 2006/b, IVÁNYI, Jr., et al, 2006/c).

CHAPTER 4

Numerical Analysis

In this chapter the different structural details for the stiffener of an orthotropic plate will be investigated numerically (IVÁNYI, Jr., et al 2006). Furthermore the effect of the different structural detail of the stiffener on the ultimate limit state of the orthotropic plate will be studied. Three arrangements are considered: rigid (R), standard (S) and the suggested economic (E). (I note here again, that the rigid structural detail is not used in practice due to fatigue problems, therefore it is used here only as a comparison.)

Two types of numerical analysis are discussed in this chapter. First a linear 3D finite element analysis which will help in the creation of the design formulas. Second a non-linear 3D finite element analysis is carried out which will help to analyse the different phenomenon (significant plastic deformations, plate buckling and material failure) that were experienced during the experiments. (IVÁNYI, Jr., IVÁNYI, P, 2007)

4.1 Linear 3D finite element analysis

In the frame of this program a linear 3D finite element model has been analysed to study the different structural details and connection between the longitudinal, trapezoidal stiffener and the cross girder with open cross section in an orthotropic plate. The aim of the analysis was to obtain enough information, which can be utilized in the determination of the "initial" stiffnesses. First of all the investigation the effect of

the different structural details of the stiffener of the orthotropic plate on the local and global behaviour of the plates has been investigated.

For the analysis the LUSAS (2000) finite element program has been used. LUSAS is a commercially available general finite element program, which has some specialised modules for civil engineers. For example one module can help the designer in combining the different load cases since the program can automatically do the load combination.

4.1.1 The finite element model

It was decided from the beginning that a full model will be created. It means that no symmetry condition will be used. The main reason for this decision is that the model has to be analysed under not only moment loading but shear loading. Fig. 4.1 shows the schematic layout of the model under sagging moment, Fig. 4.2 shows the layout of the model under hogging moment and Fig. 4.3 shows the model in the case of shear loading. These models correspond directly to the experimental setup of the different structural details.

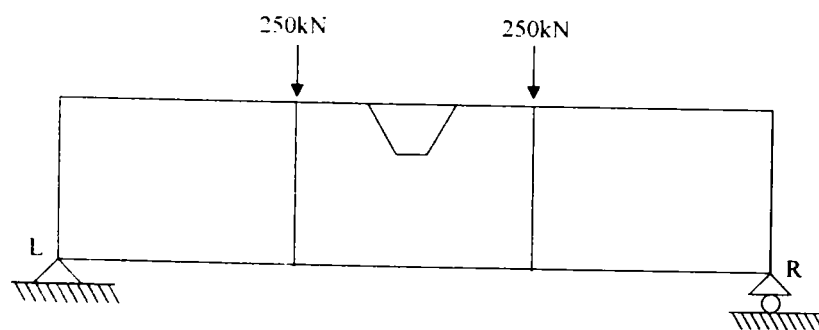


Fig. 4.1. Schematic layout of the model under sagging moment

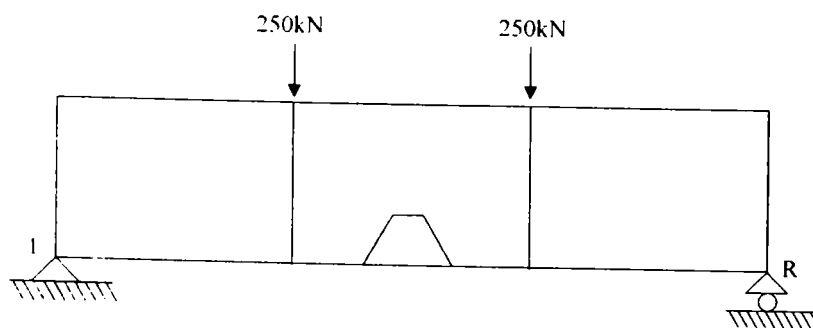


Fig. 4.2. Schematic layout of the model under hogging moment

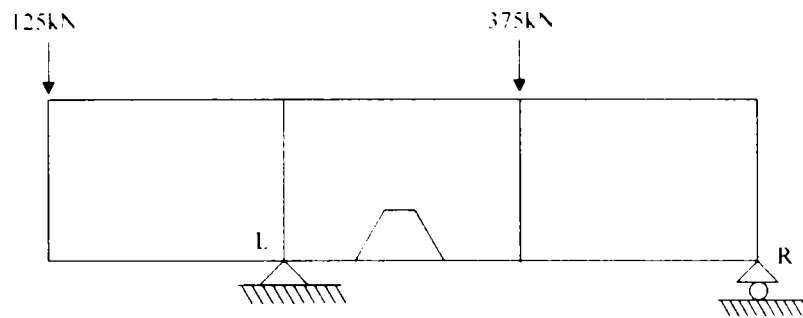


Fig. 4.3. Schematic layout of the model in the case of shear loading

Fig. 4.1 - 4.3 show that the models are simple supported beams. It means that the left hand side boundary condition (point L) restricts the displacements in all directions, X, Y and Z but allows rotations. The boundary condition on the right hand side (point R) models a rolling condition as it allows the displacements in the X direction, but restricts displacements in the Y and Z directions. The rotations at point L are also free to develop.

Since these analysis will be used in the determination of the "initial" stiffnesses of the different structural details a linear, elastic material model is used with standard steel properties:

Young modulus: 210 000 000 kN/m²,

Poisson's ratio: 0.3.

The loading conditions can also be seen in Fig. 4.1 - 4.3 for the different experimental setups.

Since the finite element mesh represents the full structure the mesh has to be designed carefully. It means that most of the elements must be concentrated around the area of interest. Naturally the area of interest is the trapezoidal stiffener and its surroundings, which is the middle of the structure. The annex beams connect to the middle section "rigidly" as there is a very strong plate between the middle section and the annex beams as it was discussed in Chapter 3. This also means that the number of finite elements in the annex beams can be very few. The meshes were generated automatically by the program.

Another important decision is that mainly quadrilateral elements must be used in the finite element meshes for precision. The LUSAS program can only generate a quadrilateral dominant mesh, where most of the elements are quadrilaterals, however there are some triangles in the mesh' as well. The name of the quadrilateral element in the LUSAS program is QSI4, which is a flat thin shell element. The element takes into account both membrane and flexural deformations and as required by thin plate theory, transverse shearing deformations are excluded.

Fig. 4.4 shows the full finite element mesh of the model for the rigid (R) type of connection and Fig. 4.5 shows a magnified view of the same mesh. Fig. 4.6 and 4.7 shows the finite element mesh of the model for the standard (S) type of connection. (It must be noted that in the experimental specimens no hole is cut out from the web of the cross girder at the corner of the trapezoidal specimen where it connects to the plate. On the other hand this hole is present in the numerical models.) Finally Fig. 4.8. and 4.9 show the finite element mesh of the model for the economic (E) type of connection.

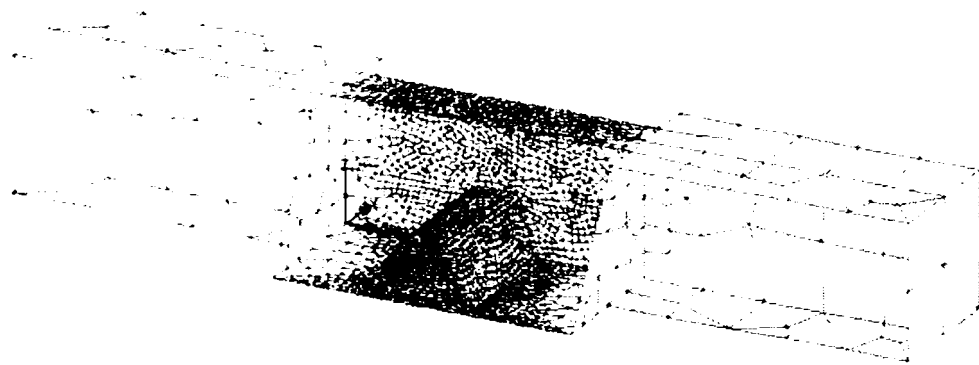


Fig. 4.4. Overview of the finite element mesh (rigid, R connection)

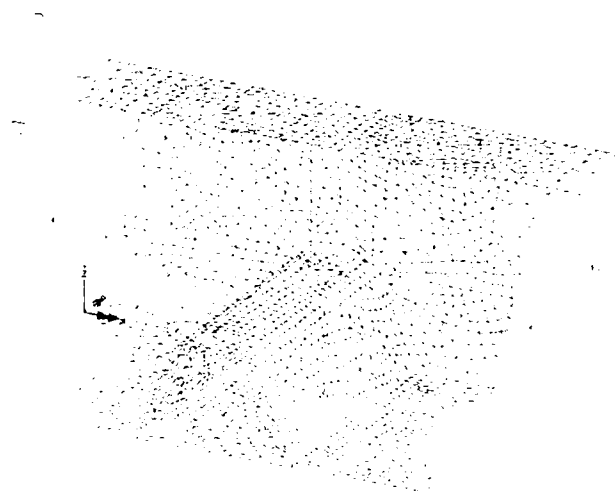
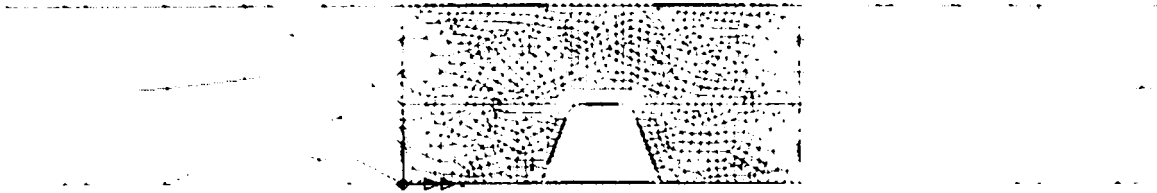
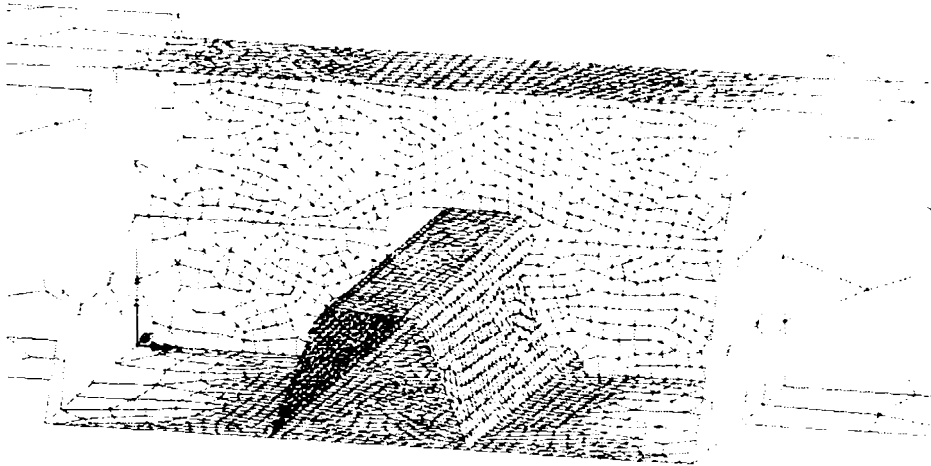


Fig. 4.5. Finite element mesh around the trapezoidal stiffener (rigid, R connection)



**Fig. 4.6. Overview of the finite element mesh
(standard, S connection)**



**Fig. 4.7. Finite element mesh around the trapezoidal stiffener
(standard, S connection)**

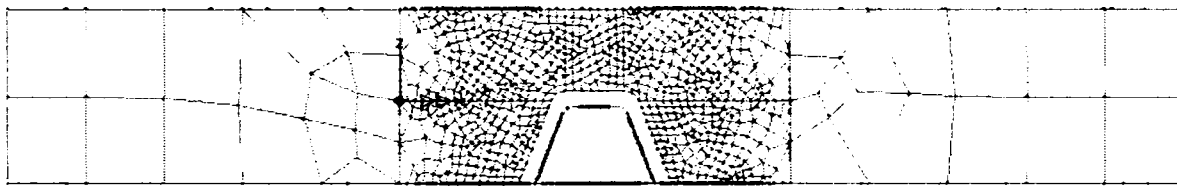
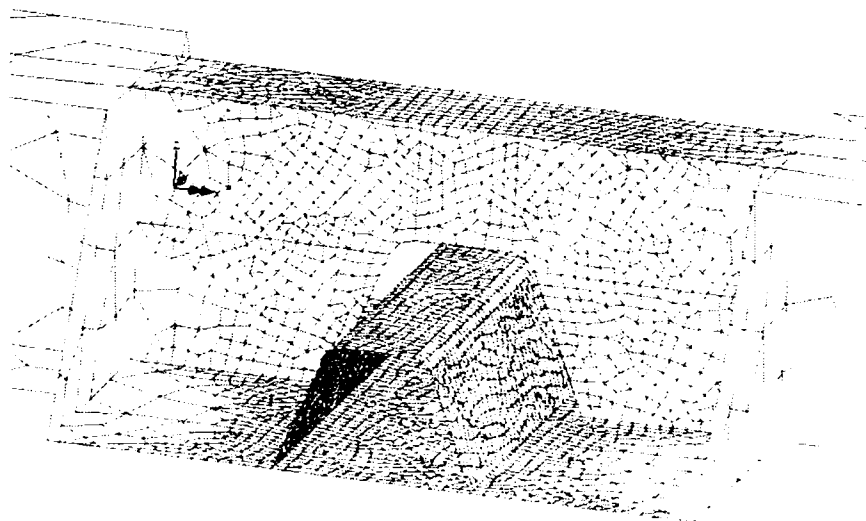


Fig. 4.8. Overview of the finite element mesh(economic, E connection)



**Fig. 4.9. Finite element mesh around the trapezoidal stiffener
(economic, E connection)**

The number of elements in the meshes is shown in Table 4.1.

Type of connection	Number of elements
Rigid	4729
Standard	4700
Economic	4631

Table 4.1. Number of elements in the meshes

4.1.2. Results of the linear 3D finite element analysis for the shear load

Fig. 4.10 shows the magnified displacements of the finite element mesh with rigid (R) connection when shear loading is applied on the model. Fig. 4.11 shows the magnified displacements for the standard (S) connection and Fig. 4.12 shows the magnified displacements for the economic (E) connection under shear loading.

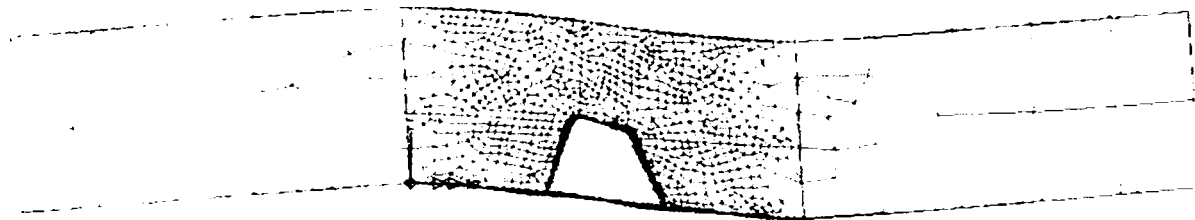


Fig. 4.10. Displacement of the finite element mesh under shear loading (rigid, R connection)

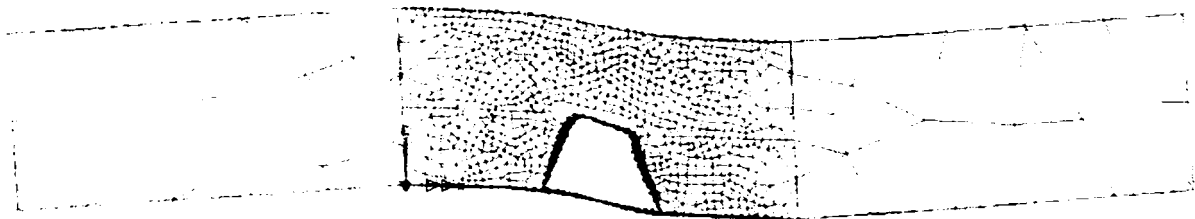


Fig. 4.11. Displacement of the finite element mesh under shear loading (standard, S connection)

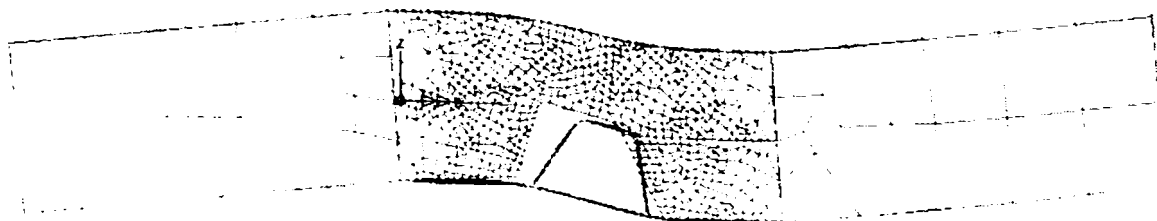


Fig. 4.12. Displacement of the finite element mesh under shear loading (economic, E connection)

In Fig. 4.12 the contact between the trapezoidal stiffener and web of the cross girder is artificial, it only occurs because the displacements are magnified.

The results of the analysis of the models under shear loading will be used in the determination of the static properties of the cross girders. I assume – based on the experimental results – that the different (R, S, E) connections between the orthotropic plate and the cross girder can be modelled as an elastic connection. It is assumed that there is an elastic layer between the two structural parts and its physical properties can be expressed by ε .

The ε parameter of the elastic connection for the different structural details between the orthotropic plate and the cross girder can be determined from the results when the model is under shear loading. During the loading – due to the geometric and loading arrangement of the model – large shear forces will develop in the studied area of the structure. The bending moments can be neglected in the same area, thus with respect to the elastic “layer” connection this behaves as a "push-out test". Fig. 4.13 shows the shear forces and bending moments in the model.

To determine the ε parameter of the elastic connection the relative displacement between points A and D must be determined as shown in Fig. 4.13. The determined deformation state will be discussed in Chapter 5 along with the experimental results.

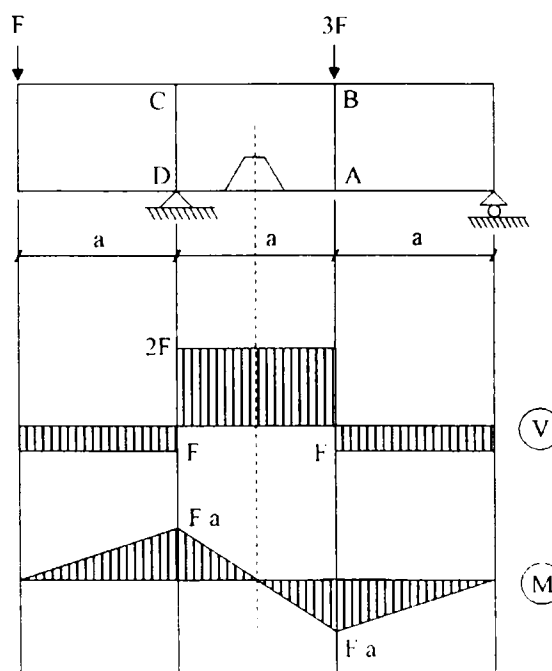


Fig. 4.13. Shear forces and bending moments in the model

4.1.3. Results of the linear 3D finite element analysis for the sagging moment

The magnified displacements of the finite element meshes under sagging moment are shown in Fig. 4.14 for the rigid (R) connection, in Fig. 4.15 for the standard (S) connection and in Fig. 4.16 for the economic (E) connection.

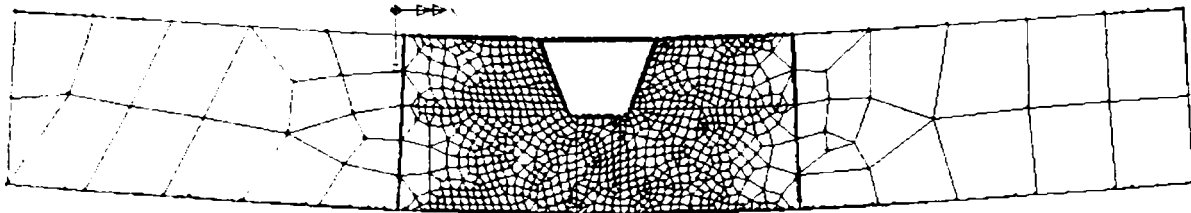


Fig. 4.14. Displacement of the finite element mesh under sagging moment (rigid, R connection)

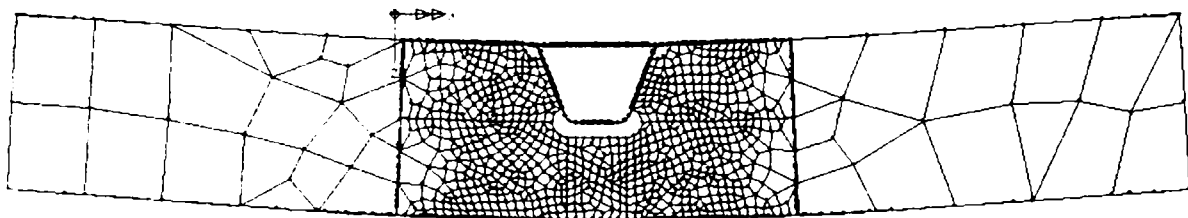


Fig. 4.15. Displacement of the finite element mesh under sagging moment (standard, S connection)

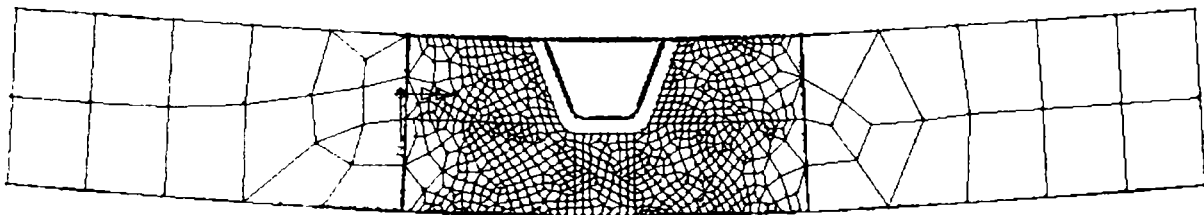


Fig. 4.16. Displacement of the finite element mesh under sagging moment (economic, E connection)

4.1.4. Results of the linear 3D finite element analysis for the hogging moment

The magnified displacements of the finite element meshes under hogging moment are shown in Fig. 4.17 for the rigid (R) connection, in Fig 4.18 for the standard (S) connection and in Fig. 4.19 for the economic (E) connection.

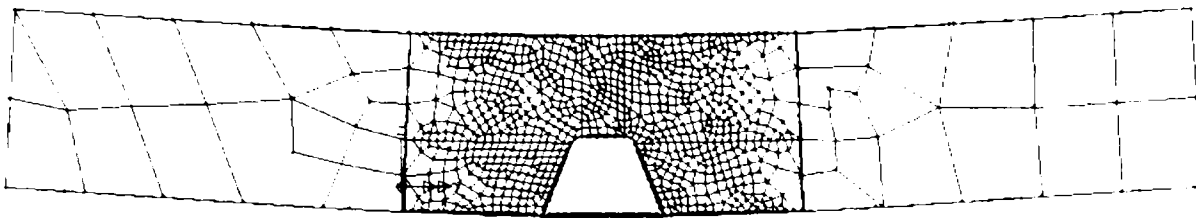


Fig. 4.17. Displacement of the finite element mesh under hogging moment
(rigid, R connection)

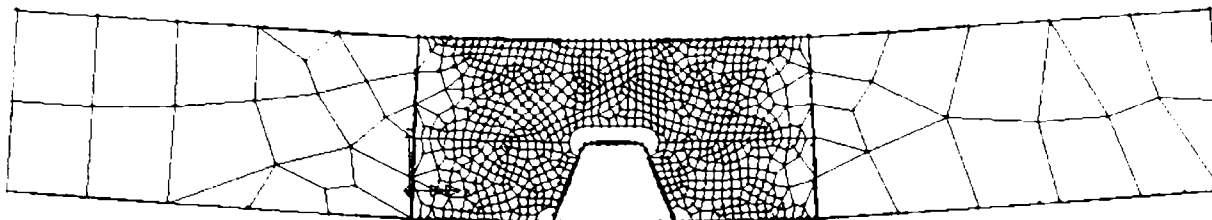


Fig. 4.18. Displacement of the finite element mesh under hogging moment
(standard, S connection)

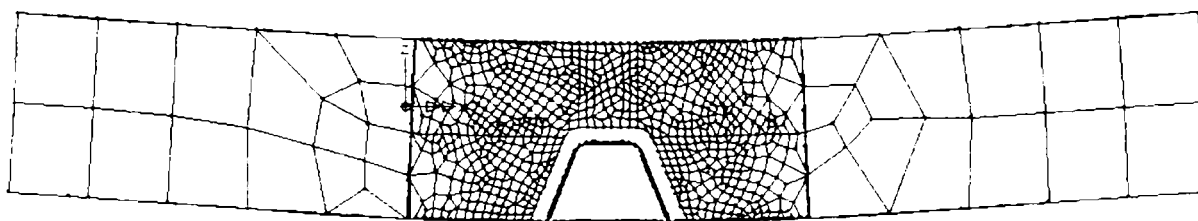


Fig. 4.19. Displacement of the finite element mesh under hogging moment
(economic, E connection)

4.2 Non-linear 3D finite element analysis

In the program a couple of non-linear 3D finite element analysis has also been performed. The purpose of these tests to study the effect of the different structural details of the connection between the trapezoidal stiffener and the cross girder on the regional area. Similarly to the linear tests all three structural details, rigid (R), standard (S) and economic (E) have been investigated. Considering the results of the experiments the aim was to perform a non-linear 3D FE analysis under shear loading.

For the non-linear finite element calculation the LS-DYNA (2001) package has been utilised. LS-DYNA has some special features which are required during the non-linear calculation. LS-DYNA can perform an explicit finite element analysis. In this

case no global stiffness matrix must be assembled and the load is applied to the structure in an increasing manner as time passes. Basically a pseudo dynamic analysis will be performed where it is possible to study the path to the ultimate state but we are more interested in the final state, in a "static" solution. However, performing a "static" analysis in this helps to account for geometric and material nonlinearities.

Another important feature of the LS-DYNA program has, that it can handle material failure. Unfortunately not many finite element packages can model material failure and even the methodology of LS-DYNA is not perfect. In LS-DYNA material failure is modelled in such a way, that when in an element the plastic strain reaches a specified limit then the element ceases to exist. The element is taken out of the model. The consequence of this element removal, however is that there is no mass and energy conservation in the model. Some discussion about this kind of material modelling can be found in a paper by IVÁNYI, P., et al (2006). The experience of Iványi is that with this type of material failure modelling the failure mechanism can be modelled quite well, however the forces and displacements may not match with the experimental results.

It is also important to note that in the finite element analysis "real" material properties have been used. These material properties have been determined by experiments. Details about these experiments can be found in Chapter 3. Fig. 4.20 shows the strain-stress relations for the steel material that was used in the experimental specimens for the numerical simulations.

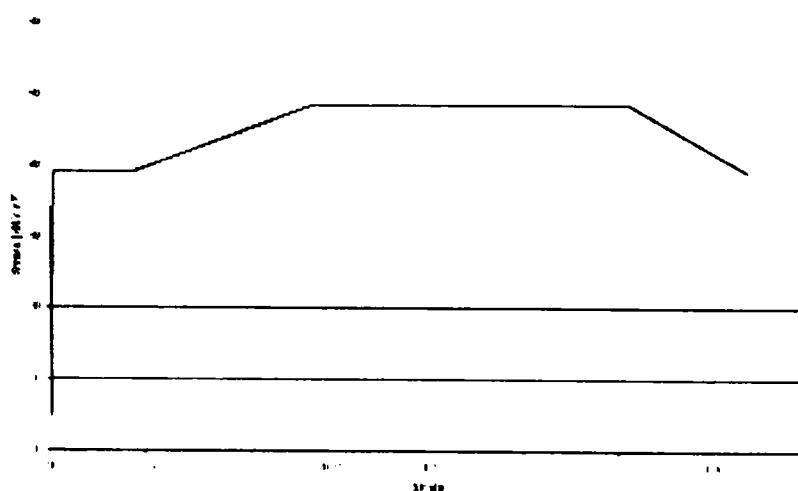


Fig. 4.20. Stress-strain relation for the steel material

Unfortunately the finite element mesh had to be built from scratch for the LS-DYNA program. In this case only quadrilateral elements are used in the mesh and the program has some constraints on the quality of the elements. The number of elements in the finite element meshes are shown in Table 4.2.

Type of connection	Number of elements
Rigid (R)	1887
Standard (S)	1937
Economic (E)	1767

Table 4.2. Number of elements in the meshes

The selected quadrilateral element is SHELL 163. SHELL 163 is a 4-node shell element with bending and membrane capabilities. The element has 12 degrees of freedom at each node: translations, accelerations, and velocities in the nodal x, y, and z directions and rotations about the nodal x, y, and z-axes.

Fig. 4.21 shows the plates in the finite element model. There is another important difference compared to the linear elastic analysis, that the loading has been applied on the structure through rigid plates. These plates can be seen in Fig. 4.21, in the upper flange. These plates are modelled as rigid as it is assumed that they will not deform. The main reason to use them is that in this way the load can be applied as a concentrated load on the rigid plates. The use of these plates is also realistic as they model the real loading device. Furthermore in this way the amount of computation time can be reduced. The calculation of rigid elements is very short compared to an elastic or plastic element.

Fig. 4.22 – Fig. 4.24 show the side view of the finite element mesh for all three connection types, rigid, standard, economic. The finite element mesh around the trapezoidal stiffener can be seen in Fig. 4.25 – Fig. 4.27.

The execution of one these finite element models is approximately 6 hours.

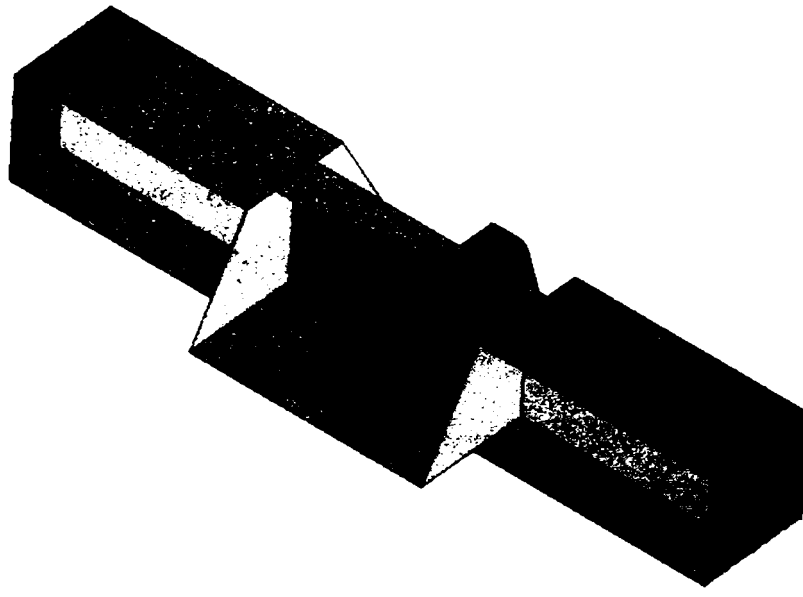


Fig. 4.21. Geometry of the finite element model in the case of the economic connection

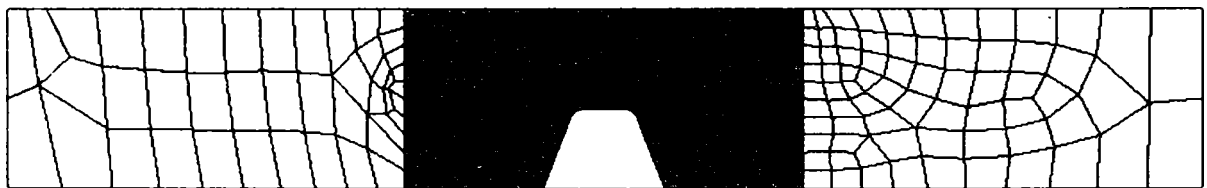


Fig. 4.22. Overview of the finite element mesh (rigid (R) connection)

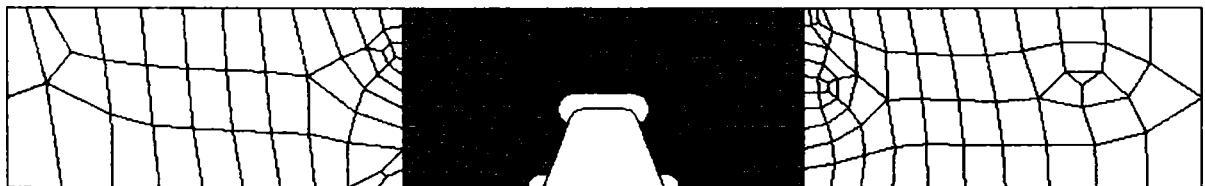


Fig. 4.23. Overview of the finite element mesh (standard (S) connection)



Fig. 4.24. Overview of the finite element mesh (economic (E) connection)

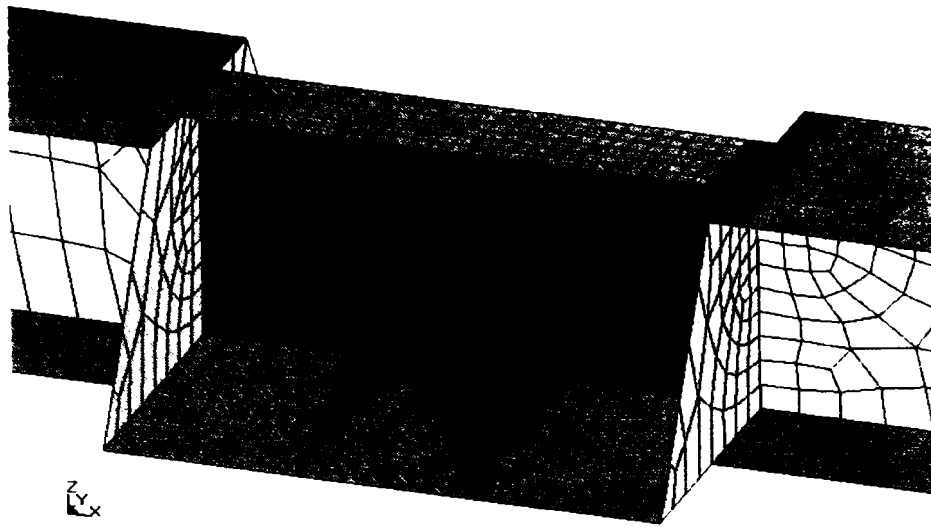


Fig. 4.25. Finite element mesh around the trapezoidal stiffener (rigid (R) connection)

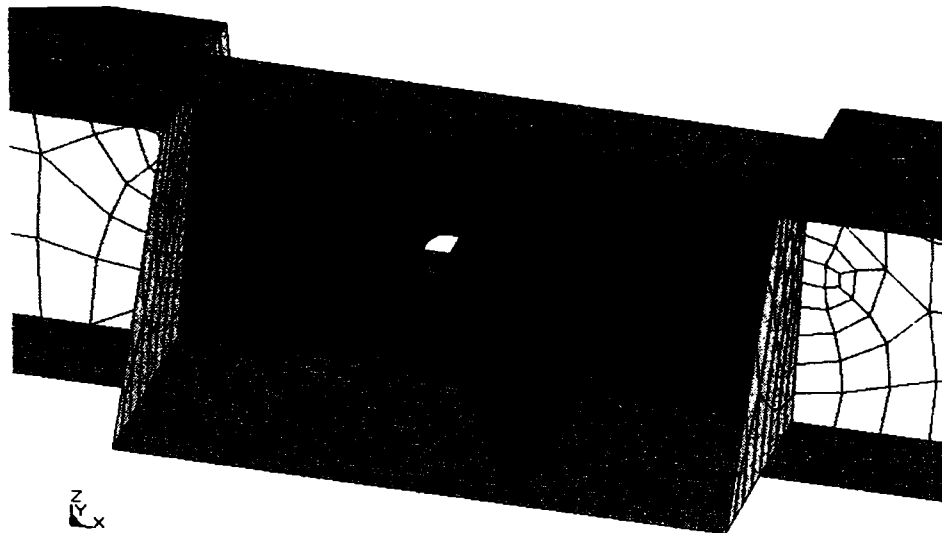


Fig. 4.26. Finite element mesh around the trapezoidal stiffener (standard (S) connection)

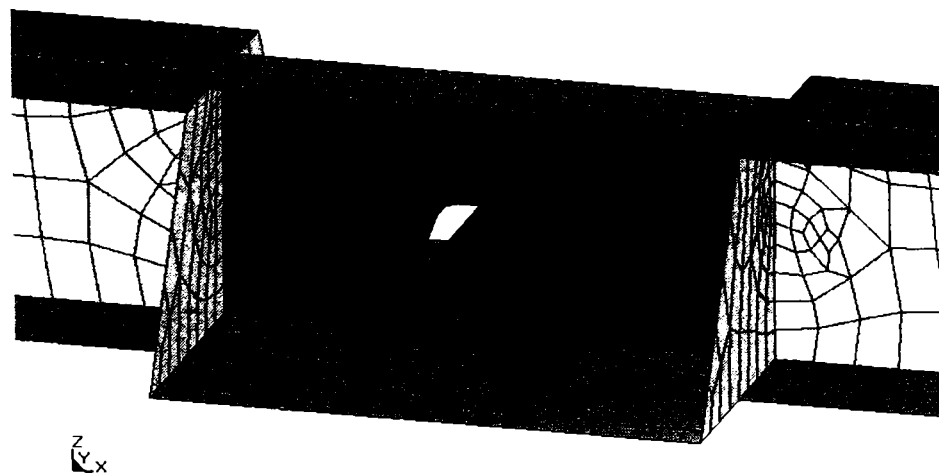


Fig. 4.27. Finite element mesh around the trapezoidal stiffener (economic (E) connection)

4.2.1 The imperfections according to EC 3 Part 1.5

The assumed elastic “layer” connection between the two parts of the structural cross section is an important part of the static model. To determine the properties of the elastic connection the load case with shear loading must be considered, therefore these analysis will focus on them.

The full analysis with attention to every detail requires significant computation power therefore only “limited” versions of the analysis were performed. I tried to perform analysis, which have few number of elements but at the same time they can provide information about the local behaviour of the structural details of the connections.

4.2.2 Comparison of the experimental and numerical tests

The load carrying capacity is very high in the case of the rigid connection between the trapezoidal stiffener and the cross girder in the orthotropic plate (see Chapter 3). The web of the cross section that is close to the trapezoidal stiffener buckles, as shown in Fig. 4.28 – Fig. 4.36. The full diagonal buckling cannot form since the trapezoidal stiffener has a strong supporting effect. The numerical results show very similar behaviour.

In the case of the standard, (S) connection the load carrying capacity is significantly lower than the load carrying capacity of the rigid (R) connection type (see Chapter 3). The web of the cross girder buckles around the cut-out holes at the top of the trapezoidal stiffener. Later on there is a material failure on the tensioned side, as shown in Fig. 4.28 – Fig. 4.36.



Fig. 4.28. Arrangement of the rigid (R) test

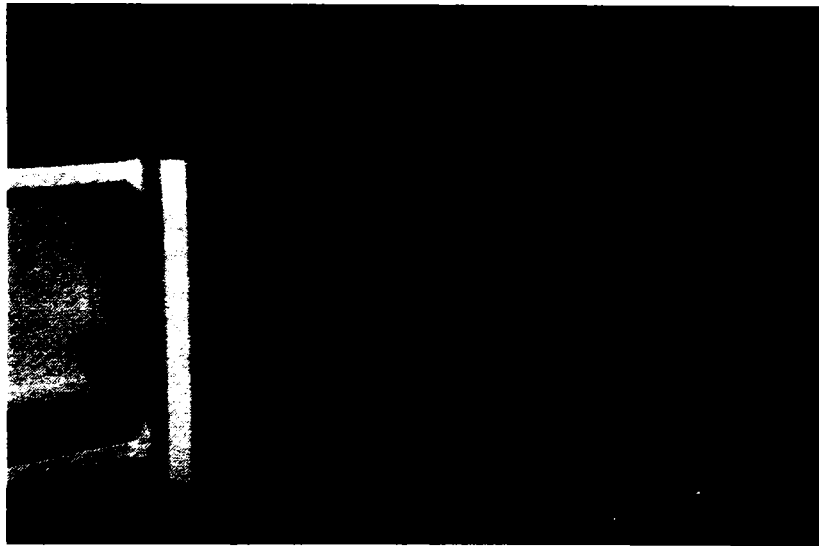


Fig. 4.29. (R) specimen

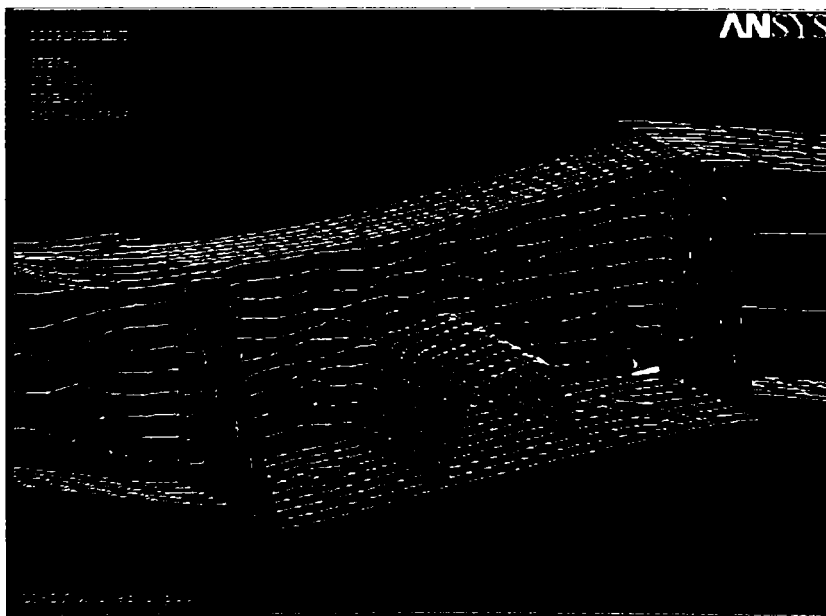


Fig. 4.30. FEM analysis of R specimen



Fig. 4.31. Arrangement of the standard (S) test

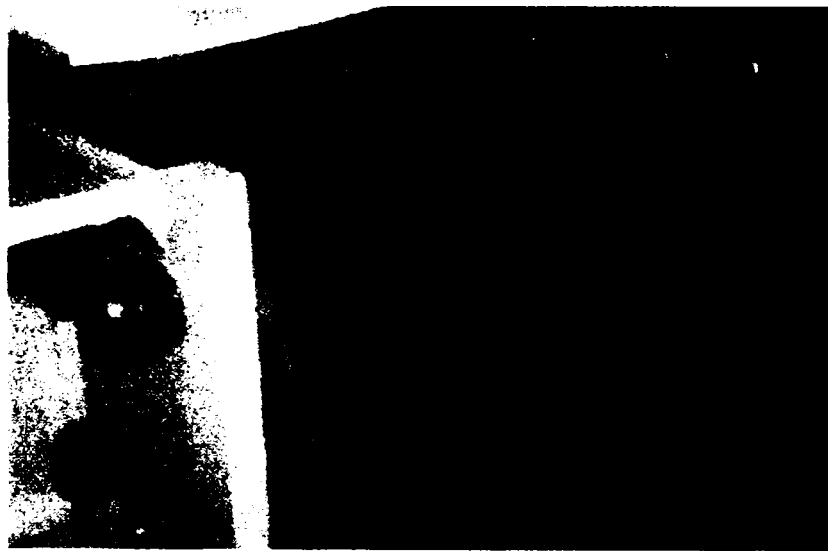


Fig. 4.32. (S) specimen

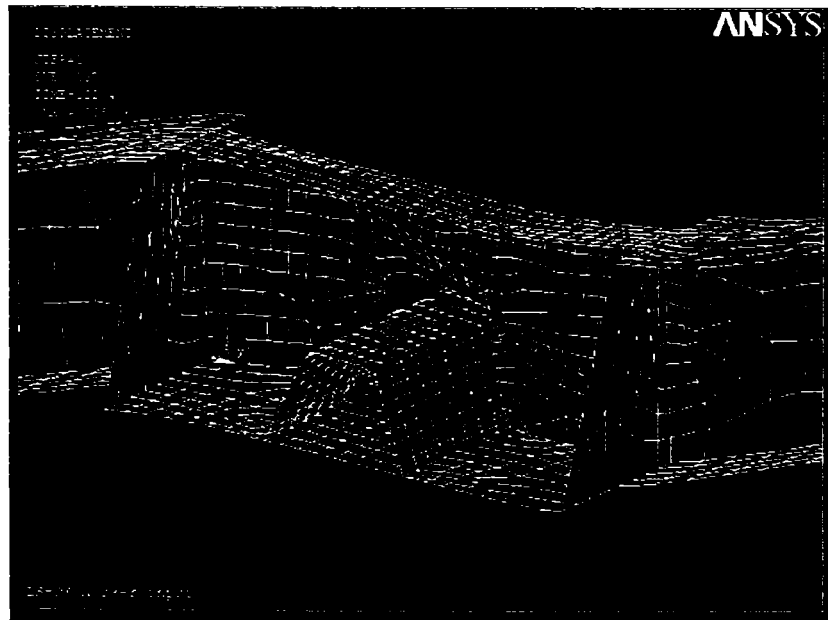


Fig. 4.33. FEM analysis of S specimen



Fig. 4.34. Arrangement of the economic (E) test

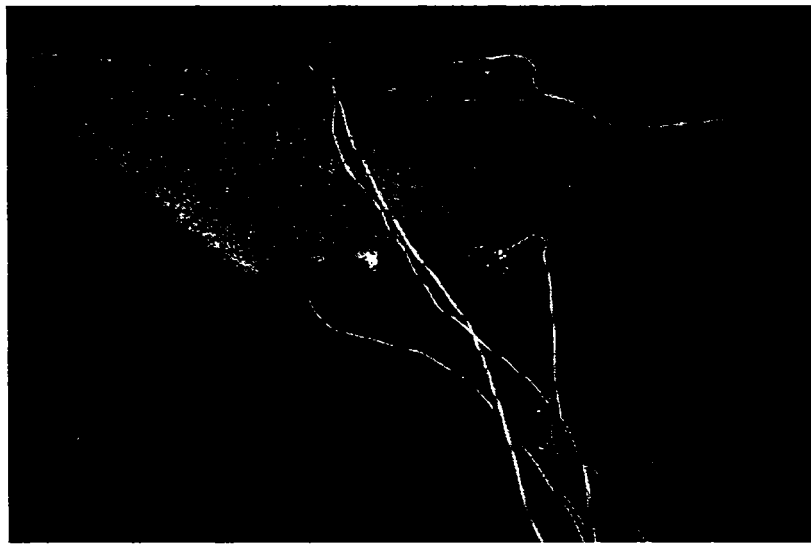


Fig. 4.35. (E) specimen

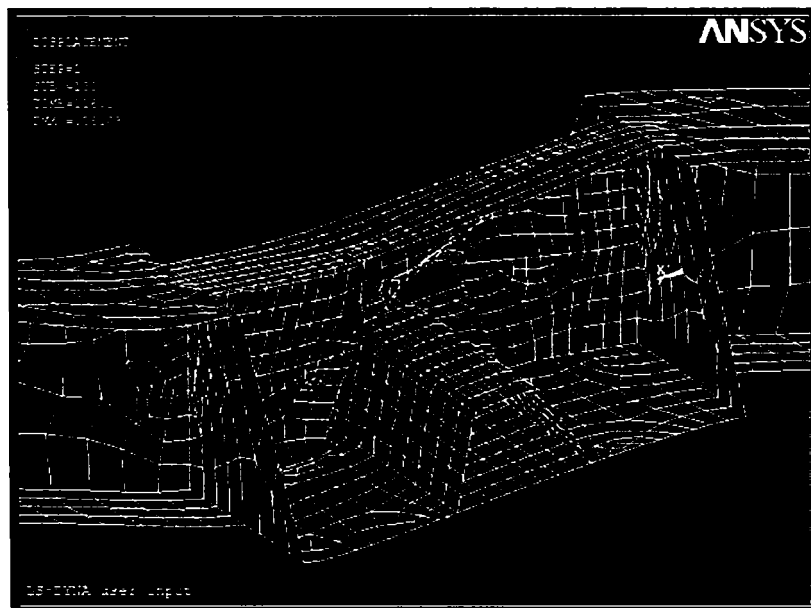


Fig. 4.36. FEM analysis of E specimen

In the case of the economic, E connection a reduced load carrying capacity can be observed. (It is important to note, that the stiffness of the connection does not exhibit this large reduction.) The web of the cross girder buckles in a larger area due to the hole, however the buckling shape is very similar to the buckling shape which occurred in the case of the standard, S connection type. In the case of the economic, E connection the tensioned part of the structure also fails later on.

In the design of the standard (S) connection the information that can be gained from the experimental and numerical analysis can also be utilised, that the behaviour of the rigid (R) and standard (S) connections differ significantly. This observation is very important since in the traditional design process this difference is not considered. (It can be noted that there are also differences between the standard (S) and economic (E) connections, but the differences are not that significant.)

4.3 Conclusions

Different structural details of the stiffeners of orthotropic plates have been investigated by numerical analysis in this chapter. The linear 3D finite element analysis helps to analyze the different structural details as elastic connections. In the case of the non-linear 3D finite element analysis only the effect of the shear forces have been investigated. These simulations help to study the local behaviour of the connections after the elastic range, during buckling and failure. The reason to perform only the analysis with shear forces as the calculation requires significant computational power. (IVÁNYI, et al 2006/b, IVÁNYI, Jr., IVÁNYI, P., 2007)

CHAPTER 5

Behaviour and Design of Plated Steel Structures

This chapter introduces the uses of plates and plated assemblies in steel structures. It describes the basic behaviour of plate panels subject to in-plane or out-of-plane loading, highlighting the importance of geometry and boundary conditions. Basic buckling modes and mode interaction are presented. It introduces the concept of effective width and describes the influence of imperfections on the behaviour of practical plates. It also gives an introduction to the behaviour of stiffened plates.

The load distribution for unstiffened plate structures loaded in-plane is discussed. The critical buckling loads are derived using linear elastic theory. The effective width method for determining the ultimate resistance of the plate is explained as are the requirements for adequate finite element modelling of a plate element. Out-of-plane loading is also considered and its influence on the plate stability discussed. The requirements for finite element models of stiffened plates are outlined using those for unstiffened plates as a basis.

5.1. Introduction to plate behaviour and design

5.1.1. Introduction

Plates are very important elements in steel structures. They can be assembled into complete members by the basic rolling process (as hot rolled sections), by folding (as cold formed sections) and by welding. The efficiency of such sections is due to their

use of the high in-plane stiffness of one plate element to support the edge of its neighbour, thus controlling the out-of-plane behaviour of the latter.

The size of plates in steel structures varies from about 0,6mm thickness and 70mm width in a corrugated steel sheet, to about 100mm thick and 3m width in a large industrial or offshore structure. Whatever the scale of construction the plate panel will have a thickness t that is much smaller than the width b , or length a . As will be seen later, the most important geometric parameter for plates is b/t and this will vary, in an efficient plate structure, within the range 30 to 250.

TIMOSHENKO-WINOWSY-KRIEGER (1959), BLEICH (1952), SZILÁRD (1974), WOLMIR (1962), DUBAS, GHERI (1986), BRUSH, ALMROTH (1975), PETERSEN (1982)

5.1.2. Basic behaviour of a plate panel

Understanding of plate structures has to begin with an understanding of the modes of behaviour of a single plate panel.

5.1.2.1. Geometric and boundary conditions

The important geometric parameters are thickness t , width b (usually measured transverse to the direction of the greater direct stress) and length a , see Fig. 5.1. The ratio b/t , often called the plate slenderness, influences the local buckling of the plate panel; the aspect ratio a/b may also influence buckling patterns and may have a significant influence on strength.

In addition to the geometric proportions of the plate, its strength is governed by its boundary conditions. Fig. 5.1 shows how response to different types of actions is influenced by different boundary conditions. Response to in-plane actions that do not cause buckling of the plate is only influenced by in-plane, plane stress, boundary conditions, Fig. 5.1b Initially, response to out-of-plane action is only influenced by the boundary conditions for transverse movement and edge moments, Fig. 5.1c. However, at higher actions, responses to both types of action conditions are

influenced by all four boundary conditions. Out-of-plane conditions influence the local buckling, see Fig. 5.1d; in-plane conditions influence the membrane action effects that develop at large displacements ($>t$) under lateral actions, see Fig. 5.1e.

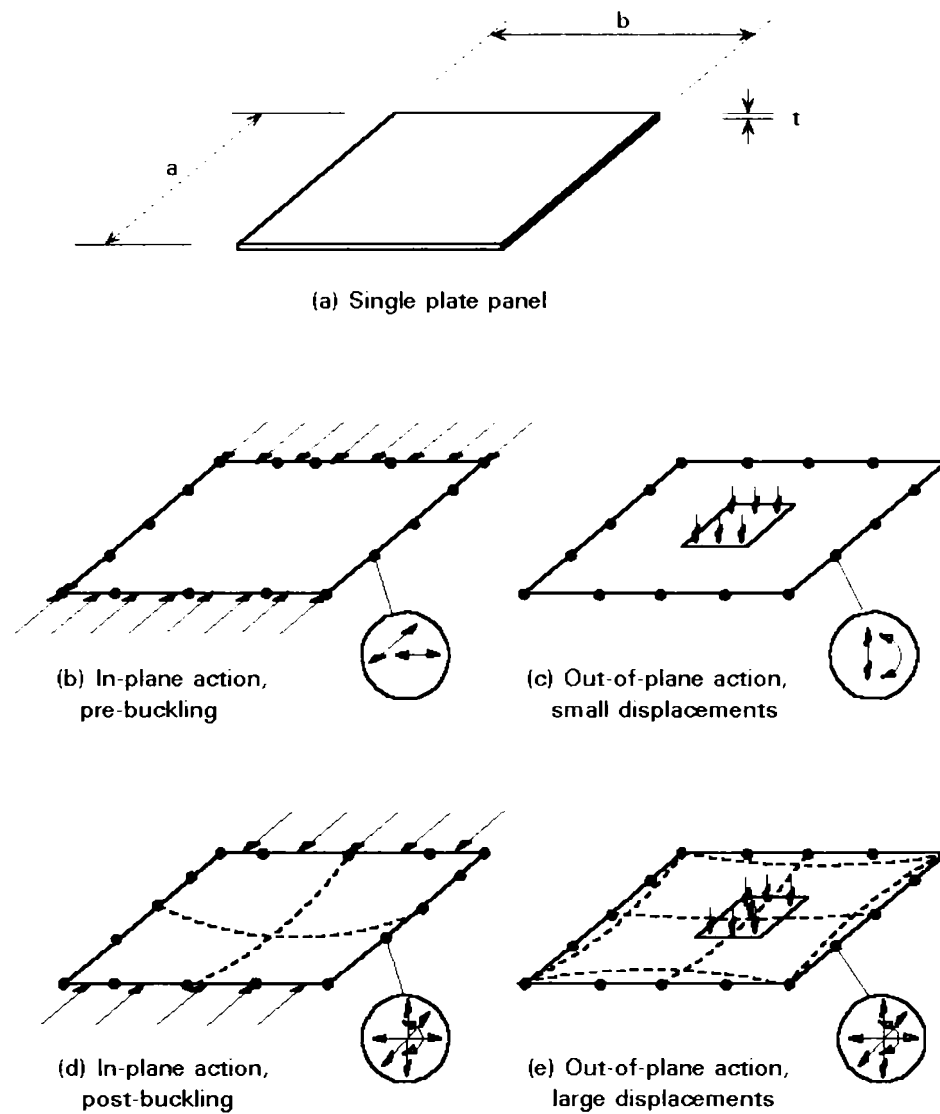


Fig. 5.1. Significant boundary conditions for plate panels

5.1.2.2. In-plane Actions

As shown in Fig. 5.2a, the basic types of in-plane actions to the edge of a plate panel are the distributed action that can be applied to a full side, the patch action or point action that can be applied locally.

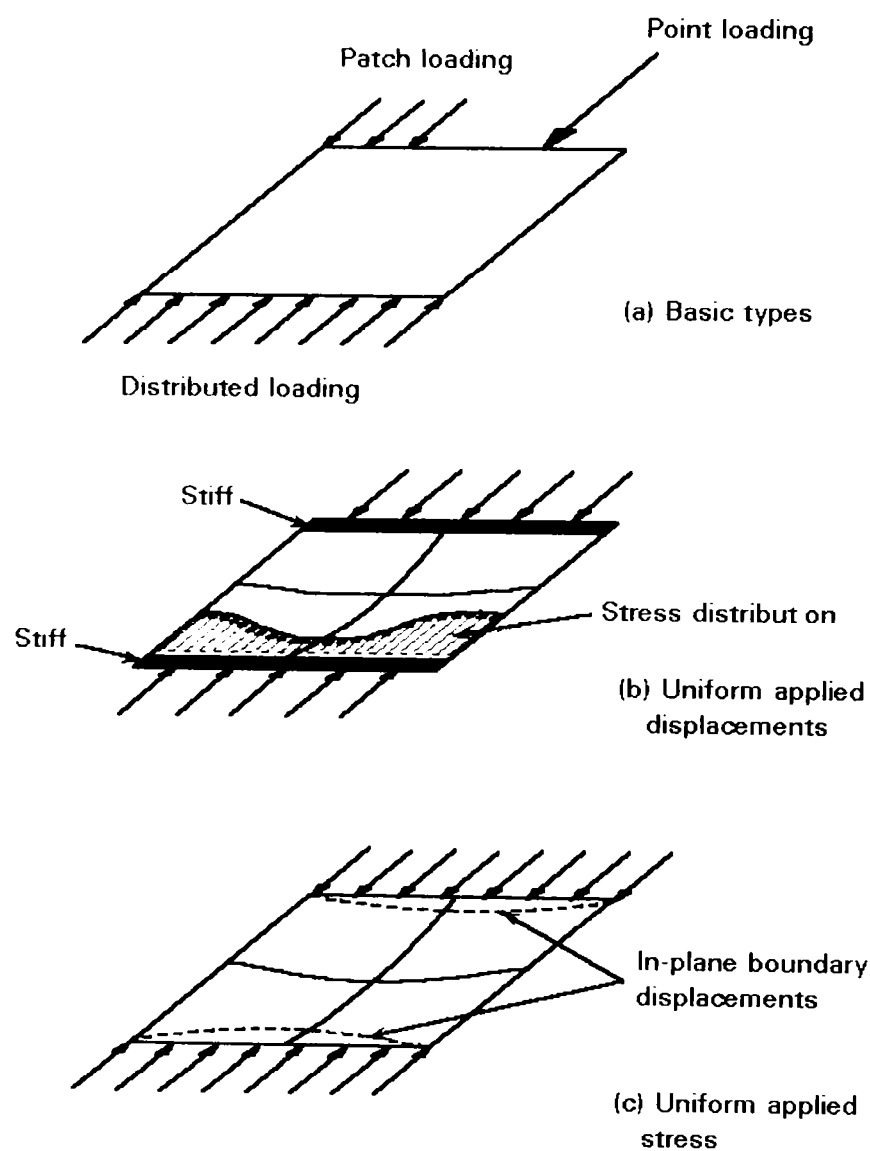


Fig. 5.2. Types of in-plane action

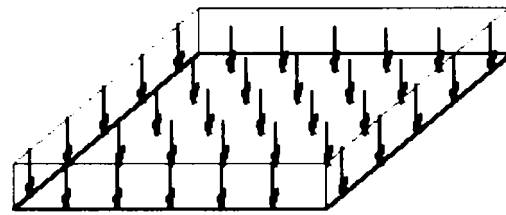
When the plate buckles, it is particularly important to differentiate between applied displacements, see Fig. 5.2b and applied stresses, see Fig. 5.2c. The former permits a redistribution of stress within the panel; the more flexible central region sheds stresses to the edges giving a valuable post buckling resistance. The latter, rarer case leads to an earlier collapse of the central region of the plate with in-plane deformation of the loaded edges.

5.1.2.3. Out-of-plane Actions

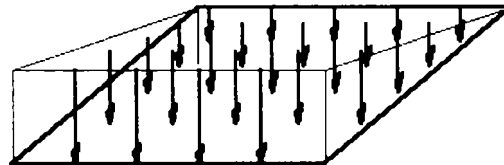
Out-of-plane loading may be:

- Uniform over the entire panel, see for example Fig. 5.3a, the base of a water tank.

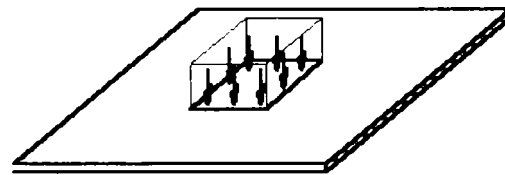
- Varying over the entire panel, see for example Fig. 5.3b, the side of a water tank.
- A local patch over part of the panel, see for example Fig. 5.3c, a wheel load on a bridge deck.



(a) Uniformly distributed loading



(b) Variable distributed loading



(c) Patch loading

Fig. 5.3. Types of out-of-plane actions

5.1.2.4. Determination of plate panel actions

In some cases, for example in Fig. 5.4a, the distribution of edge actions on the panels of a plated structure are self-evident. In other cases the in-plane flexibilities of the panels lead to distributions of stresses that cannot be predicted from simple theory. In the box girder shown in Fig. 5.4b, the in-plane shear flexibility of the flanges leads to in-plane deformation of the top flange. Where these are interrupted, for example at the change in direction of the shear at the central diaphragm, the resulting change in shear deformation leads to a non-linear distribution of direct stress across the top flange; this is called shear lag.

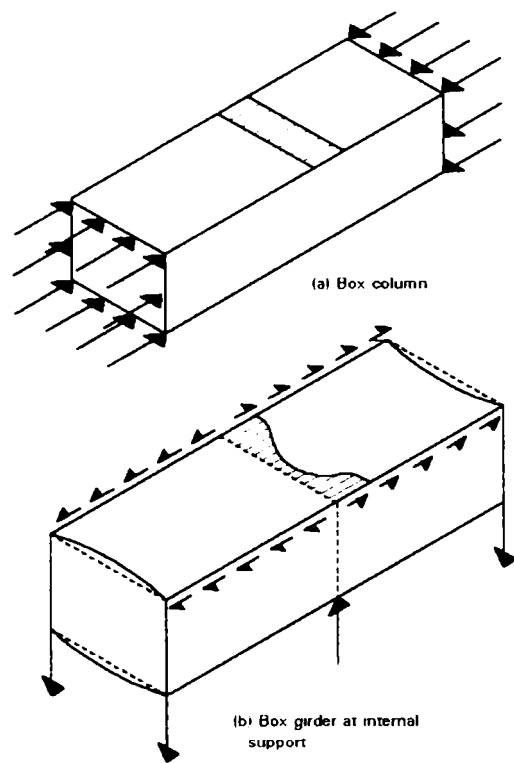


Fig. 5.4. Effect of shear lag on distribution of stresses in plated structures

In members made up of plate elements, such as the box girder shown in Fig. 5.5, many of the plate components are subjected to more than one component of in-plane action effect. Only panel A does not have shear coincident with the longitudinal compression.

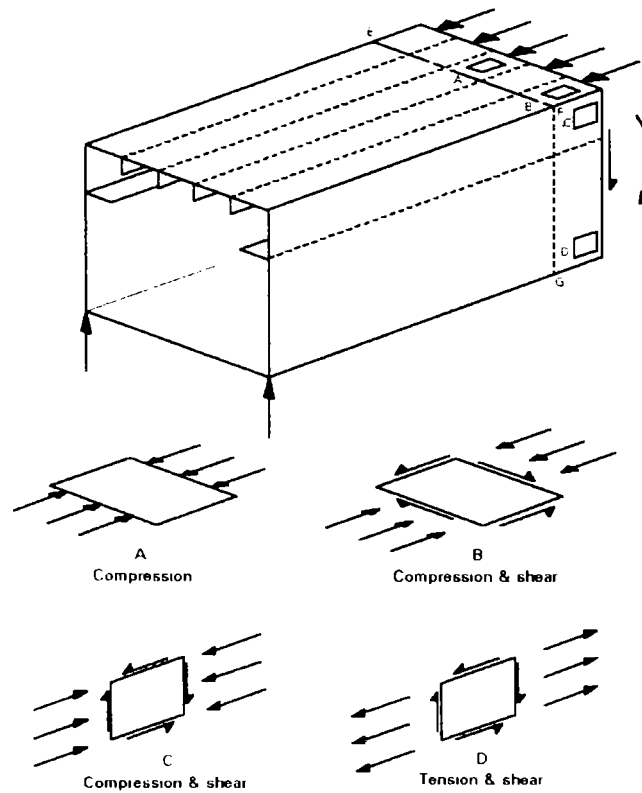


Fig. 5.5 Examples of components of action on plate panels in a box girder

If the cross-girder system EFG was a means of introducing additional actions into the box, there would also be transverse direct stresses arising from the interaction between the plate and the stiffeners.

5.1.2.5. Variations in buckled mode

i) Aspect ratio a/b

In a long plate panel, as shown in Fig. 5.6, the greatest initial inhibition to buckling is the transverse flexural stiffness of the plate between unloaded edges. (As the plate moves more into the post-buckled regime, transverse membrane action effects become significant as the plate deforms into a non-developable shape, i.e. a shape that cannot be formed just by bending).

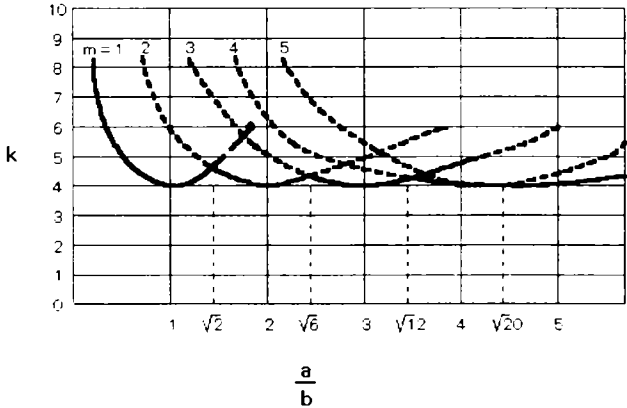
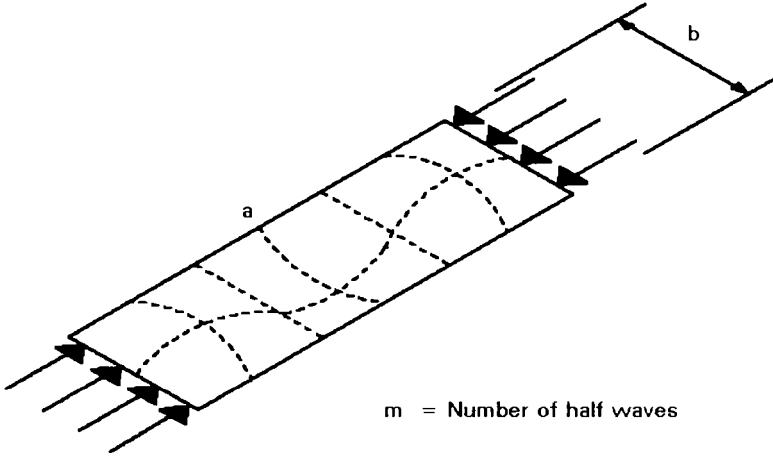


Fig. 5.6. Variations in buckled mode with aspect ratio for a plate panel in longitudinal compression

As with any instability of a continuous medium, more than one buckled mode is possible, in this instance, with one half wave transversely and in half waves longitudinally. As the aspect ratio increases the critical mode changes, tending towards the situation where the half wave length $a/m=b$. The behaviour of a long plate panel can therefore be modelled accurately by considering a simply-supported, square panel.

ii) Bending conditions

As shown in Fig. 5.7, boundary conditions influence both the buckled shapes and the critical stresses of elastic plates. The greatest influence is the presence or absence of simple supports, for example the removal of simple support to one edge between case 1 and case 4 reduces the buckling stress by a factor of $4.0/0.425$ or 9.4. By contrast introducing rotational restraint to one edge between case 1 and case 2 increases the buckling stress by 1.35.

$$\sigma_{cr} = k \frac{\pi^2 Et}{12(1-\nu^2)b}$$

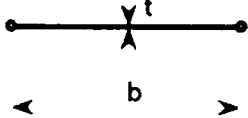
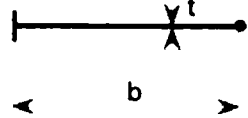
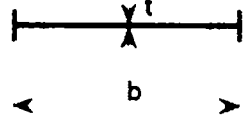
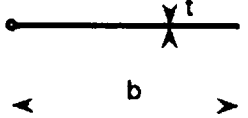
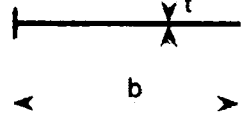
Case	Description of support at the unloaded edges	k
1	Both edges simply supported 	4.00
2	One edge simply supported, the other fixed 	5.42
3	Both edges fixed supported 	6.97
4	One edge simply supported, the other free 	0.425
5	One edge fixed the other free 	1.277

Fig. 5.7. Coefficients for plate buckling in compression for various boundary conditions

iii) Interaction of modes

Where there is more than one action component, there will be more than one mode and therefore there may be interaction between the modes. Thus in Fig. 5.8bi the presence of low transverse compression does not change the mode of buckling. However, as shown in Fig. 5.8bii, high transverse compression will cause the panel to deform into a single half wave. (In some circumstances this forcing into a higher mode may increase strength; for example, in case 5.8bii, predeformation/transverse compression may increase strength in longitudinal compression.) Shear buckling as shown in Fig. 5.8c is basically an interaction between the diagonal, destabilising compression and the stabilising tension on the other diagonal.

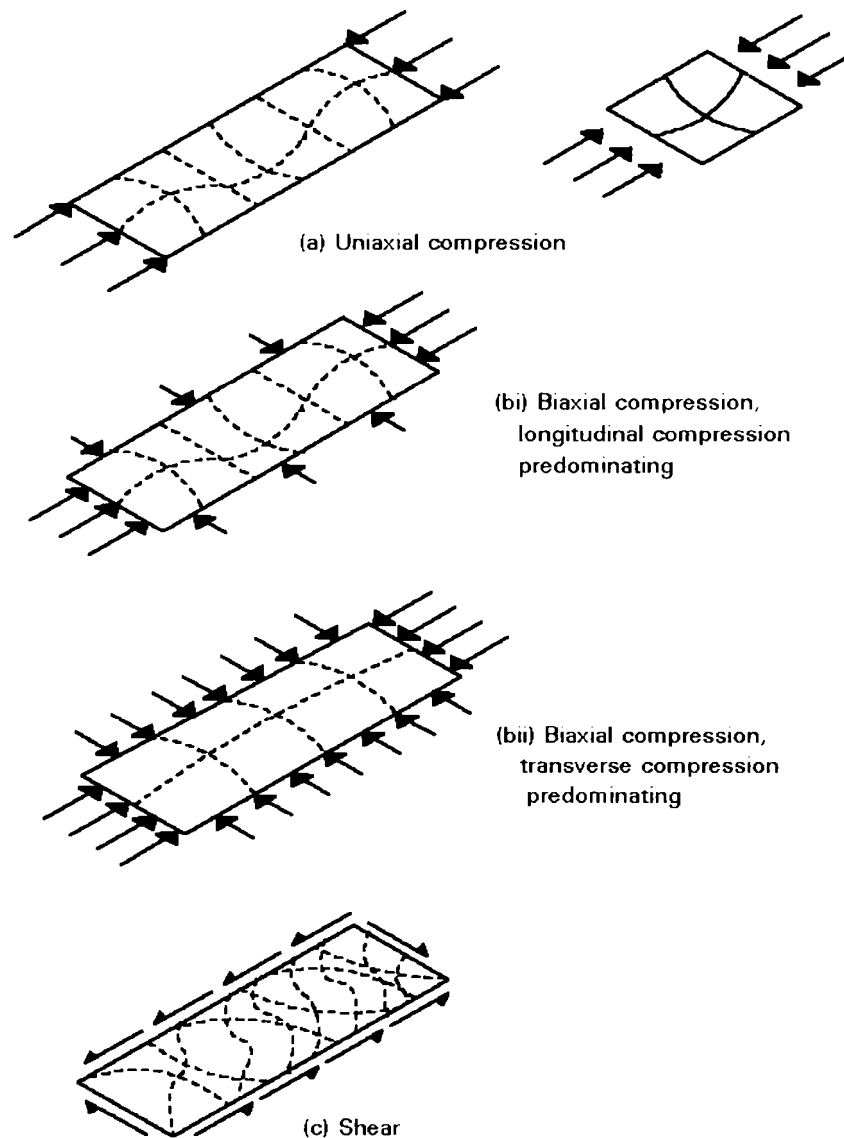


Fig. 5.8. Buckling modes for plate panels

Where buckled modes under the different action effects are similar, the buckling stresses under the combined actions are less than the addition of individual action

effects. Fig 5.9 shows the buckling interactions under combined compression, and uniaxial compression and shear.

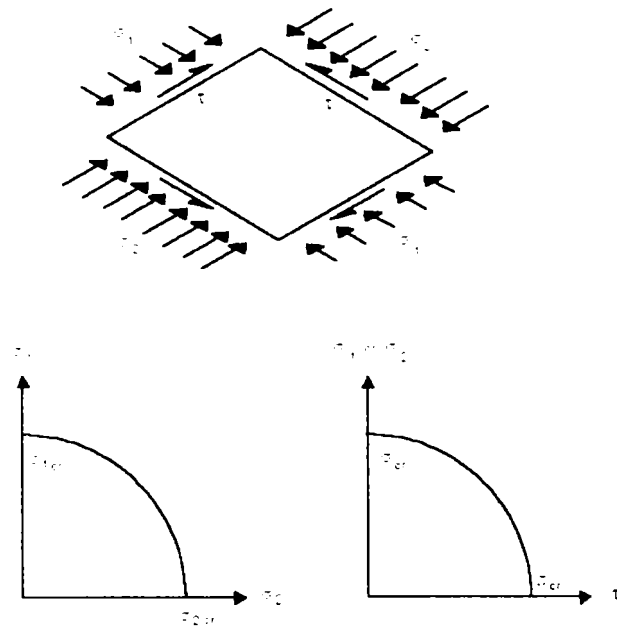


Fig. 5.9. Interaction of buckling modes for square plate panel

5.1.2.6. Grillage analogy for plate buckling

One helpful way to consider the buckling behaviour of a plate is as the grillage shown in Fig. 5.10. A series of longitudinal columns carry the longitudinal actions. When they buckle, those nearer the edge have greater restraint than those near the centre from the transverse flexural members. They therefore have greater post buckling stiffness and carry a greater proportion of the action. As the grillage moves more into the post buckling regime, the transverse buckling restraint is augmented by transverse membrane action.

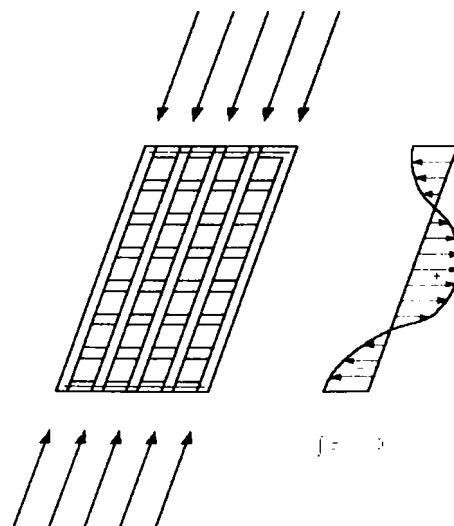


Fig. 5.10. Grid model of plate in compression

5.1.2.7 Post buckling behaviour and effective widths

Fig. 5.11a, 5.11b and 5.11c describes in more detail the changing distribution of stresses as a plate buckles following the equilibrium path shown in Fig. 5.11d. As the plate initially buckles the stresses redistribute to the stiffer edges. As the buckling continues this redistribution becomes more extreme (the middle strip of slender plates may go into tension before the plate fails). Also transverse membrane stresses build up. These are self equilibrating unless the plate has clamped in-plane edges; tension at the mid panel, which restrains the buckling is resisted by compression at the edges, which are restrained from out-of-plane movement.

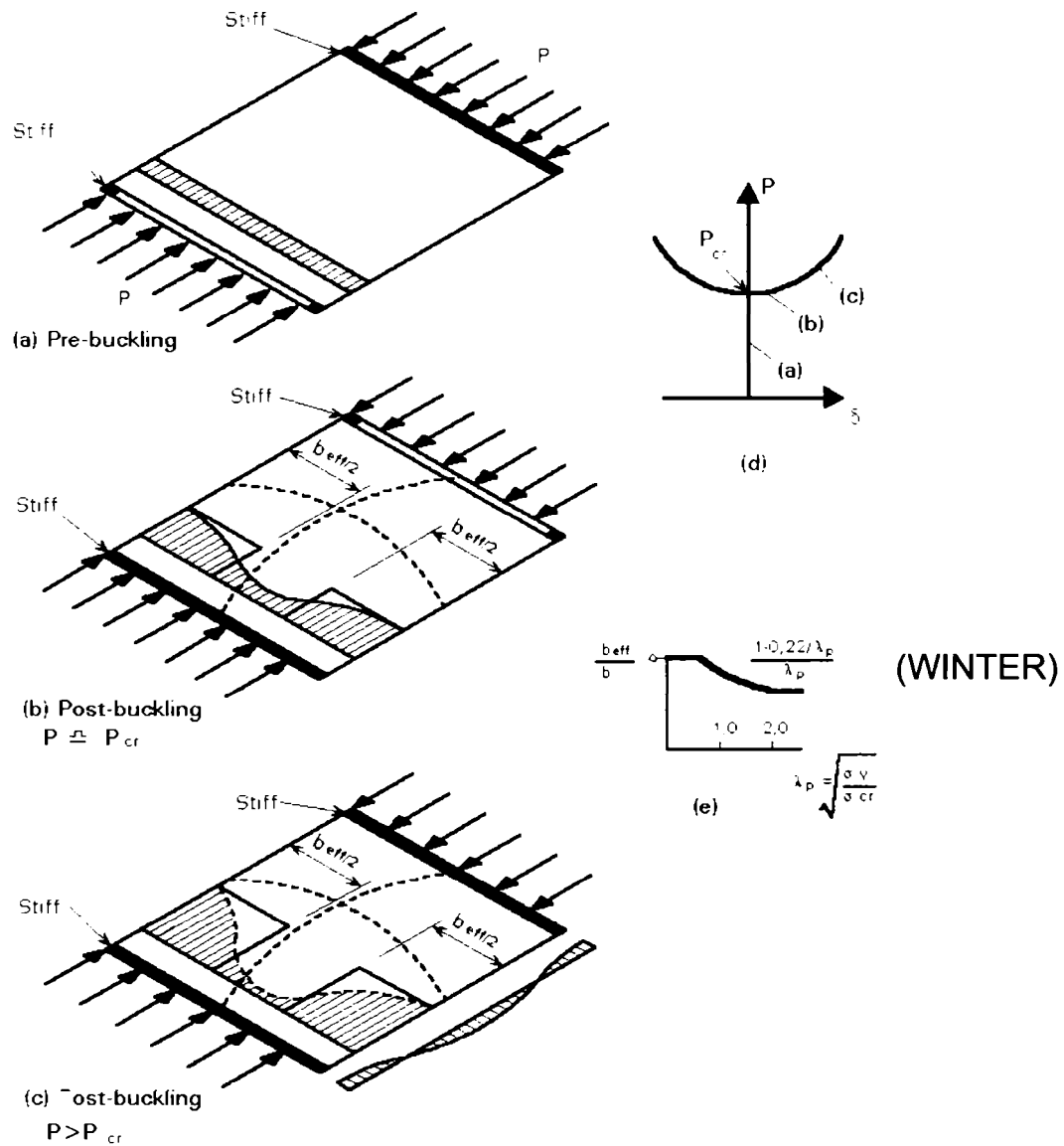
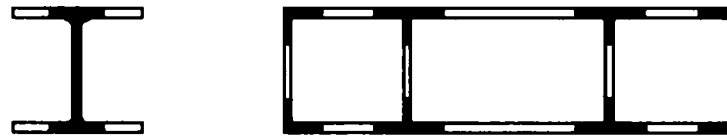


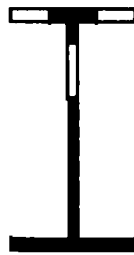
Fig. 5.11. Buckling behaviour of square plate in compression with simply supported edges, free to pull in but held straight

An examination of the non-linear longitudinal stresses in Fig. 5.11a and 5.11c show that it is possible to replace these stresses by rectangular stress blocks that have the same peak stress and same action effect. This effective width of plate (comprising $b_{eff}/2$ on each side) proves to be a very effective design concept. Fig. 5.11e shows how effective width varies with slenderness (λ_p is a measure of plate slenderness that is independent of yield stress; $\lambda_p = 1,0$ corresponds to values of b/t of 57, 53 and 46 for f_y of 235N/mm², 275N/mm² and 355N/mm² respectively).

Fig. 5.12 shows how effective widths of plate elements may be combined to give an effective cross-section of a member.



(a) Effective section (shaded) for typical members in axial compression



(b) Effective section (shaded) for typical plate girder under sagging moment

Fig. 5.12. The application of effective width of plate panels to determine effective cross-sections

5.1.2.8 The influences of imperfections on the behaviour of actual plates

As with all steel structures, plate panels contain residual stresses from manufacture and subsequent welding into plate assemblies, and are not perfectly flat. The previous discussions about plate panel behaviour all relate to an ideal, perfect plate.

As it is shown in Fig. 5.13 these imperfections modify the behaviour of actual plates. For a slender plate the behaviour is asymptotic to that of the perfect plate and there is little reduction in strength. For plates of intermediate slenderness (which frequently occur in practice), an actual imperfect plate will have a considerably lower strength than that predicted for the perfect plate.

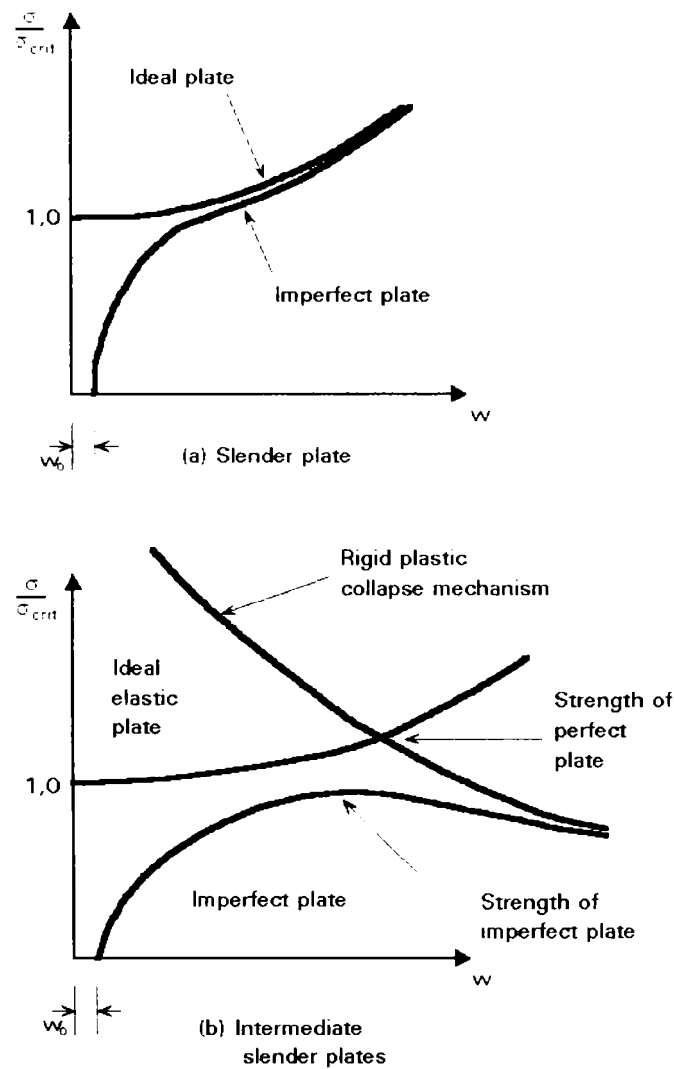


Fig. 5.13. The influence of imperfections on the behaviour of plates of different slenderness in compression

Fig. 5.14 summarises the strength of actual plates of varying slenderness. It shows the reduction in strength due to imperfections and the post buckling strength of slender plates.

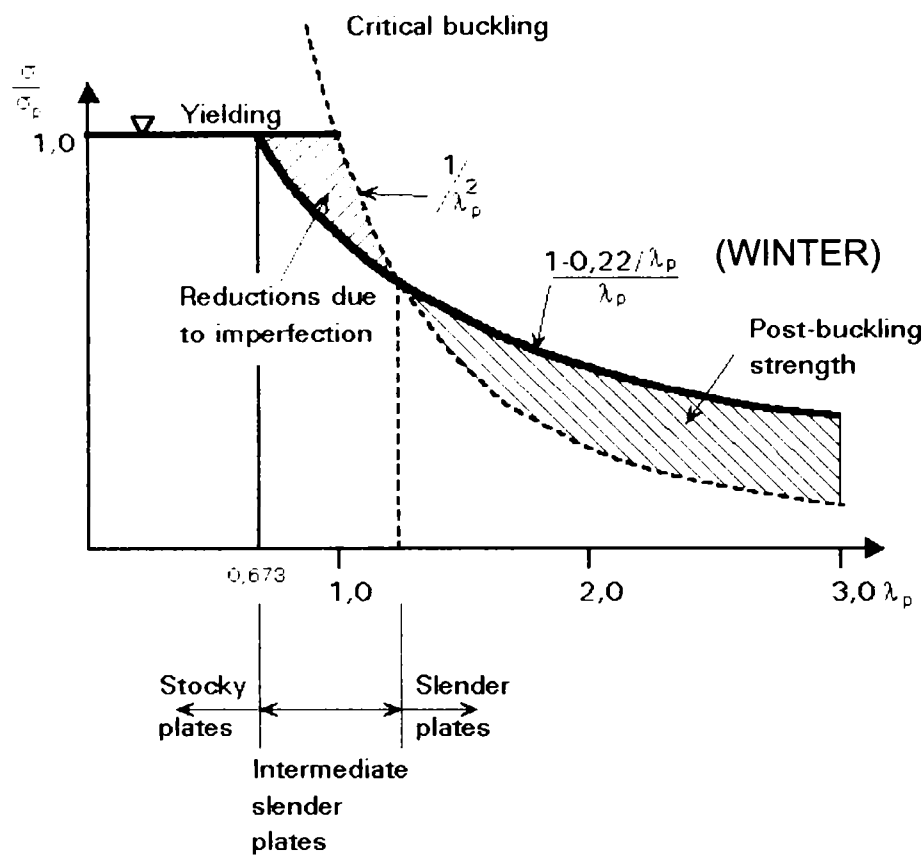


Fig. 5.14. Relationship between plate slenderness and strength in compression

5.1.2.9. Elastic behaviour of plates under lateral actions

Fig. 5.15 contrasts the behaviour of a similar plate with different boundary conditions.

The elastic behaviour of laterally loaded plates is considerably influenced by its support conditions (Fig. 5.15a). If the plate is resting on simple supports as in Fig. 5.15b, it will deflect into a shape approximating a saucer and the corner regions will lift off their supports. If it is attached to the supports, as in Fig. 5.15c, for example by welding, this lift off is prevented and the plate stiffness and action capacity increases. If the edges are encastre as in Fig. 5.15d, both stiffness and strength are increased by the boundary restraining moments.

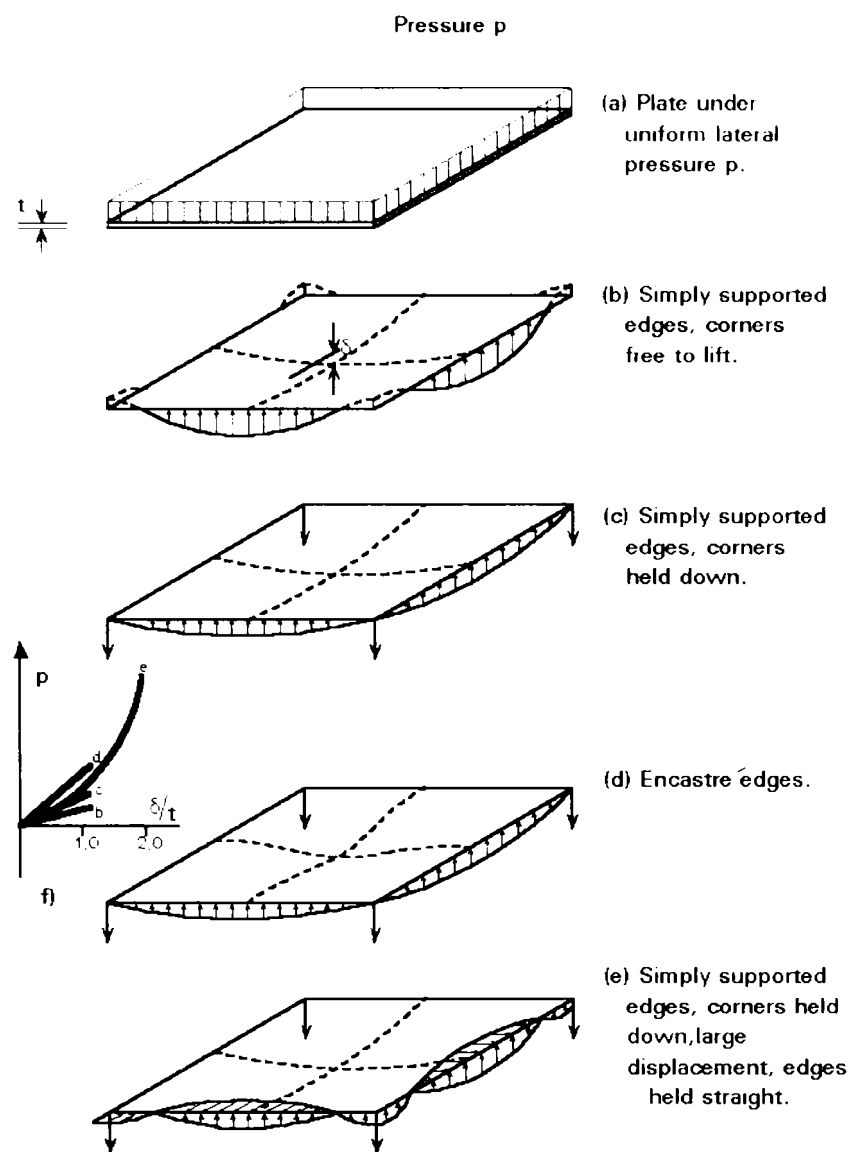


Fig. 5.15. Elastic behaviour of square plate under lateral actions with different boundary conditions

Slender plates may well deflect elastically into a large displacement regime (typically where $\delta > t$). In such cases the flexural response is significantly enhanced by the membrane action of the plate. This membrane action is at its most effective if the edges are fully clamped. Even if they are only held partially straight by their own in-plane stiffness, the increase in stiffness and strength is most noticeable at large deflections.

Fig. 5.16 shows the modes of behaviour that occur if the plates are subject to sufficient load for full yield line patterns to develop. The greater number of yield lines as the boundary conditions improve is a qualitative measure of the increase in resistance.

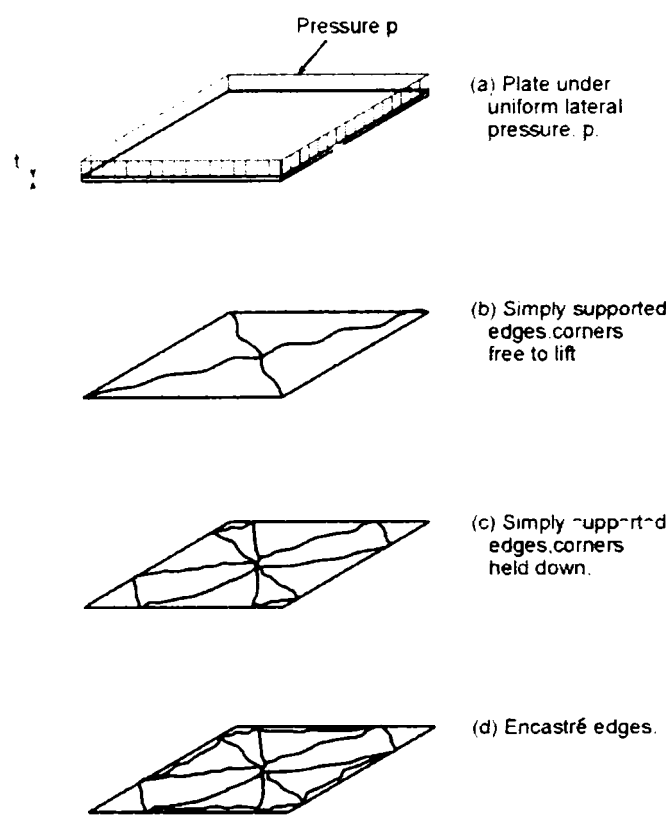


Fig. 5.16. Yield line patterns for square plates under lateral loading with various boundary conditions

5.1.3. Behaviour of stiffened plate

Many aspects of stiffened plate behaviour can be deduced from a simple extension of the basic concepts of behaviour of unstiffened plate panels. However, in making these extrapolations it should be recognised that:

- "Smearing" the stiffeners over the width of the plate can only model overall behaviour.
- Stiffeners are usually eccentric to the plate. Flexural behaviour of the equivalent tee section induces local direct stresses in the plate panels.
- Local effects on plate panels and individual stiffeners need to be considered separately.
- The discrete nature of the stiffening introduces the possibility of local modes of buckling. For example, the stiffened flange shown in Fig. 5.17a shows several modes of buckling. Examples are:

- (i) plate panel buckling under overall compression plus any local compression arising from the combined action of the plate panel with its attached stiffening, Fig. 5.17b.
- (ii) stiffened panel buckling between transverse stiffeners, Fig. 5.17c. This occurs if the latter have sufficient rigidity to prevent overall buckling. Plate action is not very significant because the only transverse member is the plate itself. This form of buckling is best modelled by considering the stiffened panel as a series of tee sections buckling as columns. It should be noted that this section is monosymmetric and will exhibit different behaviour if the plate or the stiffener tip is in greater compression.
- (iii) overall or orthotropic buckling, Fig. 5.17d. This occurs when the cross girders are flexible. It is best modelled by considering the plate assembly as an orthotropic plate.

(In this Doctoral Thesis I have created such a design process which can take into account the stiffness of the cross girders. The calculations were performed according to EC 3-1-5 and the stiffness of the cross girders were calculated according to the concept of the "ideal" cross section.)

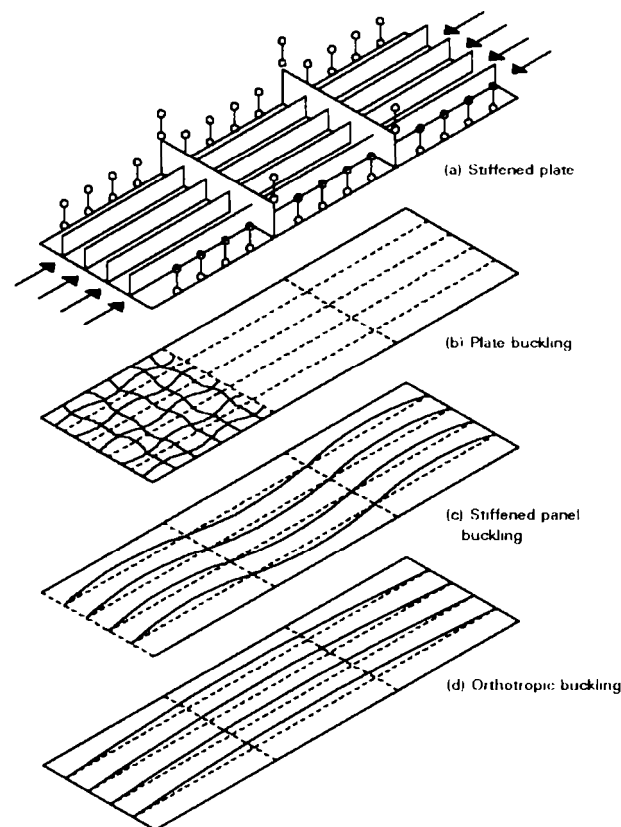


Fig. 5.17. Buckling modes for stiffened plates in compression

5.2. Behaviour and design of unstiffened plate

5.2.1. Introduction

Thin-walled members, composed of thin plate panels welded together, are increasingly important in modern steel construction. In this way, by appropriate selection of steel quality, geometry, etc., cross-sections can be produced that best fit the requirements for strength and serviceability, thus saving steel.

Recent developments in fabrication and welding procedures allow the automatic production of such elements as plate girders with thin-walled webs, box girders, thin-walled columns, etc. (Fig. 5.18a); these can be subsequently transported to the construction site as prefabricated elements.

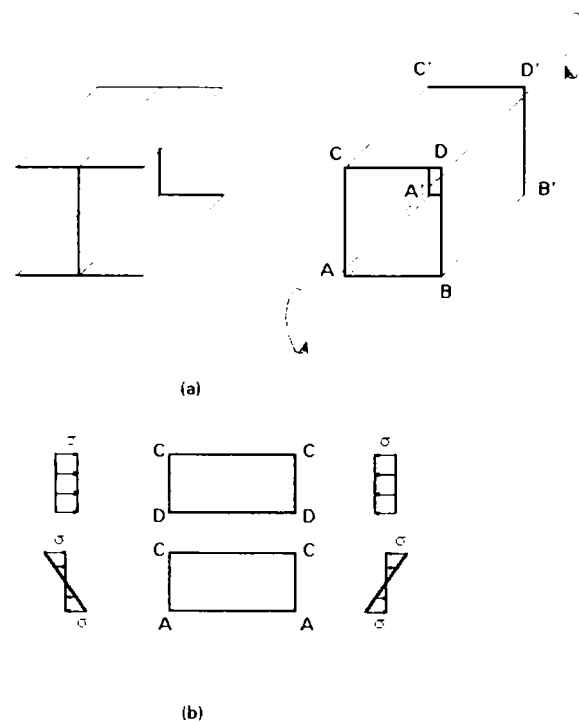


Fig. 5.18. Typical sections (a) examples, (b) in-plane stress conditions for box girder subpanels

Due to their relatively small thickness, such plate panels are basically not intended to carry actions normal to their plane. However, their behaviour under in-plane actions is of specific interest (Fig. 5.18b). Two kinds of in-plane actions are distinguished:

- those transferred from adjacent panels, such as compression or shear.
- those resulting from locally applied forces (patch loading) which generate zones of highly concentrated local stress in the plate.

The behaviour under patch action is a specific problem on plate girders. This subchapter deals with the more general behaviour of unstiffened panels subjected to in-plane actions (compression or shear) which is governed by plate buckling. It also discusses the effects of out-of-plane actions on the stability of these panels.

5.2.2. Unstiffened plates under in-plane loading

5.2.2.1 Load distribution

5.2.2.1.1. Distribution resulting from membrane theory

The stress distribution in plates that react to in-plane loading with membrane stresses may be determined, in the elastic field, by solving the plane stress elastostatic problem governed by Navier's equations.

5.2.2.1.2 Distribution resulting from linear elastic theory using Bernouilli's hypothesis

For slender plated structures, where the plates are stressed as membranes, the application of Airy's stress function is not necessary due to the hypothesis of plane strain distributions, which may be used in the elastic as well as in the plastic range, (see Fig. 5.19).

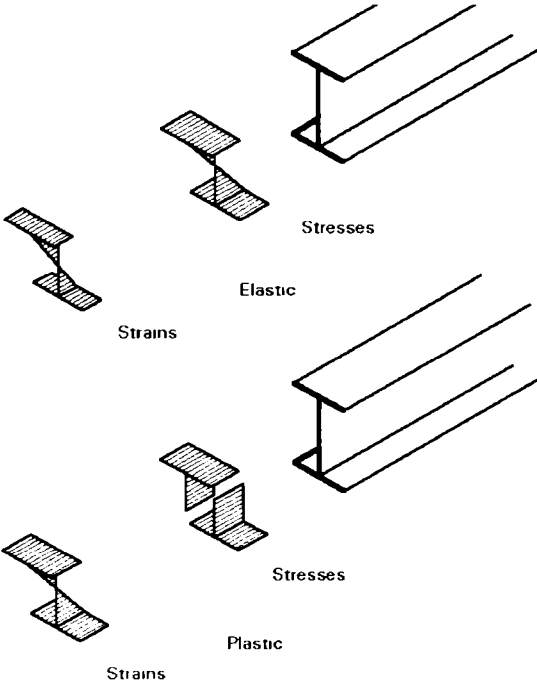


Fig. 5.19. Plane stress distribution

However, for wide flanges of plated structures, the application of Airy's stress function leads to significant deviations from the plane strain hypothesis, due to the shear lag effect, (Fig. 5.20). Shear lag may be taken into account by taking a reduced flange width.

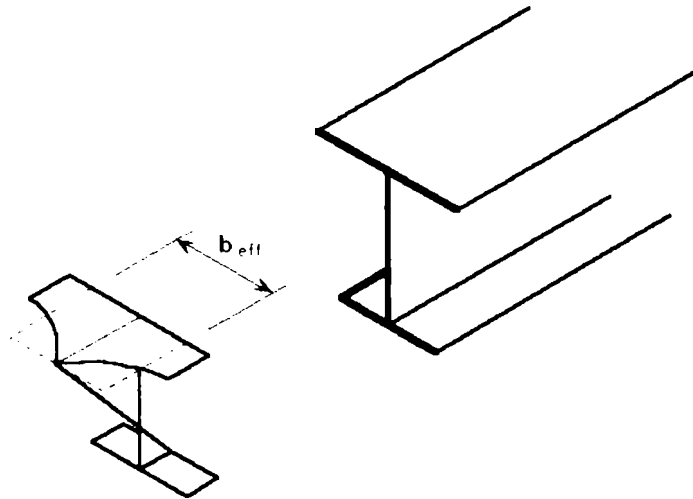


Fig. 5.20. Effective width due to shear lag

5.2.2.1.3. Distribution resulting from finite element methods

When using finite element methods for the determination of the stress distribution, the plate can be modelled as a perfectly flat arrangement of plate sub-elements. Attention must be given to the load introduction at the plate edges so that shear lag effects will be taken into account. The results of this analysis can be used for the buckling verification.

5.2.2.2. Stability of unstiffened plates

5.2.2.2.1 Linear buckling theory

The buckling of plate panels was investigated for the first time by BRYAN in 1891, in connection with the design of a ship hull (BRYAN, 1891). The assumptions for the plate under consideration (Fig. 5.21a), are those of thin plate theory Kirchhoff's theory, see (SZILARD, (1974), BRUSH, et al (1975), WOLMIR, (1962), TIMOSHENKO, et al (1959)):

- a) The material is linear elastic, homogeneous and isotropic.
- b) The plate is perfectly plane and stress free.

- c) The thickness "t" of the plate is small compared to its other dimensions.
- d) The in-plane actions pass through its middle plane.
- e) The transverse displacements w are small compared to the thickness of the plate.
- f) The slopes of the deflected middle surfaces are small compared to unity.
- g) The deformations are such that straight lines, initially normal to the middle plane, remain straight lines and normal to the deflected middle surface.
- h) The stresses normal to the thickness of the plate are of a negligible order of magnitude.

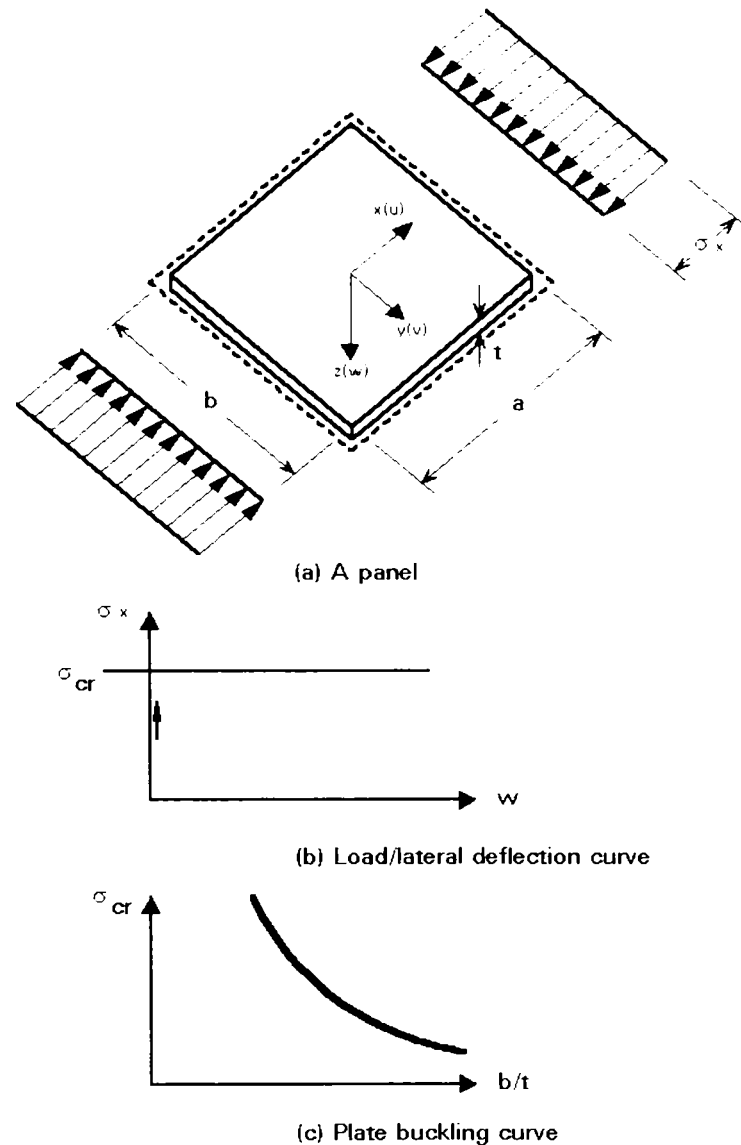


Fig. 5.21. Linear buckling theory-notation

Due to assumption (e) the rotations of the middle surface are small and their squares can be neglected in the strain displacement relationships for the stretching of the middle surface.

An important consequence of this assumption is that there is no stretching of the middle surface due to bending, and the differential equations governing the deformation of the plate are linear and uncoupled. This theory, in which the equations are linear, is referred to as linear buckling theory.

Of particular interest is the application of the linear buckling theory to rectangular plates, subjected to constant edge loading (Fig. 5.21a). The load lateral deflection curve is given by Fig. 5.21b. In this case the critical action, which corresponds to the Euler buckling load of a compressed strut, may be written as:

$$\sigma_{cr} = k_s \sigma_E \text{ or } \tau_{cr} = k_t \sigma_E, \quad (5.1)$$

$$\text{where } \sigma_E = \frac{\pi^2 E}{12(1-\nu^2) \left(\frac{b}{t}\right)^2}, \quad (5.2)$$

and k_s, k_t are dimensionless buckling coefficients.

Only the form of the buckling surface may be determined by this theory but not the magnitude of the buckling amplitude. The relationship between the critical stress σ_{cr} , and the slenderness of the panel $\lambda = b/t$, is given by the buckling curve. This curve, shown in Fig. 5.21c, has a hyperbolic shape and is analogous to the Euler hyperbola for struts.

The buckling coefficients, "k", may be determined either analytically or numerically, using the energy method, the method of transfer matrices, etc. Values of k_s and k_t for various actions and support conditions are shown in Fig. 5.22 as a function of the aspect ratio of the plate $\alpha = a/b$. The curves for k_s have α "garland" form. Each garland corresponds to a buckling mode with a certain number of waves. For a plate subjected to uniform compression, as shown in Fig. 5.22. Obviously, the buckling mode that gives the smallest value of k is the decisive one. For practical reasons a single value of k_s is chosen for plates subjected to normal stresses. This is the smallest value for the garland curves independent of the value of the aspect ratio. In the example given in Fig. 5.22 k_s is equal to 4 for a plate which is simply supported on all four sides and subjected to uniform compression.

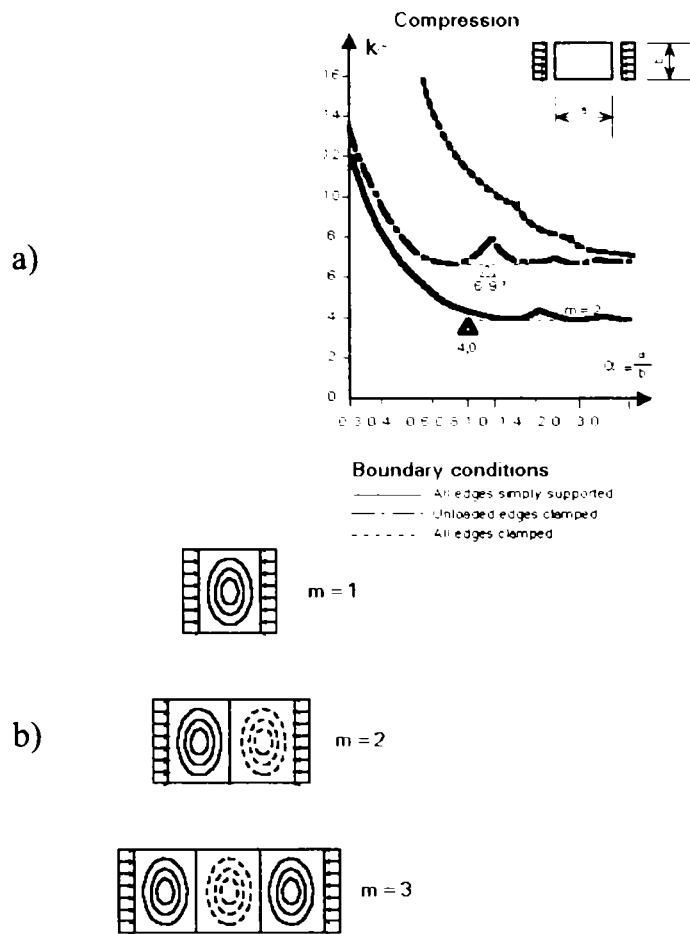


Fig. 5.22a-b. Buckling coefficients k_{σ} for kompression and buckling modes

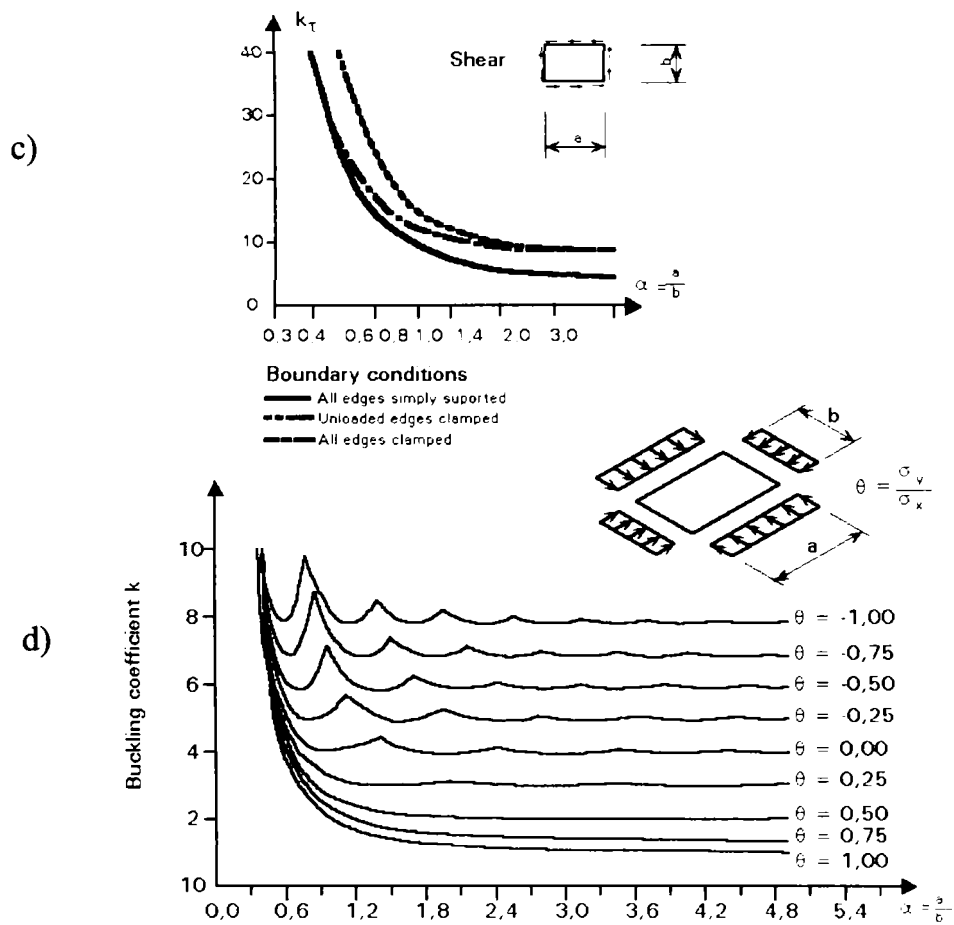


Fig 5.22c-d. Buckling coefficients k_{τ} for shear

Combination of stresses σ_x , σ_y and τ

For practical design situations some further approximations are necessary. They are illustrated by the example of a plate girder, shown in Fig.5.23.

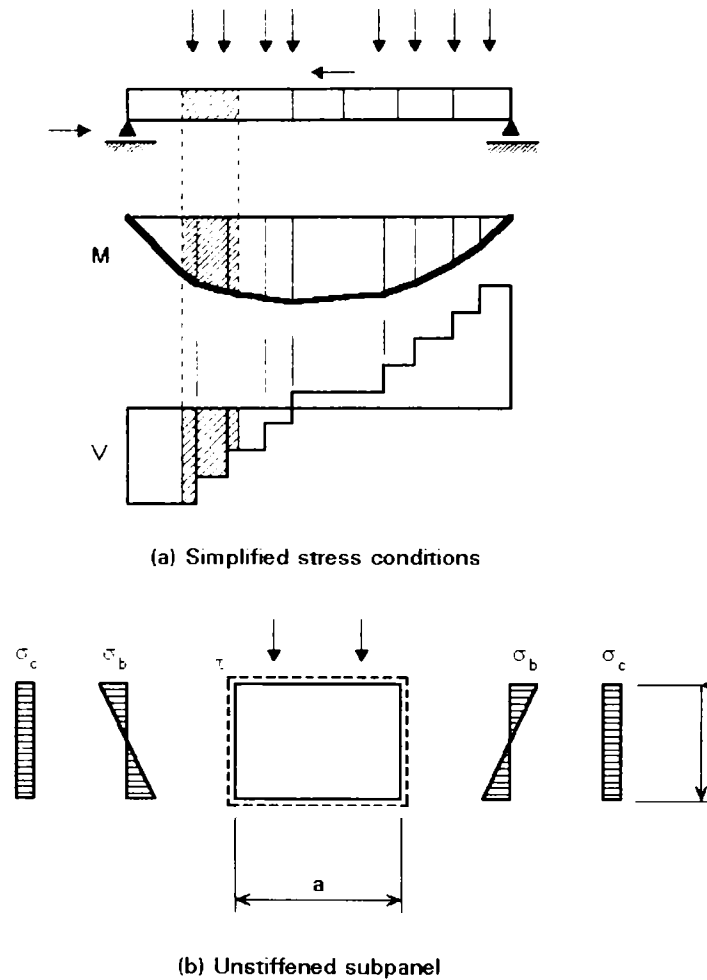


Fig. 5.23. Separation of unstiffened subpanels for a plate girder

The normal and shear stresses, σ_x and τ respectively, at the opposite edges of a subpanel are not equal, since the bending moments M and the shear forces V vary along the panel. However, M and V are considered as constants for each subpanel and equal to the largest value at an edge (or equal to the value at some distance from it). This conservative assumption leads to equal stresses at the opposite edges for which the charts of k_s and k_t apply. The verification is usually performed for two subpanels; one with the largest value of σ_x and one with the largest value of t . In most cases, as in Fig. 5.23 each subpanel is subjected to a combination of normal and shear stresses. A direct determination of the buckling coefficient for a given combination of stresses is possible; but it requires considerable numerical effort. For

practical situations an equivalent buckling stress σ_{cr}^{eq} is found by an interaction formula after the critical stresses σ_{cr}^{eq} and τ_{cr}^0 , for independent action of s and t have been determined. The interaction curve for a plate subjected to normal and shear stresses, σ_x and τ respectively, varies between a circle and a parabola (CHWALLA (1944)), depending on the value of the ratio ψ of the normal stresses at the edges (Fig. 5.24)

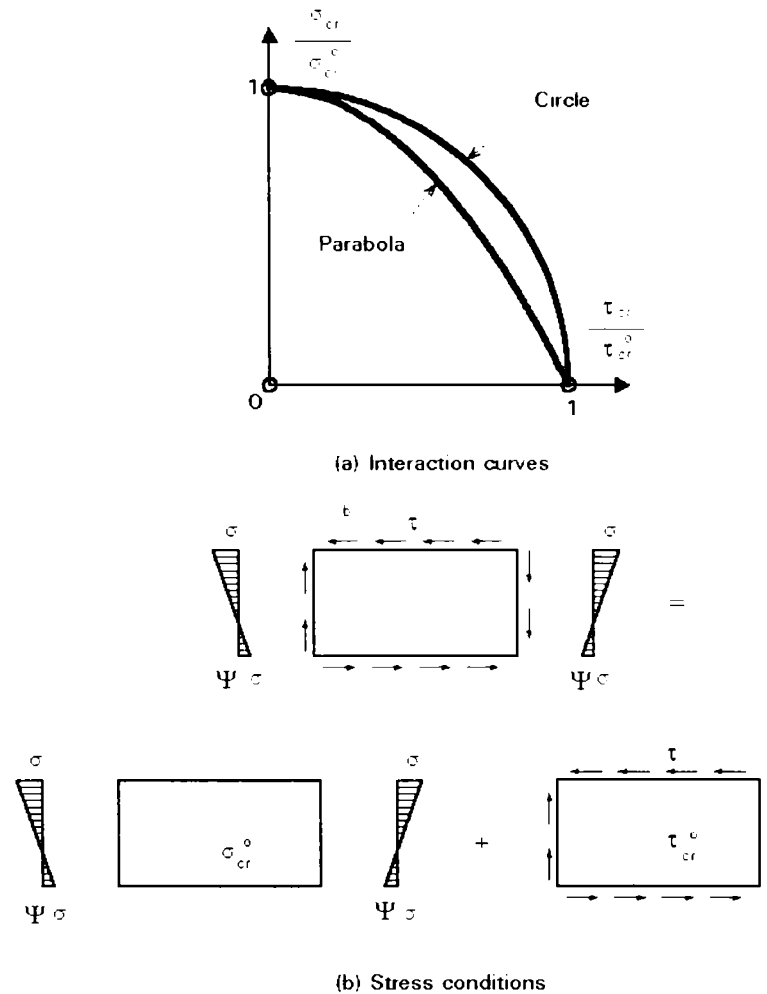


Fig. 5.24. Consideration of plate under combined shear and direct in plane stresses

5.2.2.2 Ultimate resistance of an unstiffened plate

General

The linear buckling theory described in the previous section is based on assumptions from (a) to (h) in 5.2.2.1, that are never fulfilled in real structures. The consequences for the buckling behaviour when each of these assumptions is removed is now discussed.

The first assumption of unlimited linear elastic behaviour of the material is obviously not valid for steel. If the material is considered to behave as linear elastic-ideal plastic, the buckling curve must be cut off at the level of the yield stress σ_y (Fig. 5.25b).

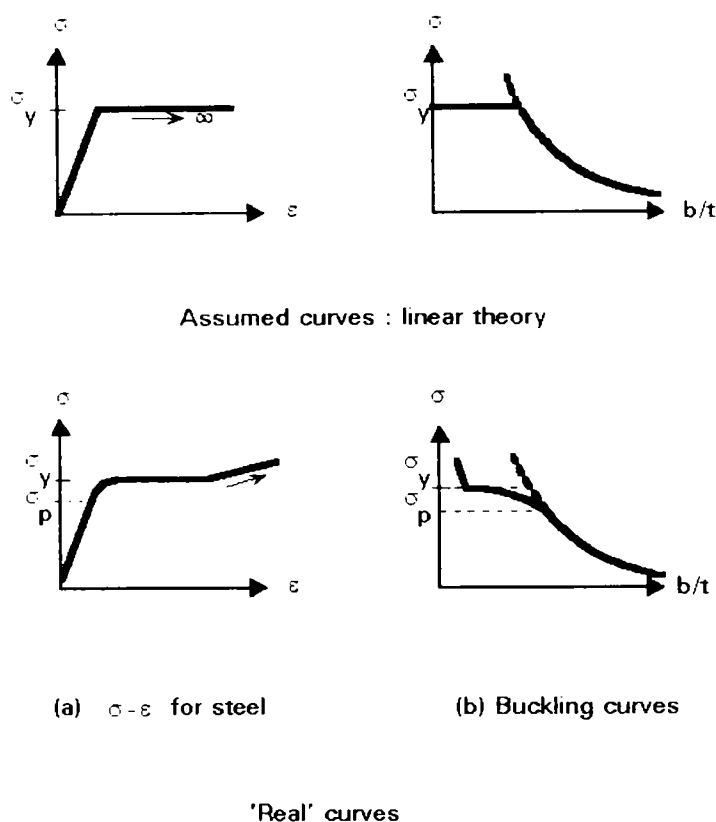
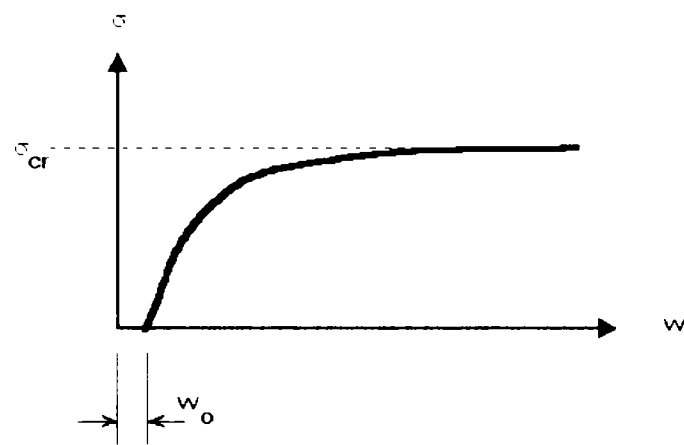


Fig. 5.25. σ - ϵ diagrams for steel and corresponding buckling curves

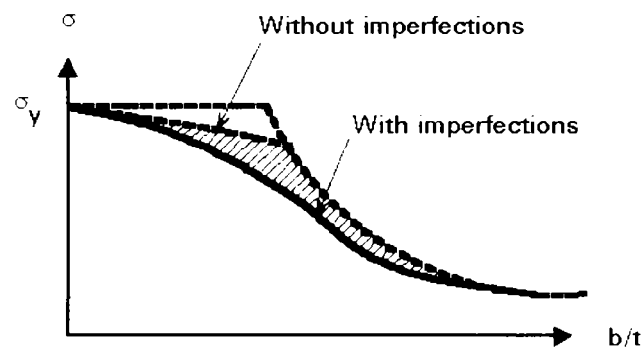
When the non-linear behaviour of steel between the proportionality limit σ_p and the yield stress σ_y is taken into account, the buckling curve will be further reduced (Fig. 5.25b). When strain hardening is considered, values of σ_{cr} larger than σ_y , as experimentally observed for very stocky panels, are possible. In conclusion, it may be stated that the removal of the assumption of linear elastic behaviour of steel results in a reduction of the ultimate stresses for stocky panels.

The second and fourth assumptions of a plate without geometrical imperfections and residual stresses, under symmetric actions in its middle plane, are also never fulfilled in real structures. If the assumption of small displacements is still retained, the analysis of a plate with imperfections requires a second order analysis. This analysis has no bifurcation point since for each level of stress the corresponding displacements w may be determined. The equilibrium path (Fig. 5.26a) tends

asymptotically to the value of σ_{cr} for increasing displacements, as is found from the second order theory.



(a) Action-lateral deflection curve for plate with imperfections



(b) Buckling curves for linear theory with plasticity

Fig. 5.26. Action-deflection curve for a plate with imperfections and buckling curve for linear theory with plasticity

However the ultimate stress is generally lower than σ_{cr} since the combined stress due to the buckling and the membrane stress is limited by the yield stress. This limitation becomes relevant for plates with geometrical imperfections, in the region of moderate slenderness, since the value of the buckling stress is not small (Fig. 5.26b). For plates with residual stresses the reduction of the ultimate stress is primarily due to the small value of σ_p (Fig. 5.25b) at which the material behaviour becomes non-linear. In conclusion it may be stated that imperfections due to geometry, residual stresses and eccentricities of loading lead to a reduction of the ultimate stress, especially in the range of moderate slenderness.

The assumption of small displacements (e) in 5.2.2.2.1. is not valid for stresses in the vicinity of σ_{cr} as shown in Fig. 5.26a. When large displacements are considered the equations are known as the von Karman equations (TIMOSHENKO, et al (1959)). They constitute the basis of the (geometrically) non-linear buckling theory. For a plate without imperfections the equilibrium path still has a bifurcation point at σ_{cr} , but, unlike the linear buckling theory, the equilibrium for stresses $\sigma > \sigma_{cr}$ is still stable (Fig. 5.27).

The equilibrium path for plates with imperfections tends asymptotically to the same curve. The ultimate stress may be determined by limiting the stresses to the yield stress. It may be observed that plates possess a considerable post-critical carrying resistance. This post-critical behaviour is more pronounced the more slender the plate, i.e. the smaller the value of σ_{cr} .

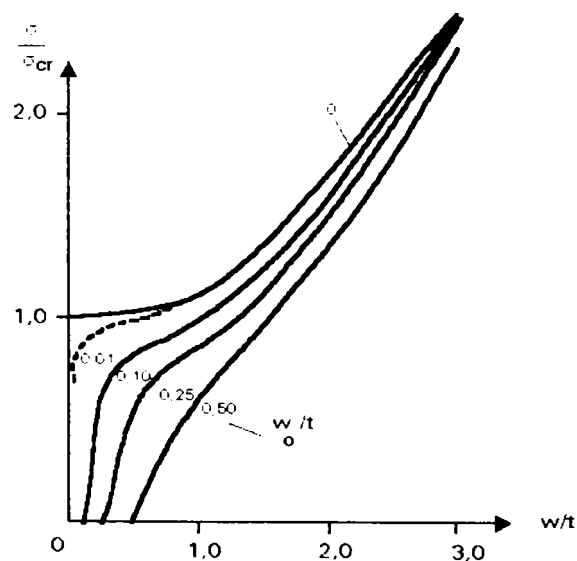


Fig. 5.27. Action-deflection curves of plates with imperfections for (geometrically) non-linear buckling theory

Buckling curve

For the reasons outlined above, it is evident that the Euler buckling curve for linear buckling theory (Fig. 5.22c) may not be used for design. A lot of experimental and theoretical investigations have been performed in order to define a buckling curve that best represents the true behaviour of plate panels. For relevant literature reference should be made to Dubas and Gehri (DUBAS, et al (1986)). For design

purposes it is advantageous to express the buckling curve in a dimensionless form as described below.

The slenderness of a panel may be written according to Eq. 5.1 and Eq. 5.2 as:

$$\lambda_p = \left(\frac{b}{t}\right) \sqrt{\frac{12(1-\nu^2)}{k_s}} = \pi \sqrt{\frac{E}{\sigma_{cr}}} \quad (5.3)$$

If a reference slenderness given by:

$$\lambda_y = \pi \sqrt{\frac{E}{f_y}} \quad (5.4)$$

is introduced, the relative slenderness becomes:

$$\bar{\lambda}_p = \frac{\lambda_p}{\lambda_y} = \sqrt{\frac{\sigma_y}{\sigma_{cr}}} \quad (5.5)$$

The ultimate stress is also expressed in a dimensionless form by introducing a reduction factor:

$$k = \frac{\sigma_u}{\sigma_y} \quad (5.6)$$

Dimensionless curves for normal and for shear stresses as proposed by Eurocode 3 (EUROCODE 3 (1992)) are illustrated in Fig. 5.28.

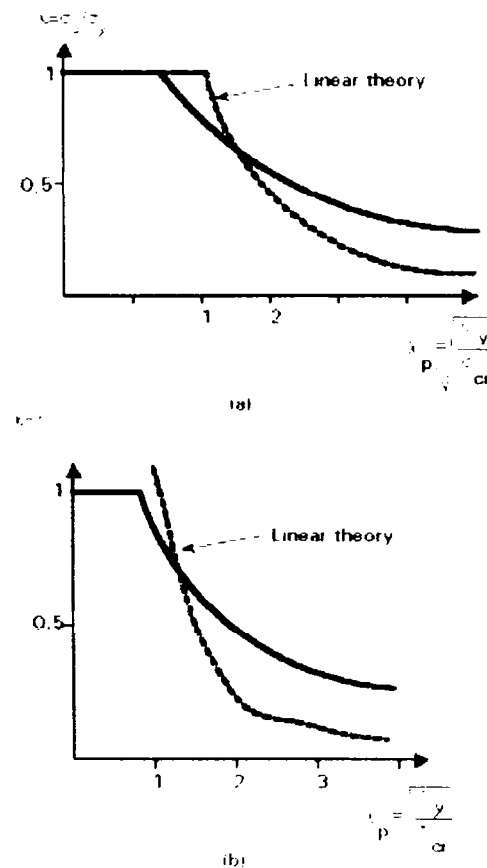


Fig. 5.28. Buckling curves (a) normal and (b) shear stresses

These buckling curves have higher values for large slendernesses than those of the Euler curve due to post critical behaviour and are limited to the yield stress. For intermediate slendernesses, however, they have smaller values than those of Euler due to the effects of geometrical imperfections and residual stresses.

Although the linear buckling theory is not able to describe accurately the behaviour of a plate panel, its importance should not be ignored. In fact this theory, as in the case of struts, yields the value of an important parameter, namely $\bar{\lambda}_p$, that is used for the determination of the ultimate stress.

Effective width method

This method has been developed for the design of thin walled sections subjected to uniaxial normal stresses. It will be illustrated for a simply-supported plate subjected to uniform compression (Fig. 5.29a).

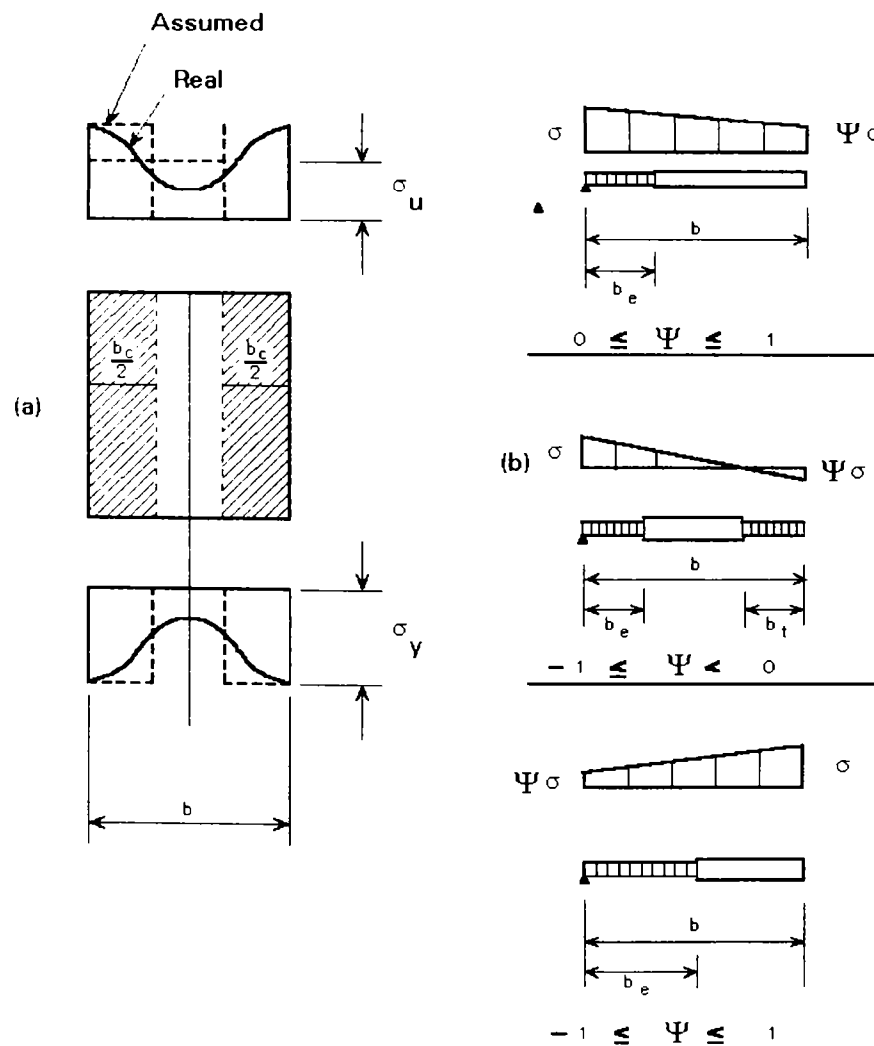


Fig. 5.29. Definition of the effective width for a plate supported on one side

The stress distribution which is initially uniform, becomes non-uniform after buckling, since the central parts of the panel are not able to carry more stresses due to the bowing effect. The stress at the stiff edges (towards which the redistribution takes place) may reach the yield stress. The method is based on the assumption that the non-uniform stress distribution over the entire panel width may be substituted by a uniform one over a reduced "effective" width. This width is determined by equating the resultant forces:

$$b\sigma_u = b_e\sigma_y, \quad (5.7)$$

and accordingly

$$b_e = \frac{\sigma_u b}{\sigma_y} = kb, \quad (5.8)$$

which shows that the value of the effective width depends on the buckling curve adopted. For uniform compression the effective width is equally distributed along the two edges (Fig. 5.29a). For non-uniform compression and other support conditions it is distributed according to rules given in the various regulations. Some examples of the distribution are shown in Fig. 5.29b. The effective width may also be determined for values of $\sigma < \sigma_u$. In such cases Eq. 5.8 is still valid, but $\overline{\lambda}_p$, which is needed for the determination of the reduction factor k , is not given by Eq. 5.5 but by the relationship

$$\overline{\lambda}_p = \sqrt{\frac{\sigma}{\sigma_{cr}}}. \quad (5.9)$$

The design of thin walled cross-sections is performed according to the following procedure:

- For given actions conditions the stress distribution at the cross-section is determined. At each subpanel the critical stress σ_{cr} , the relative slenderness $\overline{\lambda}_p$ and the effective width b_e are determined according to Eq. 5.1, Eq. 5.5 and Eq. 5.8, respectively. The effective width is then distributed along the panel as illustrated by the examples in Fig. 5.29b. The verifications are finally based on the characteristic A_e , I_e , and W_e of the effective cross-section. For the cross-section of Fig. 5.30b, which is

subjected to normal forces and bending moments, the verification is expressed as:

$$\sigma = \frac{N}{A} + \frac{M + Ne}{I} y \leq \frac{\sigma_y}{\gamma_m}, \quad (5.10)$$

where e is the shift in the centroid of the cross-section to the tension side and γ_m the partial safety factor of resistance.

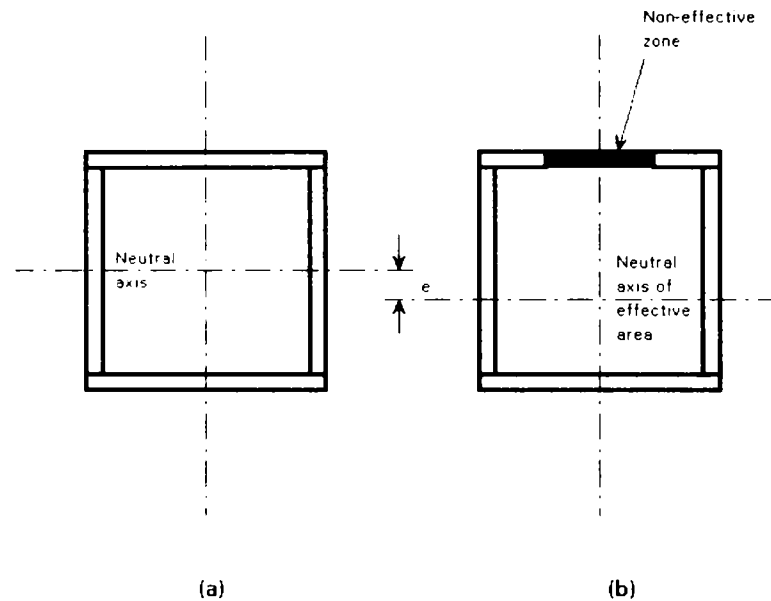


Fig. 5.30. Determination of the effective cross-section

Finite element methods

When using finite element methods to determine the ultimate resistance of an unstiffened plate one must consider the following aspects:

- The modelling of the plate panel should include the boundary conditions as accurately as possible with respect to the conditions of the real structure, see Fig. 5.31. For a conservative solution, hinged conditions can be used along the edges.
- Thin shell elements should be used in an appropriate mesh to make yielding and large curvatures (large out-of-plane displacements) possible.
- The plate should be assumed to have an initial imperfection similar in shape to the final collapse mode.

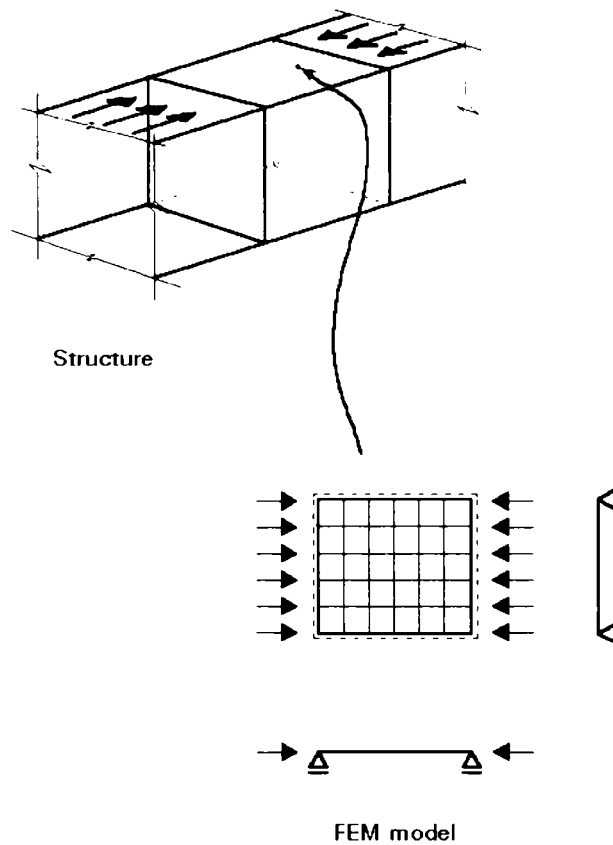
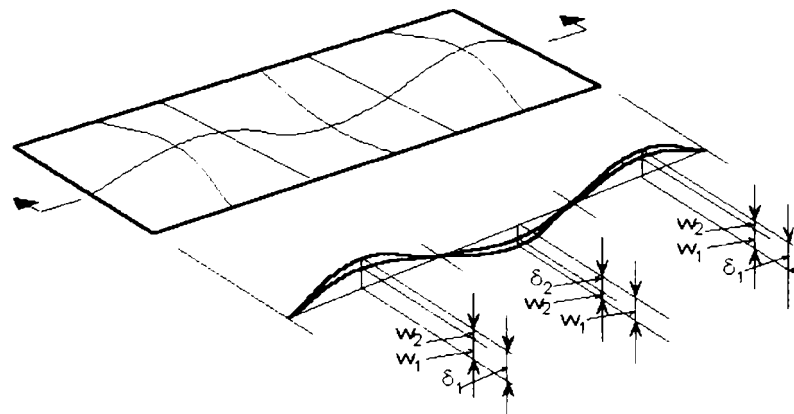


Fig. 5.31. FEM modeling from the real structure

The first order Euler buckling mode can be used as a first approximation to this shape. In addition, a disturbance to the first order Euler buckling mode can be added to avoid snap-through problems while running the programme, see Fig. 5.32. The amplitude of the initial imperfect shape should relate to the tolerances for flatness.



w_1 is the amplitude of the Euler buckling mode
The size is related to the tolerances for fabrication.

w_2 is the amplitude of the disturbance.
 $w_2 \approx 5 - 10\%$ of w_1

$\delta_1 = w_1 + w_2$
 $\delta_2 = w_1 - w_2$ } are the initial imperfections

Fig. 5.32. Initial imperfections for FEM model

The program used must be able to take a true stress-strain relationship into account, see Fig. 5.33 and if necessary an initial stress pattern. The latter can also be included in the initial shape.

The computer model must use a loading which is equal to the design loading multiplied by an action factor. This factor should be increased incrementally from zero up to the desired action level (load factor = 1). If the structure is still stable at the load factor = 1, the calculation process can be continued up to collapse or even beyond collapse into the region of unstable behaviour (Fig. 5.34). In order to calculate the unstable response, the program must be able to use more refined incremental and iterative methods to reach convergence in equilibrium.

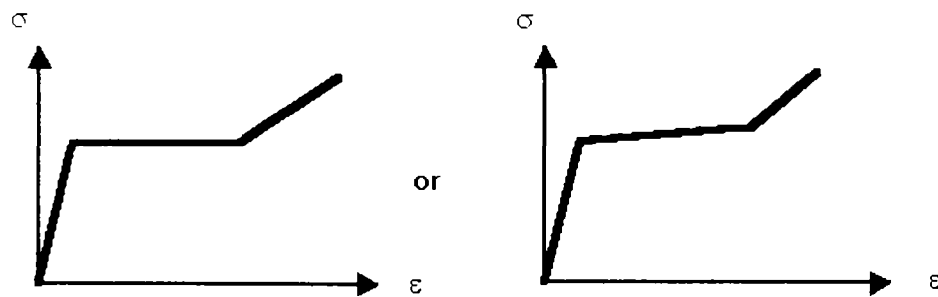


Fig. 5.33. Material model for FEM model

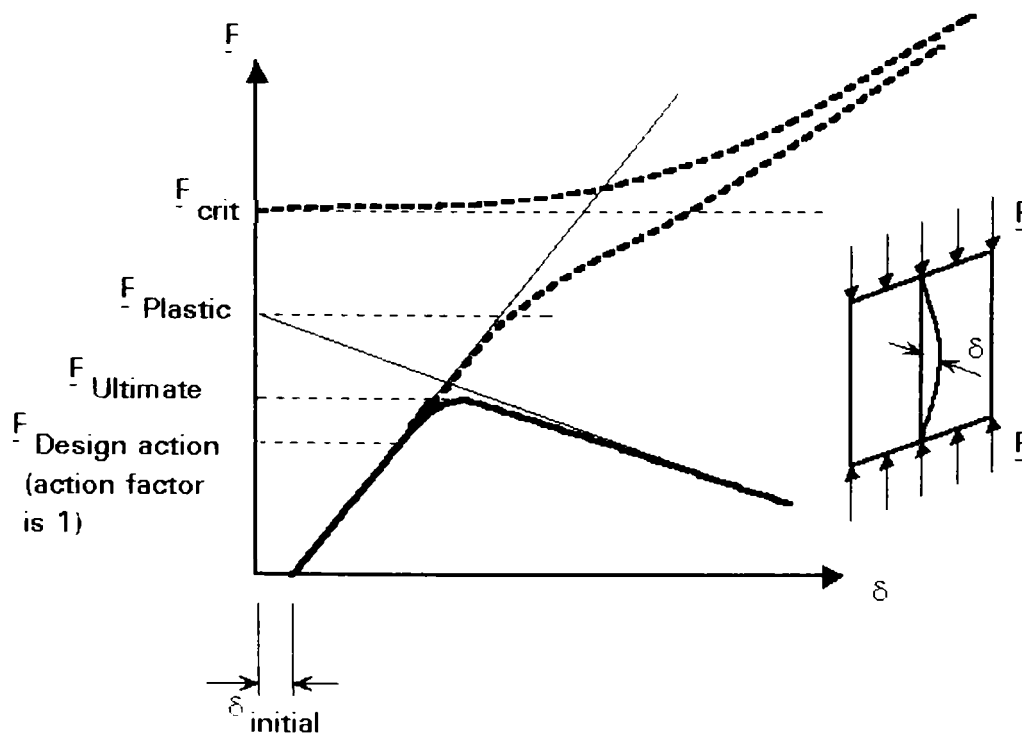


Fig. 5.34. In-plane action – out-of-plane displacement characteristic

5.2.3. Unstiffened plates under out-of-plane actions

5.2.3.1. Action distribution

5.2.3.1.1. Distribution resulting from plate theory

If the plate deformations are small compared to the thickness of the plate, the middle plane of the plate can be regarded as a neutral plane without membrane stresses. This assumption is similar to beam bending theory. The actions are held in equilibrium only by bending moments and shear forces. The stresses in an isotropic plate can be calculated in the elastic range by solving a fourth order partial differential equation, which describes equilibrium between actions and plate reactions normal to the middle plane of the plate.

An approximation may be obtained by modelling the plate as a grid and neglecting the twisting moments.

Plates in bending may react in the plastic range with a pattern of yield lines which, by analogy to the plastic hinge mechanism for beams, may form a plastic mechanism in the limit state (Fig. 5.35). The position of the yield lines may be determined by minimum energy considerations.

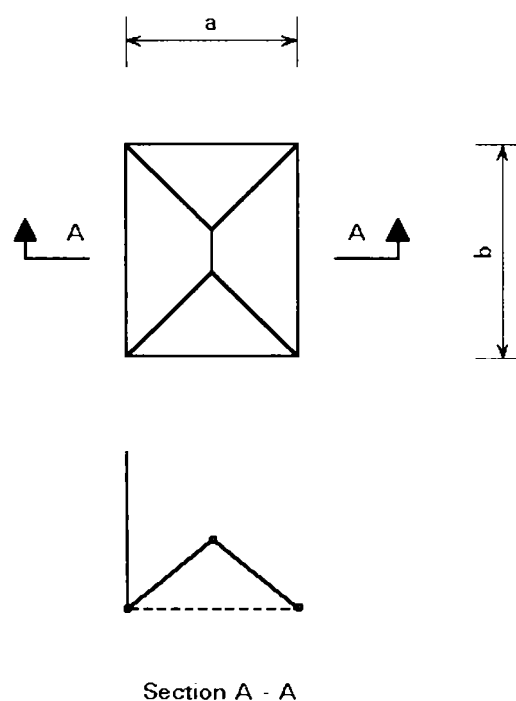


Fig. 5.35. Yield mechanism in a plate

If the plate deformations are of the order of the plate thickness or even larger, the membrane stresses in the plate can no longer be neglected in determining the plate reactions.

The membrane stresses occur if the middle surface of the plate is deformed to a curved shape. The deformed shape can be generated only by tension, compression and shear strains in the middle surface.

This behaviour can be illustrated by the deformed circular plate shown in Fig. 5.36b. It is assumed that the line $a c b$ (diameter d) does not change during deformation, so that a', c', b' is equal to the diameter d . The points which lie on the edge "akb" are now on a', k', b' , which must be on a smaller radius compared with the original one.

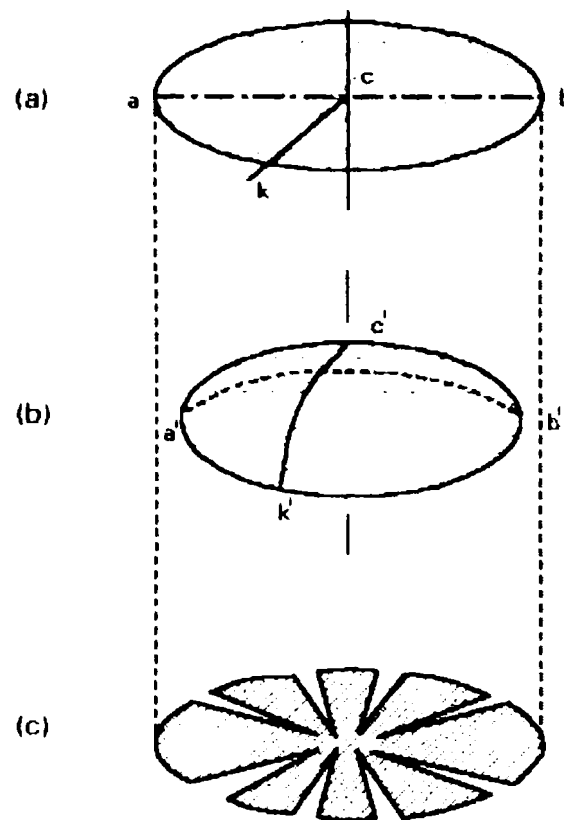


Fig. 5.36. Model to show membrane action in a circular plate under out-of-plane actions

Therefore the distance akb becomes shorter, which means that membrane stresses exist in the ring fibres of the plate. The distribution of membrane stresses can be visualised if the deformed shape is frozen.

It can only be flattened out if it is cut into a number of radial cuts, Fig. 5.36c, the gaps representing the effects of membrane stresses; this explains why curved surfaces are much stiffer than flat surfaces and are very suitable for constructing elements such as cupolas for roofs, etc.

The stresses in the plate can be calculated with two fourth order coupled differential equations, in which an Airy-type stress function which describes the membrane state, has to be determined in addition to the unknown plate deformation.

In this case the problem is non-linear. The solution is far more complicated in comparison with the simple plate bending theory which neglects membrane effects. The behaviour of the plate is governed by von Karman's equations.

5.2.3.1.2. Distribution resulting from finite element methods (FEM)

More or less the same considerations hold when using FEM to determine the stress distribution in plates which are subject to out-of-plane action as when using FEM for plates under in-plane actions, except for the following:

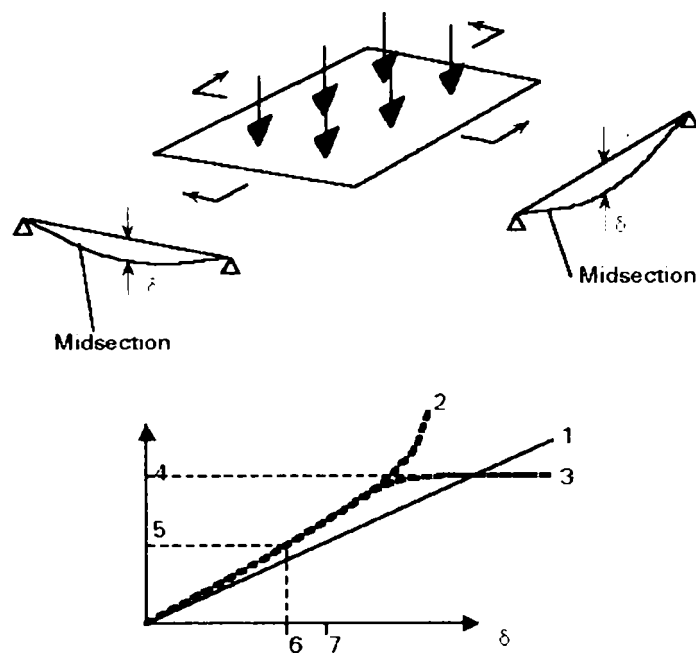
- The plate element must be able to describe large deflections out-of-plane.
- The material model used should include plasticity.

5.2.3.2. Deflection and ultimate resistance

5.2.3.2.1. Deflections

Except for the yield line mechanism theory, all analytical methods for determining the stress distributions will also provide the deformations, provided that the stresses are in the elastic region.

Using adequate finite element methods leads to accurate determination of the deflections, which take into account the decrease in stiffness due to plasticity in certain regions of the plate. Most design codes contain limits to these deflections which have to be met at serviceability load levels (see Fig.5.37).



1. Linear - elastic relationships
2. Non - linear elastic relationship due to membrane action
3. Elastic - plastic behaviour
4. Ultimate resistance
5. Action level at serviceability
6. Deflection due to serviceability action level
7. Deflection limit at serviceability action level

Fig. 5.37. Out-of-plane displacement

5.2.3.2.2 Ultimate resistance

The resistance of plates, determined using the linear plate theory only, is normally much underestimated since the additional strength due to the membrane effect and the redistribution of forces due to plasticity is neglected.

An upper bound for the ultimate resistance can be found using the yield line theory. More accurate results can be achieved using FEM.

Via an incremental procedure, the action level can increase from zero up to the desired design action level or even up to collapse (see Fig. 5.37).

5.2.4. Influence of the out-of-plane actions on the stability of unstiffened plates

The out-of-plane action has an unfavourable effect on the stability of an unstiffened plate panel in those cases where the deformed shape due to the out-of-plane action is similar to the buckling collapse mode of the plate under in-plane action only.

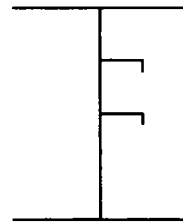
The stability of a square plate panel, therefore, is highly influenced by the presence of out-of-plane (transversely directed) actions.

When adequate Finite Element Methods are used, the complete behaviour of the plate can be simulated taking the total action combination into account.

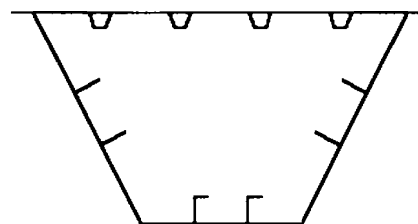
5.3. Behaviour and design of stiffened plates

5.3.1. Introduction

The automation of welding procedures and the need to design elements not only to have the necessary resistance to external actions but also to meet aesthetic and serviceability requirements leads to an increased tendency to employ thin-walled, plated structures, especially when the use of rolled sections is excluded, due to the form and the size of the structure. Through appropriate selection of plate thicknesses, steel qualities and form and position of stiffeners, cross-sections can be best adapted to the actions applied and the serviceability conditions, thus saving material weight. Examples of such structures, shown in Fig.5.38 are webs of plate girders, flanges of plate girders, the walls of box girders, thin-walled roofing, facades, etc.



(a)



(b)

Fig. 5.38. Examples of stiffened plates

Plated elements carry simultaneously:

- a) actions normal to their plane,
- b) in-plane actions.

Out-of-plane action is of secondary importance for such steel elements since, due to the typically small plate thicknesses involved, they are not generally used for carrying transverse actions. In-plane action, however, has significant importance in plated structures.

The intention of design is to utilise the full strength of the material. Since the slenderness of such plated elements is large due to the small thicknesses, their carrying resistance is reduced due to buckling. An economic design may, however, be achieved when longitudinal and/or transverse stiffeners are provided. Such stiffeners may be of open or of torsionally rigid closed sections, as shown in Fig. 5.39. When these stiffeners are arranged in a regular orthogonal grid, and the spacing is small enough to 'smear' the stiffeners to a continuum in the analysis, such a stiffened plate is called an orthogonal anisotropic plate or in short, an orthotropic plate (Fig. 5.40).

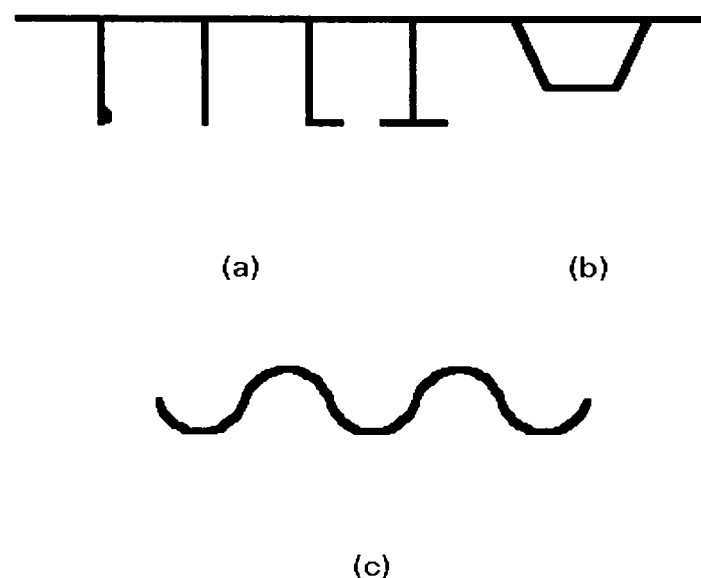


Fig. 5.39. Stiffened plate with (a) open, (b) closed stiffeners, (c) corrugated plate

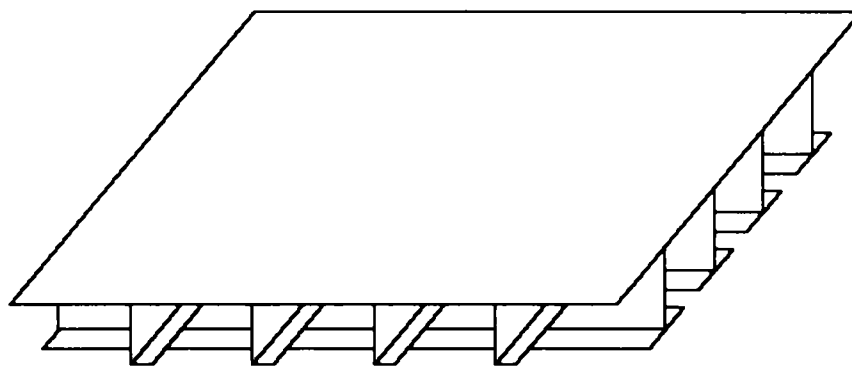


Fig. 5.40. Orthotropic plate

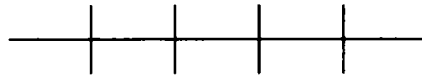
There is an extensive literature about the investigation and design of stiffened plates (orthotropic plates). The differential equation for an orthotropic plate has been written by HUBERT (1914). Other authors were studying this differential equation, including: TROITSKY (1987), HAWRANEK, STEINHARDT (1958), HARDING (1989), HALÁSZ, HUNYADI (1959), KLÖPPEL, MÖLLER (1968), KLÖPPEL, SCHEER (1960), MASSONNET, MAQUOI (1971), PELIKAN, ESSLINGER (1957), SEDLACEK (1992), SKALLOUD, et al (1965), IVANYI (2003)

5.3.2. Stiffened plates under in-plane loading

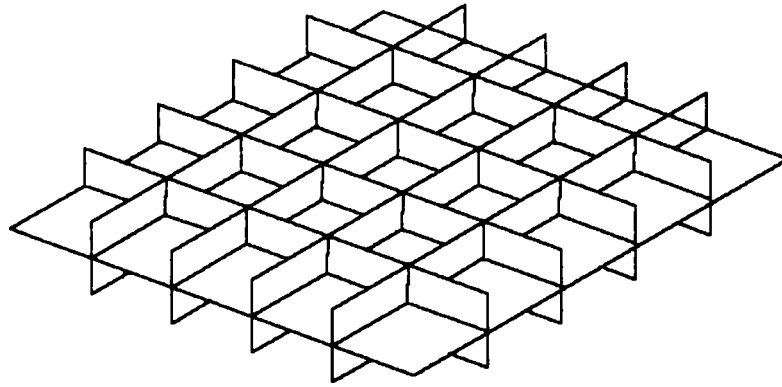
5.3.2.1 Action distribution

5.3.2.1.1 Distribution resulting from membrane theory

The stress distribution can be determined from the solutions of Navier's equations, but, for stiffened plates, this is limited to plates where the longitudinal and transverse stiffeners are closely spaced, symmetrical to both sides of the plate, and produce equal stiffness in the longitudinal and transverse direction, see Fig. 5.41. This configuration leads to an isotropic behaviour when the stiffeners are smeared out. In practice this way of stiffening is not practical and therefore not commonly used.



(a)



(b)

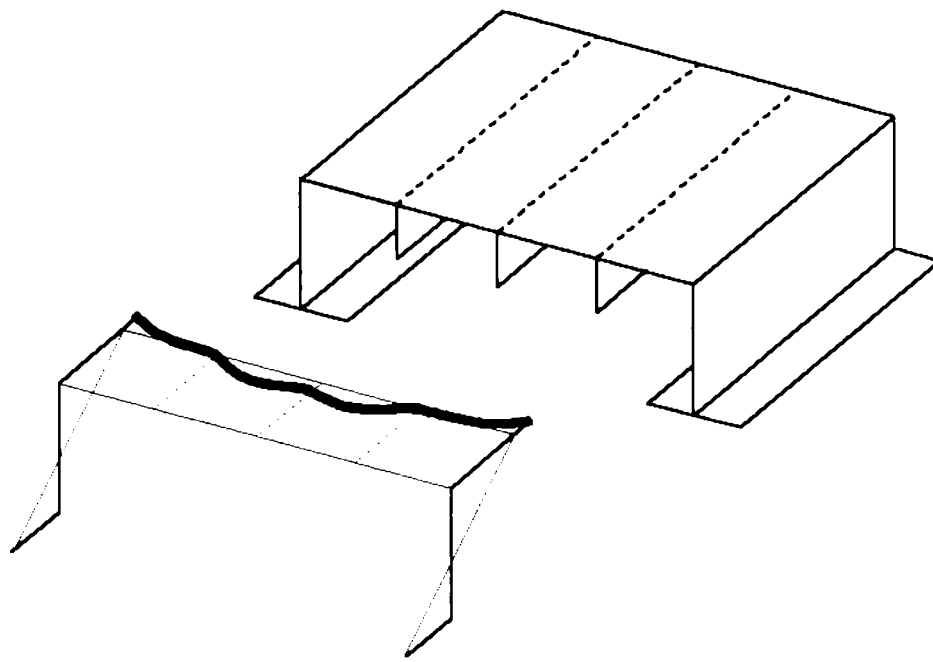
Fig. 5.41. Isotropic behaviour of symmetrically stiffened plate

All deviations from the "ideal" situation (eccentric stiffeners, etc.) have to be taken into account when calculating the stress distribution in the plate.

5.3.2.1.2 Distribution resulting from linear elastic theory using Bernoulli's hypothesis

As for unstiffened plates the most practical way of determining the stress distribution in the panel is using the plane strain hypothesis. Since stiffened plates have a relatively large width, however, the real stress distribution can differ substantially from the calculated stress distribution due to the effect of shear lag.

Shear lag may be taken into account by a reduced flange width concentrated along the edges and around stiffeners in the direction of the action (see Fig. 5.42).



Stress distribution in a stiffened flange plate differs from the distribution based on the plain section hypothesis, due to shear lag.

Fig. 5.42. Shear lag in stiffened plate panel

5.3.2.1.3 Distribution resulting from finite element methods

The stiffeners can be modelled as beam-column elements eccentrically attached to the plate elements.

In the case where the stiffeners are relatively deep beams (with large webs) it is better to model the webs with plate elements and the flange, if present, with a beam-column element.

5.3.2.2 Stability of stiffened plates

5.3.2.2.1 Linear buckling theory

The knowledge of the critical buckling load for stiffened plates is of importance not only because design was (and to a limited extent still is) based on it, but also because it is used as a parameter in modern design procedures. The assumptions for the linear buckling theory of plates are as follows:

- a) The plate is perfectly plane and stress free.

- b) The stiffeners are perfectly straight.
- c) The loading is absolutely concentric.
- d) The material is linear elastic.
- e) The transverse displacements are relatively small.

The equilibrium path has a bifurcation point which corresponds to the critical action (Fig. 5.43).

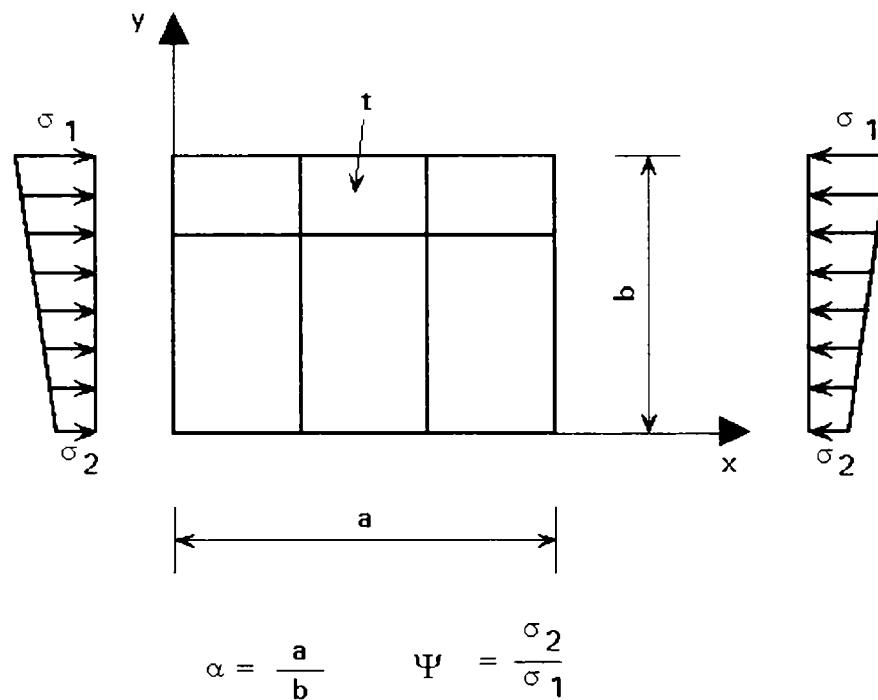


Fig. 5.43. Idealised stiffened plate under de-stabilising loading

Analytical solutions, through direct integration of the governing differential equations are, for stiffened plates, only possible in specific cases; therefore, approximate numerical methods are generally used. Of greatest importance in this respect is the Rayleigh-Ritz approach, which is based on the energy method.

The most extensive studies on rectangular, simply supported stiffened plates were carried out by KLÖPPEL and SCHEER (1960) and KLÖPPEL and MÖLLER (1968). They give charts, as shown in Fig. 5.44 for the determination of k as a function of the coefficients δ and γ , previously described, and the parameters $\alpha = a/b$ and $\psi = \sigma_2/\sigma_1$ as defined in Fig. 5.43. Some solutions also exist for specific cases of plates with fully restrained edges, stiffeners with substantial torsional rigidity, etc. For relevant

literature the reader is referred to books by PETERSEN (1982) and by DUBAS and GEHRI (1986).

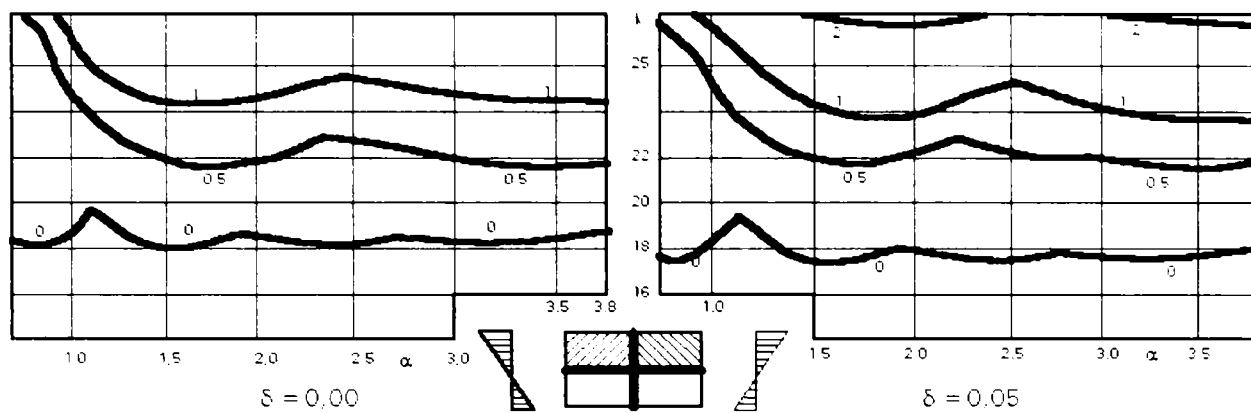


Fig. 5.44. Buckling coefficient for a stiffened plate

When the number of stiffeners in one direction exceeds two, the numerical effort required to determine k becomes considerable. Practical solutions may be found by "smearing" the stiffeners over the entire plate. The plate then behaves orthotropically, and the buckling coefficient may be determined by the same procedure as described before.

An alternative to stiffened plates, with a large number of equally spaced stiffeners and the associated high welding costs, are corrugated plates, see Fig. 5.39c. These plates may also be treated as orthotropic plates, using equivalent orthotropic rigidities (BRIASSOULIS(1986)).

So far only the application of simple action has been considered. For combinations of normal and shear stresses a linear interaction, as described by Dunkerley, is very conservative (Fig. 5.45). On the other hand direct determination of the buckling coefficient fails due to the very large number of combinations that must be considered, therefore an approximate method has been developed, which is based on the corresponding interaction for unstiffened plates, provided that the stiffeners are so stiff that buckling in an unstiffened sub-panel occurs before buckling of the stiffened plate.

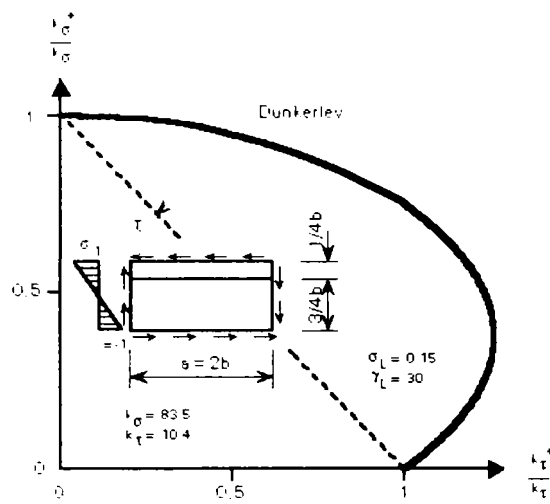


Fig. 5.45. Interaction diagram

Optimum rigidity of stiffeners

Three types of optimum rigidity of stiffeners γ^* , based on linear buckling theory, are usually defined (CHWALLA,(1944)). The first type γ_I^* , is defined such that for values $\gamma > \gamma_I^*$ no further increase of k is possible, as shown in Fig. 5.46a, because for $\gamma = \gamma_I^*$ the stiffeners remain straight.

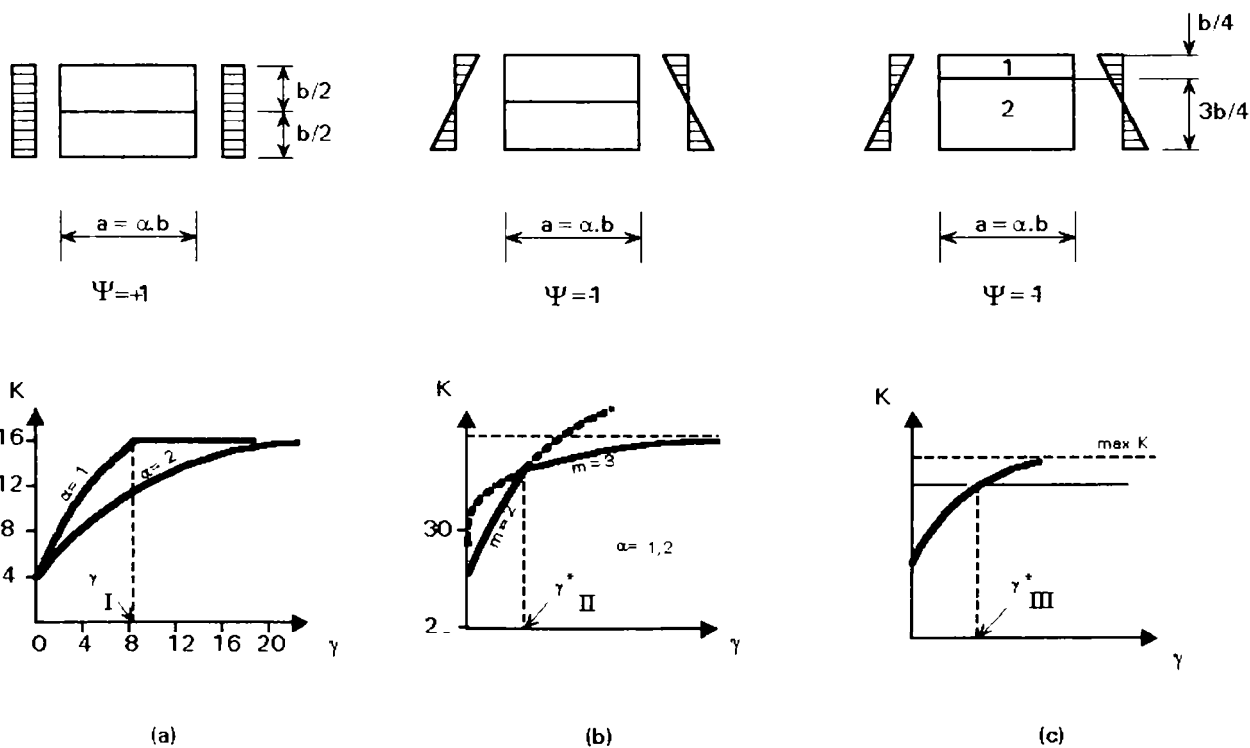


Fig.5.46. Definition of the optimum rigidities

The second type γ_{II}^* , is defined as the value for which two curves of the buckling coefficients, belonging to different numbers of waves, cross (Fig. 5.46b). The

buckling coefficient for $\gamma < \gamma_{II}^*$ reduces considerably, whereas it increases slightly for $\gamma > \gamma_{II}^*$. A stiffener with $\gamma = \gamma_{II}^*$ deforms at the same time as the plate buckles.

The third type γ_{III}^* is defined such that the buckling coefficient of the stiffened plate becomes equal to the buckling coefficient of the most critical unstiffened subpanel (Fig. 5.46c).

The procedure to determine the optimum or critical stiffness is, therefore, quite simple. However, due to initial imperfections of both plate and stiffeners as a result of out of straightness and welding stresses, the use of stiffeners with critical stiffness will not guarantee that the stiffeners will remain straight when the adjacent unstiffened plate panels buckle.

This problem can be overcome by multiplying the optimum (critical) stiffness by a factor m , when designing the stiffeners.

The factor is often taken as $m = 2,5$ for stiffeners which form a closed cross-section together with the plate, and as $m = 4$ for stiffeners with an open cross-section such as flat, angle and T-stiffeners.

5.3.2.2 Ultimate resistance of stiffened plates

Behaviour of stiffened plates

Much theoretical and experimental research has been devoted to the investigation of stiffened plates. This research was intensified after the collapses, in the 1970's, of 4 major steel bridges in Austria, Australia, Germany and the UK, caused by plate buckling. It became evident very soon that linear buckling theory cannot accurately describe the real behaviour of stiffened plates. The main reason for this is its inability to take the following into account:

- a) the influence of geometric imperfections and residual welding stresses.
- b) the influence of large deformations and therefore the post buckling behaviour.
- c) the influence of plastic deformations due to yielding of the material.

d) the possibility of stiffener failure.

Concerning the influence of imperfections, it is known that their presence adversely affects the carrying resistance of the plates, especially in the range of moderate slenderness and for normal compressive (not shear) stresses.

Large deformations, on the other hand, generally allow the plate to carry loads in the post-critical range, thus increasing the action carrying resistance, especially in the range of large slenderness. The post-buckling behaviour exhibited by unstiffened panels, however, is not always present in stiffened plates. Take, for example, a stiffened flange of a box girder under compression, as shown in Fig. 5.47. Since the overall width of this panel, measured as the distance between the supporting webs, is generally large, the influence of the longitudinal supports is rather small. Therefore, the behaviour of this flange resembles more that of a strut under compression than that of a plate. This stiffened plate does not, accordingly, possess post-buckling resistance.

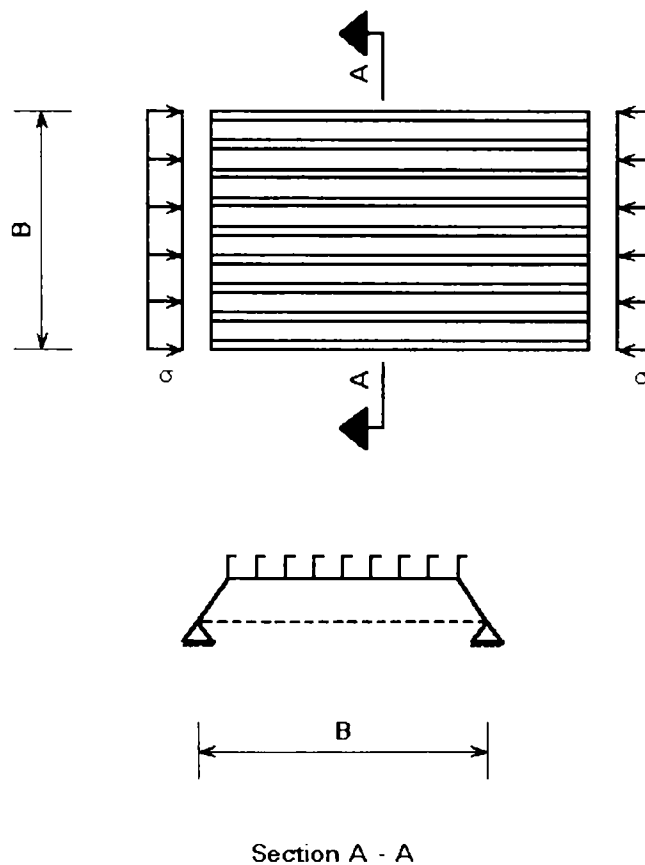


Fig. 5.47. Strut model of a stiffened plate, i.e. each stiffener considered separately

As in unstiffened panels, plastic deformations play an increasingly important role as the slenderness decreases, producing smaller ultimate actions.

The example of a stiffened plate under compression, as it is shown in Fig. 5.48, is used to illustrate why linear buckling theory is not able to predict the stiffener failure mode. For this plate two different modes of failure may be observed: the first mode is associated with buckling failure of the plate panel; the second with torsional buckling failure of the stiffeners. The overall deformations after buckling are directed in the first case towards the stiffeners, and in the second towards the plate panels, due to the up or downward movement of the centroid of the middle cross-section. Experimental investigations on stiffened panels have shown that the stiffener failure mode is much more critical for both open and closed stiffeners as it generally leads to smaller ultimate loads and sudden collapse. Accordingly, not only the magnitude but also the direction of the imperfections is of importance.

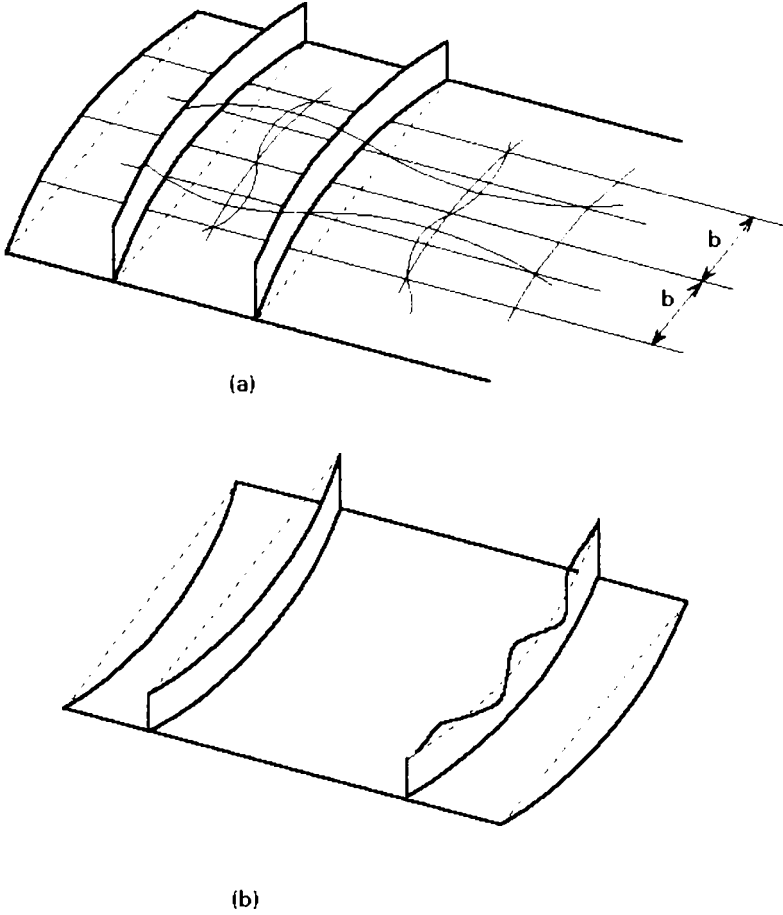


Fig. 5.48. Geometrical imperfections favouring (a) plate failure, (b) stiffener failure

Due to the above mentioned deficiencies in the way that linear buckling theory describes the behaviour of stiffened panels, two different design approaches have been recently developed. The **first**, as initially formulated by the ECCS-Recommendations (1978) for **allowable stress design** and later expanded by DIN 18800, part 3 (1990) to ultimate limit state design, still uses values from linear buckling theory for stiffened plates. The **second**, as formulated by recent EC3-1-5, is based instead on **various simple limit state models** for specific geometric configurations and loading conditions. Both approaches have been checked against experimental and theoretical results:

(A) Design approach with values from the linear buckling theory

With reference to a stiffened plate supported along its edges (Fig. 5.49), distinction is made between individual panels, e.g. IJKL, partial panels, i.e. EFGH, and the overall panel ABCD. The design is based on the condition that the design stresses of all the panels shall not exceed the corresponding design resistances. The adjustment of the linear buckling theory to the real behaviour of stiffened plates is basically made by the following provisions:

- a) Introduction of buckling curves as illustrated in Fig. 5.49b.
- b) Consideration of effective widths, due to local buckling, for flanges associated with stiffeners.
- c) Interaction formulae for the simultaneous presence of stresses σ_x , σ_y and τ at the ultimate limit state.
- d) Additional reduction factors for the strut behaviour of the plate.
- e) Provision of stiffeners with minimum torsional rigidities in order to prevent lateral-torsional buckling.

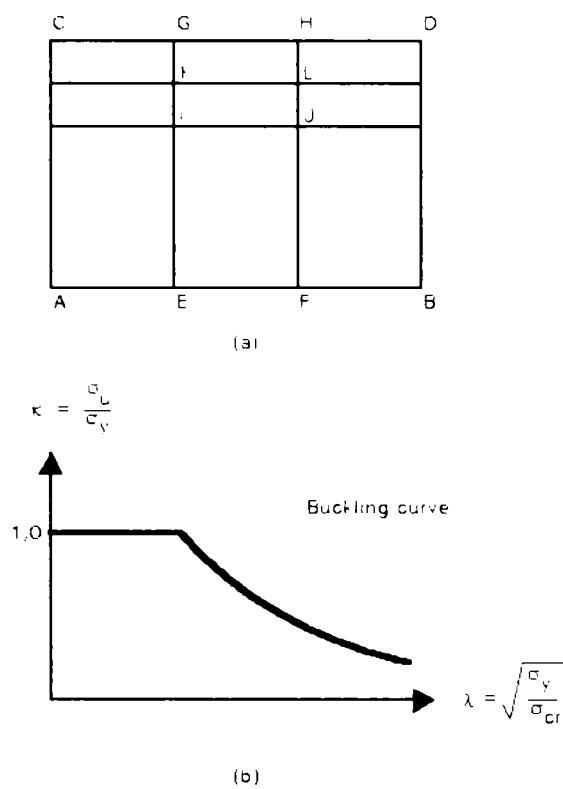


Fig. 5.49. (a) Definition of subpanels for a stiffened plate, (b) buckling curve

(B) Design approach with simple limit state models

The stiffened plate can be considered as a grillage of beam-columns loaded in compression column buckling attitude and plate (plate buckling attitude) loaded in impression, which consist of the stiffeners themselves together with the adjacent effective plate widths. This effective plate width is determined by buckling of the unstiffened plates. The bending resistance M_u , reduced as necessary due to the presence of axial forces, is determined using the characteristics of the effective cross-section. Where both shear forces and bending moments are present simultaneously an interaction formula is given.

The resistance of a box girder flange subjected to compression can be determined using the method presented in the EC3-1-5 referred to previously, by considering a strut composed of a stiffener and an associated effective width of plating. The design resistance is calculated using the Perry-Robertson formula. Shear forces due to torsion or beam shear are taken into account by reducing the yield strength of the material according to the von Mises yield criterion. An alternative approach using orthotropic plate properties is also given.

Generally this approach gives rigidity and strength requirements for the stiffeners which are stricter than those mentioned previously.

Discussion of the design approaches

Both approaches have advantages and disadvantages.

The main advantage of the **first approach** is that it covers the design of both unstiffened and stiffened plates subjected to virtually any possible combination of actions using the same method. Its main disadvantage is that it is based on the limitation of stresses and, therefore, does not allow for any plastic redistribution at the cross-section.

The **second approach** also has some disadvantages: there are a limited number of cases of geometrical and loading configurations where these models apply; there are different methodologies used in the design of each specific case and considerable numerical effort is required, especially using the tension field method.

Another important point is the fact that reference is made to webs and flanges that cannot always be defined clearly, as shown in the examples of Fig. 5.50.

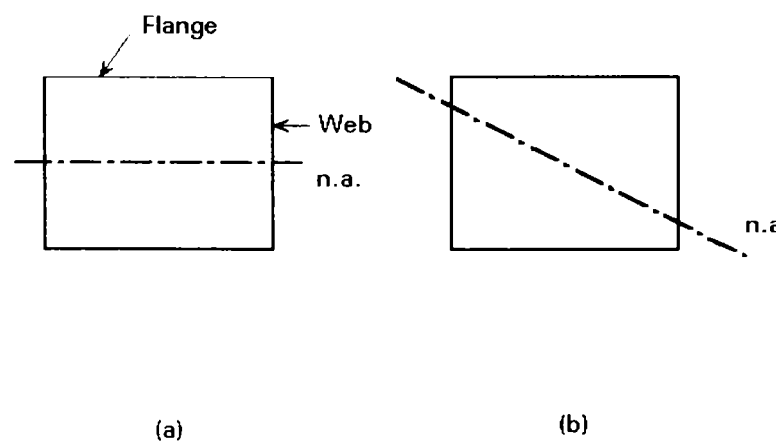


Fig. 5.50. Definition of webs and flanges

For a box girder subjected to uniaxial bending (Fig. 5.50a) the compression flange and the webs are defined. This is however not possible when biaxial bending is present (Fig. 5.50b).

Finite Element Methods

In determining the stability behaviour of stiffened plate panels, basically the same considerations hold as described in previous subchapter. In addition it should be noted that the stiffeners have to be modelled by shell elements or by a combination of shell and beam-column elements. Special attention must also be given to the initial imperfect shape of the stiffeners with open cross-sections.

It is difficult to describe all possible failure modes within one and the same finite element model. It is easier, therefore, to describe the beam-column behaviour of the stiffeners together with the local and overall buckling of the unstiffened plate panels and the stiffened assemblage respectively and to verify specific items such as lateral-torsional buckling separately (see Fig. 5.51). Only for research purposes is it sometimes necessary to model the complete structure such that all the possible phenomena are simulated by the finite element model.

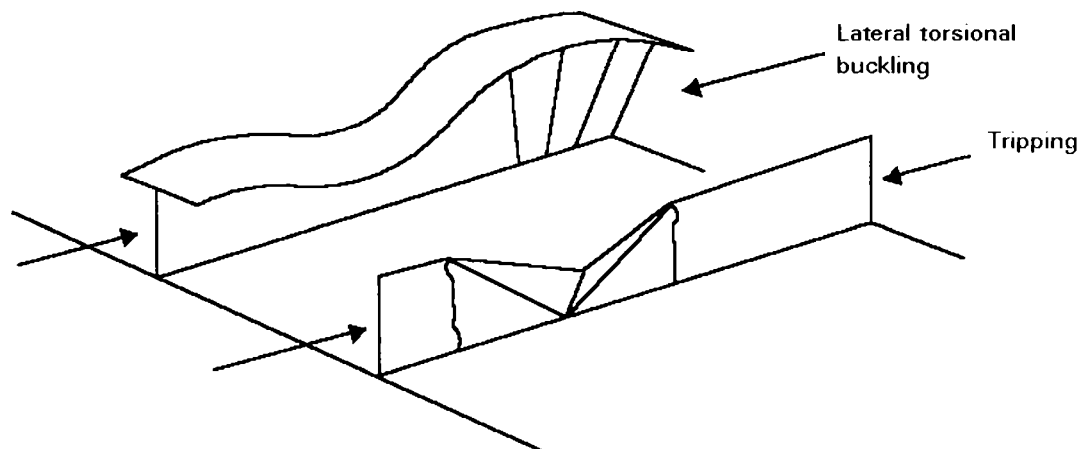


Fig. .5.51. Lateral buckling and tripping

5.3.3. Stiffened plates under out-of-plane action application

5.3.3.1 Action distribution

(i) Distribution resulting from plate theory

The theory described previous points can only be applied to stiffened plates if the stiffeners are sufficiently closely spaced so that orthotropic behaviour occurs. If this is not the case it is better to consider the unstiffened plate panels in between the stiffeners separately. The remaining grillage of stiffeners must be considered as a beam system in bending.

(ii) Distribution resulting from a grillage under lateral actions filled in with unstiffened sub-panels

The unstiffened sub-panels can be analysed previous points.

The remaining beam grillage is formed by the stiffeners which are welded to the plate, together with a certain part of the plate. The part can be taken as for buckling, namely the effective width. In this way the distribution of forces and moments can be determined quite easily.

(iii) Distribution resulting from finite element methods (FEM)

Similar considerations hold for using FEM to determine the force and moment distribution in stiffened plates which are subject to out-of-plane actions as for using FEM for stiffened plates loaded in-plane except that the finite elements used must be able to take large deflections and elastic-plastic material behaviour into account.

5.3.3.2 Deflection and ultimate resistance

All considerations mentioned in previous points for unstiffened plates are valid for the analysis of stiffened plates both for deflections and ultimate resistance. It should be noted, however, that for design purposes it is easier to verify specific items, such as lateral-torsional buckling, separately from plate buckling and beam-column behaviour.

5.4. Planar orthotropic plated structures without transverse loading according to EC 3 (Part 1.5)

EC 3 (Part 1.5) studies the planar plated structures without transverse loading. To be compliant with EC3 for the rest of this chapter, the following definitions will apply:

elastic critical stress: Stress at which an elastic structure without imperfections becomes unstable according to small deformation theory.

gross cross-section: The total cross-sectional area of a member but excluding longitudinal stiffeners that are not continuous, battens and splice material.

effective cross-section: The gross cross-section reduced for the effects of plate buckling and shear lag.

membrane stress: Stress at mid-depth of the plate.

plated structure: A structure that is built up from nominally flat plates which are welded together. The plates may be stiffened or unstiffened.

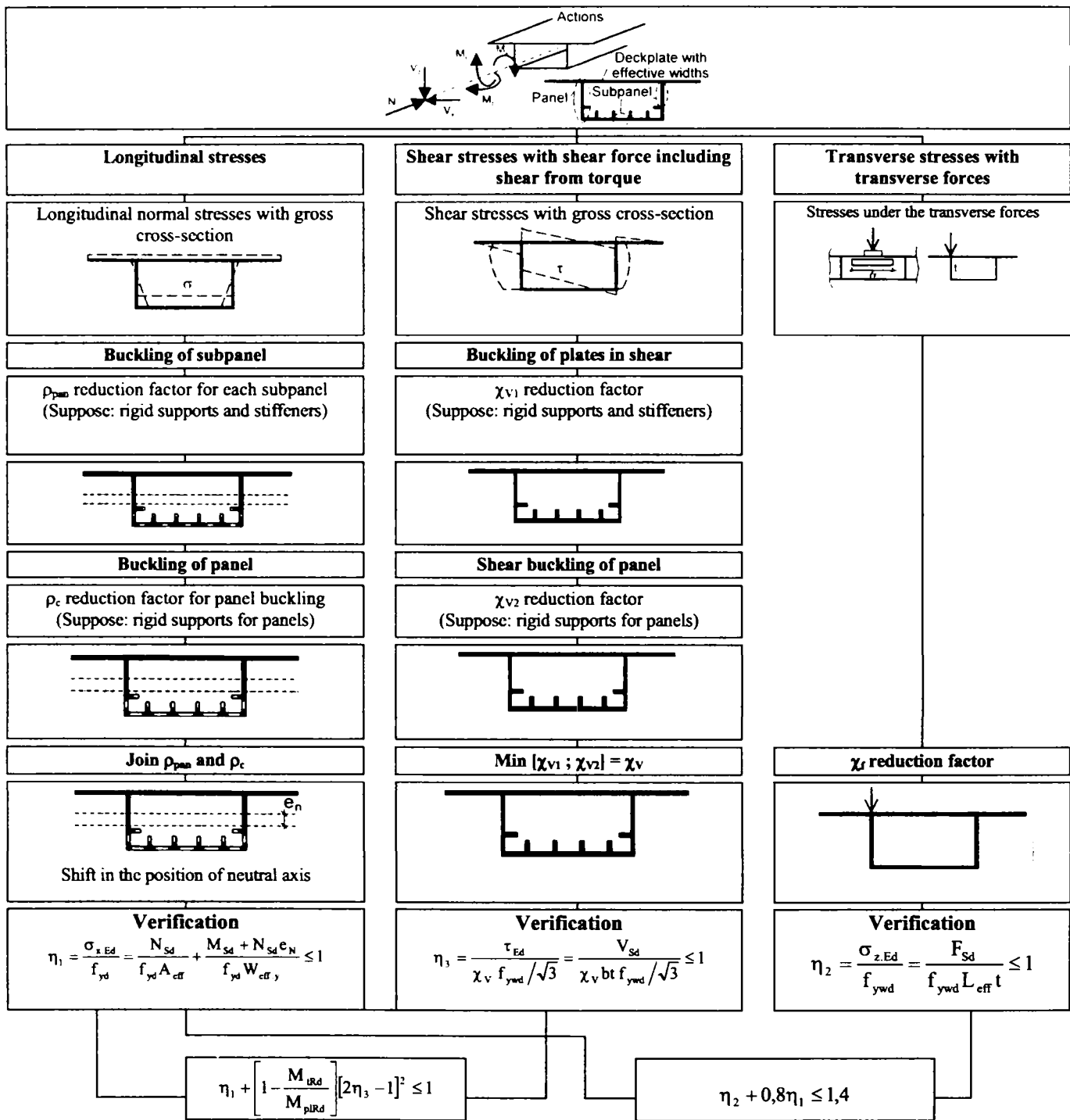
stiffener: A plate or rolled section attached to a plate with the purpose of delaying or preventing buckling of the plate or reinforcing it against local loads. A stiffener is denoted:

- longitudinal if its direction is parallel to that of the member;
- transverse if its axis is perpendicular to that of the member.

stiffened plate: Plate with transverse and/or longitudinal stiffeners.

subpanel: Unstiffened plate surrounded by flanges or stiffeners.

The suggested methods for the design of planar plated structures have been summarised by JOHANSSON et al (1999) and JOHANSSON et al (2001) and they are repeated here for completeness (see Fig. 5.52- Fig. 5.56):



Interaction between shear force, bending moment, axial and transverse force

Fig. 5.52. Flow chart describing the general procedure for the design of plated structures according to EC3, Part 1.5.

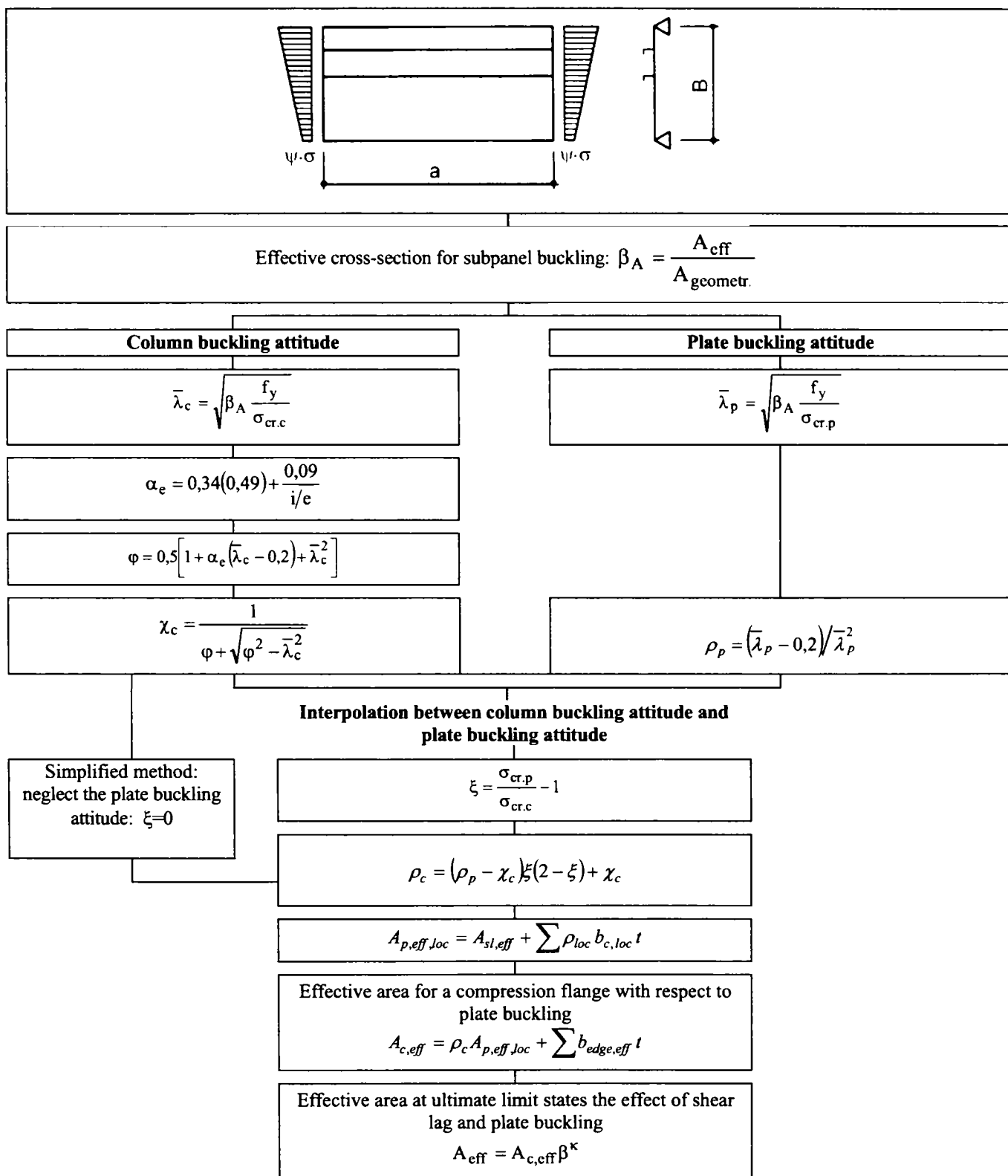


Fig. 5.53. Flow chart describing the procedure for the determination of effective cross-section properties of a longitudinally stiffened class 4 panel

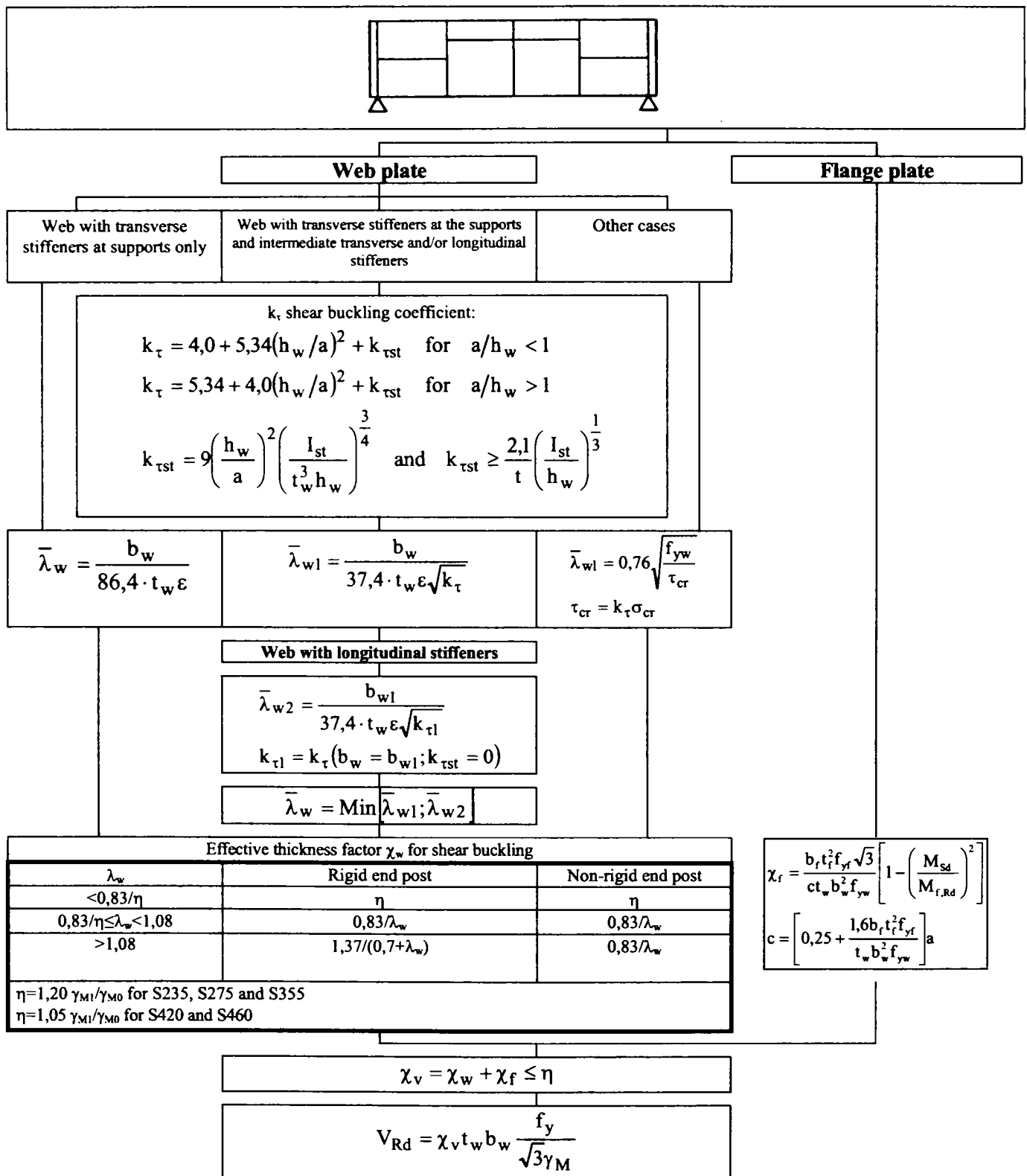


Fig. 5.54. Flow chart describing the procedure for the determination of effective cross-section resistance in the shear buckling

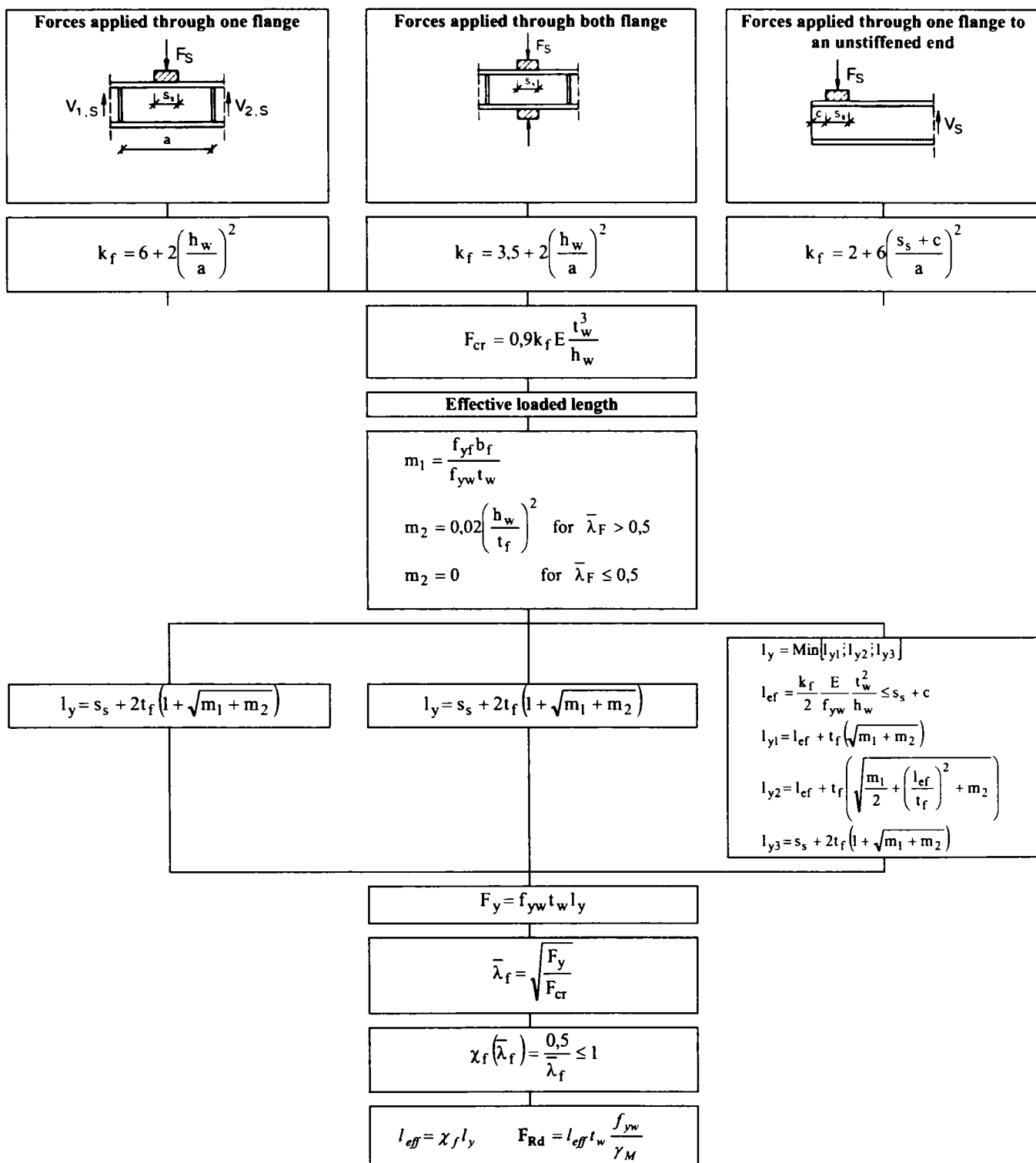
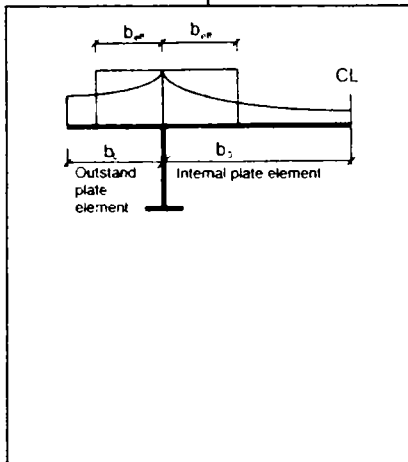
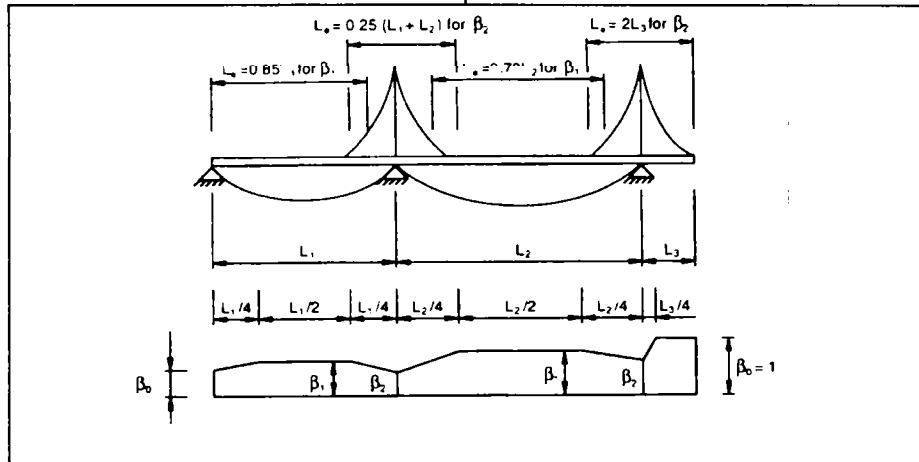


Fig. 5.55. Flow chart describing the procedure for the determination of the cross-section resistance under patch loading

Definitions of notations for shear lag

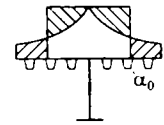


Effective length L_e for continuous beam and distribution of effective width



A_{sl} : Area of all longitudinal stiffeners

$$\alpha_0 = \sqrt{1 + \frac{A_{sl}}{b_0 t}} \quad \kappa = \alpha_0 b_0 / L_e$$



Effective width factor β

$\kappa = \frac{\alpha_0 b_0}{L_e}$	Location for verification	β - Value
$\leq 0,02$		$\beta = 1,0$
0,02 - 0,07	Sagging bending	$\beta = \beta_1 - \frac{1}{1 + 6,4\kappa^2}$
	Hogging bending	$\beta = \beta_2 - \frac{1}{1 + 6,0\left(\kappa - \frac{1}{2500\kappa}\right) + 1,6\kappa^2}$
$> 0,70$	Sagging bending	$\beta = \beta_1 - \frac{1}{5,9\kappa}$
	Hogging bending	$\beta = \beta_2 - \frac{1}{8,6\kappa}$
all κ	End support	$\beta_0 = (0,55 + 0,025/\kappa)\beta_1$, but $\beta_0 < \beta_1$
all κ	Cantilever	$\beta = \beta_2$ at support, $\beta_0 = 1,0$ at the end

Effective width under serviceability limit state
 $b_{eff} = \beta b_0$

Effective area under ultimate limit state
 $A_{eff} = A_{c,eff} \beta^\kappa$

Fig. 5.56. Interaction between effective widths due to shear lag effects and effective widths from plate buckling

EC 3 (Part 1.5) section describes the general steps to perform for the analysis of planar orthotropic plated structures, however EC3 describes the analysis of the plate section only between two cross girders in detail in Annex A and the stiffness of the cross girders is examined separately. In this way only the effect of stiffened panel buckling is investigated by EC3 (Fig. 5.57) and it may also be necessary to investigate to effect of **orthotropic buckling**. (Fig. 5.17 is repeated here as it is important in respect of this section.)

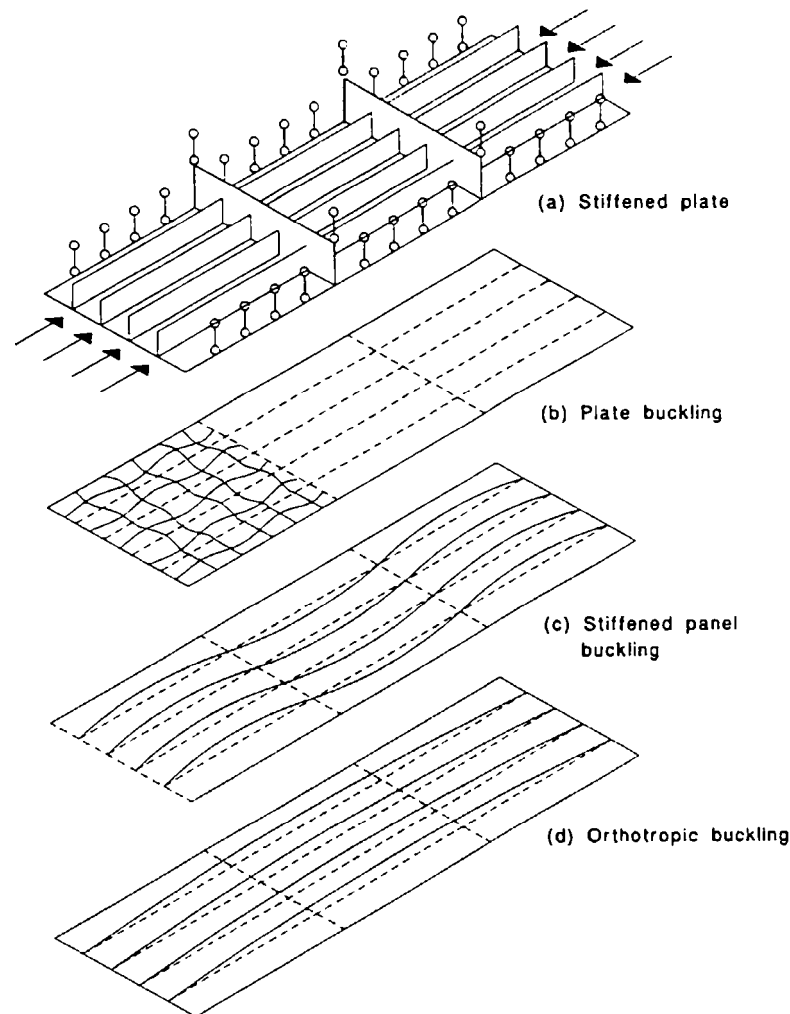


Fig. 5.57. Buckling modes for stiffened plates in compression.

The aim of the research: Analysis of compressed stiffened plates

- To study the effect of the orthotropic buckling a special model is required which takes into account this phenomenon and is based on the results of known analytical methods.
- For the analysis of the effect of the orthotropic buckling the value of

$\sigma_{cr,c}$ column buckling type and

$\sigma_{cr,p}$ plate buckling type

formulas are required (Fig. 5.53). In this way the results of the analytical methods can be rearranged and introduced into a calculation according to EC 3.

- The rearranged formulas must be checked for those equations of EC 3 Part 1.5 that are provided for the effect of stiffened plate buckling.
- To be able to analyse the effect of the orthotropic buckling the structural details of the cross girder must be known the effect and behaviour of the cross girder must be taken into account. In other words the connection between the web of the cross girder and the longitudinal stiffeners must be considered.
- During the investigation the results of the experiments and numerical studies must be taken into account. The results presented in this chapter are compared to the results obtained during the design of the composite floodplain Danube bridges at Szekszard. Furthermore by executing a parametric study advices are provided to perform a design procedure according to the regulations of EC 3 Part 1.5.

5.5. Orthotropic buckling of compressed stiffened plates

The book (HANDBOOK OF STRUCTURAL STABILITY (1971)) published by the "Column Research Committee of Japan" is one of the most complete collection in this research area. In the following sections the basic assumption are collected with the aid of this book.

(A) Column buckling attitude, $\sigma_{cr,c}$

HANDBOOK (1971) Chapter "2-25 II Frames and Curved Members", Reference No. 105 (PIN-YU, MICHELSON 1969) provides easily manageable formulas for the investigation of the column buckling attitude of the orthotropic buckling of compressed, stiffened plates. Fig. 5.58 shows the corresponding page from the HANDBOOK (1971).

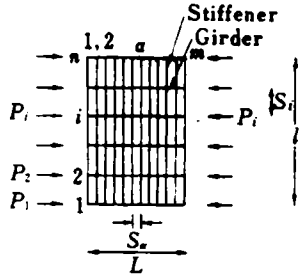
conditions	results	ref.
<p>105 Grillage beams</p>  <p>Assumptions</p> <ol style="list-style-type: none"> (1) The stiffeners are identical in properties and in spacing. (2) The spacing of stiffeners is small. (3) The axial forces are proportional to the moment of inertia of the girders. 	<p>(1) All ends are built-in. The criterion for the critical buckling load $b_i \sinh a_i L \pm a_i \sin b_i L = 0$</p> <p>where</p> $a_i = \sqrt{\frac{1}{2} \sqrt{\beta_i} - \frac{1}{4} \alpha}, \quad b_i = \sqrt{\frac{1}{2} \sqrt{\beta_i} + \frac{1}{4} \alpha}$ $\alpha = \frac{q}{E}, \quad \beta_i = \frac{1}{S_a E \lambda_i}, \quad P_i = q I_i$ <p>λ_i = Eigen-values of flexibility matrix $[I_i^{1/2}] [a_{ij}] [I_i^{1/2}]$ for girders, in which a_{ij} is the influence coefficient of stiffener</p> <p>I_i = moment of inertia of ith girder ($i=1, 2, \dots, n$)</p> <p>The envelope of the curves which can be plotted to show P_i for different grillages is approximately expressed by</p> $P_{cr,i} = \left[4 + 0.0866 \frac{L^2}{\sqrt{S_a E \lambda_0}} \right] P_e, \quad \text{if } \frac{P_{cr,i}}{P_e} \leq 5$ $P_{cr,i} = \left[3 + 0.202 \frac{L^2}{\sqrt{S_a E \lambda_0}} \right] P_e, \quad \text{if } \frac{P_{cr,i}}{P_e} > 5$ <p>where</p> $\lambda_0 = \max \{ \lambda_i \}, \quad P_e = \frac{\pi^2 EI}{l^2}$ <p>When the girders are identical in size and in spacing,</p> $\lambda_0 = [0.020833 + 0.01022(n-1)] \frac{l^3}{EI_s} I_g$ <p>where</p> <p>n = the number of girders I_s, I_g = moment of inertia for stiffeners or girders</p> <p>(2) All ends are simply supported.</p> $P_{cr,i} = \left[1 + 0.0866 \frac{L^2}{\sqrt{S_a E \lambda_0}} \right] P_e, \quad \text{if } \frac{P_{cr,i}}{P_e} \leq 2$ $P_{cr,i} = 0.202 \frac{L^2}{\sqrt{S_a E \lambda_0}} \cdot P_e, \quad \text{if } \frac{P_{cr,i}}{P_e} < 2$	49

Fig. 5.58. Column buckling attitude of the orthotropic buckling of compressed, stiffened plates (HANDBOOK, 1971)

Formulas under subsection (2) will be used as it is assumed that all ends are simply supported.

Using the notation of EC 3 Part 1.5 the equations in Fig. 5.58 can be rewritten as follows. The arrangement of the stiffeners and cross girders can be seen in Fig. 5.59.

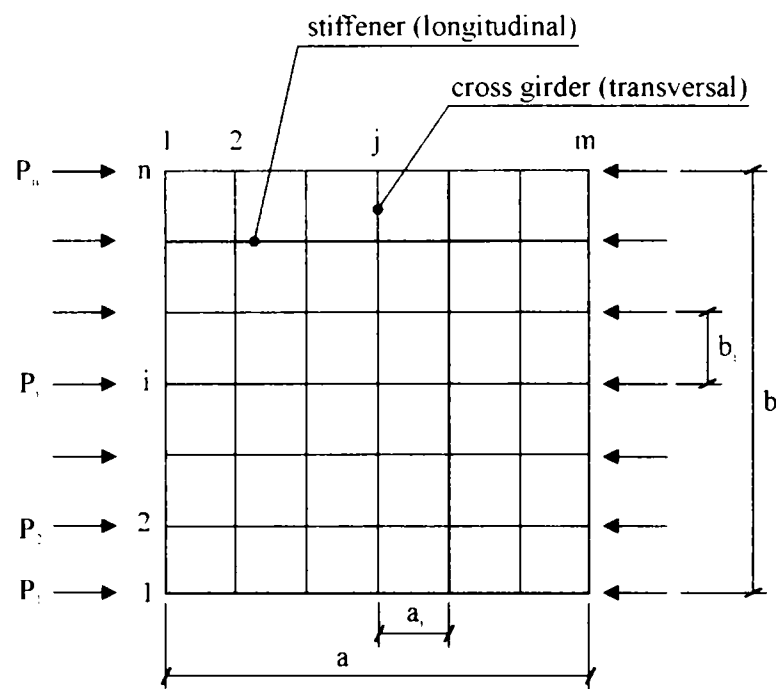


Fig. 5.59. Arrangement of the stiffeners and cross girders

When the stiffeners are identical in size and in spacing

$$a = (m - 1) a_j,$$

$$b = (n - 1) b_j,$$

then

$$\lambda_0 = [0.020833 + 0.01022(n - 1)] \frac{b^3}{EI_b} I_{st_1}, \quad (5.11)$$

where I_{st_1} is the inertia of the stiffener, I_b is the inertia of the girder, n is the number of stiffeners including the webs of the main girder, b is the length of the bottom flange of the main girder and E is the Young's modulus. Eq. 5.11 is usually written in the short form of

$$\lambda_0 = Z \frac{b^3}{EI_b} I_{st_1}, \quad (5.12)$$

where $Z = [0.020833 + 0.01022(n - 1)]$.

When all ends are simply supported:

$$P_{cr,i} = \left[1 + 0.0866 \frac{a^2}{\sqrt{a_j E \lambda_0}} \right] P_e \quad \text{if} \quad \frac{P_{cr}}{P_e} \leq 2, \quad (5.13)$$

where a and a_j can be seen in Fig. 5.58 and P_e is $P_e = \frac{\pi^2 E I_{sl}}{a^2}$.

Eq. 5.13 can be rearranged into the form of

$$\frac{P_{cr}}{P_e} = 1 + 0.0866 \frac{\alpha^2 b^2}{\sqrt{\frac{\alpha b}{m-1} E Z \frac{b^3}{E I_b} I_{sl}}}, \quad (5.14)$$

where $\alpha = \frac{a}{b}$. Further rearrangement result in the following equation:

$$\frac{P_{cr}}{P_e} = 1 + 0.0866 \frac{\alpha^2}{\sqrt{\frac{\alpha}{m-1} Z K}} = \frac{\sigma_{cr,c}}{\sigma_{cr,sl}} \leq 2, \quad (5.15)$$

where $K_0 = \frac{I_{sl}}{I_b}$.

When $\frac{P_{cr,i}}{P_e} > 2$ then

$$\frac{P_{cr,i}}{P_e} = 0.202 \frac{a^2}{\sqrt{a_j E \lambda_0}}, \quad (5.16)$$

which can be rearranged into the form of

$$\frac{P_{cr,i}}{P_e} = 0.202 \frac{\alpha^2}{\sqrt{\frac{\alpha}{m-1} Z K_0}} = \frac{\sigma_{cr,c}}{\sigma_{cr,sl}} > 2. \quad (5.17)$$

(i) Comparison

Comparing the derived results to the results of EC 3 Part 1.5 Annex A the following conclusions can be drawn. If $a = a_j$ and the cross girders are simply supported then the second component of Eq. 5.15 disappears and the method to study the stiffened panel buckling is obtained.

(ii) Parametric study

Fig. 5.60 – Fig. 5.62 show the relation between the P_{cr} force and the α parameter of the plate. The different figures show the results for different number of trapezoidal

stiffeners (n) and cross girders (m). In a figure the different curves represent different ratio of the inertia between the trapezoidal stiffener and cross girder.

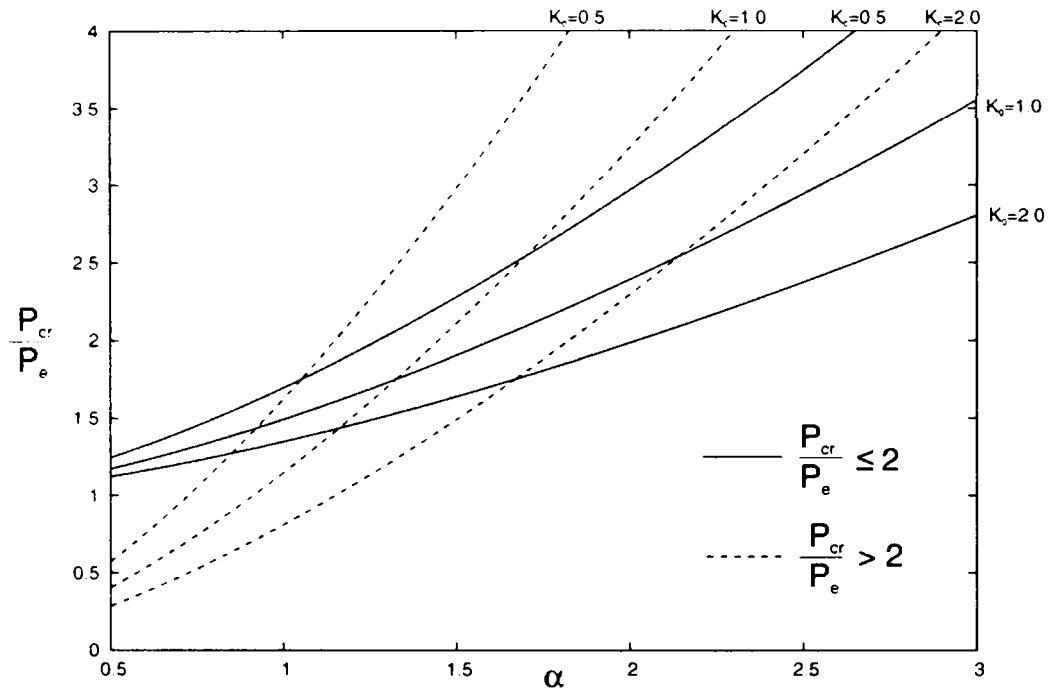


Fig. 5.60. The relation of P_{cr} and α in the case of $n=2, m=2$

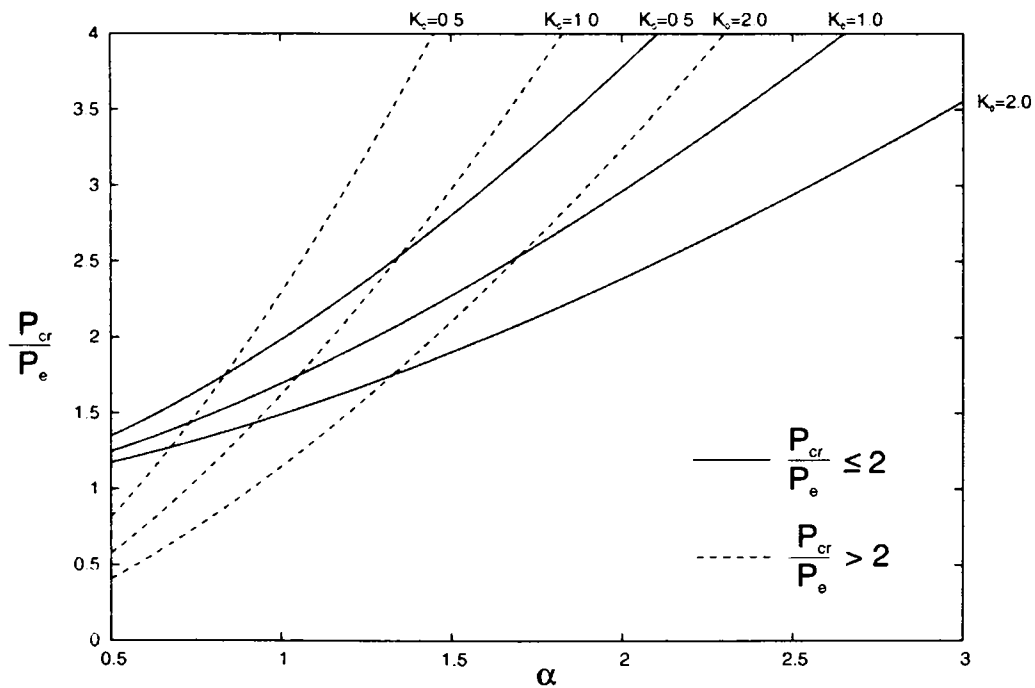


Fig. 5.61. The relation of P_{cr} and α in the case of $n=2, m=3$

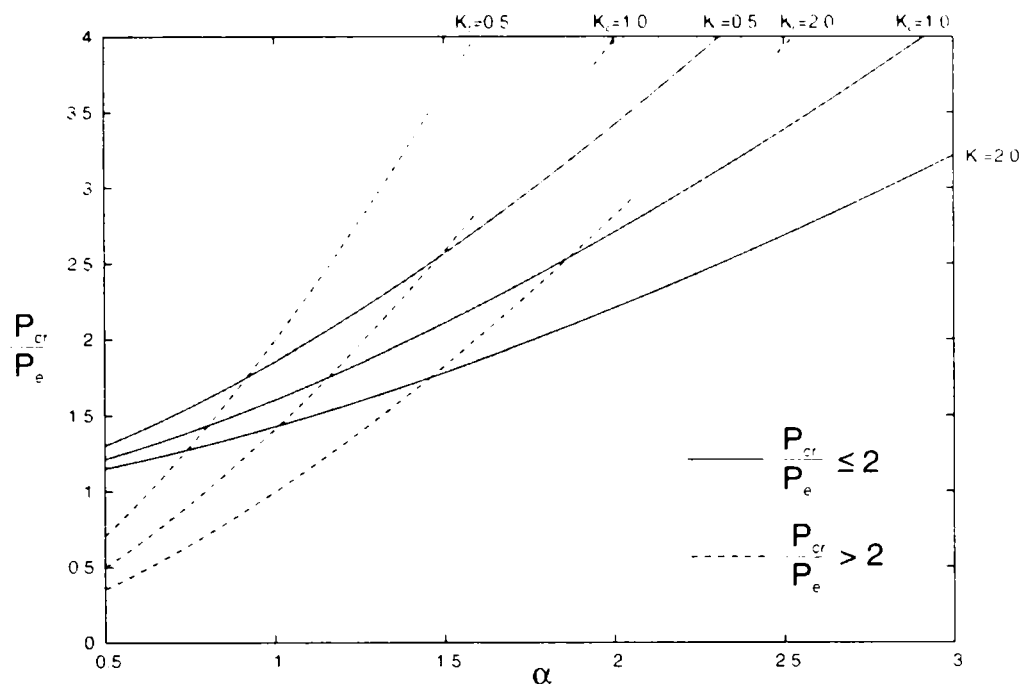


Fig. 5.62. The relation of P_{cr} and α in the case of $n=3, m=3$

(B) Plate buckling attitude, $\sigma_{cr,p}$

HANDBOOK (1971) Chapter "3-158 III Plates", Reference No. 203 (OKURA, ARIMA 1922) provides easily manageable formulas for the investigation of the plate buckling attitude of the orthotropic buckling of compressed, stiffened plates (see Fig. 5.63).

conditions	results	ref.
<p>203 Many longitudinal and transverse stiffeners equally spaced</p>	<p>(i) All edges simply supported $\sigma_k = \frac{\pi^2 a E}{b t} \left\{ \frac{I_a (m+1)}{a^3} + \frac{I_b (n+1)}{b^3} \right\}$ </p> <p>(ii) All edges clamped $\sigma_k = \frac{4 \pi^2 a E}{b t} \left\{ \frac{I_a (m+1)}{a^3} + \frac{I_b (n+1)}{b^3} \right\}$ </p> <p>(iii) a-edges clamped, b-edges simply supported $\sigma_k = \frac{16 \pi^2 a E}{3 b t} \left\{ \frac{3 I_a (m+1)}{16 a^3} + \frac{I_b (n+1)}{b^3} \right\}$ </p> <p>(iv) a-edges simply supported, b-edges clamped $\sigma_k = \frac{4 \pi^2 a E}{b t} \left\{ \frac{I_a (m+1)}{a^3} + \frac{3 I_b (n+1)}{16 b^3} \right\}$ </p> <p>m, n = the number of stiffeners in a- and b-directions, respectively</p>	339

Fig. 5.63. The plate buckling attitude of the orthotropic buckling of compressed, stiffened plates, HANDBOOK (1971)

Formulas under subsection (i) will be used as it is assumed that all ends are simply supported.

Using the notation of EC 3 Part 1.5 the equations in Fig. 5.63 can be rewritten as follows. The arrangement of the stiffeners and cross girders can be seen in Fig. 5.64.

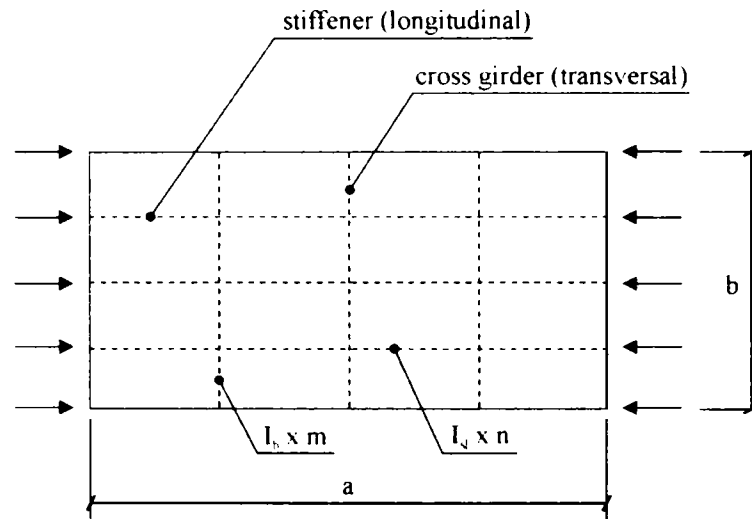


Fig. 5.64. Arrangement of the stiffeners and cross girders

When the stiffeners are identical in size and in spacing:

$$\sigma_k = \frac{\pi^2 E a}{t b} \left(\frac{I_{sl}(n+1)}{a^3} \right) \left\{ 1 + \frac{\frac{I_b(m+1)}{b^3}}{\frac{I_{sl}(n+1)}{a^3}} \right\}. \quad (5.18)$$

When Eq. 5.18 is multiplied and divided by $[bt^3 12(1-\nu^2)]$ and by b and rearranged then its form will be

$$\frac{\sigma_K}{\sigma_e} = (1-\nu^2) \frac{I_{sl}(n+1)12}{\alpha^2 t^3 b} \left\{ 1 + \frac{1}{K_0} \frac{m+1}{n+1} \alpha^3 \right\}, \quad (5.19)$$

where $\sigma_e = \frac{\pi^2 E}{12(1-\nu^2)} \left(\frac{t}{b} \right)^2$, and $\alpha = \frac{a}{b}$, and $K_0 = \frac{I_{sl}}{I_b}$. When introducing the inertia

of the plate $I_p = \frac{t^3 b}{12(1-\nu^2)}$ and $g = \frac{I_{sl}}{I_p}$ then

$$\frac{\sigma_K}{\sigma_e} = g \frac{(n+1)}{\alpha^2} \left\{ 1 + \frac{1}{K_0} \frac{m+1}{n+1} \alpha^3 \right\} = \frac{\sigma_{cr,p}}{\sigma_e} = k \sigma_p. \quad (5.20)$$

(i) Comparison

Comparing the derived results to the results of EC 3 Part 1.5 Annex A the following conclusions can be drawn. Annex A examines the influence of stiffened plate buckling on only one plate. Considering the bottom flange around the middle pier of the floodplain Danube bridge at Szekszard the calculation according to Annex A gives

$$k_{\sigma_p} = 235.428 .$$

Using the newly derived Eq. 5.9 and $n=4$, $I_{sl} = 10415\text{cm}^2$, $I_b = 402.9\text{cm}^2$ and $\alpha = 0.6618$ then

$$k_{\sigma_p} = (1 - \nu^2) g \frac{n+1}{\alpha^2} = (1 - 0.3^2) \frac{10415}{402.9} \frac{4+1}{0.6618^2} = 268.54 .$$

In the case of this example the newly derived method provides a 13% higher value.

(ii) Parametric study

Fig 5.65-Fig. 5.69 show the relation between the k_{σ_p} parameter and the α parameter of the plate. The different figures show the results for different number of trapezoidal stiffeners (n) and cross girders (m). In a figure the different curves represent different ratio of the inertia between the trapezoidal stiffener and cross girder.

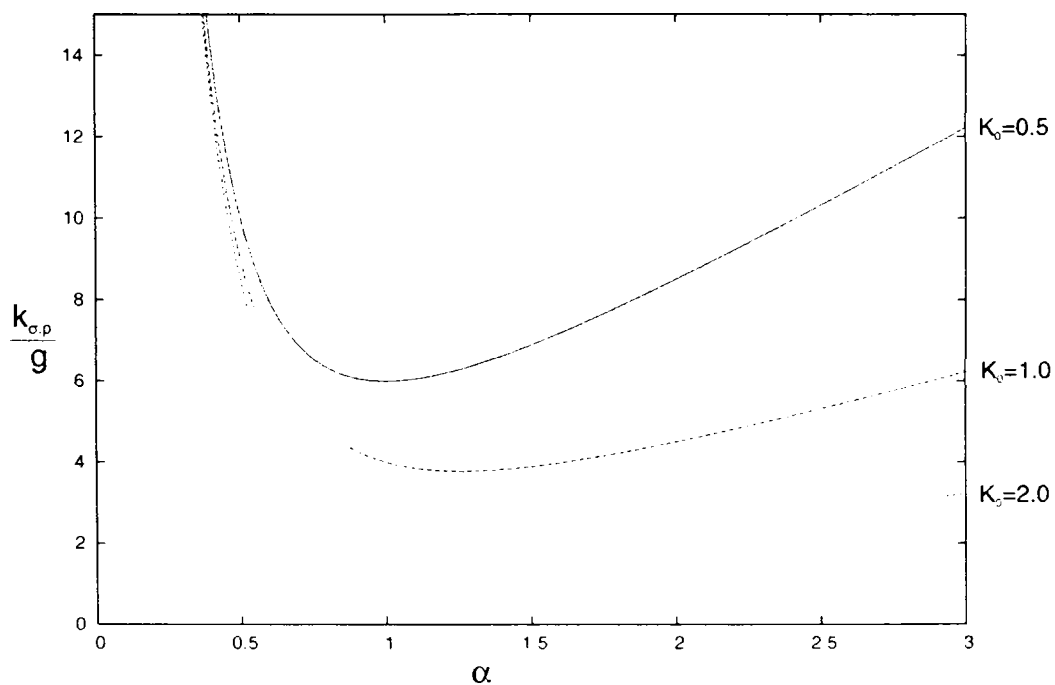


Fig. 5.65. The relation of k_{σ_p} and α in the case of $n=1$, $m=1$

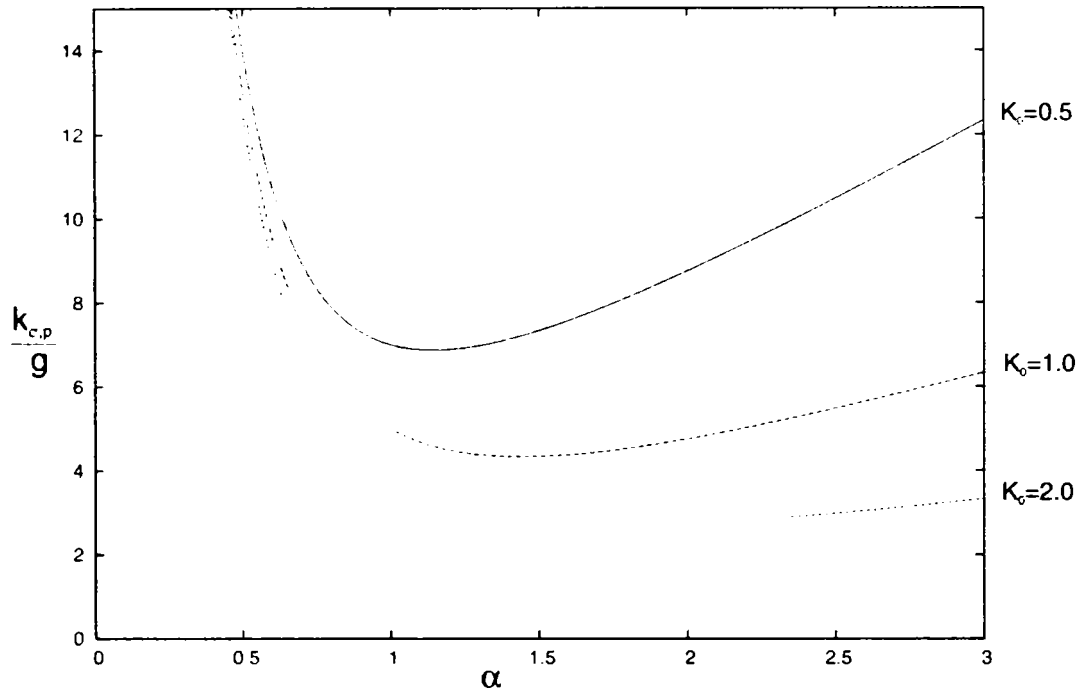


Fig. 5.66. The relation of $k_{\sigma p}$ and α in the case of $n=2, m=1$

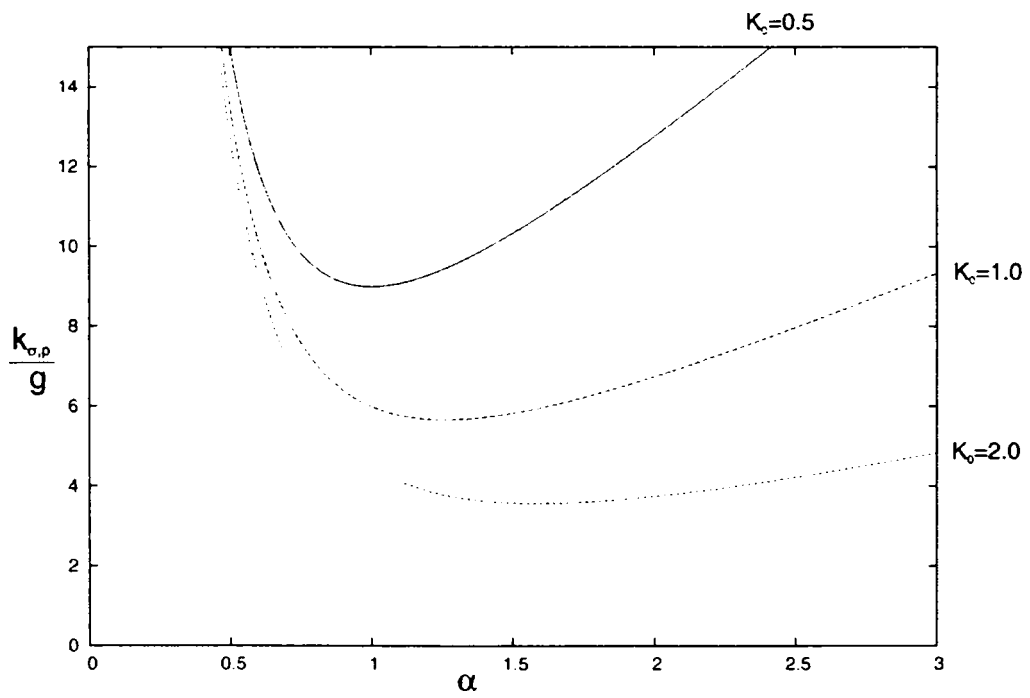


Fig. 5.67. The relation of $k_{\sigma p}$ and α in the case of $n=2, m=2$

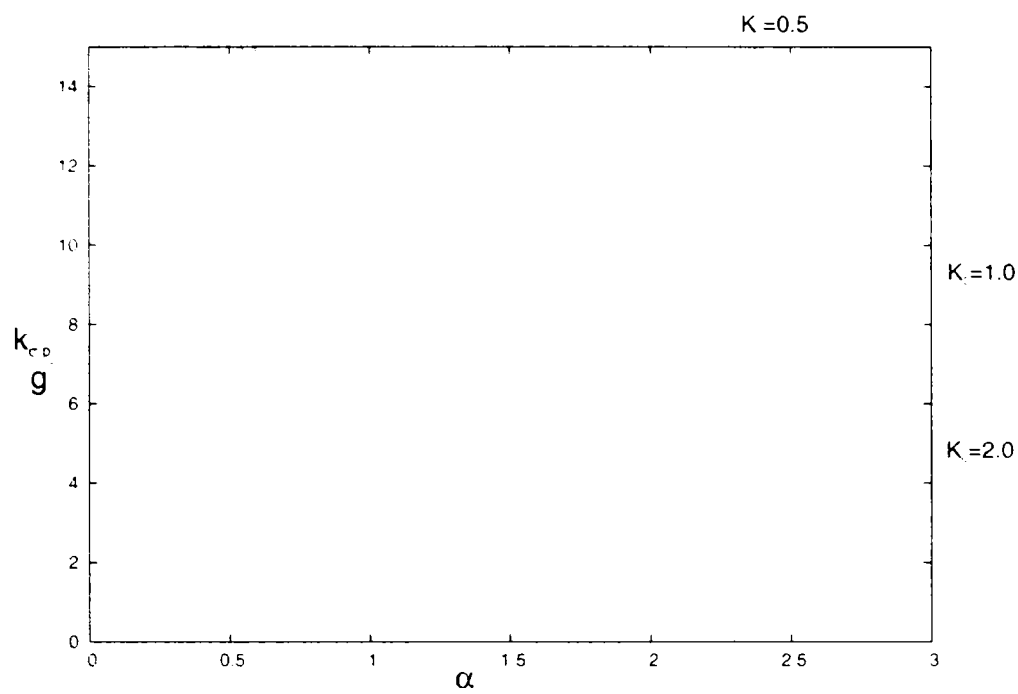


Fig. 5.68. The relation of $k_{\sigma p}$ and α in the case of $n=3, m=2$

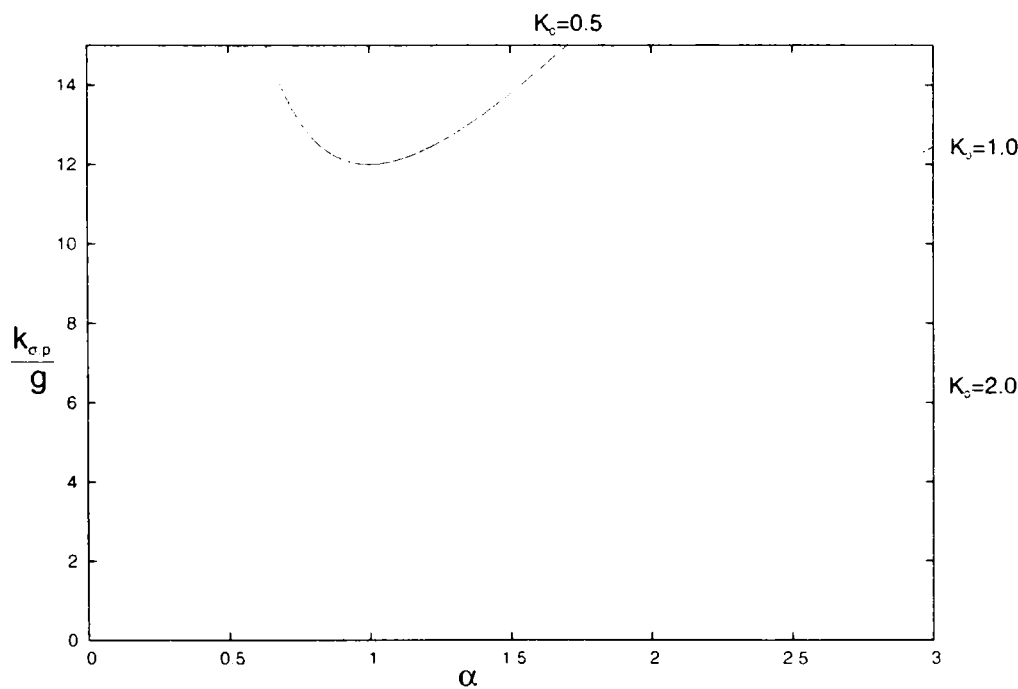


Fig. 5.69. The relation of $k_{\sigma p}$ and α in the case of $n=3, m=3$

5.6. The analysis of elastically “layer” connected structures, The concept of the “ideal” cross section

FALKE (1983) (1984) suggested a new technique to analyze the orthotropic plates based on the method used for composite structures where the parts of the structure are elastically connected. Several other researched have worked on the problem of elastically connected structures. Several other researched have worked on the

problem of elastically connected structures (SATTLER (1955), LESKELA (1986), STÜSSI (1943), TOMMOLA, JUTILA (2001), SZABO (2006), PLATTHY (1965), COSENZA, MAZZOLANI (1994), ARIBERT (1990))

(see Fig. 5.70)

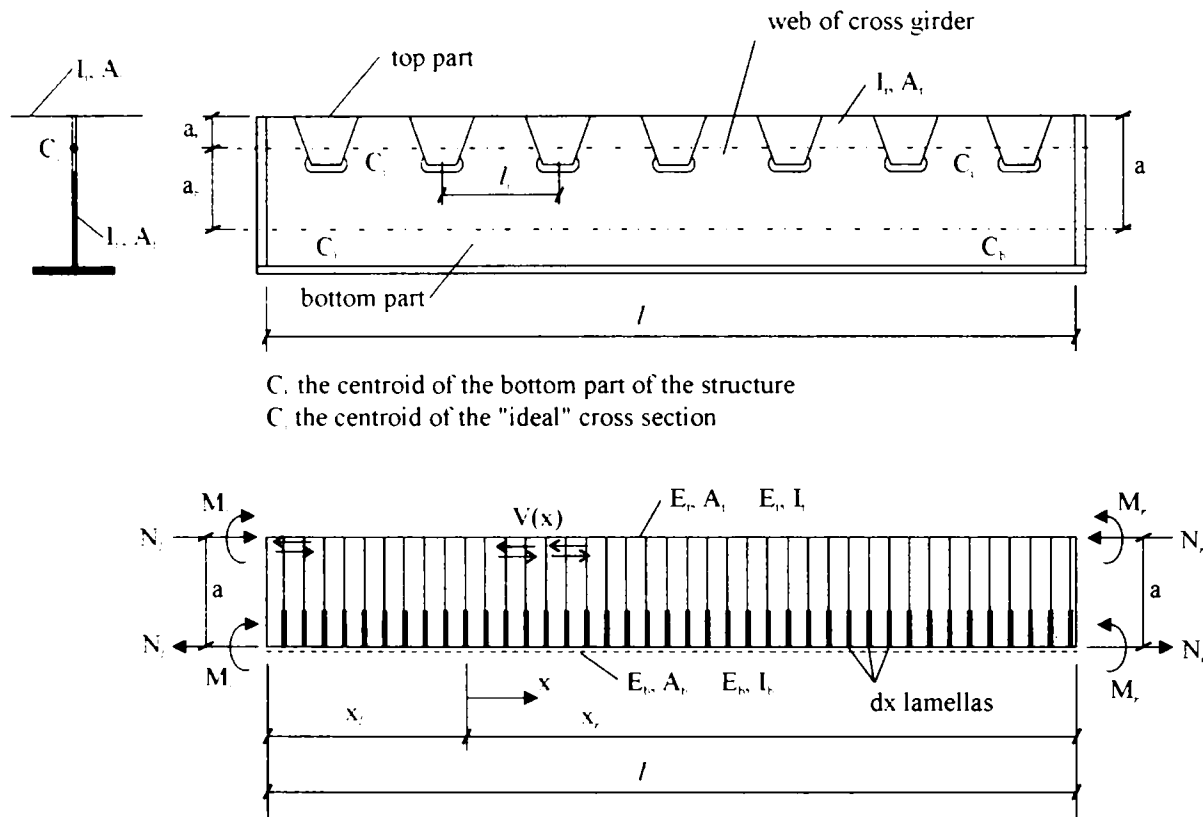


Fig. 5.70. Elastic "layer" connection model

One of the basic assumptions in the case of elastically connected structures is that the connection between the two parts of the structural cross section is continuous. This means that the model can be viewed as a structure where there is a continuous, elastic layer between the two parts (see Fig. 5.71). The differential equation to describe the behaviour of the static model of the orthotropic plate can be formulated after FALKE (1984). If the spring constant of the "layer" is denoted by ε then the change of the length of the layer due to $V(x)$ force can be written as

$$\delta(x) = \varepsilon V(x).$$

In this case the relative elongation is

$$\frac{d\delta(x)}{dx} = \varepsilon \frac{dV(x)}{dx}. \quad (5.23)$$

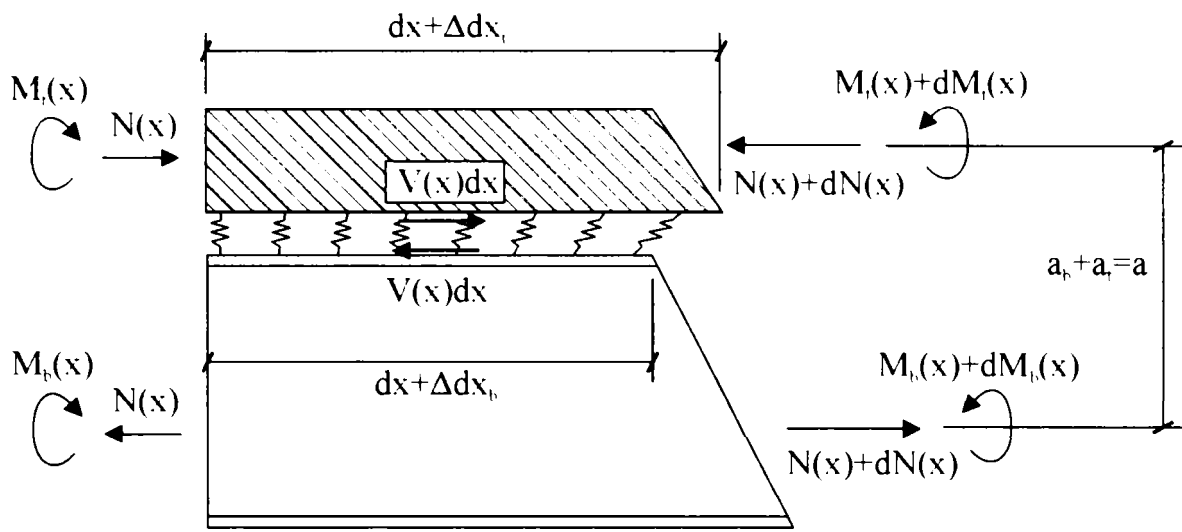


Fig. 5.71. State of equilibrium considering an "elastic" layer

On the other hand Eq. 5.23 can be written as the function of the relative elongation of the two parts of the structure. To perform this rewriting an infinitesimally small part of the structure (with length dx) will be considered and the displacements will be investigated at the connection. It can be easily understood that the elastic layer has to counter the relative displacements of the two parts of the structure, thus

$$(dx + \Delta dx_b) - (dx + \Delta dx_t) = d\delta(x) \quad (5.24)$$

Substituting Eq. 5.23 into Eq. 5.24 the following can be written

$$\frac{\Delta dx_b}{dx} - \frac{\Delta dx_t}{dx} = \frac{d\delta(x)}{dx} = \varepsilon \frac{dV(x)}{dx} \quad (5.25)$$

However knowing the internal forces, M_b , M_t , and N it is possible to write

$$\frac{\Delta dx_b}{dx} = \frac{N}{E_b A_b} - \frac{M_b}{E_b I_b} a_b,$$

and

$$\frac{\Delta dx_t}{dx} = \frac{N}{E_t A_t} - \frac{M_t}{E_t I_t} a_t,$$

Considering that $a_t + a_b = a$ and taking advantage of the equal rotation

$$\frac{M_t}{E_t I_t} = \frac{M_b}{E_b I_b}.$$

Eq. 5.25 can be written as

$$N(x) \left[\frac{1}{E_b A_b} + \frac{1}{E_t A_t} \right] - M_b(x) \frac{a}{E_b I_b} = \varepsilon \frac{dV(x)}{dx} . \quad (5.26)$$

The right hand side of Eq. 5.26 can be rewritten, since from the condition of equilibrium (see Fig. 5.71)

$$\sum N(x) = N(x) + V(x) dx - N(x) - dN(x) = 0 ,$$

thus

$$\frac{dN(x)}{dx} = V(x) , \quad (5.27)$$

and

$$\frac{dV(x)}{dx} = \frac{d^2 N(x)}{dx^2} . \quad (5.28)$$

Furthermore from the equation of equilibrium

$$M = M_b + M_t + a N ,$$

if M_t is neglected we get

$$M_b \approx M - a N . \quad (5.29)$$

Using Eq. 5.27, 5.28 and 5.29 then Eq. 5.26 can be rewritten as

$$\frac{d^2 N}{dx^2} - \frac{\frac{1}{E_t A_t} + \frac{1}{E_b A_b} + \frac{a^2}{E_b I_b}}{\varepsilon} N + \frac{a}{\varepsilon E_b I_b} M = 0 ,$$

in a second order differential equation. By introducing the following two new notations

$$\omega = \frac{a}{\varepsilon E_b I_b} ,$$

and

$$\lambda^2 = \frac{\frac{1}{E_t A_t} + \frac{1}{E_b A_b} + \frac{a^2}{E_b I_b}}{\varepsilon} ,$$

the differential equation has the form of

$$\frac{d^2 N(x)}{dx^2} - \lambda^2 N(x) + \omega M(x) = 0 , \quad (5.30)$$

which is the usual form of the differential equation for elastically connected structures. Eq. 5.30 is solved for load cases that can occur in practice, for example in the book of SATTLER (1955) several approximate methods can be found.

HOMBERG (1952), HOISCHEN (1954), PLATTHY (1965) had suggested a new method where instead of solving the elastically connected composite structures by differential equation the problem is solved by an energy method. In this case an "ideal" stiffness can be determined and then the elastically connected composite structure can be calculated as a normal beam structure. One of them conclusions that the displacements of the elastically connected, simple supported composite beam are similar to the displacements of a homogeneous beam.

(i) The difference is in the stiffness (EI) and for an **elastically connected composite structure** it can be written as:

$$(EI)_i = E_b I_b + E_t I_t + \frac{a^2}{K + \frac{\nu^2 \pi^2}{l^2} \varepsilon} \quad (5.31)$$

which is the "reduced" or "ideal" stiffness, where E_b and E_t are the Young's modulus of the bottom and the top structural details, a is the sum of the distance between the centre of gravity of the top part and the centre of gravity of the whole structural cross section and the distance between the centre of gravity of the bottom part and the centre of gravity of the whole cross section.

$$K = \frac{1}{E_b A_b} + \frac{1}{E_t A_t}, \text{ where} \quad (5.32)$$

A_b and A_t are the areas of the bottom and top part [cm^2]

l is the span [cm],

ε is the elastic "layer" parameter [cm^2/kN]

$\nu = 2n+1; n=0, 1, 2, \dots$

When $\varepsilon=0$ – the structure is infinitely stiff – then the "ideal" stiffness gives the same formula which is used for composite structure:

$$(EI)_i = E_b I_b + E_t I_t + \frac{a^2}{K} = E_b I_b + E_t I_t + E_b a_b^2 A_b + E_t a_t^2 A_t, \quad (5.33)$$

where a_t is the distance between the centre of gravity of the top part and the centre of gravity of the whole cross section, a_b is the distance between the centre of gravity of the bottom part and the centre of gravity of the whole cross section ($a = a_t + a_b$).

When $\varepsilon = \infty$ then there is no connection between the parts of the structural cross section and

$$(EI)_i = E_b I_b + E_t I_t. \quad (5.34)$$

The intermediate values for ε are schematically shown in Fig. 5.72.

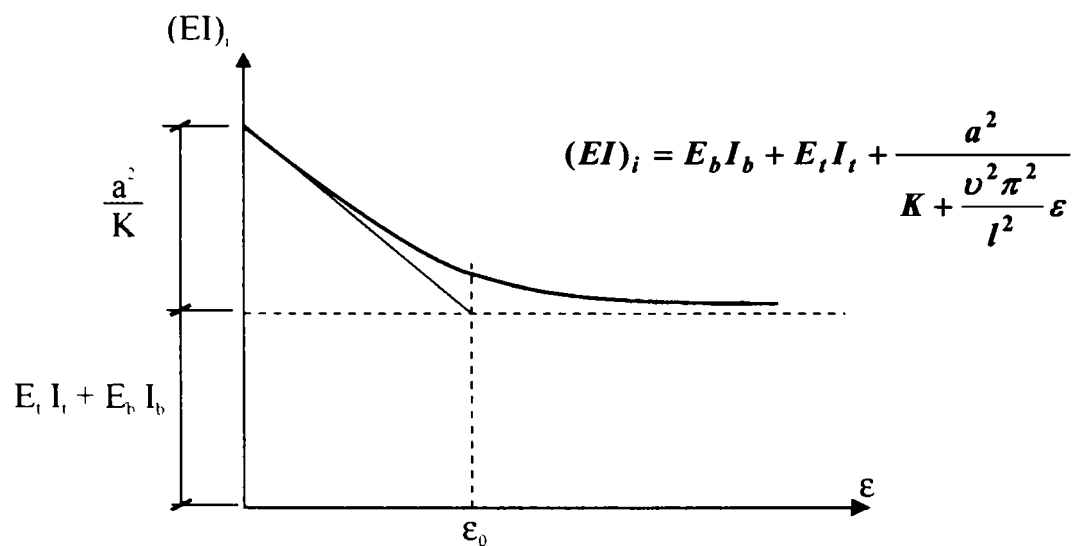


Fig. 5.72. Stiffness of elastically connected composite structure

(ii) The "ideal stiffness" in relation to the ε elastic "layer" parameter can be approximated with the **exponential function** (see Fig. 5.73) :

$$(EI)_i = E_t I_t + E_b I_b + \frac{a^2}{K} e^{-\frac{\varepsilon}{\varepsilon_0}}, \quad (5.35)$$

$$\varepsilon = 0, \quad (EI)_i = E_t I_t + E_b I_b + \frac{a^2}{K}, \quad (5.36)$$

$$\varepsilon = \varepsilon_0, \quad (EI)_i = E_t I_t + E_b I_b + \frac{a^2}{K} \frac{1}{e}, \quad (5.37)$$

$$\varepsilon = \infty, \quad (EI)_i = E_t I_t + E_b I_b. \quad (5.38)$$

The ε elastic parameter to take into account the structural detail of the orthotropic plate has been determined by a numerical analysis and it was compared to the experimental results.

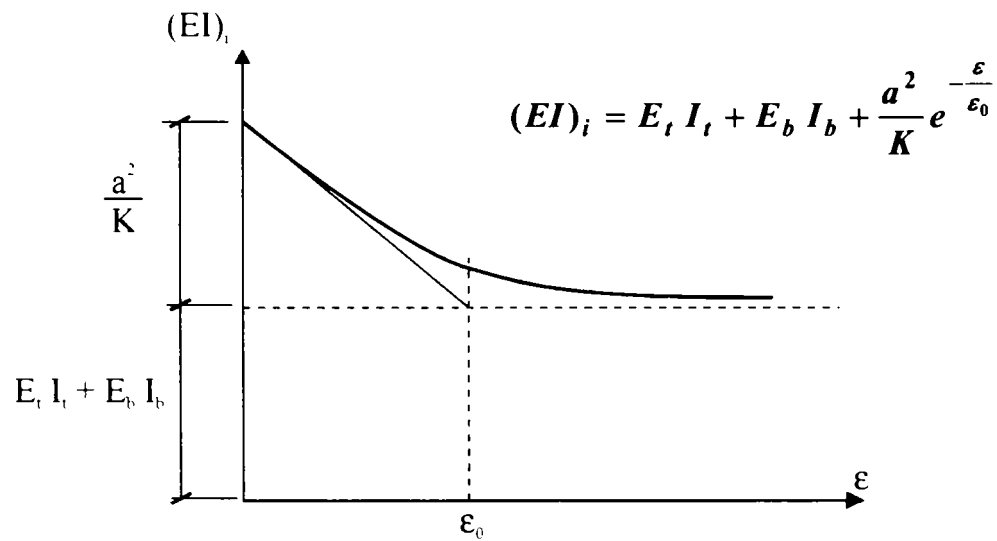


Fig. 5.73. Elastic "layer" parameter with exponential function

5.7. Application of an „ideal” cross section

5.7.1. The inertia of the "ideal" (reduced) cross section for the experimental models

Lets determine the inertia of the ideal cross section for the cases investigated by the experiments (R, S, E).

$$(EI)_i = EI_t + EI_b + \frac{a^2}{E \left[K + \frac{\nu^2 \pi^2}{l^2} \varepsilon \right]}$$

$$I_b = \frac{50 \cdot 0,6^3}{12} = 0,9 \text{ cm}^4,$$

$$(I_t)_R = 194,9 \text{ cm}^4, \quad (I_t)_{S,E} = 106,38 \text{ cm}^4,$$

where a is the distance between the centroids of the top and bottom sides

$$a_R = 19,835 \text{ cm}, \quad a_{S,E} = 20,759 \text{ cm},$$

$$(EK)_R = \frac{E}{EA_t} + \frac{E}{EA_b} = \frac{1}{30} + \frac{1}{12,25} = 0,11496 \left[\frac{1}{cm^2} \right],$$

$$(EK)_{S,E} = \frac{1}{30} + \frac{1}{11} = 0,12424 \left[\frac{1}{cm^2} \right],$$

$$E \frac{\nu^2 \pi^2}{l^2} \varepsilon = 21000 \frac{\pi^2}{50^2} \varepsilon = 82,90\varepsilon ,$$

$$\nu = 2n+1, (n = 0,1,2,\dots),$$

$$\nu = 1,$$

$$(I_i)_R = 0,9 + 194,9 + \frac{19,835^2}{0,11496 + 82,90\varepsilon},$$

$$(I_i)_{S,E} = 0,9 + 106,38 + \frac{20,759^2}{0,12424 + 82,90\varepsilon}.$$

The ε spring constant of the elastic “layer” can be determined by numerical experiments and it is checked with the experimental results.

5.7.2. Results of the numerical analysis and the experimental tests

A 3D linear finite element model has been calculated in the numerical analysis. The elastic layer is defined between the two structural components, thus the ε spring constant can be determined by the length change due to shearing.

In the numerical analysis the displacements due to V shear force have been determined. The ε spring constant can be calculated according to the displacement difference between point A and D. In this way the analysis of the elastic “layer” between the two structural parts means a “push-out” test (Fig. 5.74).

Numerical analysis has been performed at the load level N=125 kN, Table 5.1 summarizes the results.

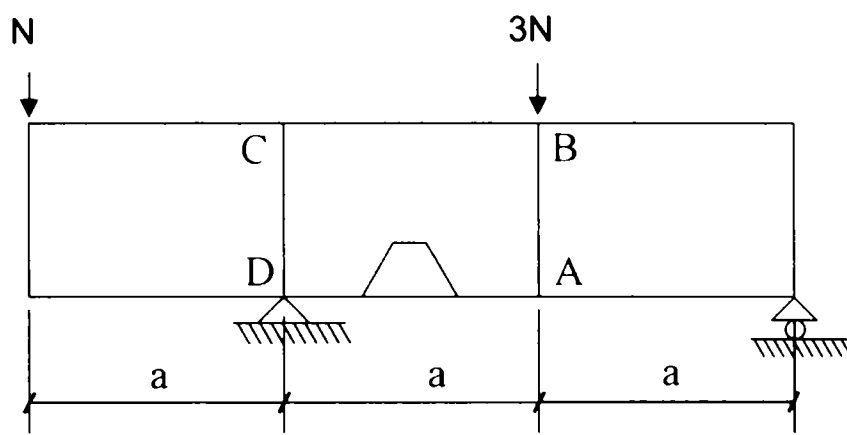


Fig. 5.74. The effect of shear load

TR R-3	C	x	$-0,3821 \times 10^{-3} \text{ m}$	B	$-0,3814 \times 10^{-3} \text{ m}$
		y	$-1,0 \times 10^{-8} \text{ m}$		$-0,1284 \times 10^{-6} \text{ m}$
		z	$-0,2906 \times 10^{-4} \text{ m}$		$-0,1553 \times 10^{-2} \text{ m}$
	A	x	$-0,17928 \times 10^{-4} \text{ m}$	D	0
		y	$-0,1240 \times 10^{-7} \text{ m}$		0
		z	$-0,1459 \times 10^{-2} \text{ m}$		0
TR S-3	C	x	$-0,56313 \times 10^{-3} \text{ m}$	B	$-0,56256 \times 10^{-3} \text{ m}$
		y	$-0,2239 \times 10^{-8} \text{ m}$		$-0,31574 \times 10^{-6} \text{ m}$
		z	$-0,2787 \times 10^{-4} \text{ m}$		$-0,19549 \times 10^{-2} \text{ m}$
	A	x	$-0,42429 \times 10^{-4} \text{ m}$	D	0
		y	$-0,40876 \times 10^{-7} \text{ m}$		0
		z	$-0,18582 \times 10^{-2} \text{ m}$		0
TR E-3	C	x	$-0,65531 \times 10^{-3} \text{ m}$	B	$-0,6473 \times 10^{-3} \text{ m}$
		y	$-0,17002 \times 10^{-7} \text{ m}$		$-0,17684 \times 10^{-7} \text{ m}$
		z	$-0,274471 \times 10^{-4} \text{ m}$		$-0,20464 \times 10^{-2} \text{ m}$
	A	x	$-0,5387 \times 10^{-4} \text{ m}$	D	0
		y	$-0,73969 \times 10^{-7} \text{ m}$		0
		z	$-0,19498 \times 10^{-2} \text{ m}$		0

Table 5.1. Deflections of different point (ABCD) by numerical analysis

In case of $N=125\text{kN}$ the relative displacements in the x direction of point A and D calculated by the numerical analysis are:

R rigid: $(e_{Ax})_R=0.001793$ cm,
 S standard: $(e_{Ax})_S=0.004243$ cm,
 E economic: $(e_{Ax})_E=0.005387$ cm.

The load level in the experiments were $N=50$ kN when the relative displacements have been measured in the experiments (Chapter 3). After adjusting the values by considering the load difference the relative displacement and their relation to the numerically determined relative displacements are:

R rigid:	$(e_{Ax})_R=0.0015$ cm,	88%
S standard:	$(e_{Ax})_S=0.0038$ cm,	90%
E economic:	$(e_{Ax})_E=0.0058$ cm.	108%

In the calculations the numerical results have been used.

5.7.3. Structural details investigated by experimental models

The ε spring parameter for the inertia of “ideal” structural cross section can be determined of the elastic “layer”. (Geometry of the models can be found in Chapter 3.) In this section a fourth structural details is considered, full connection. In this case the web of the cross girder is continuously welded to the orthotropic plate, the trapezoidal stiffeners do not cut a hole into this web.

(i) (F) Full connection

$$\varepsilon = 0,$$

$$I_F = 0,9 + 194,9 + \frac{19,835^2}{0,11496} = 0,9 + 194,9 + 3422,3 = 3618,1 \text{ cm}^4.$$

The ratio between the inertia of a structural detail (R,S,E) and the inertia of the structural details with full (F) connection

(ii) R-rigid connection

$$\varepsilon_R = \frac{e_{AX} a}{2N} = \frac{0,001793[\text{cm}] \cdot 50[\text{cm}]}{250[\text{kN}]} = 0,0003586 \frac{\text{cm}^2}{\text{kN}},$$

$$(I_i)_R = 195,8 + 2532,6 = 2728,5 \text{ cm}^4. \quad 75,4\%$$

(iii) S-standard connection

$$\varepsilon_S = \frac{e_{AX}^a}{2N} = \frac{0,004243 \cdot 50}{250} = 0,0008486 \frac{cm^2}{kN},$$

$$(I_i)_S = 107,28 + 2214,6 = 2321,9 cm^4. \quad 64,1\%$$

(iv) E-economic connection

$$\varepsilon_E = \frac{e_{AX}^a}{2N} = \frac{0,005387 \cdot 50}{250} = 0,0010774 \frac{cm^2}{kN},$$

$$(I_i)_E = 107,28 + 2017,9 = 2125,2 cm^4. \quad 58,7\%$$

(v) When there is no connection between the two structural components:

$$\varepsilon = \infty,$$

$$I_0 = 195,8 cm^4.$$

5.7.4. Case study of the floodplain bridge at Szekszárd over the Danube

The inertia of the ideal (reduced) cross section of the floodplain bridge at Szekszárd over the Danube will be determined in this section. The studied orthotropic plate section is under compression, therefore the bottom flange near the middle pier will be considered (Fig. 5.75).

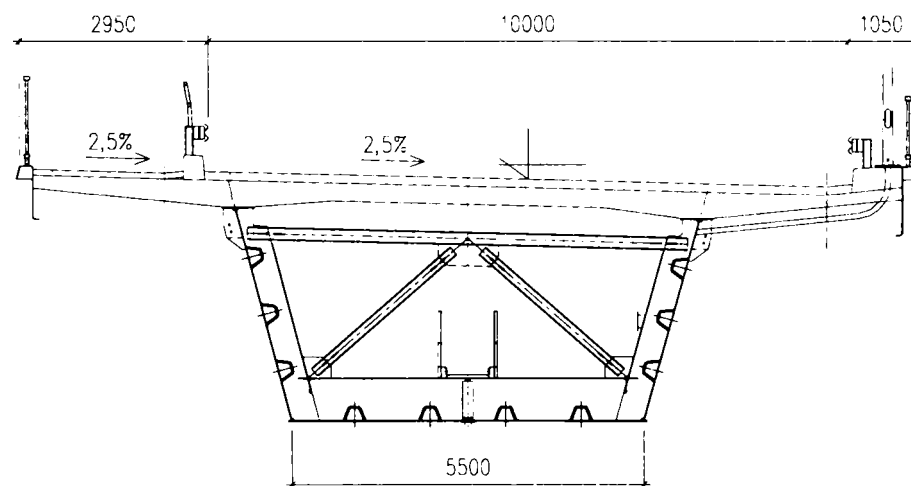


Fig. 5.75. The cross section of the floodplain Danube bridge at Szekszárd

$$I_i = I_t + I_b + \frac{a^2}{E \left[K + \frac{\nu^2 \pi^2}{l^2} \varepsilon \right]},$$

$$I_b = \frac{100 \cdot 1,2^3}{12} = 14,4 \text{ cm}^4.$$

It has been assumed that that the ε spring constant can be used in the case of the floodplain bridge at Szekszárd over the Danube.

(i) F-full connection

$$I_F = 58431 \text{ cm}^4$$

(ii) R-rigid connection

$$(I_t)_R = 3118,5 \text{ cm}^4, \quad (I_t)_{S,E} = 1523,6 \text{ cm}^4,$$

$$a_R = 46,2 - 6,53 = 39,67 \text{ cm}, \quad a_{S,E} = 46,2 - 5,04 = 41,16 \text{ cm},$$

$$K_R = \frac{1}{A_t} + \frac{1}{A_b} = \frac{1}{49,0} + \frac{1}{120} = 0,02874 \left[\frac{1}{\text{cm}^2} \right],$$

$$K_{S,E} = \frac{1}{45} + \frac{1}{120} = 0,030555 \left[\frac{1}{\text{cm}^2} \right],$$

$$E \frac{\nu^2 \pi^2}{l^2} \varepsilon = 21000 \frac{\pi^2}{110^2} \varepsilon = 17,128 \varepsilon,$$

$$l = \frac{b}{5} = 110 \text{ cm},$$

$$\varepsilon_R = 0,00035285 \left[\frac{\text{cm}^2}{\text{kN}} \right],$$

$$(I_i)_R = 14,4 + 3118,5 + \frac{39,67^2}{0,02874 + 17,128 \varepsilon} = 48375 \text{ cm}^4. \quad (82,5\%)$$

The ratio between the inertia of a structural detail (R,S,E) and the inertia of the structural details with full (F) connection

(iii) S-standard connection

$$\varepsilon_S = 0,00084859 \left[\frac{\text{cm}^2}{\text{kN}} \right],$$

$$(I_i)_S = 14,4 + 1523,6 + \frac{41,16^2}{0,030555 + 17,1288\varepsilon} = 39111 \text{ cm}^4. \quad (72,9\%)$$

(iv) E-economic connection

$$\varepsilon_E = 0,0010774 \left[\frac{\text{cm}^2}{\text{kN}} \right],$$

$$(I_i)_E = 14,4 + 1523,6 + \frac{41,16^2}{0,030555 + 17,1288\varepsilon} = 36105 \text{ cm}^4. \quad (67,3\%)$$

5.7.5. Study of the bottom flange at the middle pier in the floodplain bridge at Szekszárd over the Danube when an exponential function is used

To determine ε_0 first the inertia must be calculated

R-rigid connection

$$(I_i)_R = 14,4 + 3118,5 + \frac{39,67^2}{0,02874} \frac{1}{2,7183} = 23276,6 \text{ cm}^4$$

S-standard and E-economic connection

$$(I_i)_{S,E} = 14,4 + 1523,6 + \frac{41,16^2}{0,030555} \frac{1}{2,7183} = 21935,2 \text{ cm}^4$$

The values of ε_0 :

$$\text{„R”} \quad 17,1288\varepsilon_0 = \frac{39,67^2}{20143,7} - 0,02874, \quad \varepsilon_0 = 0,0028832 \frac{\text{cm}^2}{\text{kN}}$$

$$\text{„S”, „E”} \quad 17,1288\varepsilon_0 = \frac{41,16^2}{20397} - 0,030555, \quad \varepsilon_0 = 0,0030652 \frac{\text{cm}^2}{\text{kN}}$$

Percentages
compared to the
inertia determined
in Section 5.7.4

The inertia in the case of different structural details:

$$\text{„R”} \quad (I_i)_R = 3132,9 + \frac{39,67^2}{0,02874} e^{-\frac{0,00035285}{0,0028832}} = 46001,4 \text{ cm}^4 \quad (5\%)$$

$$\text{„S”} \quad (I_i)_S = 1538 + \frac{41,16^2}{0,030555} e^{-\frac{0,00084859}{0,0030652}} = 43575,4 \text{ cm}^4 \quad (11\%)$$

$$„E” \quad (I_i)_E = 1538 + \frac{41,16^2}{0,030555} e^{-\frac{0,0010774}{0,0030652}} = 40551,6 \text{ cm}^4 \quad (12\%)$$

Thus it is possible to investigate the effects of the different structural details with the approximation of an exponential function which does not contain l .

5.7.6. Study of the floodplain bridge at Szekszárd over the Danube

In this section first the ultimate limit state of the bottom flange will be calculated considering the "ideal" cross section of the cross girders.

(Full) cross girder: $I_F = 58431 \text{ cm}^4$,
 (Rigid): $(I_i)_R = 48375 \text{ cm}^4$,
 (Standard): $(I_i)_S = 39111 \text{ cm}^4$,
 (Economic): $(I_i)_E = 36105 \text{ cm}^4$.

The calculation has been performed on a part of the stiffened panel sections with the effect of stiffener of cross girders.

The calculations were carried out by the MathCAD program and the details can be found in the Appendices.

Appendix 1 contains the analysis of one plate section between two cross girders according to EC 3-1-5 (2005). The values of $\sigma_{cr,p}$ and $\sigma_{cr,c}$ have been determined according to Annex 1 of EC 3.

The load bearing capacity is $N_{R,d} = 32109 \text{ kN}$.

The load bearing capacity considering shear lag is $N_{R,d \text{ shear lag}} = 19551 \text{ kN}$.

Appendix 2 contains the analysis of one plate section between two cross girders according to prENV EC 3-1-5 (1992). These analysis were performed following the examples of EISEL et al (1995) and BANCILA (1996).

The load bearing capacity is $N_{R,d} = 29439 \text{ kN}$.

The load bearing capacity considering shear lag is $N_{R,d \text{ shear lag}} = -$.

Appendix 3 contains the analysis of two plate sections with three cross girders according to EC 3-1-5 (2005). To be able to determine $\sigma_{cr,p}$ and $\sigma_{cr,c}$ the stiffness of the cross girders is required. In this case the full cross section of the cross girder is taken into account. The results are shown in Table 5.2.

Appendix 4 contains an analysis similar to the analysis in Appendix 3 with the exception that in this case the stiffness of the cross girder has been determined with the concept of the "ideal" cross section (Section 5.7.4) and the connection between the trapezoidal stiffener and the cross girders is rigid (R). The results are shown in Table 5.2.

Appendix 5 contains an analysis similar to the analysis in Appendix 4 with the exception that in this case the connection between the trapezoidal stiffener and the cross girders is the type of standard (S). The results are shown in Table 5.2.

Appendix 6 contains an analysis similar to the analysis in Appendix 4 with the exception that in this case the connection between the trapezoidal stiffener and the cross girders is the type of economic (E). The results are shown in Table 5.2.

Based on these calculations the following conclusions can be drawn:

- The stiffness of the cross girders is significantly different when using different structural details (R, S, E).
- The load bearing capacity of the structure with two compressed plates is influenced in a less significant way by the structural details (R, S, E). Furthermore the structural detail of the connection between the stiffener and the cross girder has smaller effect on the load bearing capacity when considering shear lag.

	$(I)_{F,R,S,E}$ [mm ⁴]	$\frac{(I_i)_{R,S,E}}{I_F}$	$N_{R,d}$ [kN]	$\frac{N_{R,d,i}}{N_{R,d}}$	$N_{R,d, shear}$ [kN]	$\frac{N_{R,d, sheatag}}{N_{R,d}}$
App. 3 F (Full)	5.84 10 ⁸	1.000	38 290	1.000	22 428	1.000
App. 4 R (Rigid)	4,837 10 ⁸	0.825	37 577	0.981	22 103	0.985
App. 5 S (Standard)	3.911 10 ⁸	0.669	36 691	0.958	21 698	0.967
App. 6 E (Economic)	3,611 10 ⁸	0.618	36 337	0.948	21 535	0.960

Table 5.2. The effect of the structural detail in the stiffness and the load bearing capacity

5.7.7. “Supporting” effect of the cross girders

In the case of traditional structural details the connection between the longitudinal stiffeners and the cross girders is direct and thus the supporting effect is also direct. On the other hand the supporting effect is not direct and therefore it is worth to study in the structural detail investigated in this thesis.

(i) It is important to note that EC 3 Part 1.5 is still valid for the type of orthotropic steel plates that are going to be investigated in this chapter. The main assumption that there are no transversal loading on the plates.

(ii) The Japanese-Hungarian joint research work (IVÁNYI, 2001) discussed in the introduction of this chapter have investigated the requirements for the automatic welding (with robots) and studied the structural details of the open cross section, non continuous stiffeners for plates. The conclusion of this research was that a gap, causing the disruption in the continuity of the stiffeners, do not significantly affect the load carrying capacity if its size do not exceed a certain size. Thus this structural details is acceptable for stiffeners.

In the engineering practice there are well-known basic problems where due to the lack of direct support the structure utilizes an indirect support. Classic example is the stability analysis of the top flange of an open truss system, where the columns and cross beams form a U-shaped frame and the stiffness of this frame determines the elastic support of the compressed flange. Another example is the elastically supported, compressed bar (HALÁSZ-IVÁNYI, 2001). This example can be seen in Fig. 5.76.

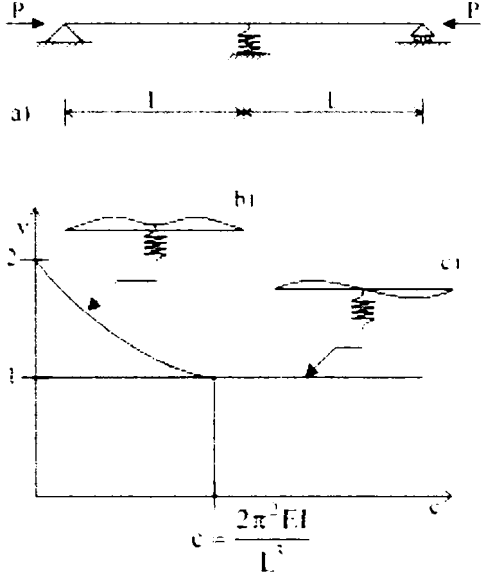


Fig. 5.76. Elastically supported, compressed bar

Beyond a certain value of the elastic parameter the buckling of the bar is not influenced, however below this value the buckling length is modified.

In this study, in the case economic (E) structural detail there is no direct connection between the trapezoidal stiffener and the web of the cross girders, however the “neighbouring” plates can provide indirect support. In this section this problem will be investigated with a simple engineering model (see Fig. 5.77).

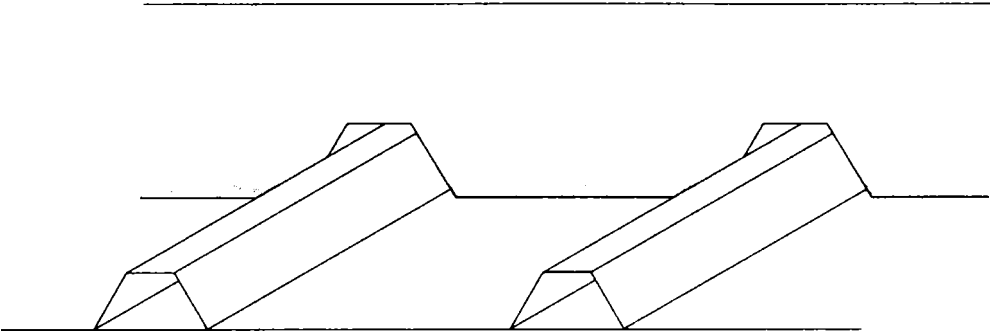


Fig. 5.77. Stiffened plate between stiffeners with economic (E) connections

The web of the cross girder is connected directly to the plate. It is assumed that the trapezoidal stiffeners provide a simple support for the plates. Lets examine two adjacent plates, or in other words only one cross girder is assumed. To determine the elastic parameter it is required to calculate the elastic displacement of plate that is simple supported at all four sides and loaded by a partial distributed load. SZILARD (1974) provides a solution for this problem:

$$w(x, y) = \frac{16p_0}{D\pi^6} \sum_{m=1}^{\infty} \sum_{n=1}^{\infty} \frac{\sin(m\pi\xi/a)\sin(n\pi\eta/b)\sin(m\pi c/2a)\sin(n\pi d/2b)}{mn\left[\left(m^2/a^2\right)+\left(n^2/b^2\right)\right]^2} \sin\frac{m\pi x}{a}\sin\frac{n\pi y}{b} \quad (5.39)$$

where the explanation of the variables can be seen in Fig. 5.78. The convergence of this solution is relatively fast, provided that the dimensions a and b are not too small. The displacement can be obtained with sufficient accuracy by taking the first four terms of the series.

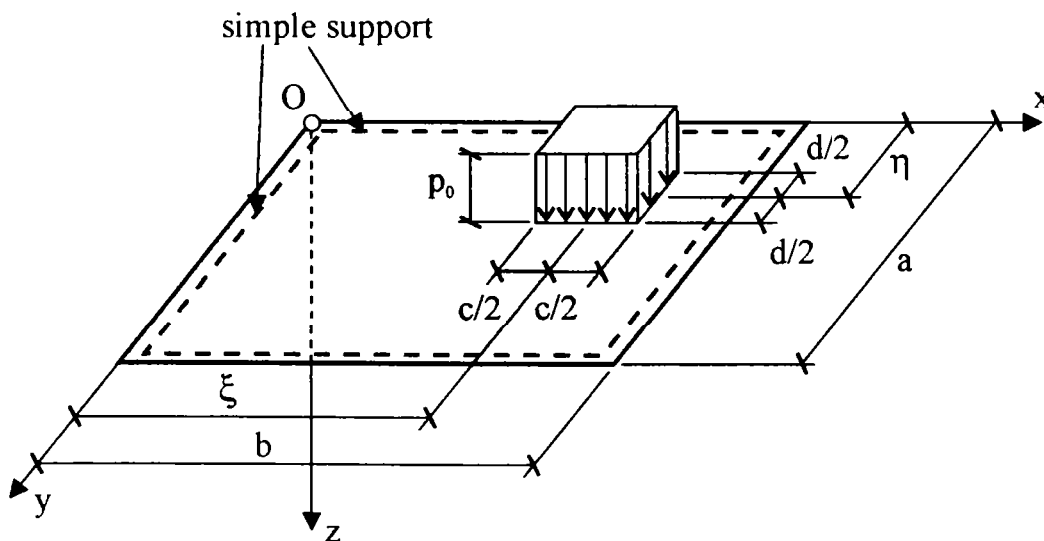


Fig. 5.78. Uniform load over a small rectangular area

It is also assumed that the area of the partial load is equivalent to the cross section area of the cross girder and assuming $p=1 \text{ N/m}^2$ load then the deflection of the plate will provide the elastic parameter. By knowing this elastic parameter the stability model can be solved now (see Fig. 5.79 – Fig. 5.80).

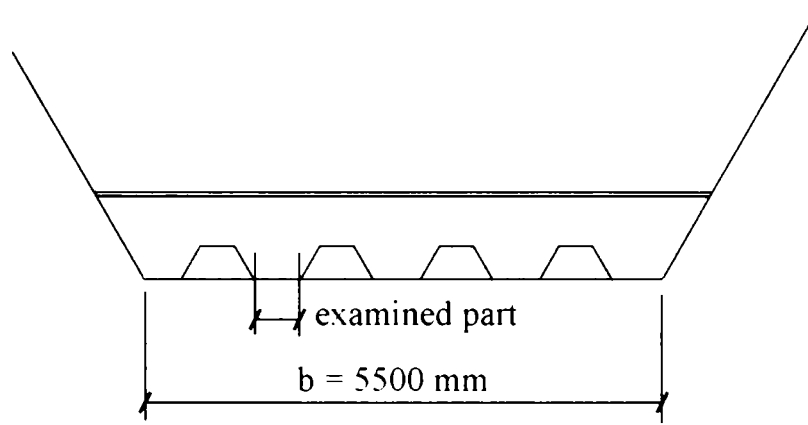


Fig. 5.79. The examined cross section

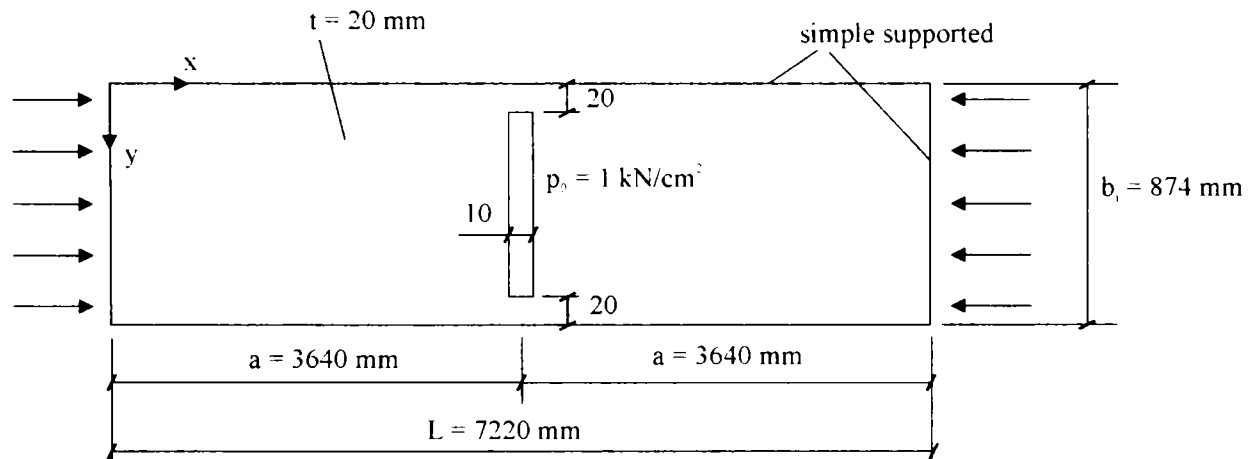


Fig. 5.80. Structural model for the calculation of the plate displacement

The area and inertia of the cross section of the trapezoidal stiffener:

$$A_{sl} = \frac{132136}{4} = 33034 \text{ mm}^2,$$

$$I_{sl} = \frac{4,123 \cdot 10^8}{4} = 1,0307 \cdot 10^8 \text{ mm}^4,$$

Loading is $p_0 = 1 \frac{\text{kN}}{\text{cm}^2}$.

The loading surface of the web of the cross girde is $A = 83,4 \text{ cm}^2$.

The deflection at the examined point: $e_z = 0,427 \text{ cm}$,

$$C = \frac{p_0 A}{e_z} = \frac{1 \cdot 83,4}{0,427} = 195,3 \frac{\text{kN}}{\text{cm}},$$

$$c = \frac{C L^3}{E I_{sl}} = \frac{1953 \cdot 722^3}{21000 \cdot 10307} = 340.$$

In the case of the simple supported beam that is elastically supported in the middle the elastic parameter can be taken from TABLE (2004)

If the elastic parameter is larger than 150, which is the case here, the support can be considered rigid.

5.8. Conclusions

I have studied the connection of the stiffeners of a stiffened plate. It can be stated that the economic (E) connection can also provide sufficient support for the longitudinal stiffeners.

The concept of the ideal cross section can be recommended to determine the stiffness of the cross girders. The formula can be generalized using the exponential function

$$(EI)_i = E_t I_t + E_b I_b + \frac{a^2}{K} e^{-\frac{\varepsilon}{\varepsilon_0}}$$

where t is the top of the cross section,

b is the bottom of the cross section,

a is distance between the centroids of the two parts of the structure,

$$K = \frac{1}{E_b A_b} + \frac{1}{E_t A_t}.$$

The recommended values for the ε elastic “layer” parameter:

In the case of **S** standard structural detail: $(\varepsilon)_s = 0,00084859 \text{ [cm}^2/\text{kN]}$,

In the case of **E** economic structural detail: $(\varepsilon)_E = 0,0010774 \text{ [cm}^2/\text{kN]}$.

The value of ε_0 parameter when the structural detail of the cross girder of the floodplain bridge at Szekszárd is used: $(\varepsilon)_0 = 0,0030652 \text{ [cm}^2/\text{kN]}$,

(IVANYI, Jr., BANCILA, 2006, IVANYI, Jr., et al, 2007),

CHAPTER 6

Summary and Conclusions

I have investigated the connection between the trapezoidal stiffener and the open cross section girder in an orthotropic plate which is loaded only in its plane. The calculations determine the effect of the different connection types on the load bearing capacity of the orthotropic plate.

6.1. Examining the design process

The basis of the analysis is the EC 3-1-5 standard and determines the values of $\sigma_{cr,p}$ (plate buckling attitude) and $\sigma_{cr,c}$ (column buckling attitude). In Annex 1 of EC 3-1-5 contains formulas only for the design of one plate section between two cross girders.

- (i) The method discussed in this study makes it possible to examine two plate sections with three cross girders.
- (ii) I have also presented a method which can take into account the different structural detail between the cross girders and the trapezoidal stiffeners in a compressed plate with stiffeners. In this way it is possible to study the "orthotropic buckling" phenomena.
- (iii) I have examined three structural details for the connection between the trapezoidal stiffener and the cross girder. In the case of the rigid (R) connection the web of the cross girder is fully welded to the plate. Two other types of connections have been considered, the standard (S) (the

traditional used) and the economic (E) (the newly proposed). The results have shown that the structural details have little effect on the load bearing capacity, even when shear lag is considered.

- (iv) The structural detail has a significant effect on the stiffness of the cross girder. For the calculations the concept of the "ideal" cross section has been introduced which can take into account the effect of the structural detail through the introduction of an elastic layer.
- (v) The elastic parameter for the elastic layer has been determined by numerical analysis and experiments.
- (vi) The "ideal" cross section has also been determined by the exponential function which is well known in the engineering practice.

6.2. Experiments

- (vii) I have designed and carried out experiments to study the different structural details (R, S, E) between a trapezoidal stiffener and a cross girder. The experimental specimens were loaded by sagging and hogging moments and by shear forces.
- (viii) The results of the experiments show that the stiffnesses of the different structural details (R, S, E) are significantly different.
- (ix) It can also be concluded that the plastic behaviour of the different structural details under different loadings is different, especially under shear loading.
- (x) It can be similarly stated that the deformation capacities are also different under different loading considering different structural connections.

6.3. Numerical simulation

- (xi) I have designed and executed numerical simulations to study the different structural details (R, S, E) between a trapezoidal stiffener and a cross girder. Using a linear 3D finite element analysis the effect of the different structural details (R, S, E) could be studied.
- (xii) In the frame of non-linear 3D finite element analysis I have studied the behaviour of the different connection types (R, S, E) under shear loading. In this case the plate buckling and material failure could be modelled at the final stages of the loading.

6.4. New Scientific Results

Thesis 1.

I have design and performed an experimental program on half scale test under static loading in bending and shear with the purpose of defining the static load bearing capacity and behaviour of the joints between the trapezoidal stiffeners and the web of the cross beam for orthotropic plate.

On the basis of the experimental results I have characterized the static behaviour of the joints as follows:

- a) I determined the load bearing capacity of the tested joints and characterized the different failure modes (web buckling around the different structural details of the joints). Based on the results I described the effect of the “Rigid”, “Standard” and “Economical” solutions of joints.
- b) I determined the elastic behaviour of the joints under bending and shear separately. The effect of the shear forces gave very important experimental information of the behaviour of the different structural details. It was a special push-out experimental program.

Thesis 2.

I have performed an investigation on the stiffness of the different structural details of joints between the trapezoidal stiffeners and the web of the cross girder by a 3D linear element model on the basis of the application of the experimentally determined characteristics of the special “push-out test” for shear forces.

- a) I showed that the determination of joint-stiffness based on push-out test contains several uncertainties due to the observed initial nonlinearity in the behaviour, consequently, I proposed the approximate consideration of the joint stiffness by stiffness coefficient.
- b) By a parametric study I proved the accuracy of the application of the stiffness coefficient in design.

- c) Comparing the numerical and test results I established that the proposed linear model gives good prediction – despite of the observed nonlinearity – until the load level belonging to the serviceability limit state is reached.

Thesis 3.

I have developed a 3D nonlinear finite element model for the investigation of the different joints structural details between the trapezoidal stiffeners and the web of the cross girder. The model is built by shell and solid elements and considers the geometrical and material nonlinearities, the model includes the “special push-out test” for shear forces based joints characteristics.

- a) Based on the comparison of numerical and experimental results I determined the model level that is required to describe the complex behaviour (accuracy) and permit the practical application (efficiency).
- b) By numerical analysis I determined the effect of each behavioural component on the nonlinear behaviour of the joints between the trapezoidal stiffeners and the web of the cross girder.
- c) I proved numerically the development of the slip distribution in the shear effect that is one of the basic assumptions of the design model.

Thesis 4.

Since the Eurocodes (3 and 4) do not give recommendation as to the evaluation of the design resistance of the different structural details of joints, I have performed analytical studies of these joints types based on the component method. The results of these analytical studies are summarized as follows:

- a) I developed a design method to evaluate the so called “orthotropic buckling” case when the effect of the plate elements, the trapezoidal stiffeners and the cross girders joint to each other different cases (Rigid, Standard and Economical solutions) – I verified and validated the design method using the test and numerical analysis results.
- b) I developed a EC3 compatible design method for the joints. With the application of the developed method the design resistance of the joints

including the “column type attitude” and “plate type attitude” for the “orthotropic buckling”.

Thesis 5.

Based on the comparison of the experimental, numerical and analytical results I have derived practical design rules that ensure favourable ultimate behaviour and resistance.

- a) I demonstrated that within certain limits the “Economical” solution for the joints has enough stiffness for the ultimate limit states of the orthotropic plate.
- b) I verified the design method based on the numerical analysis and experimental results of half-scale beam test. I proved that the failure load and the stress distribution in the ultimate state are in good agreement if the measured material properties are used.

CHAPTER 7

Bibliography

Andra, H.P. (1990) Economical Shear Connectors with High Fatigue Strength, Proc. IABSE Symposium on Mixed Structures, Brussels.

Aribert, J.M. and Abdel A. K. (1985) Calculation of Composite Beams up to Ultimate State with the Effect of Uplift at Steel-Concrete Interface, Revue Construction Métallique, No. 4, pp. 3-36.

Aribert, J.M. (1990) Span Limitations in Design of Composite Steel and Concrete Beams with a Partial Shear Connection, IABSE Symposium Brussels, Belgium - Theme 1 - September 5-7.

ANSI/AWS (1985) American Welding Society Structural Welding Code Steel, (Appendix K) Doc. D1, pp. 1-85.

Bancila, R. (1996) "Noile norme Europeene: EC 3/2 extras selectiv" Al II-lea Seminar de Poduri "Directii actuale in calculul si proiectarea podurilor", Universitatea "Politehnica" Timisoara, pp. 97-149

Bjorhovde, R. (2005) Current Steel Structures Research, Engineering Journal, Second Quarter p. 117.

Bleich, F. (1952) Buckling Strength of Metal Structures, McGraw-Hill Book, New York.

Bondariuc, V., Bancila, R. (1987) Poduri Metalice Curs, Elemente de Calcul Si Alcatuire, (in Romanian) Institutul Politehnic "Traian Vuia" Timisoara, Timisoara.

Bower, J. E. (1966) Elastic stress around holes in wide-flange beams, Journal Structural Div., ASCE, Vol. 92, No.2., pp. 85-101.

Bower, J. E. (1968) Ultimate strength of beams with rectangular holes, Journal Structural Div., ASCE, Vol. 94, No.6., pp. 1315-1337.

Briassoulis, D. (1986) Equivalent Orthotropic Properties of Corrugated Sheets, Computers and Structures, pp. 129-138.

Brush, D. O. and Almroth, B. O. (1975) Buckling of Bars, Plates and Shells, McGraw-Hill, New York.

Bryan, G. K. (1891) On the Stability of a Plane Plate under Thrusts in its own Plane with Application on the "Buckling" of the Sides of a Ship, Math. Soc. Proc., 54.

Chwalla, E. (1944) Über die Biegebeulung der langversteiften Platte und das Problem der Mindeststeifigkeit, Stahlbau 17, pp. 84-88.

Cosenza, E., Mazzolani, S., (1994) Composite steel-concrete structures and Eurocode 4. New Research Results, Behaviour in Service of Beams with Partial Shear Connectors. Eurocodes 3 and 4 in the Light of (I) Other Design Rules (II) New Research Results, International Advanced School, Technical report, Budapest, pp. 345-374.

DIN 18800 Teil 3 (1990), "Stahlbauten, Stabilitätsfalle, Plattenbeulen", Berlin: Beuth.

Dowling, P.J., Knowles, P., Owens, G. W. (1988) Structural Steel Design, Steel Construction Institute, Butterworths, London.

Dubas, P. and Gehri, E. (1986) Behaviour and Design of Steel Plated Structures, ECCS.

Dunai, L., Okura, I., Késmárky, Z., Nagy A. and Iványi M. (1998) Effects of Stiffener-End-Gaps on Ultimate Behaviour of Thin-Walled Girders. Journal of Constructional Steel Research, Vol. 46, No. 1-3, pp. 428-429. (full paper on CD-ROM)

ECCS (1978) Conventional design rules based on the linear buckling theory.

ECCS (1989) Design of longitudinally stiffened webs of plate and box girders, Draft.

ECCS (1989) "Stiffened compression flanges of box girders", Draft.

Eisel, H., Müller, C. and Sedlacek, G. (1995) Worked examples to demonstrate the use of design rules of Eurocode 3 – Part 2., Institute of Steel Construction, RWTH Aachen.

ESDEP, (1994) European Steel Design Education Program, British Steel, administrated by The Steel Construction Institute.

Eurocode 3, (1992) Design of Steel Structures: ENV 1993-1-1: Part 1.1: General rules and rules for buildings, CEN, 1992.

Eurocode 3, (2005) Design of steel structures: EN 1993-1-1: Part 1.1: General rules and rules for building, CEN.

Eurocode 4, (2004) Design of composite steel and concrete structures: EN 1994-1-1: Part 1.1: General rules and rules for building, CEN.

Eurocode 4, Design of Composite Steel and Concrete Structures: ENV1994-1-1: Part 1.1: General rules and rules for building, CEN (in press).: Single Span Beams

Falke, J., (1983) Die Berechnung relemasig gegliederter Trager als Kontinuum, Bauingenieur, Vol. 58, pp. 341-347.

Falke, J., (1984) Theoretische und experimentelle Untersuchungen zu Quertragern orthotroper Platten unde deren naherungsweise Berechnung, Bauingenieur, Vol. 59, pp. 131-136.

Halász, O., Hunyadi, F. (1959) Ortotrop pályalemezes hidak szerkezeti és számítási kérdései (in Hungarian), Analysis of design of orthotropic deck for bridges, Mérnöki Továbbképző Intézet kiadványa, Felsőoktatási Jegyzetellátó Vállalat, Budapest

Halász, Iványi, (2001) Stabilitáselmélet. Acélszerkezetek méretezésének elvei és módszerei. (in Hungary). Stability Theory. Principles and Methods for the Design of Steel Structures. Akadémiai Kiadó, Budapest.

Handbook of Structural Stability, (1971) Edited by Column Research Committee of Japan, Corona Publishing Company, Ltd, Tokyo.

Harding, J. E. (1989) Interaction of direct and shear stresses on Plate Panels in Plated Structures, Stability and Strength. Narayanan (ed.), Applied Science Publishers, London.

Hawranek, A., Steinhardt, O., (1958) Theorie und Berechnung der Stahlbrucken (Theory and analysis of steel bridges), Springer-Verlag, Berlin, pp. 381-414.

Hoischen, A. (1954) Verbundtrager mit elastischer und unterbrochener Verdubelung (Composite girder with discrete elastic connectors) Der Bauingenieur, Vol. 29, pp. 241-244.

Homberg, H. (1952) Brucke mit elastischem Verbund zwischen den Stahlhaupttragern und der Betonfahrbahntafel (Composite bridge with elastic connections between steel main beam and concrete slab), Der Bauingenieur, Vol. 27, No. 7, pp. 213-216.

Hubert, M.T. (1914) Die Grundlagen einer Rationellen Berechnung der Kreuzweise Bewehrten Eisenbetonplatten. Zeitschrift des Osterreichischen Ingenieur-u. Architekten-Vereines, Vol. 66, No. 30

Ito, M., Fujiwara, K., Okazaki, K., (1991) Ultimate Strength of Beams with U-Shaped holes in Top of Web, Journal of Structural Engineering, ASCE, Vol. 117, No. 7, pp. 1929-1945.

Ivanyi, M., (2001) (Editor) Interaction of Automatic Fabrication and Behaviour of Steel Structures, Muegyetemi Kiado, Budapest.

Ivanyi, M., (2003) Orthotropic steel bridges, Muegyetemi Kiado, Budapest and Helsinki University of Technology Publications in Bridge Engineering, Espoo, TKK-SRT-33.

Ivanyi, M. Jr., (2004) Recent composite bridge designs by Uvater Co., in Proceedings of Bridges in Danube Basin–Bridges across the Danube, B. Stipanic (Editor), Euro Gardi Group, Novi–Sad, Serbia, pp. 201–206.

Ivanyi, M., Ivanyi, M. Jr., (2005) Modern steel bridges in Hungary, in Konferencija Savremena Gradeniska Praksa Fakultat Technickih Nauka, Novi Sad, Serbia, pp. 39–54.

Ivanyi, M. Jr., (2005) Design problems of composite bridges, in Festtagung aus Anlass des 60. Geburtstags des Herrn Prof. Dr. Ing. Radu Bancila, E. Petzek (Editor), Technische Universitat “Politehnica”, Timisoara, Romania, pp. 83–86.

Ivanyi, M. Jr., Bancila, R., (2006) Ultimate strength and behavior of a new type of orthotropic plate, in Proceedings of Steel–A New and Traditional Material for Building, Taylor and Francis/Balkema, London UK, pp. 159–164.

Ivanyi, M. Jr., Bancila, R., Ivanyi, M., (2006/a) Behaviour of a new type orthotropic plate for composite bridges, Pollack Periodica, Vol. 1, No. 2, pp. 45-60

Ivanyi, M. Jr., Bancila, R., Ivanyi, M., (2006/b) Numerical and Experimental Analysis of New Type of Orthotropic Plates, ECT 2006.

Ivanyi, M. Jr., Bancila, R., Ivanyi, M., (2006/c) Experimental tests of a new type of orthotropic steel plate for composite bridges, 21st Czech and Slovak International Conference Steel Structures and Bridges 2006, Bratislava, p. 8.

Ivanyi, M. Jr., Bancila, R. And Ivanyi, M., (2007) Analysis of Ultimate Limit State of Orthotropic Steel Plates for Composite Bridges According to Eurocodes, in 6th International Conference on Bridges across the Danube 2007, „Bridges in Danube Basin“ Budapest, szept 12-14. 2007. Proceedings (Ed. M. Ivanyi, R. Bancila), Műegyetem Kiadó, Budapest, pp. 81-104.

Ivanyi, M. Jr., Ivanyi, P., (2007) Numerical Analysis of the structural details on Orthotropic Steel Plates, in 6th International Conference on Bridges across the Danube 2007, „Bridges in Danube Basin“ Budapest, szept 12-14. 2007. Proceedings (Ed. M. Ivanyi, R. Bancila), Műegyetem Kiadó, Budapest, pp. 257-272.

Ivanyi P., Zygomalas M. and Baniotopoulos C.C. (2006) On the pull-out phenomenon of bolts from steel bolted plate connections : A laboratory testing and numerical approach, Gizejowski M. A., Kozlowski A., Slecicka L. and Ziolkowski J. (Editors) Progress in Steel, Composite and Aluminium Structures, Proc. XI International Conference on Metal Structures, Taylor & Francis/Balkema, The Netherlands, pp. 221-228.

Johansson, B., Maquoi, R., Sedlacek, G., Müller, C. and Schneider, R. (1999) Die Behandlung des Beulens bei dünnwandigen, Stahlkonstruktionen in ENV 1993-Teil 1,5. (Eurocode 3-1-5), Stahlbau 68, Heft 11.

Johansson, B., Maquoi, R., and Sedlacek, G. (2001) New design rules for plated structures in Eurocode 3, Journal of Constructional Steel Research, Vol.57, No.3, pp. 279-311.

Johnson, R.P. (1975) Composite Structures of Steel and Concrete - Vol. 1., Crosby Lockwood.

Johnson, R.P. and Buckby, R. J. (1979) Composite Structures of Steel and Concrete - Vol. 2., Granada, St. Albans.

Kloppel, K. and Moller, K. H. (1968) Beulwerte Ausgesteifter Rechteckplatten, Bd. 2, Berlin, W. Ernst u. Sohn.

Kloppel, K. and Scheer, J. (1960) Beulwerte Ausgesteifter Rechteckplatten, Bd. 1, Berlin, W. Ernst u. Sohn.

Kovacs, Zs. (2002) Statical calculation of the superstructure, (in Hungarian) UVATERV Co. Budapest.

Kunert, K. (1967) Einige Überlagerungen zu Projektierung von Stahlbrücken am Beispiel der Mainbrücke Hovchbeim, (in German) Bauingenieur, 42, pp. 213-226.

Kunert, K. and Wagner, P. (1968) Quarrippen orthotrop Platten mit an deru Duchdringungspunkten der Langrippen geschlitzten Stegen., (in German) Bauingenieur, 43, pp. 244-253.

Leskela, M., (1986) Calculation models for concrete-steel composite beams, considering partial interaction, Department of Civil Engineering, University of Oulo, Acta. Univ. Oulu, C. 36.7986, Artes Constr. 8. Oulu, Finland, p. 158.

LS-DYNA (2001) User Manual, Livermore Software Technology Corporation.

LUSAS (2000) Lusas User Manual, Kingston upen Thames, UK.

Maquoi, R., Massonnet, C., (1971) Thésie non-linearia de la resistance postcritique des grandes pouters en caissons raidies. IABSE Publications, Zürich, Vol. 31-II, pp. 91-140.

Naruse, T. (1975) Structural properties of Golden Horn Bridge, (in Japanese) Proc. Japan Soc. Civil Engineering., 241, pp. 25-38.

Néző, J., Dunai, L., Okura, I. and Iványi, M. (1999). Interaction of Local and Global Phenomena in the Ultimate Behaviour of Plate Girders. 2nd European Conference on Steel Structures, Proceedings, Praha, Vol. 1, pp. 39-43.

Okura, K. and Arima, T. (1922) Strength and Frequency of Natural Vibration of Rectangular Thin Plates with Longitudinal and Lateral Stiffeners (Part I, II) J. Soc. Naval Arch. Japan, Vol. 58, p. 59 and Vol. 59, p. 163.

Okura, I., Kazashi, A., Késmárky, Z. and Nagy, A. (1997). Effects of Stiffener-End-Gaps on Ultimate Strength of Girders under Bending. Technology Reports of Osaka University, 47:2294, pp. 225-235.

Okura, I., Kawarabayashi M. and Kazashi A. (1999). Reduction of Ultimate Strength of Girders Due to Stiffener-End-Gaps. The 6th International Colloquium on Stability and Ductility of Steel Structures, Proceedings, Timisoara, pp. 159-166

Okura, I., Nezo, J., Dunai, L., Ivanyi, M., (2000) Finite element analysis of local strains in plate girders, Ivanyi M, Muzeau J.P., Topping B.H.V. (Editors) Computational Steel Structures Technology, Civil-Comp Press, Edinburgh, pp. 27-34.

Pelikan, W. and Esslinger, M. (1957). Die Stahlfahrbahn – Berchnung und Konstruktion, MAN Forschungsheft, No. 7.

Petersen, C. (1982) Statik und Stabilität der Baukonstruktionen, (in German) Braunschweig, Vieweg.

Pin-Yu, C. and Michelson, F.S. (1969) On the Stability of Grillage Beams, Journal of Ship Research, Vol. 13-1, pp. 23-31.

- Platthy, P., (1965) Rugalmas kapcsolatu folytatolagos oszvertartok szamitasa (Calculation of continuous composite girders having elastic connectors), EKME Tud. Kozl (Scientific Publication of BUTE) XI. No. 3-4, Budapest, pp. 261-270.
- Redwood, R. G. (1969) The strength of steel beams with unreinforced web holes, Civil Engineering, Public Works Re., pp. 559-562.
- Sattler, K. (1955) Ein allgemeines Berechnungsverfahren fur Tragwerke mit elastischem Verbund (A general calculation method for load-carrying structures with elastic connectors), Koln, Stahlbau-Verlag, p. 52.
- Sedlacek, G. (1992). Orthotropic Plate Bridge Decks, In Dowling, P.J., Harding, J.E. and Bjorhovde, R., editors: Construction Steel Design. An International Guide, Elsevier Applied Science, London and New York.
- Skaloud, M. and Novotny, R. (1965). Post-critical behaviour of an initially curved uniformly compressed panel, reinforced in its middle by longitudinal stiffener (in German), Acta Tech., ČSAV, No. 2
- Stark, J.W.B., Hove, B.W.E., (1990) Composite Steel and Concrete Beams with Partial Shear Connection, Heron, Vol. 34, No. 4.
- Stussi, F., (1943) Beitrage zur Berechnung und Ausbildung zusammengesetzter Vollwandtrager, (Contributions to analysis and detailing of riveted plate girders) Schweizerische Bauzeitung, Vol. 121, No. 9, pp. 87-89, pp. 102-104.
- Szabo, B., (2006) Influence of shear connectors on the elastic behaviour of composite girders, Muegyetemi Kiado, Budapest and Helsinki University of Technology Publications in Bridge Engineering, Espoo, TKK-SRT-36.
- Szatmari, I., Farkas, Gy., (2003) Technical report about test loading of the flood bridge at Szekszárd over the Danube, (in Hungarian) Budapest University of Technology and Economics, Budapest.

Szillard, R. (1974) Theory and Analysis of Plates, Prentice-Hall, Englewood Cliffs, New Jersey.

Table, (2004) Table for design of steel structures according EC3 (in Hungary), (Ivanyi, M.) Műegyetem Kiadó, Budapest.

Timoshenko, S. and Woinowsky-Krieger, S. (1959) Theory of Plates and Shells, McGraw Hill.

Tommola, J., Jutila, A. (2001) Analysis of wood-concrete composite girder with discrete shear connectors, Proceedings of IABSE Conference LAHTI 2001 (Innovative Wooden Structures and Bridges), Finland, pp. 489-494.

Troitsky, M.S. (1987). Orthotropic Bridges. Theory and Design, The James F. Lincoln Arc Weld Found, Cleveland, Ohio.

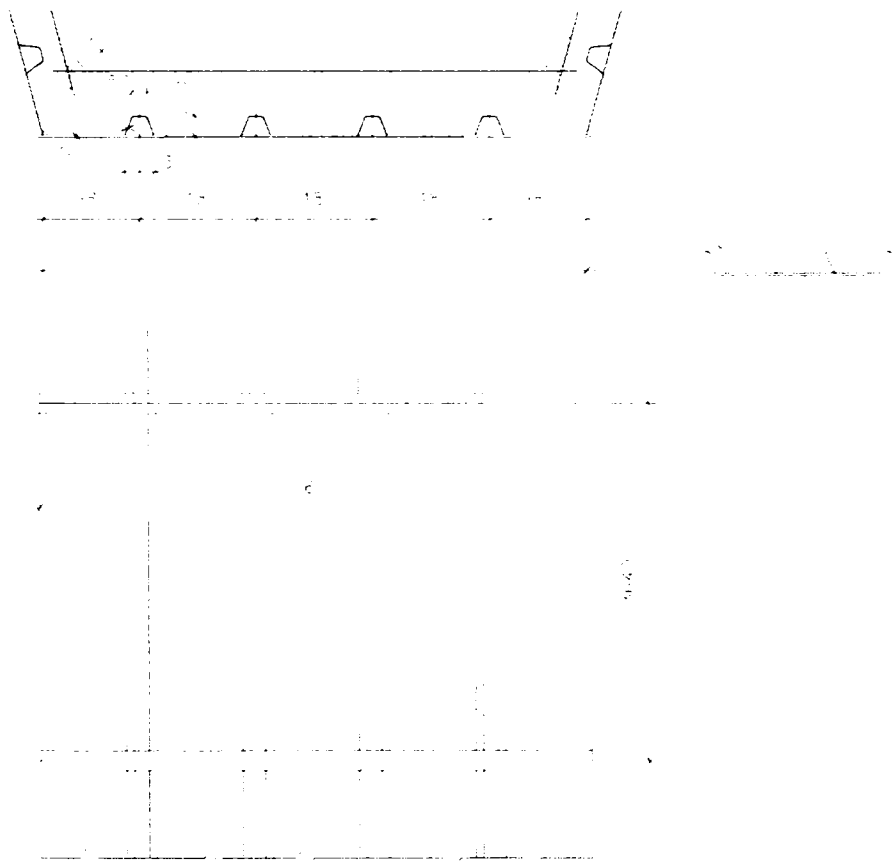
Wolchuk, R., Ostapenko, A. (1992) Secondary Stresses in Closed Orthotropic Deck Ribs at Floor Beams, Journal of Structural Engineering, ASCE, Vol. 118, No. 2, pp. 582-595.

Wolmir, A. S. (1962) Biegsame Platten und Schalen, VEB Verlag für Bauwesen, Berlin.

Yam, L.C.P. and Chapman, J.C. (1968) "The Inelastic Behaviour of Simply-supported Composite Beams of Steel and Concrete", Proc. I.C.E., 41, pp. 651-684.

APPENDIX 1

Analysis of one stiffened plate section between two cross girders according to prEN 1993-1-5 (2005)



$$N := \text{kg} \cdot \frac{\text{m}}{\text{sec}^2} \quad \text{kN} := 1000 \cdot N$$

$$v := 0.3 \quad E := 210000 \cdot \frac{\text{N}}{\text{mm}^2}$$

$$f_y := 355 \cdot \frac{\text{N}}{\text{mm}^2}$$

$$\varepsilon := \sqrt{\frac{235 \cdot \frac{\text{N}}{\text{mm}^2}}{f_y}} \quad \varepsilon = 0.814$$

Bottom of the trapezoidal stiffener: $b_{tr} := 306 \cdot \text{mm}$

Hight of the trapezoidal stiffener $h_{tr} := 200 \cdot \text{mm}$

Cross section area of the trapezoidal stiffener $A_{sl1} := 5534 \cdot \text{mm}^2$

Inertia of the trapezoidal stiffener $I_{sl1} := 1.0415 \cdot 10^8 \cdot \text{mm}^4$ to the edge of the plate

$$y_{sl1} := 121 \cdot \text{mm} \quad e := y_{sl1}$$

$$i_{sl1} := \sqrt{\frac{I_{sl1}}{A_{sl1}}} \quad i_{sl1} = 137.186 \text{ mm}$$

No. of the trapezoidal stiffener $n := 4$

Distance between the cross girders $a := 3640 \cdot \text{mm}$

Width of the plate $b := 5500 \cdot \text{mm}$

Thickness of the plate $t := 20 \cdot \text{mm}$

Cross sectional area of the plate $A_p := b \cdot t \quad A_p = 110000 \text{ mm}^2$

Inertia of the plate $I_p := \frac{(b \cdot t^3)}{12 \cdot (1 - v^2)} \quad I_p = 4.029 \times 10^6 \text{ mm}^4$

Bottom flange and trapezoidal stiffeners $A := b \cdot t + 4 \cdot A_{sl1} \quad A = 1.321 \times 10^5 \text{ mm}^2$

$$I_{sl} := 4.123 \cdot 10^8 \cdot \text{mm}^4$$

Distance between the center of gravity and the edge of the bottom flange $y_t := 32 \cdot \text{mm}$

PLATE BUCKLING ATTITUDE

$$\sigma_E := \frac{\pi^2 \cdot E \cdot t^2}{12 \cdot (1 - \nu^2) \cdot b^2} \quad \sigma_E = 2.51 \frac{\text{N}}{\text{mm}^2}$$

$$\psi := 1 \quad \gamma_n := \frac{I_{sl}}{I_p} \quad \gamma_n = 102.325 \quad \begin{array}{l} I_{sl} - \text{plate+stiffeners} \\ I_p - \text{only plate} \end{array}$$

$$\gamma_L := \frac{\gamma_n}{n} \quad \gamma_L = 25.581$$

$$\gamma := (n + 1) \cdot \gamma_L \quad \gamma = 127.907$$

$$\delta_n := \frac{(n \cdot A_{sl1})}{A_p} \quad \delta_n = 0.201 \quad \begin{array}{l} A_{sl1} - \text{area of the all stiffeners} \\ A_p - \text{area of the plate} \end{array}$$

$$\delta_L := \frac{\delta_n}{n} \quad \delta_L = 0.05$$

$$\delta := (n + 1) \cdot \delta_L \quad \delta = 0.252$$

$$\alpha := \frac{a}{b} \quad \alpha = 0.662 \quad g := \sqrt[4]{\gamma} \quad g = 3.363$$

$$k_{\sigma p} := \begin{cases} \frac{(1 + \alpha^2)^2 + \gamma}{\left(\frac{\alpha^2}{2}\right) \cdot (1 + \psi) \cdot (1 + \delta)} & \text{if } \alpha \leq \sqrt[4]{\gamma} \\ 4 \cdot \frac{1 + \sqrt{\gamma}}{(\psi + 1) \cdot (1 + \delta)} & \text{if } \alpha > \sqrt[4]{\gamma} \end{cases} \quad k_{\sigma p} = 237.102$$

$$\sigma_{crp} := k_{\sigma p} \cdot \sigma_E \quad \sigma_{crp} = 595.066 \frac{\text{N}}{\text{mm}^2}$$

COLUMN BUCKLING ATTITUDE

Closest stiffener to the edge of the plate where the compression stresses highest
 calculation of the effective plate: (Fig.:4.1) in the EC3

$$b_1 := 827 \cdot \text{mm}$$

$$b_2 := 874 \cdot \text{mm}$$

$$b_{1\text{inf}} := \left(\frac{3 - \psi}{5 - \psi} \right) \cdot b_1 \quad b_{1\text{inf}} = 413.5 \text{ mm}$$

$$b_{2\text{sup}} := \left(\frac{2}{5 - \psi} \right) \cdot b_2 \quad b_{2\text{sup}} = 437 \text{ mm}$$

width of the effective plate adjacent to the stiffener

$$b_{\text{tot}} := b_{1\text{inf}} + b_{\text{tr}} + b_{2\text{sup}} \quad b_{\text{tot}} = 1156.5 \text{ mm}$$

area of the stiffener and the adjacent effective plate

$$A_{\text{sl1_tot}} := A_{\text{sl1}} + b_{\text{tot}} \cdot t \quad A_{\text{sl1_tot}} = 28664 \text{ mm}^2$$

$$\sigma_{\text{crc}} := \frac{\pi^2 \cdot E \cdot I_{\text{sl1}}}{A_{\text{sl1_tot}} \cdot a^2} \quad \sigma_{\text{crc}} = 568.38 \frac{\text{N}}{\text{mm}^2}$$

Determination of β_{AC} , β_{AP} for λ slenderness

a) flange of the trapezoidal stiffener

$$b_{\text{tr_flange}} := 150 \cdot \text{mm} \quad t_{\text{tr_flange}} := 10 \cdot \text{mm}$$

$$\sigma_{\text{E_tr_flange}} := \frac{\pi^2 \cdot E \cdot t_{\text{tr_flange}}^2}{12 \cdot (1 - \nu^2) \cdot b_{\text{tr_flange}}^2} \quad \sigma_{\text{E_tr_flange}} = 843.556 \frac{\text{N}}{\text{mm}^2}$$

$$k_{\sigma_{\text{p_tr_flange}}} := 4 \quad (\text{Table 4.1) in the EC3}$$

$$\sigma_{\text{crp_tr_flange}} := k_{\sigma_{\text{p_tr_flange}}} \cdot \sigma_{\text{E_tr_flange}}$$

$$\sigma_{\text{crp_tr_flange}} = 3374.224 \frac{\text{N}}{\text{mm}^2}$$

$$\lambda_{\text{p_tr_flange}} := \sqrt{\frac{f_y}{\sigma_{\text{crp_tr_flange}}}}$$

$$\lambda_{\text{p_tr_flange}} = 0.324$$

$$\rho_{\text{p_tr_flange}} := 1$$

b) web of the trapezoidal stiffener

$$b_{tr_web} := 214.67 \cdot \text{mm} \quad t_{tr_web} := 10 \cdot \text{mm}$$

$$\sigma_{E_tr_web} := \frac{\pi^2 \cdot E \cdot t_{tr_web}^2}{12 \cdot (1 - \nu^2) \cdot b_{tr_web}^2} \quad \sigma_{E_tr_web} = 411.864 \frac{\text{N}}{\text{mm}^2}$$

$$k_{\sigma p_tr_web} := 4 \quad (\text{Table 4.1) in the EC3}$$

$$\sigma_{crp_tr_web} := k_{\sigma p_tr_web} \cdot \sigma_{E_tr_web} \quad \sigma_{crp_tr_web} = 1647.455 \frac{\text{N}}{\text{mm}^2}$$

$$\lambda_{p_tr_web} := \sqrt{\frac{f_y}{\sigma_{crp_tr_web}}} \quad \lambda_{p_tr_web} = 0.464$$

$$\rho_{p_tr_web} := 1$$

c) b_1 plate

$$b_1 = 827 \text{ mm} \quad t = 20 \text{ mm}$$

$$\sigma_{E_1} := \frac{\pi^2 \cdot E \cdot t^2}{12 \cdot (1 - \nu^2) \cdot b_1^2} \quad \sigma_{E_1} = 111.006 \frac{\text{N}}{\text{mm}^2}$$

$$k_{\sigma p_1} := 4 \quad (\text{Table 4.1) in the EC3}$$

$$\sigma_{crp_1} := k_{\sigma p_1} \cdot \sigma_{E_1} \quad \sigma_{crp_1} = 444.023 \frac{\text{N}}{\text{mm}^2}$$

$$\lambda_{p_1} := \sqrt{\frac{f_y}{\sigma_{crp_1}}} \quad \lambda_{p_1} = 0.894$$

$$\rho_1 := \frac{\lambda_{p_1} - 0.055 \cdot (3 + \psi)}{\lambda_{p_1}^2} \quad \rho_1 = 0.843$$

d) b_2 plate

$$b_2 = 874 \text{ mm} \quad t = 20 \text{ mm}$$

$$\sigma_{E_2} := \frac{\pi^2 \cdot E \cdot t^2}{12 \cdot (1 - \nu^2) \cdot b_2^2} \quad \sigma_{E_2} = 99.388 \frac{\text{N}}{\text{mm}^2}$$

$$k_{\text{op}_2} := 4 \quad (\text{Table 4.1) in the EC3})$$

$$\sigma_{\text{crp}_2} := k_{\text{op}_2} \cdot \sigma_{E_2} \quad \sigma_{\text{crp}_2} = 397.552 \frac{\text{N}}{\text{mm}^2}$$

$$\lambda_{p_2} := \sqrt{\frac{f_y}{\sigma_{\text{crp}_2}}} \quad \lambda_{p_2} = 0.945$$

$$\rho_2 := \frac{\lambda_{p_2} - 0.055 \cdot (3 + \psi)}{\lambda_{p_2}^2} \quad \rho_2 = 0.812$$

$$A_{s1_eff_tot} := A_{s1} + t \cdot \left(\rho_1 \cdot \frac{b_1}{2} + b_{tr} + \rho_2 \cdot \frac{b_2}{2} \right) \quad A_{s1_eff_tot} = 25723.045 \text{ mm}^2$$

$$\beta_{AC} := \frac{A_{s1_eff_tot}}{A_{s1_tot}} \quad \beta_{AC} = 0.897$$

$$A_p = 1.1 \times 10^5 \text{ mm}^2 \quad A_{s1_eff} := 4 \cdot A_{s1} \quad A_{s1_eff} = 22136 \text{ mm}^2$$

$$A_{p_eff_loc} := A_{s1_eff} + 2 \cdot \rho_1 \cdot \frac{b_1}{2} \cdot t + 4 \cdot b_{tr} \cdot t + 3 \cdot \rho_2 \cdot \frac{b_2}{2} \cdot t \cdot 2 \quad A_{p_eff_loc} = 103136.929 \text{ mm}^2$$

$$\beta_{AP} := \frac{A_{p_eff_loc}}{A_p} \quad \beta_{AP} = 0.938$$

λ slenderness

Plate buckling attitude:

$$\lambda_p := \sqrt{\frac{\beta_{AP} \cdot f_y}{\sigma_{crp}}} \quad \lambda_p = 0.748$$

$$\rho_p := \begin{cases} 1 & \text{if } \lambda_p \leq 0.673 \\ \frac{\lambda_p - 0.055(3 + \psi)}{\lambda_p^2} & \text{if } \lambda_p > 0.673 \end{cases} \quad \rho_p = 0.944$$

Column buckling attitude:

$$\lambda_c := \sqrt{\frac{\beta_{AC} \cdot f_y}{\sigma_{crc}}} \quad \lambda_c = 0.749$$

$$\alpha_{stiff} := 0.34$$

$$\alpha_e := \alpha_{stiff} + \frac{0.09}{\left(\frac{isl1}{e}\right)} \quad \alpha_e = 0.419$$

$$\phi := 0.5 \cdot \left[1 + \alpha_e \cdot (\lambda_c - 0.2) + \lambda_c^2 \right] \quad \phi = 0.895$$

$$\chi_c := \frac{1}{\phi + \sqrt{\phi^2 - \lambda_c^2}} \quad \chi_c = 0.721$$

$$\xi := \frac{\sigma_{crp}}{\sigma_{crc}} - 1 \quad \xi = 0.047$$

$$\rho_c := (\rho_p - \chi_c) \cdot \xi \cdot (2 - \xi) + \chi_c \quad \rho_c = 0.742$$

$$A_{c_eff} := \rho_c \cdot A_{p_eff_loc} + 2 \cdot \rho_1 \cdot \frac{b_1}{2} \cdot t \quad A_{c_eff} = 90448.472 \text{ mm}^2$$

$$\gamma_M := 1$$

$$N_{Rd} := A_{c_eff} \cdot f_y \cdot \frac{1}{\gamma_M} \quad N_{Rd} = 32109.208 \text{ kN}$$

Appendix 1- 7

Taking into account the SHEAR LAG

section 3.3

$$b_0 := \frac{b}{2} \quad b_0 = 2750 \text{ mm}$$

$$L_e := 0.25 \cdot 2 \cdot 65500 \text{ mm} \quad L_e = 32750 \text{ mm} \quad \frac{L_e}{50} = 655 \text{ mm}$$

must be examine

$$\alpha_0 := \sqrt{\frac{A_{c_eff}}{b_0 \cdot t}} \quad \alpha_0 = 1.282$$

$$\kappa := \alpha_0 \cdot \frac{b_0}{L_e} \quad \kappa = 0.108$$

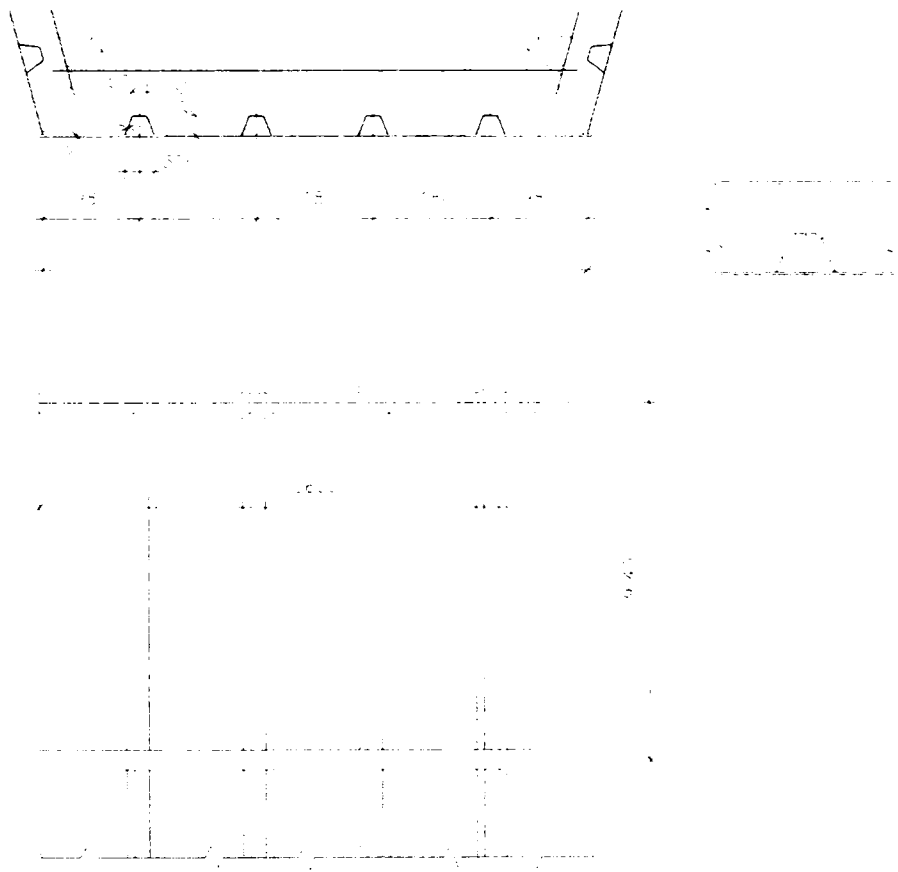
$$\beta := \begin{cases} 1.0 & \text{if } \kappa \leq 0.02 \\ \frac{1}{1 + 6 \cdot \left(\kappa - \frac{1}{2500 \cdot \kappa} \right) + 1.6 \cdot \kappa^2} & \text{if } 0.02 < \kappa \wedge \kappa \leq 0.70 \\ \frac{1}{8.6 \cdot \kappa} & \text{if } \kappa > 0.70 \end{cases} \quad \beta = 0.609$$

$$A_{eff_shearlag} := \beta \cdot A_{c_eff} \quad A_{eff_shearlag} = 55072.497 \text{ mm}^2$$

$$NRd_shearlag := A_{eff_shearlag} \cdot f_y \cdot \frac{1}{\gamma_M} \quad NRd_shearlag = 19550.737 \text{ kN}$$

APPENDIX 2

Analysis of one stiffened plate section between two cross girders according to prEN 1993-1-5 (1992)



$$N := \text{kg} \cdot \frac{\text{m}}{\text{sec}^2} \quad \text{kN} := 1000 \cdot N$$

$$v := 0.3 \quad E := 210000 \cdot \frac{N}{\text{mm}^2} \quad f_y := 355 \cdot \frac{N}{\text{mm}^2}$$

Bottom of the trapezoidal stiffener	$b_{tr} := 306 \cdot \text{mm}$
Bottom of the trapezoidal stiffener	$h_{tr} := 200 \cdot \text{mm}$
Cross section area of the trapezoidal stiffener	$A_{sl1} := 5534 \cdot \text{mm}^2$
Inertia of the trapezoidal stiffener	$I_{sl1} := 1.0415 \cdot 10^8 \cdot \text{mm}^4$ to the edge of the plate
	$y_{sl1} := 121 \cdot \text{mm} \quad e := y_{sl1}$
	$i_{sl1} := \sqrt{\frac{I_{sl1}}{A_{sl1}}} \quad i_{sl1} = 137.186 \text{ mm}$
No. of the trapezoidal stiffener	$n := 4$
Distance between the cross girders	$a := 3640 \cdot \text{mm}$
Width of the plate	$b := 5500 \cdot \text{mm}$
Thickness of the plate	$t := 20 \cdot \text{mm}$
Cross sectional area of the plate	$A_p := b \cdot t \quad A_p = 110000 \text{ mm}^2$
Inertia of the plate	$I_p := \frac{(b \cdot t^3)}{12 \cdot (1 - v^2)} \quad I_p = 4.029 \times 10^6 \text{ mm}^4$
Bottom flange and trapezoidal stiffeners	$A := b \cdot t + 4 \cdot A_{sl1} \quad A = 1.321 \times 10^5 \text{ mm}^2$ $I_{sl} := 4.123 \cdot 10^8 \cdot \text{mm}^4$
Distance between the center of gravity and the edge of the bottom flange	$y_t := 32 \cdot \text{mm}$

$$D_x := \frac{E \cdot I_{sl}}{b} \quad D_x = 15.742 \text{ m}^3 \frac{N}{\text{mm}^2}$$

$$D_y := \frac{E \cdot t^3}{12 \cdot (1 - v^2)} \quad D_y = 0.154 \text{ m}^3 \frac{N}{\text{mm}^2}$$

$$\gamma := \sqrt{\frac{D_x}{D_y}} \quad \gamma = 10.116$$

$$\alpha := \frac{a}{b} \quad \alpha = 0.662$$

$$\sigma_E := \frac{\pi^2 \cdot E \cdot t^2}{12 \cdot (1 - v^2) \cdot b^2} \quad \sigma_E = 2.51 \frac{N}{\text{mm}^2}$$

$$\psi := 1$$

$$\alpha_1 := \frac{\alpha}{\sqrt{\gamma}}$$

$$\alpha_1 = 0.208$$

$$k_{\sigma p} := \left(\alpha + \frac{\gamma}{\alpha} \right)^2$$

$$k_{\sigma p} = 254.287$$

$$\sigma_{\text{crp}} := k_{\sigma p} \cdot \sigma E$$

$$\sigma_{\text{crp}} = 638.198 \frac{\text{N}}{\text{mm}^2}$$

$$\sigma_{\text{crc}} := \frac{\pi^2 \cdot D_x}{a^2 \cdot t}$$

$$\sigma_{\text{crc}} = 586.323 \frac{\text{N}}{\text{mm}^2}$$

$$\lambda_p := \sqrt{\frac{f_y}{\sigma_{\text{crp}}}}$$

$$\lambda_p = 0.746$$

$$\rho_p := \frac{(\lambda_p - 0.22)}{\lambda_p^2}$$

$$\rho_p = 0.945$$

$$\lambda_c := \sqrt{\frac{f_y}{\sigma_{\text{crc}}}}$$

$$\lambda_c = 0.778$$

$$i := \sqrt{\frac{b \cdot D_x}{A \cdot E}}$$

$$i = 55.859 \text{ mm}$$

$$\alpha_- := 0.34 + \frac{0.09}{\frac{i}{e}}$$

$$\alpha_- = 0.535$$

$$\phi_c := 0.5 \cdot [1 + \alpha_- \cdot (\lambda_c - 0.2) + \lambda_c^2]$$

$$\phi_c = 0.957$$

$$\rho_c := \frac{1}{\phi_c + \sqrt{\phi_c^2 - \lambda_c^2}}$$

$$\rho_c = 0.66$$

$$\xi := \frac{\sigma_{\text{crp}}}{\sigma_{\text{crc}}} - 1$$

$$\xi = 0.088$$

$$\rho := (\rho_p - \rho_c) \cdot \xi \cdot (2 - \xi) + \rho_c$$

$$\rho = 0.708$$

Appendix 2- 3

a) flange of the trapezoidal stiffener

$$b_{tr_flange} := 150 \cdot \text{mm} \quad t_{tr_flange} := 10 \cdot \text{mm}$$

$$\sigma_{E_tr_flange} := \frac{\pi^2 \cdot E \cdot t_{tr_flange}^2}{12 \cdot (1 - \nu^2) \cdot b_{tr_flange}^2} \quad \sigma_{E_tr_flange} = 843.556 \frac{\text{N}}{\text{mm}^2}$$

$$k_{\sigma_{crp_tr_flange}} := 4$$

$$\sigma_{crp_tr_flange} := k_{\sigma_{crp_tr_flange}} \cdot \sigma_{E_tr_flange}$$

$$\sigma_{crp_tr_flange} = 3374.224 \frac{\text{N}}{\text{mm}^2}$$

$$\lambda_{p_tr_flange} := \sqrt{\frac{f_y}{\sigma_{crp_tr_flange}}} \quad \lambda_{p_tr_flange} = 0.324$$

$$\rho_{p_tr_flange} := \frac{\lambda_{p_tr_flange} - 0.22}{\lambda_{p_tr_flange}^2} \quad \rho_{p_tr_flange} = 0.992$$

b) web of the trapezoidal stiffener

$$b_{tr_web} := 214.67 \cdot \text{mm} \quad t_{tr_web} := 10 \cdot \text{mm}$$

$$\sigma_{E_tr_web} := \frac{\pi^2 \cdot E \cdot t_{tr_web}^2}{12 \cdot (1 - \nu^2) \cdot b_{tr_web}^2} \quad \sigma_{E_tr_web} = 411.864 \frac{\text{N}}{\text{mm}^2}$$

$$k_{\sigma_{crp_tr_web}} := 4$$

$$\sigma_{crp_tr_web} := k_{\sigma_{crp_tr_web}} \cdot \sigma_{E_tr_web}$$

$$\sigma_{crp_tr_web} = 1647.455 \frac{\text{N}}{\text{mm}^2}$$

$$\lambda_{p_tr_web} := \sqrt{\frac{f_y}{\sigma_{crp_tr_web}}} \quad \lambda_{p_tr_web} = 0.464$$

$$\rho_{p_tr_web} := \frac{\lambda_{p_tr_web} - 0.22}{\lambda_{p_tr_web}^2} \quad \rho_{p_tr_web} = 1.133$$

$$\rho_{p_tr_web} := 1$$

c) b₁ plate

$$b_1 := 827\text{mm} \quad t = 20\text{mm}$$

$$\sigma_{E_1} := \frac{\pi^2 \cdot E \cdot t^2}{12 \cdot (1 - \nu^2) \cdot b_1^2} \quad \sigma_{E_1} = 111.006 \frac{\text{N}}{\text{mm}^2}$$

$$k_{\sigma p_1} := 4 \quad (\text{Table 4.1) in the EC3}$$

$$\sigma_{crp_1} := k_{\sigma p_1} \cdot \sigma_{E_1} \quad \sigma_{crp_1} = 444.023 \frac{\text{N}}{\text{mm}^2}$$

$$\lambda_{p_1} := \sqrt{\frac{f_y}{\sigma_{crp_1}}} \quad \lambda_{p_1} = 0.894$$

$$\rho_1 := \frac{\lambda_{p_1} - 0.22}{\lambda_{p_1}^2} \quad \rho_1 = 0.843$$

d) b₂ plate

$$b_2 := 874\text{mm} \quad t = 20\text{mm}$$

$$\sigma_{E_2} := \frac{\pi^2 \cdot E \cdot t^2}{12 \cdot (1 - \nu^2) \cdot b_2^2} \quad \sigma_{E_2} = 99.388 \frac{\text{N}}{\text{mm}^2}$$

$$k_{\sigma p_2} := 4 \quad (\text{Table 4.1) in the EC3}$$

$$\sigma_{crp_2} := k_{\sigma p_2} \cdot \sigma_{E_2} \quad \sigma_{crp_2} = 397.552 \frac{\text{N}}{\text{mm}^2}$$

$$\lambda_{p_2} := \sqrt{\frac{f_y}{\sigma_{crp_2}}} \quad \lambda_{p_2} = 0.945$$

$$\rho_2 := \frac{\lambda_{p_2} - 0.22}{\lambda_{p_2}^2} \quad \rho_2 = 0.812$$

e) b_3 plate

$$b_3 := 306\text{mm} \quad t = 20\text{mm}$$

$$\sigma_{E_3} := \frac{\pi^2 \cdot E \cdot t^2}{12 \cdot (1 - \nu^2) \cdot b_3^2}$$

$$\sigma_{E_3} = 810.8 \frac{\text{N}}{\text{mm}^2}$$

$$k_{\sigma p_3} := 4 \quad (\text{Table 4.1) in the EC3}$$

$$\sigma_{crp_3} := k_{\sigma p_3} \cdot \sigma_{E_3}$$

$$\sigma_{crp_3} = 3243.199 \frac{\text{N}}{\text{mm}^2}$$

$$\lambda_{p_3} := \sqrt{\frac{f_y}{\sigma_{crp_3}}}$$

$$\lambda_{p_3} = 0.331$$

$$\rho_3 := \frac{\lambda_{p_3} - 0.22}{\lambda_{p_3}^2}$$

$$\rho_3 = 1.013$$

$$\rho_3 := 1$$

$$A_{sl_eff} := 4 \cdot A_{sl1} \quad A_{sl_eff} = 22136 \text{mm}^2$$

$$A_c := A_{sl_eff} + (2 \cdot \rho_1 \cdot b_1 \cdot t + 4 \cdot b_{tr} \cdot t + 3 \cdot \rho_2 \cdot b_2 \cdot t)$$

$$A_c = 117083.599 \text{mm}^2$$

$$A_{c_eff} := \rho \cdot A_c$$

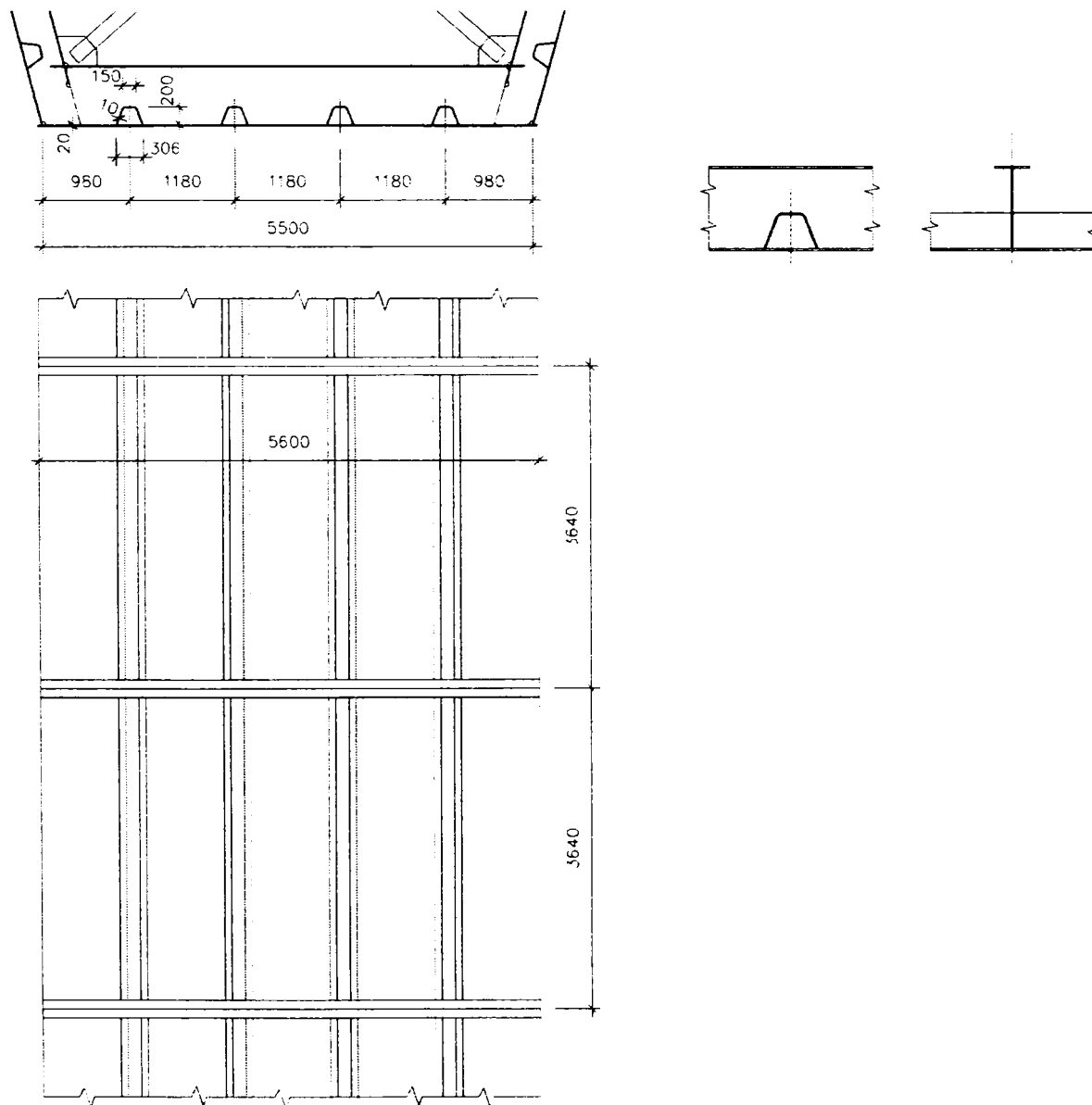
$$A_{c_eff} = 82925.873 \text{mm}^2$$

$$N_{Rd} := A_{c_eff} \cdot f_y$$

$$N_{Rd} = 29438.685 \text{kN}$$

APPENDIX 3

Analysis of two stiffened plate sections between three cross girders
according to prEN 1993-1-5 (2005) (F) full



Appendix 3-1

$$N := \text{kg} \cdot \frac{\text{m}}{\text{sec}^2}$$

$$\text{kN} := 1000 \cdot N$$

$$\nu := 0.3$$

$$E := 210000 \cdot \frac{N}{\text{mm}^2}$$

$$f_y := 355 \cdot \frac{N}{\text{mm}^2}$$

No. of the trapezoidal stiffener

$$n := 4$$

Bottom of the trapezoidal stiffener

$$b_{tr} := 306 \cdot \text{mm}$$

Distance of the trapezoidal stiffeners

$$b_i := \begin{pmatrix} 980\text{mm} \\ 1180\text{mm} \\ 1180\text{mm} \\ 1180\text{mm} \\ 980\text{mm} \end{pmatrix}$$

$$b := \sum b_i$$

$$b = 5500 \text{ mm}$$

Cross sectional area of the trapezoidal stiffener

$$A_{sl1} := 5534 \cdot \text{mm}^2$$

Inertia of the trapezoidal stiffener

$$I_{sl1} := 1.0415 \cdot 10^8 \cdot \text{mm}^4 \text{ to the edge of the plate}$$

$$y_{sl1} := 121 \cdot \text{mm}$$

$$e := y_{sl1}$$

$$i_{sl1} := \sqrt{\frac{I_{sl1}}{A_{sl1}}}$$

$$i_{sl1} = 137.186 \text{ mm}$$

No. of the cross girders

$$m := 3$$

Distance between the cross girder

$$a_j := 3640 \cdot \text{mm}$$

Cross sectional area of the cross girder

$$A_b := 18900 \text{ mm}^2$$

Inertia of the cross girder

$$I_b := 5.84 \cdot 10^8 \text{ mm}^4$$

$$a := (m - 1) \cdot a_j$$

$$a = 7.28 \text{ m}$$

Thickness of the plate

$$t := 20 \text{ mm}$$

Cross sectional area of the plate

$$A_p := b \cdot t$$

$$A_p = 110000 \text{ mm}^2$$

$$\alpha := \frac{a}{b}$$

$$\alpha = 1.324$$

$$P_e := \frac{\pi^2 E \cdot I_{sl1}}{a^2}$$

$$P_e = 4.073 \times 10^3 \text{ kN}$$

$$K := \frac{I_{sl1}}{I_b}$$

$$K = 0.178$$

Appendix 3- 2

Plate buckling attitude

$$\sigma_E := \frac{\pi^2 \cdot E \cdot t^2}{12 \cdot (1 - \nu^2) \cdot b^2} \quad \sigma_E = 2.51 \frac{\text{N}}{\text{mm}^2}$$

Inertia of the plate

$$I_p := \frac{t^3 \cdot b}{12(1 - \nu^2)} \quad I_p = 4.029 \times 10^6 \text{ mm}^4$$

$$g := \frac{I_{sl1}}{I_p} \quad g = 25.848$$

$$\sigma_{crp} := g \cdot \frac{n+1}{\alpha^2} \cdot \left(1 + \frac{1}{K} \cdot \frac{m+1}{n+1} \cdot \alpha^3 \right) \cdot \sigma_E \quad \sigma_{crp} = 2111.076 \frac{\text{N}}{\text{mm}^2}$$

Column buckling attitude

$$z := 0.020833 + 0.01022 \cdot (n - 1) \quad z = 0.051$$

$$\lambda_0 := (z) \cdot \frac{b^3}{E \cdot I_b} \cdot I_{sl1} \quad \lambda_0 = 7.276 \times 10^{-12} \text{ m}^4 \text{ sec}^2 \text{ kg}^{-1}$$

$$P_{cr_a1} := 1 + 0.0866 \cdot \frac{\alpha^2}{\sqrt{\frac{\alpha}{m-1} \cdot z \cdot K}} \quad P_{cr_a1} = 2.946$$

$$P_{cr_a2} := 0.202 \cdot \frac{\alpha^2}{\sqrt{\frac{\alpha}{m-1} \cdot z \cdot K}} \quad P_{cr_a2} = 4.54$$

$$P_{cr_ai} := \begin{cases} P_{cr_a1} & \text{if } P_{cr_a1} \leq 2 \\ P_{cr_a2} & \text{if } P_{cr_a2} > 2 \\ \text{"hiba"} & \text{otherwise} \end{cases} \quad P_{cr_ai} = 4.54$$

$$\sigma_{cr_sl} := \frac{P_e}{A_{sl1}} \quad \sigma_{cr_sl} = 735.998 \frac{\text{N}}{\text{mm}^2}$$

$$\sigma_{crc} := P_{cr_ai} \cdot \sigma_{cr_sl} \quad \sigma_{crc} = 3341.169 \frac{\text{N}}{\text{mm}^2}$$

$$\psi := 1$$

Calculation of the effective plate (Fig.:4.1)

$$b_1 := 827 \cdot \text{mm}$$

$$b_2 := 874 \cdot \text{mm}$$

$$b_{1\text{inf}} := \left(\frac{3 - \psi}{5 - \psi} \right) \cdot b_1 \quad b_{1\text{inf}} = 413.5 \text{ mm}$$

$$b_{2\text{sup}} := \left(\frac{2}{5 - \psi} \right) \cdot b_2 \quad b_{2\text{sup}} = 437 \text{ mm}$$

width of the effective plate adjacent to the stiffener

$$b_{\text{tot}} := b_{1\text{inf}} + b_{\text{tr}} + b_{2\text{sup}} \quad b_{\text{tot}} = 1156.5 \text{ mm}$$

area of the stiffener and the adjacent effective plate

$$A_{\text{sl1_tot}} := A_{\text{sl1}} + b_{\text{tot}} \cdot t \quad A_{\text{sl1_tot}} = 28664 \text{ mm}^2$$

$$\sigma_{\text{cr_sl}} := \frac{\pi^2 \cdot E \cdot I_{\text{sl1}}}{A_{\text{sl1_tot}} \cdot a^2} \quad \sigma_{\text{cr_sl}} = 142.095 \frac{\text{N}}{\text{mm}^2}$$

$$\sigma_{\text{cr_c}} := P_{\text{cr_ai}} \cdot \sigma_{\text{cr_sl}} \quad \sigma_{\text{cr_c}} = 645.061 \frac{\text{N}}{\text{mm}^2}$$

Determination of β_{AC} , β_{AP} for λ slenderness

a) flange of the trapezoidal stiffener

$$b_{\text{tr_flange}} := 150 \cdot \text{mm} \quad t_{\text{tr_flange}} := 10 \cdot \text{mm}$$

$$\sigma_{\text{E_tr_flange}} := \frac{\pi^2 \cdot E \cdot t_{\text{tr_flange}}^2}{12 \cdot (1 - \nu^2) \cdot b_{\text{tr_flange}}^2} \quad \sigma_{\text{E_tr_flange}} = 843.556 \frac{\text{N}}{\text{mm}^2}$$

$$k_{\sigma\text{p_tr_flange}} := 4 \quad (\text{Table 4.1) in the EC3}$$

$$\sigma_{\text{crp_tr_flange}} := k_{\sigma\text{p_tr_flange}} \cdot \sigma_{\text{E_tr_flange}}$$

$$\sigma_{\text{crp_tr_flange}} = 3374.224 \frac{\text{N}}{\text{mm}^2}$$

$$\lambda_{\text{p_tr_flange}} := \sqrt{\frac{f_y}{\sigma_{\text{crp_tr_flange}}}}$$

$$\lambda_{\text{p_tr_flange}} = 0.324$$

$$\rho_{\text{p_tr_flange}} := 1$$

b) web of the trapezoidal stiffener

$$b_{tr_web} := 214.67 \cdot \text{mm} \quad t_{tr_web} := 10 \cdot \text{mm}$$

$$\sigma_{E_tr_web} := \frac{\pi^2 \cdot E \cdot t_{tr_web}^2}{12 \cdot (1 - \nu^2) \cdot b_{tr_web}^2} \quad \sigma_{E_tr_web} = 411.864 \frac{\text{N}}{\text{mm}^2}$$

$$k_{\sigma p_tr_web} := 4 \quad (\text{Table 4.1) in the EC3}$$

$$\sigma_{crp_tr_web} := k_{\sigma p_tr_web} \cdot \sigma_{E_tr_web} \quad \sigma_{crp_tr_web} = 1647.455 \frac{\text{N}}{\text{mm}^2}$$

$$\lambda_{p_tr_web} := \sqrt{\frac{f_y}{\sigma_{crp_tr_web}}} \quad \lambda_{p_tr_web} = 0.464$$

$$\rho_{p_tr_web} := 1$$

c) b_1 plate

$$b_1 = 827 \text{ mm} \quad t = 20 \text{ mm}$$

$$\sigma_{E_1} := \frac{\pi^2 \cdot E \cdot t^2}{12 \cdot (1 - \nu^2) \cdot b_1^2} \quad \sigma_{E_1} = 111.006 \frac{\text{N}}{\text{mm}^2}$$

$$k_{\sigma p_1} := 4 \quad (\text{Table 4.1) in the EC3}$$

$$\sigma_{crp_1} := k_{\sigma p_1} \cdot \sigma_{E_1} \quad \sigma_{crp_1} = 444.023 \frac{\text{N}}{\text{mm}^2}$$

$$\lambda_{p_1} := \sqrt{\frac{f_y}{\sigma_{crp_1}}} \quad \lambda_{p_1} = 0.894$$

$$\rho_1 := \frac{\lambda_{p_1} - 0.055 \cdot (3 + \psi)}{\lambda_{p_1}^2} \quad \rho_1 = 0.843$$

d) b_2 plate

$$b_2 = 874 \text{ mm}$$

$$t = 20 \text{ mm}$$

$$\sigma_{E_2} := \frac{\pi^2 \cdot E \cdot t^2}{12 \cdot (1 - \nu^2) \cdot b_2^2}$$

$$\sigma_{E_2} = 99.388 \frac{\text{N}}{\text{mm}^2}$$

$$k_{\sigma p_2} := 4 \quad (\text{Table 4.1) in the EC3})$$

$$\sigma_{crp_2} := k_{\sigma p_2} \cdot \sigma_{E_2}$$

$$\sigma_{crp_2} = 397.552 \frac{\text{N}}{\text{mm}^2}$$

$$\lambda_{p_2} := \sqrt{\frac{f_y}{\sigma_{crp_2}}}$$

$$\lambda_{p_2} = 0.945$$

$$\rho_2 := \frac{\lambda_{p_2} - 0.055 \cdot (3 + \psi)}{\lambda_{p_2}^2}$$

$$\rho_2 = 0.812$$

$$A_p = 1.1 \times 10^5 \text{ mm}^2$$

$$A_{sl_eff} := 4 \cdot A_{sl1}$$

$$A_{sl_eff} = 22136 \text{ mm}^2$$

$$A_{p_eff_loc} := A_{sl_eff} + 2 \cdot \rho_1 \cdot \frac{b_1}{2} \cdot t + 4 \cdot b_{tr} \cdot t + 3 \cdot \rho_2 \cdot \frac{b_2}{2} \cdot t \cdot 2$$

$$A_{p_eff_loc} = 103136.929 \text{ mm}^2$$

$$\beta_{AP} := \frac{A_{p_eff_loc}}{A_p}$$

$$\beta_{AP} = 0.938$$

$$A_{sl1_eff_tot} := A_{sl1} + t \cdot \left(\rho_1 \cdot \frac{b_1}{2} + b_{tr} + \rho_2 \cdot \frac{b_2}{2} \right)$$

$$A_{sl1_eff_tot} = 25723.045 \text{ mm}^2$$

$$\beta_{AC} := \frac{A_{sl1_eff_tot}}{A_{sl1_tot}}$$

$$\beta_{AC} = 0.897$$

λ slenderness

Plate buckling attitude:

$$\lambda_p := \sqrt{\frac{\beta_{AP} \cdot f_y}{\sigma_{crp}}} \quad \lambda_p = 0.397$$

$$\rho_p := \begin{cases} 1 & \text{if } \lambda_p \leq 0.673 \\ \frac{\lambda_p - 0.055(3 + \psi)}{\lambda_p^2} & \text{if } \lambda_p > 0.673 \end{cases} \quad \rho_p = 1$$

Column buckling attitude:

$$\lambda_c := \sqrt{\frac{\beta_{AC} \cdot f_y}{\sigma_{crc}}} \quad \lambda_c = 0.309$$

$$\alpha_{stiff} := 0.34$$

$$\alpha_e := \alpha_{stiff} + \frac{0.09}{\left(\frac{|s|1}{e}\right)} \quad \alpha_e = 0.419$$

$$\phi := 0.5 \cdot \left[1 + \alpha_e \cdot (\lambda_c - 0.2) + \lambda_c^2 \right] \quad \phi = 0.57$$

$$\chi_c := \frac{1}{\phi + \sqrt{\phi^2 - \lambda_c^2}} \quad \chi_c = 0.952$$

$$\xi := \frac{\sigma_{crp}}{\sigma_{crc}} - 1 \quad \xi = -0.368$$

$$\rho_c := (\rho_p - \chi_c) \cdot \xi \cdot (2 - \xi) + \chi_c \quad \rho_c = 0.911$$

$$A_{c_eff} := \rho_c \cdot A_{p_eff_loc} + 2 \cdot \rho_1 \cdot \frac{b_1}{2} \cdot t \quad A_{c_eff} = 107859.033 \text{ mm}^2$$

$$\gamma_M := 1$$

$$N_{Rd} := A_{c_eff} \cdot f_y \cdot \frac{1}{\gamma_M} \quad N_{Rd} = 38289.957 \text{ kN}$$

Appendix 3- 7

Taking into account the SHEAR LAG:

section 3.3

$$b_0 := \frac{b}{2} \quad b_0 = 2750 \text{ mm}$$

$$L_e := 0.25 \cdot 2 \cdot 65500 \text{ mm} \quad L_e = 32750 \text{ mm} \quad \frac{L_e}{50} = 655 \text{ mm}$$

must be examine

$$\alpha_0 := \sqrt{\frac{A_{c_eff}}{b_0 \cdot t}} \quad \alpha_0 = 1.4$$

$$\kappa := \alpha_0 \cdot \frac{b_0}{L_e} \quad \kappa = 0.118$$

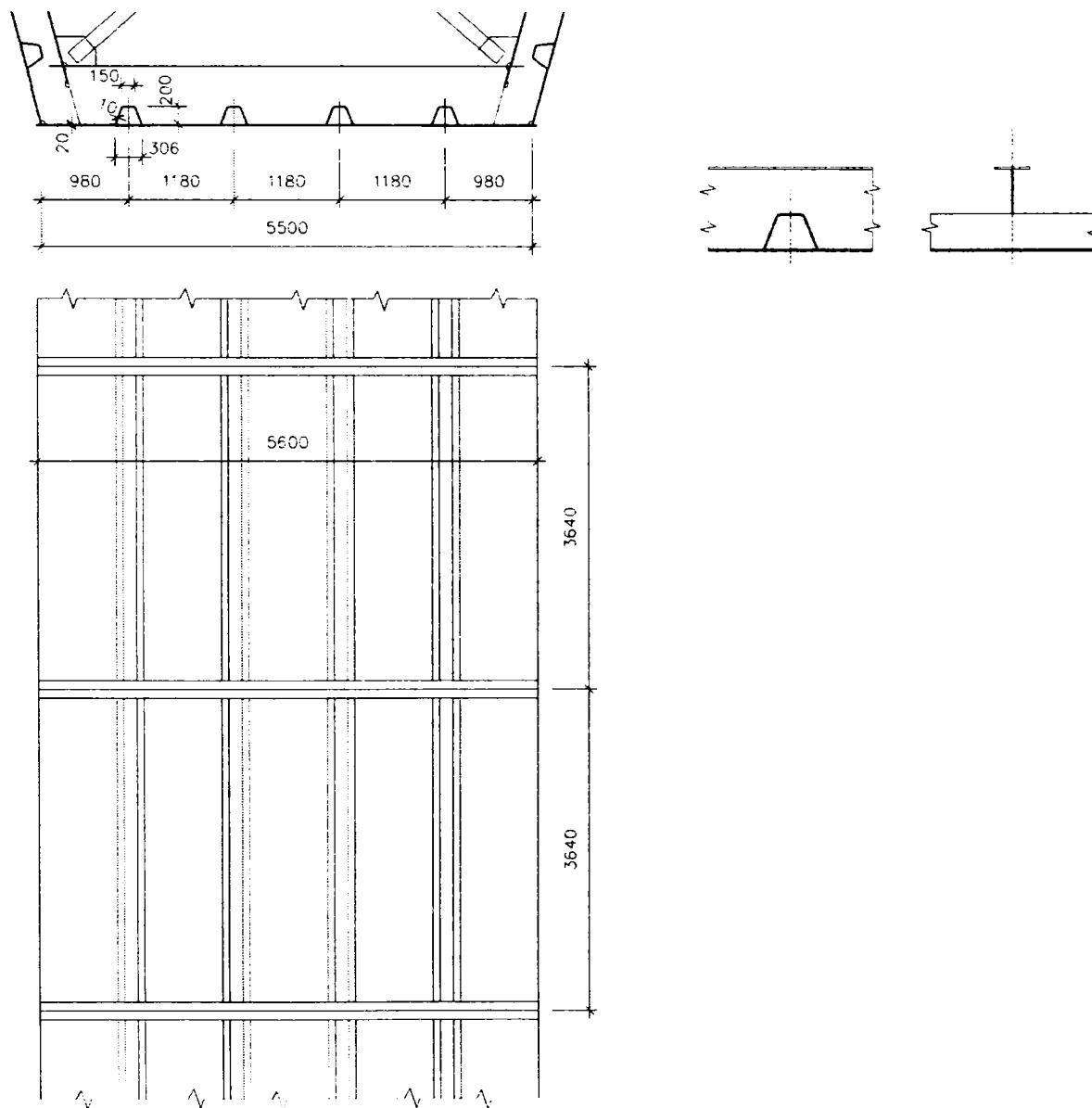
$$\beta := \begin{cases} 1.0 & \text{if } \kappa \leq 0.02 \\ \frac{1}{1 + 6 \cdot \left(\kappa - \frac{1}{2500 \cdot \kappa} \right) + 1.6 \cdot \kappa^2} & \text{if } 0.02 < \kappa \wedge \kappa \leq 0.70 \\ \frac{1}{8.6 \cdot \kappa} & \text{if } \kappa > 0.70 \end{cases}$$

$$A_{eff_shearlag} := \beta \cdot A_{c_eff} \quad A_{eff_shearlag} = 63177.049 \text{ mm}^2$$

$$N_{Rd_shearlag} := A_{eff_shearlag} \cdot f_y \cdot \frac{1}{\gamma_M} \quad N_{Rd_shearlag} = 22427.852 \text{ kN}$$

APPENDIX 4

Analysis of two stiffened plate sections between three cross girders
according to prEN 1993-1-5 (2005) (R) rigid



Appendix 4-1

$$N := \text{kg} \cdot \frac{\text{m}}{\text{sec}^2} \quad \text{kN} := 1000 \cdot N$$

$$v := 0.3 \quad E := 210000 \cdot \frac{N}{\text{mm}^2} \quad f_y := 355 \cdot \frac{N}{\text{mm}^2}$$

No. of the trapezoidal stiffener

$$n := 4$$

Bottom of the trapezoidal stiffener

$$b_{tr} := 306 \cdot \text{mm}$$

Distance of the trapezoidal stiffeners

$$b_i := \begin{pmatrix} 980\text{mm} \\ 1180\text{mm} \\ 1180\text{mm} \\ 1180\text{mm} \\ 980\text{mm} \end{pmatrix}$$

$$b := \sum b_i$$

$$b = 5500 \text{ mm}$$

Crass sectional area of the trapezoidal stiffener

$$A_{sl1} := 5534 \cdot \text{mm}^2$$

Inertia of the trapezoidal stiffener

$$I_{sl1} := 1.0415 \cdot 10^8 \cdot \text{mm}^4 \quad \text{to the edge of the plate}$$

$$y_{sl1} := 121 \cdot \text{mm}$$

$$e := y_{sl1}$$

$$i_{sl1} := \sqrt{\frac{I_{sl1}}{A_{sl1}}}$$

$$i_{sl1} = 137.186 \text{ mm}$$

No. of the cross girders

$$m := 3$$

Distance between the cross girder

$$a_j := 3640 \cdot \text{mm}$$

Cross sectional area of the cross girder

$$A_b := 18900 \text{ mm}^2$$

Inertia of the cross girder

$$I_b := 4.837 \cdot 10^8 \text{ mm}^4$$

$$a := (m - 1) \cdot a_j$$

$$a = 7.28 \text{ m}$$

Thickness of the plate

$$t := 20 \text{ mm}$$

Cross sectional area of the plate

$$A_p := b \cdot t$$

$$A_p = 110000 \text{ mm}^2$$

$$\alpha := \frac{a}{b}$$

$$\alpha = 1.324$$

$$P_e := \frac{\pi^2 E \cdot I_{sl1}}{a^2}$$

$$P_e = 4.073 \times 10^3 \text{ kN}$$

$$K := \frac{I_{sl1}}{I_b}$$

$$K = 0.215$$

Appendix 4- 2

Plate buckling attitude

$$\sigma_E := \frac{\pi^2 \cdot E \cdot t^2}{12 \cdot (1 - \nu^2) \cdot b^2} \quad \sigma_E = 2.51 \frac{\text{N}}{\text{mm}^2}$$

Inertia of the plate

$$I_p := \frac{t^3 \cdot b}{12(1 - \nu^2)} \quad I_p = 4.029 \times 10^6 \text{ mm}^4$$

$$g := \frac{I_{sl1}}{I_p} \quad g = 25.848$$

$$\sigma_{crp} := g \cdot \frac{n+1}{\alpha^2} \cdot \left(1 + \frac{1}{K} \cdot \frac{m+1}{n+1} \cdot \alpha^3 \right) \cdot \sigma_E \quad \sigma_{crp} = 1780.302 \frac{\text{N}}{\text{mm}^2}$$

Column buckling attitude

$$z := 0.020833 + 0.01022 \cdot (n - 1) \quad z = 0.051$$

$$\lambda_0 := (z) \cdot \frac{b^3}{E \cdot I_b} \cdot I_{sl1} \quad \lambda_0 = 8.784 \times 10^{-12} \text{ m}^4 \text{ sec}^2 \text{ kg}^{-1}$$

$$P_{cr_a1} := 1 + 0.0866 \cdot \frac{\alpha^2}{\sqrt{\frac{\alpha}{m-1} \cdot z \cdot K}} \quad P_{cr_a1} = 2.771$$

$$P_{cr_a2} := 0.202 \cdot \frac{\alpha^2}{\sqrt{\frac{\alpha}{m-1} \cdot z \cdot K}} \quad P_{cr_a2} = 4.131$$

$$P_{cr_ai} := \begin{cases} P_{cr_a1} & \text{if } P_{cr_a1} \leq 2 \\ P_{cr_a2} & \text{if } P_{cr_a2} > 2 \\ \text{"hiba"} & \text{otherwise} \end{cases} \quad P_{cr_ai} = 4.131$$

$$\sigma_{cr_sl} := \frac{P_e}{A_{sl1}} \quad \sigma_{cr_sl} = 735.998 \frac{\text{N}}{\text{mm}^2}$$

$$\sigma_{crc} := P_{cr_ai} \cdot \sigma_{cr_sl} \quad \sigma_{crc} = 3040.746 \frac{\text{N}}{\text{mm}^2}$$

$$\psi := 1$$

Calculation of the effective plate (Fig.:4.1)

$$b_1 := 827 \cdot \text{mm}$$

$$b_2 := 874 \cdot \text{mm}$$

$$b_{1\text{inf}} := \left(\frac{3 - \psi}{5 - \psi} \right) \cdot b_1 \quad b_{1\text{inf}} = 413.5 \text{ mm}$$

$$b_{2\text{sup}} := \left(\frac{2}{5 - \psi} \right) \cdot b_2 \quad b_{2\text{sup}} = 437 \text{ mm}$$

width of the effective plate adjacent to the stiffener

$$b_{\text{tot}} := b_{1\text{inf}} + b_{\text{tr}} + b_{2\text{sup}} \quad b_{\text{tot}} = 1156.5 \text{ mm}$$

area of the stiffener and the adjacent effective plate

$$A_{\text{sl1_tot}} := A_{\text{sl1}} + b_{\text{tot}} \cdot t \quad A_{\text{sl1_tot}} = 28664 \text{ mm}^2$$

$$\sigma_{\text{cr_sl}} := \frac{\pi^2 \cdot E \cdot I_{\text{sl1}}}{A_{\text{sl1_tot}} \cdot a^2} \quad \sigma_{\text{cr_sl}} = 142.095 \frac{\text{N}}{\text{mm}^2}$$

$$\sigma_{\text{cr_c}} := \rho_{\text{cr_ai}} \cdot \sigma_{\text{cr_sl}} \quad \sigma_{\text{cr_c}} = 587.06 \frac{\text{N}}{\text{mm}^2}$$

Determination of β_{AC} , β_{AP} for λ slenderness

a) flange of the trapezoidal stiffener

$$b_{\text{tr_flange}} := 150 \cdot \text{mm} \quad t_{\text{tr_flange}} := 10 \cdot \text{mm}$$

$$\sigma_{\text{E_tr_flange}} := \frac{\pi^2 \cdot E \cdot t_{\text{tr_flange}}^2}{12 \cdot (1 - \nu^2) \cdot b_{\text{tr_flange}}^2} \quad \sigma_{\text{E_tr_flange}} = 843.556 \frac{\text{N}}{\text{mm}^2}$$

$$k_{\sigma_{\text{p_tr_flange}}} := 4 \quad (\text{Table 4.1) in the EC3}$$

$$\sigma_{\text{crp_tr_flange}} := k_{\sigma_{\text{p_tr_flange}}} \cdot \sigma_{\text{E_tr_flange}}$$

$$\sigma_{\text{crp_tr_flange}} = 3374.224 \frac{\text{N}}{\text{mm}^2}$$

$$\lambda_{\text{p_tr_flange}} := \sqrt{\frac{f_y}{\sigma_{\text{crp_tr_flange}}}}$$

$$\lambda_{\text{p_tr_flange}} = 0.324$$

$$\rho_{\text{p_tr_flange}} := 1$$

b) web of the trapezoidal stiffener

$$b_{tr_web} := 214.67 \cdot \text{mm} \quad t_{tr_web} := 10 \cdot \text{mm}$$

$$\sigma_{E_tr_web} := \frac{\pi^2 \cdot E \cdot t_{tr_web}^2}{12 \cdot (1 - \nu^2) \cdot b_{tr_web}^2} \quad \sigma_{E_tr_web} = 411.864 \frac{\text{N}}{\text{mm}^2}$$

$$k_{\sigma p_tr_web} := 4 \quad (\text{Table 4.1) in the EC3}$$

$$\sigma_{crp_tr_web} := k_{\sigma p_tr_web} \cdot \sigma_{E_tr_web} \quad \sigma_{crp_tr_web} = 1647.455 \frac{\text{N}}{\text{mm}^2}$$

$$\lambda_{p_tr_web} := \sqrt{\frac{f_y}{\sigma_{crp_tr_web}}} \quad \lambda_{p_tr_web} = 0.464$$

$$\rho_{p_tr_web} := 1$$

c) b_1 plate

$$b_1 = 827 \text{ mm} \quad t = 20 \text{ mm}$$

$$\sigma_{E_1} := \frac{\pi^2 \cdot E \cdot t^2}{12 \cdot (1 - \nu^2) \cdot b_1^2} \quad \sigma_{E_1} = 111.006 \frac{\text{N}}{\text{mm}^2}$$

$$k_{\sigma p_1} := 4 \quad (\text{Table 4.1) in the EC3}$$

$$\sigma_{crp_1} := k_{\sigma p_1} \cdot \sigma_{E_1} \quad \sigma_{crp_1} = 444.023 \frac{\text{N}}{\text{mm}^2}$$

$$\lambda_{p_1} := \sqrt{\frac{f_y}{\sigma_{crp_1}}} \quad \lambda_{p_1} = 0.894$$

$$\rho_1 := \frac{\lambda_{p_1} - 0.055 \cdot (3 + \psi)}{\lambda_{p_1}^2} \quad \rho_1 = 0.843$$

d) b_2 plate

$$b_2 = 874 \text{ mm}$$

$$t = 20 \text{ mm}$$

$$\sigma_{E_2} := \frac{\pi^2 \cdot E \cdot t^2}{12 \cdot (1 - \nu^2) \cdot b_2^2}$$

$$\sigma_{E_2} = 99.388 \frac{\text{N}}{\text{mm}^2}$$

$$k_{\sigma p_2} := 4 \quad (\text{Table 4.1) in the EC3})$$

$$\sigma_{crp_2} := k_{\sigma p_2} \cdot \sigma_{E_2}$$

$$\sigma_{crp_2} = 397.552 \frac{\text{N}}{\text{mm}^2}$$

$$\lambda_{p_2} := \sqrt{\frac{f_y}{\sigma_{crp_2}}}$$

$$\lambda_{p_2} = 0.945$$

$$\rho_2 := \frac{\lambda_{p_2} - 0.055 \cdot (3 + \psi)}{\lambda_{p_2}^2}$$

$$\rho_2 = 0.812$$

$$A_p = 1.1 \times 10^5 \text{ mm}^2$$

$$A_{sl_eff} := 4 \cdot A_{sl1}$$

$$A_{sl_eff} = 22136 \text{ mm}^2$$

$$A_{p_eff_loc} := A_{sl_eff} + 2 \cdot \rho_1 \cdot \frac{b_1}{2} \cdot t + 4 \cdot b_{tr} \cdot t + 3 \cdot \rho_2 \cdot \frac{b_2}{2} \cdot t \cdot 2$$

$$A_{p_eff_loc} = 103136.929 \text{ mm}^2$$

$$\beta_{AP} := \frac{A_{p_eff_loc}}{A_p}$$

$$\beta_{AP} = 0.938$$

$$A_{sl1_eff_tot} := A_{sl1} + t \cdot \left(\rho_1 \cdot \frac{b_1}{2} + b_{tr} + \rho_2 \cdot \frac{b_2}{2} \right)$$

$$A_{sl1_eff_tot} = 25723.045 \text{ mm}^2$$

$$\beta_{AC} := \frac{A_{sl1_eff_tot}}{A_{sl1_tot}}$$

$$\beta_{AC} = 0.897$$

λ slenderness

Plate buckling attitude:

$$\lambda_p := \sqrt{\frac{\beta_{AP} \cdot f_y}{\sigma_{crp}}} \quad \lambda_p = 0.432$$

$$\rho_p := \begin{cases} 1 & \text{if } \lambda_p \leq 0.673 \\ \frac{\lambda_p - 0.055(3 + \psi)}{\lambda_p^2} & \text{if } \lambda_p > 0.673 \end{cases} \quad \rho_p = 1$$

Column buckling attitude:

$$\lambda_c := \sqrt{\frac{\beta_{AC} \cdot f_y}{\sigma_{crc}}} \quad \lambda_c = 0.324$$

$$\alpha_{stiff} := 0.34$$

$$\alpha_e := \alpha_{stiff} + \frac{0.09}{\left(\frac{I_{s1}}{e}\right)} \quad \alpha_e = 0.419$$

$$\phi := 0.5 \cdot \left[1 + \alpha_e \cdot (\lambda_c - 0.2) + \lambda_c^2 \right] \quad \phi = 0.578$$

$$\chi_c := \frac{1}{\phi + \sqrt{\phi^2 - \lambda_c^2}} \quad \chi_c = 0.946$$

$$\xi := \frac{\sigma_{crp}}{\sigma_{crc}} - 1 \quad \xi = -0.415$$

$$\rho_c := (\rho_p - \chi_c) \cdot \xi \cdot (2 - \xi) + \chi_c \quad \rho_c = 0.891$$

$$A_{c_eff} := \rho_c \cdot A_{p_eff_loc} + 2 \cdot \rho_1 \cdot \frac{b_1}{2} \cdot t \quad A_{c_eff} = 105849.485 \text{ mm}^2$$

$$\gamma_M := 1$$

$$N_{Rd} := A_{c_eff} \cdot f_y \cdot \frac{1}{\gamma_M} \quad N_{Rd} = 37576.567 \text{ kN}$$

Appendix 4- 7

Taking into account the SHEAR LAG:

section 3.3

$$b_0 := \frac{b}{2} \quad b_0 = 2750 \text{ mm}$$

$$L_e := 0.25 \cdot 2 \cdot 65500 \text{ mm} \quad L_e = 32750 \text{ mm} \quad \frac{L_e}{50} = 655 \text{ mm}$$

must be examine

$$\alpha_0 := \sqrt{\frac{A_{c_eff}}{b_0 \cdot t}} \quad \alpha_0 = 1.387$$

$$\kappa := \alpha_0 \cdot \frac{b_0}{L_e} \quad \kappa = 0.116$$

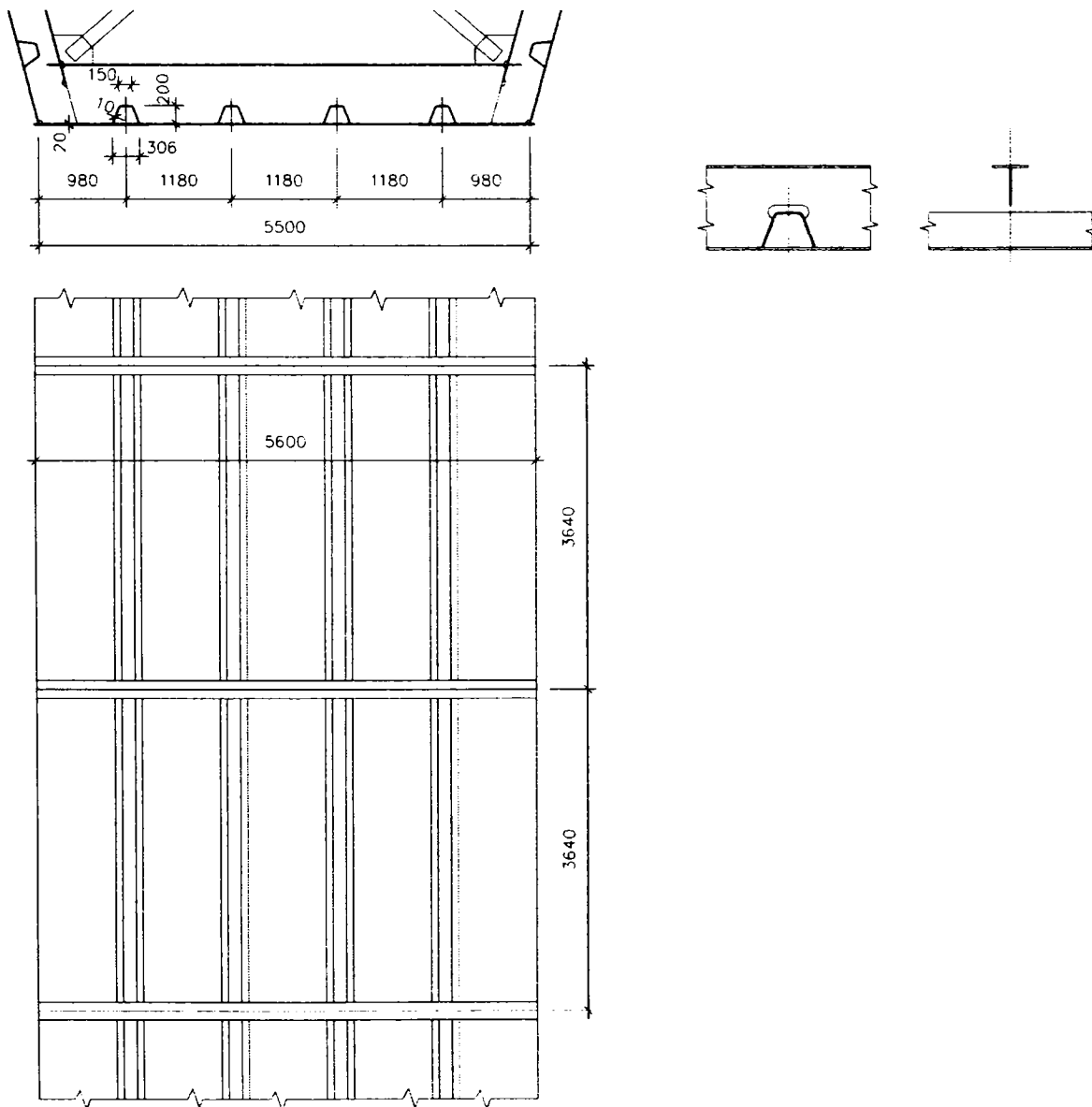
$$\beta := \begin{cases} 1.0 & \text{if } \kappa \leq 0.02 \\ \frac{1}{1 + 6 \cdot \left(\kappa - \frac{1}{2500 \cdot \kappa} \right) + 1.6 \cdot \kappa^2} & \text{if } 0.02 < \kappa \wedge \kappa \leq 0.70 \\ \frac{1}{8.6 \cdot \kappa} & \text{if } \kappa > 0.70 \end{cases}$$

$$A_{eff_shearlag} := \beta \cdot A_{c_eff} \quad A_{eff_shearlag} = 62262.871 \text{ mm}^2$$

$$N_{Rd_shearlag} := A_{eff_shearlag} \cdot f_y \cdot \frac{1}{\gamma_M} \quad N_{Rd_shearlag} = 22103.319 \text{ kN}$$

APPENDIX 5

Analysis of two stiffened plate sections between three cross girders according to prEN 1993-1-5 (2005) (S) standard



Appendix 5-1

$$N := \text{kg} \cdot \frac{\text{m}}{\text{sec}^2} \quad \text{kN} := 1000 \cdot N$$

$$v := 0.3 \quad E := 210000 \cdot \frac{N}{\text{mm}^2} \quad f_y := 355 \cdot \frac{N}{\text{mm}^2}$$

No. of the trapezoidal stiffener $n := 4$

Bottom of the trapezoidal stiffener $b_{tr} := 306 \cdot \text{mm}$

Distance of the trapezoidal stiffeners $b_i := \begin{pmatrix} 980\text{mm} \\ 1180\text{mm} \\ 1180\text{mm} \\ 1180\text{mm} \\ 980\text{mm} \end{pmatrix}$

$$b := \sum b_i \quad b = 5500 \text{ mm}$$

Cross sectional area of the trapezoidal stiffener $A_{sl1} := 5534 \cdot \text{mm}^2$

Inertia of the trapezoidal stiffener $I_{sl1} := 1.0415 \cdot 10^8 \cdot \text{mm}^4$ to the edge of the plate

$$y_{sl1} := 121 \cdot \text{mm} \quad e := y_{sl1}$$

$$i_{sl1} := \sqrt{\frac{I_{sl1}}{A_{sl1}}} \quad i_{sl1} = 137.186 \text{ mm}$$

No. of the cross girders $m := 3$

Distance between the cross girder $a_j := 3640 \cdot \text{mm}$

Cross sectional area of the cross girder $A_b := 18900 \text{ mm}^2$

Inertia of the cross girder $I_b := 3.9111 \cdot 10^8 \text{ mm}^4$

$$a := (m - 1) \cdot a_j \quad a = 7.28 \text{ m}$$

Thickness of the plate $t := 20 \text{ mm}$

Cross sectional area of the plate $A_p := b \cdot t \quad A_p = 110000 \text{ mm}^2$

$$\alpha := \frac{a}{b} \quad \alpha = 1.324$$

$$P_e := \frac{\pi^2 E \cdot I_{sl1}}{a^2} \quad P_e = 4.073 \times 10^3 \text{ kN}$$

$$K := \frac{I_{sl1}}{I_b} \quad K = 0.266$$

Appendix 5- 2

Plate buckling attitude

$$\sigma_E := \frac{\pi^2 \cdot E \cdot t^2}{12 \cdot (1 - \nu^2) \cdot b^2} \quad \sigma_E = 2.51 \frac{\text{N}}{\text{mm}^2}$$

Inertia of the plate

$$I_p := \frac{t^3 \cdot b}{12(1 - \nu^2)} \quad I_p = 4.029 \times 10^6 \text{ mm}^4$$

$$g := \frac{I_{s1}}{I_p} \quad g = 25.848$$

$$\sigma_{crp} := g \cdot \frac{n+1}{\alpha^2} \cdot \left(1 + \frac{1}{K} \cdot \frac{m+1}{n+1} \cdot \alpha^3 \right) \cdot \sigma_E \quad \sigma_{crp} = 1474.955 \frac{\text{N}}{\text{mm}^2}$$

Column buckling attitude

$$z := 0.020833 + 0.01022 \cdot (n - 1) \quad z = 0.051$$

$$\lambda_0 := (z) \cdot \frac{b^3}{E \cdot I_b} \cdot I_{s1} \quad \lambda_0 = 1.086 \times 10^{-11} \text{ m}^4 \text{ sec}^2 \text{ kg}^{-1}$$

$$P_{cr_a1} := 1 + 0.0866 \cdot \frac{\alpha^2}{\sqrt{\frac{\alpha}{m-1} \cdot z \cdot K}} \quad P_{cr_a1} = 2.593$$

$$P_{cr_a2} := 0.202 \cdot \frac{\alpha^2}{\sqrt{\frac{\alpha}{m-1} \cdot z \cdot K}} \quad P_{cr_a2} = 3.715$$

$$P_{cr_ai} := \begin{cases} P_{cr_a1} & \text{if } P_{cr_a1} \leq 2 \\ P_{cr_a2} & \text{if } P_{cr_a2} > 2 \\ \text{"hiba"} & \text{otherwise} \end{cases} \quad P_{cr_ai} = 3.715$$

$$\sigma_{cr_sl} := \frac{P_e}{A_{s11}} \quad \sigma_{cr_sl} = 735.998 \frac{\text{N}}{\text{mm}^2}$$

$$\sigma_{crc} := P_{cr_ai} \cdot \sigma_{cr_sl} \quad \sigma_{crc} = 2734.271 \frac{\text{N}}{\text{mm}^2}$$

$$\psi := 1$$

Calculation of the effective plate (Fig.:4.1)

$$b_1 := 827 \cdot \text{mm}$$

$$b_2 := 874 \cdot \text{mm}$$

$$b_{1\text{inf}} := \left(\frac{3 - \psi}{5 - \psi} \right) \cdot b_1 \quad b_{1\text{inf}} = 413.5 \text{ mm}$$

$$b_{2\text{sup}} := \left(\frac{2}{5 - \psi} \right) \cdot b_2 \quad b_{2\text{sup}} = 437 \text{ mm}$$

width of the effective plate adjacent to the stiffener

$$b_{\text{tot}} := b_{1\text{inf}} + b_{\text{tr}} + b_{2\text{sup}} \quad b_{\text{tot}} = 1156.5 \text{ mm}$$

area of the stiffener and the adjacent effective plate

$$A_{\text{sl1_tot}} := A_{\text{sl1}} + b_{\text{tot}} \cdot t \quad A_{\text{sl1_tot}} = 28664 \text{ mm}^2$$

$$\sigma_{\text{cr_sl}} := \frac{\pi^2 \cdot E \cdot I_{\text{sl1}}}{A_{\text{sl1_tot}} \cdot a^2} \quad \sigma_{\text{cr_sl}} = 142.095 \frac{\text{N}}{\text{mm}^2}$$

$$\sigma_{\text{cr_c}} := P_{\text{cr_ai}} \cdot \sigma_{\text{cr_sl}} \quad \sigma_{\text{cr_c}} = 527.891 \frac{\text{N}}{\text{mm}^2}$$

Determination of β_{AC} , β_{AP} for λ slenderness

a) flange of the trapezoidal stiffener

$$b_{\text{tr_flange}} := 150 \cdot \text{mm} \quad t_{\text{tr_flange}} := 10 \cdot \text{mm}$$

$$\sigma_{\text{E_tr_flange}} := \frac{\pi^2 \cdot E \cdot t_{\text{tr_flange}}^2}{12 \cdot (1 - \nu^2) \cdot b_{\text{tr_flange}}^2} \quad \sigma_{\text{E_tr_flange}} = 843.556 \frac{\text{N}}{\text{mm}^2}$$

$$k_{\sigma_{\text{p_tr_flange}}} := 4 \quad (\text{Table 4.1) in the EC3}$$

$$\sigma_{\text{crp_tr_flange}} := k_{\sigma_{\text{p_tr_flange}}} \cdot \sigma_{\text{E_tr_flange}}$$

$$\sigma_{\text{crp_tr_flange}} = 3374.224 \frac{\text{N}}{\text{mm}^2}$$

$$\lambda_{\text{p_tr_flange}} := \sqrt{\frac{f_y}{\sigma_{\text{crp_tr_flange}}}}$$

$$\lambda_{\text{p_tr_flange}} = 0.324$$

$$\rho_{\text{p_tr_flange}} := 1$$

b) web of the trapezoidal stiffener

$$b_{tr_web} := 214.67 \cdot \text{mm} \quad t_{tr_web} := 10 \cdot \text{mm}$$

$$\sigma_{E_tr_web} := \frac{\pi^2 \cdot E \cdot t_{tr_web}^2}{12 \cdot (1 - \nu^2) \cdot b_{tr_web}^2} \quad \sigma_{E_tr_web} = 411.864 \frac{\text{N}}{\text{mm}^2}$$

$$k_{\sigma p_tr_web} := 4 \quad (\text{Table 4.1) in the EC3}$$

$$\sigma_{crp_tr_web} := k_{\sigma p_tr_web} \cdot \sigma_{E_tr_web} \quad \sigma_{crp_tr_web} = 1647.455 \frac{\text{N}}{\text{mm}^2}$$

$$\lambda_{p_tr_web} := \sqrt{\frac{f_y}{\sigma_{crp_tr_web}}} \quad \lambda_{p_tr_web} = 0.464$$

$$\rho_{p_tr_web} := 1$$

c) b_1 plate

$$b_1 = 827 \text{ mm} \quad t = 20 \text{ mm}$$

$$\sigma_{E_1} := \frac{\pi^2 \cdot E \cdot t^2}{12 \cdot (1 - \nu^2) \cdot b_1^2} \quad \sigma_{E_1} = 111.006 \frac{\text{N}}{\text{mm}^2}$$

$$k_{\sigma p_1} := 4 \quad (\text{Table 4.1) in the EC3}$$

$$\sigma_{crp_1} := k_{\sigma p_1} \cdot \sigma_{E_1} \quad \sigma_{crp_1} = 444.023 \frac{\text{N}}{\text{mm}^2}$$

$$\lambda_{p_1} := \sqrt{\frac{f_y}{\sigma_{crp_1}}} \quad \lambda_{p_1} = 0.894$$

$$\rho_1 := \frac{\lambda_{p_1} - 0.055 \cdot (3 + \psi)}{\lambda_{p_1}^2} \quad \rho_1 = 0.843$$

d) b_2 plate

$$b_2 = 874 \text{ mm}$$

$$t = 20 \text{ mm}$$

$$\sigma_{E_2} := \frac{\pi^2 \cdot E \cdot t^2}{12 \cdot (1 - \nu^2) \cdot b_2^2}$$

$$\sigma_{E_2} = 99.388 \frac{\text{N}}{\text{mm}^2}$$

$$k_{\sigma p_2} := 4 \quad (\text{Table 4.1) in the EC3})$$

$$\sigma_{crp_2} := k_{\sigma p_2} \cdot \sigma_{E_2}$$

$$\sigma_{crp_2} = 397.552 \frac{\text{N}}{\text{mm}^2}$$

$$\lambda_{p_2} := \sqrt{\frac{f_y}{\sigma_{crp_2}}}$$

$$\lambda_{p_2} = 0.945$$

$$\rho_2 := \frac{\lambda_{p_2} - 0.055 \cdot (3 + \psi)}{\lambda_{p_2}^2}$$

$$\rho_2 = 0.812$$

$$A_p = 1.1 \times 10^5 \text{ mm}^2$$

$$A_{sl_eff} := 4 \cdot A_{sl1}$$

$$A_{sl_eff} = 22136 \text{ mm}^2$$

$$A_{p_eff_loc} := A_{sl_eff} + 2 \cdot \rho_1 \cdot \frac{b_1}{2} \cdot t + 4 \cdot b_{tr} \cdot t + 3 \cdot \rho_2 \cdot \frac{b_2}{2} \cdot t \cdot 2$$

$$A_{p_eff_loc} = 103136.929 \text{ mm}^2$$

$$\beta_{AP} := \frac{A_{p_eff_loc}}{A_p}$$

$$\beta_{AP} = 0.938$$

$$A_{sl1_eff_tot} := A_{sl1} + t \cdot \left(\rho_1 \cdot \frac{b_1}{2} + b_{tr} + \rho_2 \cdot \frac{b_2}{2} \right)$$

$$A_{sl1_eff_tot} = 25723.045 \text{ mm}^2$$

$$\beta_{AC} := \frac{A_{sl1_eff_tot}}{A_{sl1_tot}}$$

$$\beta_{AC} = 0.897$$

λ slenderness

Plate buckling attitude:

$$\lambda_p := \sqrt{\frac{\beta_{AP} \cdot f_y}{\sigma_{crp}}} \quad \lambda_p = 0.475$$

$$\rho_p := \begin{cases} 1 & \text{if } \lambda_p \leq 0.673 \\ \frac{\lambda_p - 0.055(3 + \psi)}{\lambda_p^2} & \text{if } \lambda_p > 0.673 \end{cases} \quad \rho_p = 1$$

Column buckling attitude:

$$\lambda_c := \sqrt{\frac{\beta_{AC} \cdot f_y}{\sigma_{crc}}} \quad \lambda_c = 0.341$$

$$\alpha_{stiff} := 0.34$$

$$\alpha_e := \alpha_{stiff} + \frac{0.09}{\left(\frac{|s|1}{e}\right)} \quad \alpha_e = 0.419$$

$$\phi := 0.5 \cdot \left[1 + \alpha_e \cdot (\lambda_c - 0.2) + \lambda_c^2 \right] \quad \phi = 0.588$$

$$\chi_c := \frac{1}{\phi + \sqrt{\phi^2 - \lambda_c^2}} \quad \chi_c = 0.938$$

$$\xi := \frac{\sigma_{crp}}{\sigma_{crc}} - 1 \quad \xi = -0.461$$

$$\rho_c := (\rho_p - \chi_c) \cdot \xi \cdot (2 - \xi) + \chi_c \quad \rho_c = 0.867$$

$$A_{c_eff} := \rho_c \cdot A_{p_eff_loc} + 2 \cdot \rho_1 \cdot \frac{b_1}{2} \cdot t \quad A_{c_eff} = 103356.122 \text{ mm}^2$$

$$\gamma_M := 1$$

$$N_{Rd} := A_{c_eff} \cdot f_y \cdot \frac{1}{\gamma_M} \quad N_{Rd} = 36691.423 \text{ kN}$$

Appendix 5- 7

Taking into account the SHEAR LAG:

section 3.3

$$b_0 := \frac{b}{2} \quad b_0 = 2750 \text{ mm}$$

$$L_e := 0.25 \cdot 2 \cdot 65500 \text{ mm} \quad L_e = 32750 \text{ mm} \quad \frac{L_e}{50} = 655 \text{ mm}$$

must be examine

$$\alpha_0 := \sqrt{\frac{A_{c_eff}}{b_0 \cdot t}} \quad \alpha_0 = 1.371$$

$$\kappa := \alpha_0 \cdot \frac{b_0}{L_e} \quad \kappa = 0.115$$

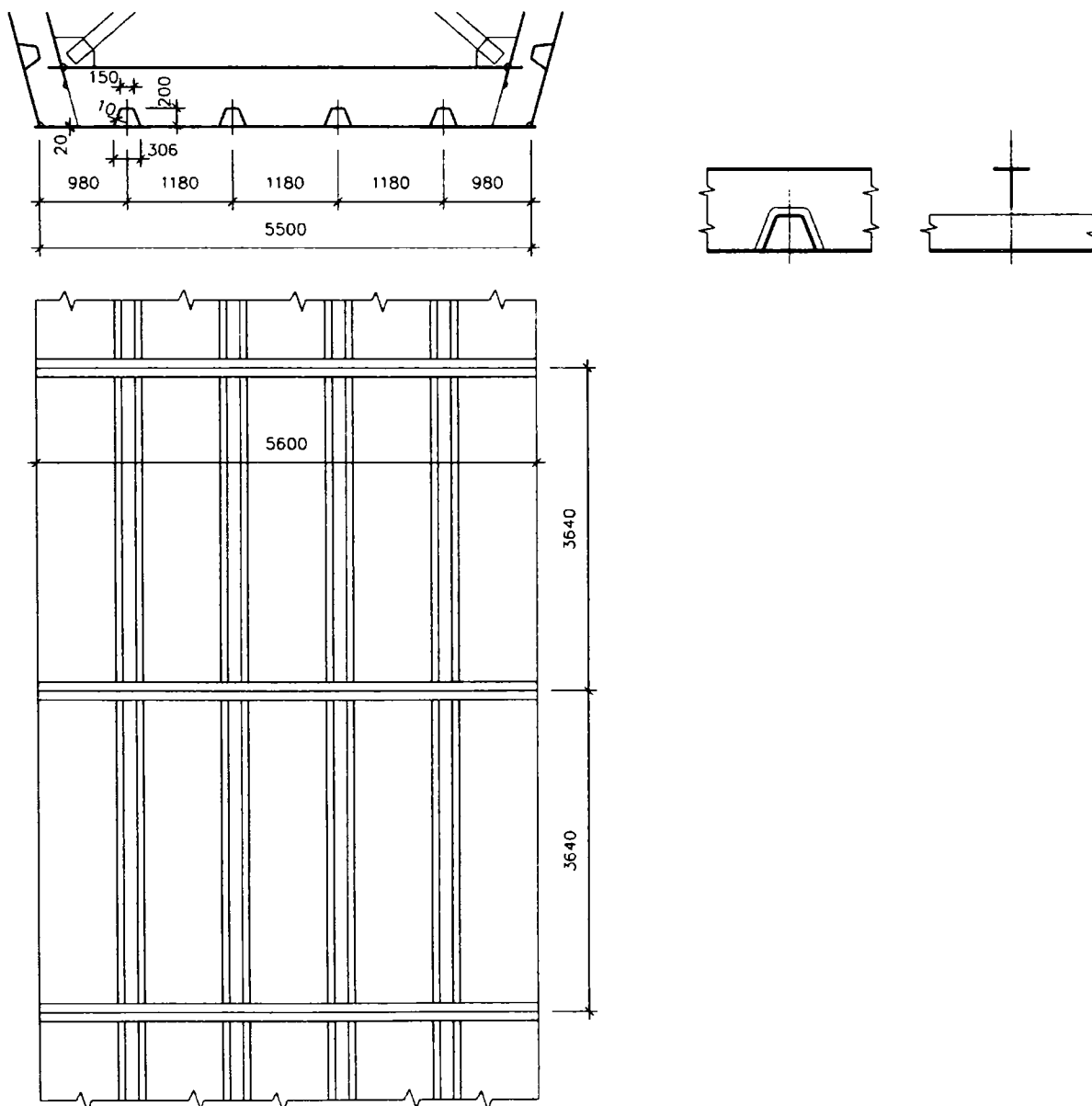
$$\beta := \begin{cases} 1.0 & \text{if } \kappa \leq 0.02 \\ \frac{1}{1 + 6 \cdot \left(\kappa - \frac{1}{2500 \cdot \kappa} \right) + 1.6 \cdot \kappa^2} & \text{if } 0.02 < \kappa \wedge \kappa \leq 0.70 \\ \frac{1}{8.6 \cdot \kappa} & \text{if } \kappa > 0.70 \end{cases}$$

$$A_{eff_shearlag} := \beta \cdot A_{c_eff} \quad A_{eff_shearlag} = 61121.217 \text{ mm}^2$$

$$NRd_shearlag := A_{eff_shearlag} \cdot f_y \cdot \frac{1}{\gamma_M} \quad NRd_shearlag = 21698.032 \text{ kN}$$

APPENDIX 6

Analysis of two stiffened plate sections between three cross girders
according to prEN 1993-1-5 (2005) (E) economic



Appendix 6-1

$$N := \text{kg} \cdot \frac{\text{m}}{\text{sec}^2} \quad \text{kN} := 1000 \cdot N$$

$$v := 0.3 \quad E := 210000 \cdot \frac{\text{N}}{\text{mm}^2} \quad f_y := 355 \cdot \frac{\text{N}}{\text{mm}^2}$$

No. of the trapezoidal stiffener $n := 4$

Bottom of the trapezoidal stiffener $b_{tr} := 306 \cdot \text{mm}$

Distance of the trapezoidal stiffeners $b_i := \begin{pmatrix} 980\text{mm} \\ 1180\text{mm} \\ 1180\text{mm} \\ 1180\text{mm} \\ 980\text{mm} \end{pmatrix}$

$$b := \sum b_i \quad b = 5500 \text{ mm}$$

Cross sectional area of the trapezoidal stiffener $A_{sl1} := 5534 \cdot \text{mm}^2$

Inertia of the trapezoidal stiffener $I_{sl1} := 1.0415 \cdot 10^8 \cdot \text{mm}^4$ to the edge of the plate

$$y_{sl1} := 121 \cdot \text{mm} \quad e := y_{sl1}$$

$$i_{sl1} := \sqrt{\frac{I_{sl1}}{A_{sl1}}} \quad i_{sl1} = 137.186 \text{ mm}$$

No. of the cross girders $m := 3$

Distance between the cross girder $a_j := 3640 \cdot \text{mm}$

Cross sectional area of the cross girder $A_b := 18900 \text{mm}^2$

Inertia of the cross girder $I_b := 3.6105 \cdot 10^8 \text{mm}^4$

$$a := (m - 1) \cdot a_j \quad a = 7.28 \text{ m}$$

Thickness of the plate $t := 20 \text{mm}$

Cross sectional area of the plate $A_p := b \cdot t \quad A_p = 110000 \text{mm}^2$

$$\alpha := \frac{a}{b} \quad \alpha = 1.324$$

$$P_e := \frac{\pi^2 E \cdot I_{sl1}}{a^2} \quad P_e = 4.073 \times 10^3 \text{ kN}$$

$$K := \frac{I_{sl1}}{I_b} \quad K = 0.288$$

Appendix 6- 2

Plate buckling attitude

$$\sigma_E := \frac{\pi^2 \cdot E \cdot t^2}{12 \cdot (1 - \nu^2) \cdot b^2} \quad \sigma_E = 2.51 \frac{\text{N}}{\text{mm}^2}$$

Inertia of the plate

$$I_p := \frac{t^3 \cdot b}{12(1 - \nu^2)} \quad I_p = 4.029 \times 10^6 \text{ mm}^4$$

$$g := \frac{I_{sl1}}{I_p} \quad g = 25.848$$

$$\sigma_{crp} := g \cdot \frac{n+1}{\alpha^2} \cdot \left(1 + \frac{1}{K} \cdot \frac{m+1}{n+1} \cdot \alpha^3 \right) \cdot \sigma_E \quad \sigma_{crp} = 1375.822 \frac{\text{N}}{\text{mm}^2}$$

Column buckling attitude

$$z := 0.020833 + 0.01022 \cdot (n - 1) \quad z = 0.051$$

$$\lambda_0 := (z) \cdot \frac{b^3}{E \cdot I_p} \cdot I_{sl1} \quad \lambda_0 = 1.177 \times 10^{-11} \text{ m}^4 \text{ sec}^2 \text{ kg}^{-1}$$

$$P_{cr_a1} := 1 + 0.0866 \cdot \frac{\alpha^2}{\sqrt{\frac{\alpha}{m-1} \cdot z \cdot K}} \quad P_{cr_a1} = 2.53$$

$$P_{cr_a2} := 0.202 \cdot \frac{\alpha^2}{\sqrt{\frac{\alpha}{m-1} \cdot z \cdot K}} \quad P_{cr_a2} = 3.569$$

$$P_{cr_ai} := \begin{cases} P_{cr_a1} & \text{if } P_{cr_a1} \leq 2 \\ P_{cr_a2} & \text{if } P_{cr_a2} > 2 \\ \text{"hiba"} & \text{otherwise} \end{cases} \quad P_{cr_ai} = 3.569$$

$$\sigma_{cr_sl} := \frac{P_e}{A_{sl1}} \quad \sigma_{cr_sl} = 735.998 \frac{\text{N}}{\text{mm}^2}$$

$$\sigma_{crc} := P_{cr_ai} \cdot \sigma_{cr_sl} \quad \sigma_{crc} = 2627.095 \frac{\text{N}}{\text{mm}^2}$$

$$\psi := 1$$

Calculation of the effective plate (Fig.:4.1)

$$b_1 := 827 \cdot \text{mm}$$

$$b_2 := 874 \cdot \text{mm}$$

$$b_{1\text{inf}} := \left(\frac{3 - \psi}{5 - \psi} \right) \cdot b_1 \quad b_{1\text{inf}} = 413.5 \text{ mm}$$

$$b_{2\text{sup}} := \left(\frac{2}{5 - \psi} \right) \cdot b_2 \quad b_{2\text{sup}} = 437 \text{ mm}$$

width of the effective plate adjacent to the stiffener

$$b_{\text{tot}} := b_{1\text{inf}} + b_{\text{tr}} + b_{2\text{sup}} \quad b_{\text{tot}} = 1156.5 \text{ mm}$$

area of the stiffener and the adjacent effective plate

$$A_{\text{sl1_tot}} := A_{\text{sl1}} + b_{\text{tot}} \cdot t \quad A_{\text{sl1_tot}} = 28664 \text{ mm}^2$$

$$\sigma_{\text{cr_sl}} := \frac{\pi^2 \cdot E \cdot I_{\text{sl1}}}{A_{\text{sl1_tot}} \cdot a^2} \quad \sigma_{\text{cr_sl}} = 142.095 \frac{\text{N}}{\text{mm}^2}$$

$$\sigma_{\text{cr_c}} := \rho_{\text{cr_ai}} \cdot \sigma_{\text{cr_sl}} \quad \sigma_{\text{cr_c}} = 507.199 \frac{\text{N}}{\text{mm}^2}$$

Determination of β_{AC} , β_{AP} for λ slenderness

a) flange of the trapezoidal stiffener

$$b_{\text{tr_flange}} := 150 \cdot \text{mm} \quad t_{\text{tr_flange}} := 10 \cdot \text{mm}$$

$$\sigma_{\text{E_tr_flange}} := \frac{\pi^2 \cdot E \cdot t_{\text{tr_flange}}^2}{12 \cdot (1 - \nu^2) \cdot b_{\text{tr_flange}}^2} \quad \sigma_{\text{E_tr_flange}} = 843.556 \frac{\text{N}}{\text{mm}^2}$$

$$k_{\sigma_{\text{p_tr_flange}}} := 4 \quad (\text{Table 4.1) in the EC3}$$

$$\sigma_{\text{crp_tr_flange}} := k_{\sigma_{\text{p_tr_flange}}} \cdot \sigma_{\text{E_tr_flange}}$$

$$\sigma_{\text{crp_tr_flange}} = 3374.224 \frac{\text{N}}{\text{mm}^2}$$

$$\lambda_{\text{p_tr_flange}} := \sqrt{\frac{f_y}{\sigma_{\text{crp_tr_flange}}}} \quad \lambda_{\text{p_tr_flange}} = 0.324$$

$$\rho_{\text{p_tr_flange}} := 1$$

b) web of the trapezoidal stiffener

$$b_{tr_web} := 214.67 \cdot \text{mm} \quad t_{tr_web} := 10 \cdot \text{mm}$$

$$\sigma_{E_tr_web} := \frac{\pi^2 \cdot E \cdot t_{tr_web}^2}{12 \cdot (1 - \nu^2) \cdot b_{tr_web}^2} \quad \sigma_{E_tr_web} = 411.864 \frac{\text{N}}{\text{mm}^2}$$

$$k_{\sigma p_tr_web} := 4 \quad (\text{Table 4.1) in the EC3}$$

$$\sigma_{crp_tr_web} := k_{\sigma p_tr_web} \cdot \sigma_{E_tr_web} \quad \sigma_{crp_tr_web} = 1647.455 \frac{\text{N}}{\text{mm}^2}$$

$$\lambda_{p_tr_web} := \sqrt{\frac{f_y}{\sigma_{crp_tr_web}}} \quad \lambda_{p_tr_web} = 0.464$$

$$\rho_{p_tr_web} := 1$$

c) b_1 plate

$$b_1 = 827 \text{ mm} \quad t = 20 \text{ mm}$$

$$\sigma_{E_1} := \frac{\pi^2 \cdot E \cdot t^2}{12 \cdot (1 - \nu^2) \cdot b_1^2} \quad \sigma_{E_1} = 111.006 \frac{\text{N}}{\text{mm}^2}$$

$$k_{\sigma p_1} := 4 \quad (\text{Table 4.1) in the EC3}$$

$$\sigma_{crp_1} := k_{\sigma p_1} \cdot \sigma_{E_1} \quad \sigma_{crp_1} = 444.023 \frac{\text{N}}{\text{mm}^2}$$

$$\lambda_{p_1} := \sqrt{\frac{f_y}{\sigma_{crp_1}}} \quad \lambda_{p_1} = 0.894$$

$$\rho_1 := \frac{\lambda_{p_1} - 0.055 \cdot (3 + \psi)}{\lambda_{p_1}^2} \quad \rho_1 = 0.843$$

d) b_2 plate

$$b_2 = 874 \text{ mm}$$

$$t = 20 \text{ mm}$$

$$\sigma_{E_2} := \frac{\pi^2 \cdot E \cdot t^2}{12 \cdot (1 - \nu^2) \cdot b_2^2}$$

$$\sigma_{E_2} = 99.388 \frac{\text{N}}{\text{mm}^2}$$

$$k_{\text{op_2}} := 4 \quad (\text{Table 4.1) in the EC3}$$

$$\sigma_{\text{crp_2}} := k_{\text{op_2}} \cdot \sigma_{E_2}$$

$$\sigma_{\text{crp_2}} = 397.552 \frac{\text{N}}{\text{mm}^2}$$

$$\lambda_{p_2} := \sqrt{\frac{f_y}{\sigma_{\text{crp_2}}}}$$

$$\lambda_{p_2} = 0.945$$

$$\rho_2 := \frac{\lambda_{p_2} - 0.055 \cdot (3 + \psi)}{\lambda_{p_2}^2}$$

$$\rho_2 = 0.812$$

$$A_p = 1.1 \times 10^5 \text{ mm}^2$$

$$A_{s1_eff} := 4 \cdot A_{s1}$$

$$A_{s1_eff} = 22136 \text{ mm}^2$$

$$A_{p_eff_loc} := A_{s1_eff} + 2 \cdot \rho_1 \cdot \frac{b_1}{2} \cdot t + 4 \cdot b_{tr} \cdot t + 3 \cdot \rho_2 \cdot \frac{b_2}{2} \cdot t \cdot 2$$

$$A_{p_eff_loc} = 103136.929 \text{ mm}^2$$

$$\beta_{AP} := \frac{A_{p_eff_loc}}{A_p}$$

$$\beta_{AP} = 0.938$$

$$A_{s1_eff_tot} := A_{s1} + t \cdot \left(\rho_1 \cdot \frac{b_1}{2} + b_{tr} + \rho_2 \cdot \frac{b_2}{2} \right)$$

$$A_{s1_eff_tot} = 25723.045 \text{ mm}^2$$

$$\beta_{AC} := \frac{A_{s1_eff_tot}}{A_{s1_tot}}$$

$$\beta_{AC} = 0.897$$

λ slenderness

Plate buckling attitude:

$$\lambda_p := \sqrt{\frac{\beta_{AP} \cdot f_y}{\sigma_{crp}}} \quad \lambda_p = 0.492$$

$$\rho_p := \begin{cases} 1 & \text{if } \lambda_p \leq 0.673 \\ \frac{\lambda_p - 0.055(3 + \psi)}{\lambda_p^2} & \text{if } \lambda_p > 0.673 \end{cases} \quad \rho_p = 1$$

Column buckling attitude:

$$\lambda_c := \sqrt{\frac{\beta_{AC} \cdot f_y}{\sigma_{crc}}} \quad \lambda_c = 0.348$$

$$\alpha_{stiff} := 0.34$$

$$\alpha_e := \alpha_{stiff} + \frac{0.09}{\left(\frac{|s|1}{e}\right)} \quad \alpha_e = 0.419$$

$$\phi := 0.5 \cdot \left[1 + \alpha_e \cdot (\lambda_c - 0.2) + \lambda_c^2 \right] \quad \phi = 0.592$$

$$\chi_c := \frac{1}{\phi + \sqrt{\phi^2 - \lambda_c^2}} \quad \chi_c = 0.934$$

$$\xi := \frac{\sigma_{crp}}{\sigma_{crc}} - 1 \quad \xi = -0.476$$

$$\rho_c := (\rho_p - \chi_c) \cdot \xi \cdot (2 - \xi) + \chi_c \quad \rho_c = 0.857$$

$$A_{c_eff} := \rho_c \cdot A_{p_eff_loc} + 2 \cdot \rho_1 \cdot \frac{b_1}{2} \cdot t \quad A_{c_eff} = 102356.5 \text{ mm}^2$$

$$\gamma_M := 1$$

$$N_{Rd} := A_{c_eff} \cdot f_y \cdot \frac{1}{\gamma_M} \quad N_{Rd} = 36336.558 \text{ kN}$$

Appendix 6- 7

Taking into account the SHEAR LAG:

section 3.3

$$b_0 := \frac{b}{2} \quad b_0 = 2750 \text{ mm}$$

$$L_e := 0.25 \cdot 2 \cdot 65500 \text{ mm} \quad L_e = 32750 \text{ mm} \quad \frac{L_e}{50} = 655 \text{ mm}$$

must be examine

$$\alpha_0 := \sqrt{\frac{A_{c_eff}}{b_0 \cdot t}} \quad \alpha_0 = 1.364$$

$$\kappa := \alpha_0 \cdot \frac{b_0}{L_e} \quad \kappa = 0.115$$

$$\beta := \begin{cases} 1.0 & \text{if } \kappa \leq 0.02 \\ \frac{1}{1 + 6 \cdot \left(\kappa - \frac{1}{2500 \cdot \kappa} \right) + 1.6 \cdot \kappa^2} & \text{if } 0.02 < \kappa \wedge \kappa \leq 0.70 \\ \frac{1}{8.6 \cdot \kappa} & \text{if } \kappa > 0.70 \end{cases}$$

$$A_{eff_shearlag} := \beta \cdot A_{c_eff} \quad A_{eff_shearlag} = 60661.176 \text{ mm}^2$$

$$NRd_shearlag := A_{eff_shearlag} \cdot f_y \cdot \frac{1}{\gamma_M} \quad NRd_shearlag = 21534.717 \text{ kN}$$